NASA Conference Publication 10033

NASA Laser Light Scattering Advanced Technology Development Workshop—1988

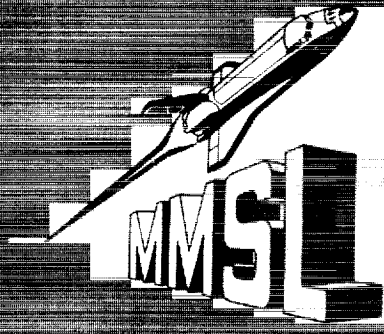

Proceedings of a workshop
sponsored by NASA Lewis Research Center
Cleveland, Ohio
September 7 and 8, 1988

NASA

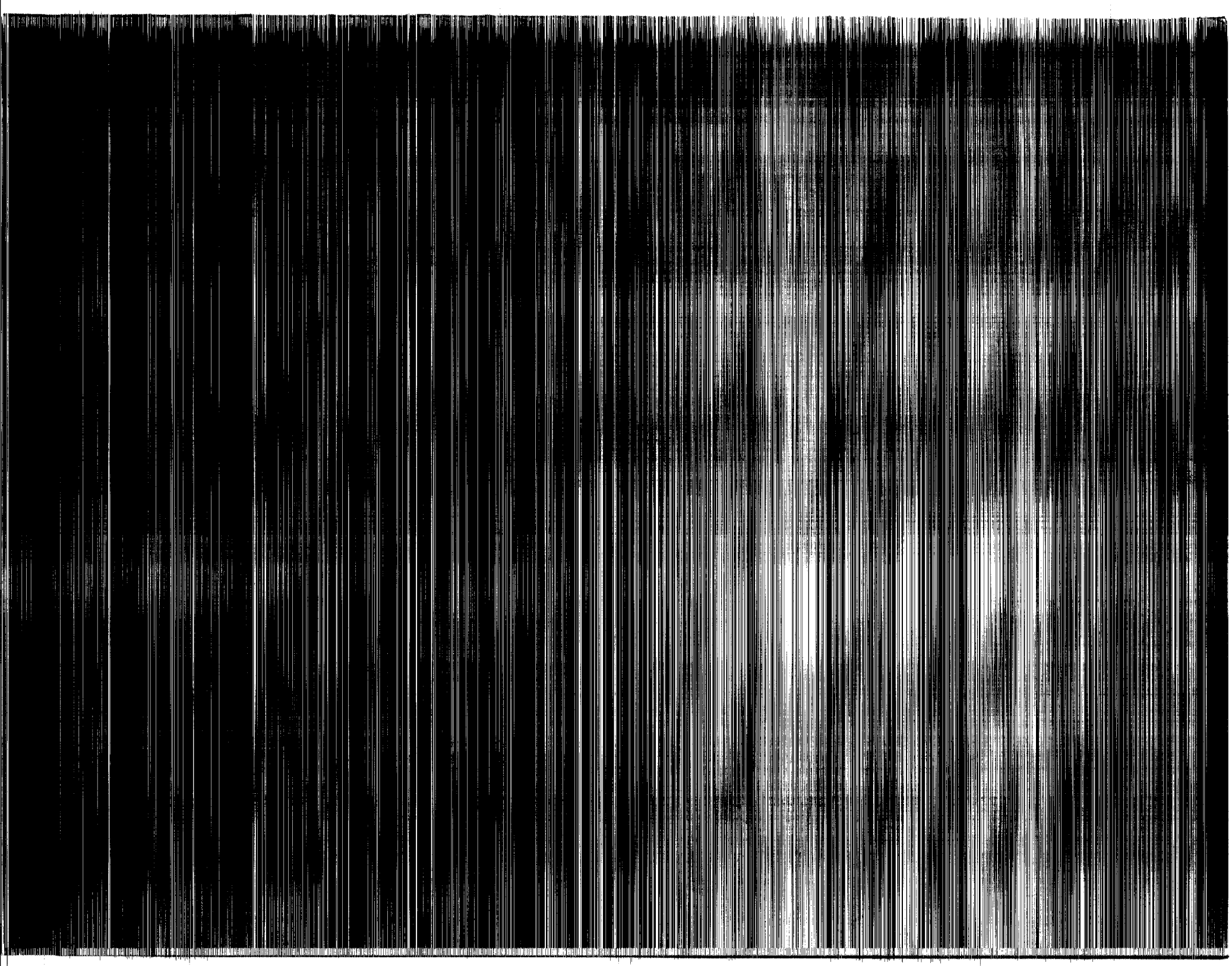

NASA Conference Publication 10033

NASA Laser Light Scattering Advanced Technology Development Workshop—1988

Proceedings of a workshop
sponsored by NASA Lewis Research Center
Cleveland, Ohio
September 7 and 8, 1988

NASA
National Aeronautics and
Space Administration

Scientific and Technical
Information Division

1989

PREFACE

The Laser Light Scattering Advanced Technology Development Workshop was held September 7 and 8, 1988, in Cleveland, Ohio. Its major objective was to explore the capabilities of existing and prospective laser light scattering (LLS) hardware and to assess user requirements and needs for an LLS instrument in a space environment (i.e., reduced gravity). This workshop, which was organized by Lewis Research Center, addressed experimental needs and stressed hardware developments. Future workshops are planned which will emphasize experiments.

Over fifty-seven individuals attended the workshop, representing a broad spectrum of experts from the United States, Canada, England, and the Federal Republic of Germany. Seventeen papers and two discussion sessions that resulted from this workshop follow. In the synopsis of the discussion sessions, it was necessary to shorten and paraphrase much of the discussion to improve clarity, and this has probably resulted in some loss of content in translating the session from the tape recording and transcriptions. If any errors have been introduced, the editor of this Proceedings apologizes.

I would like to thank all workshop participants once again for their extra effort that made it all worthwhile. Jack Harper, Richard Ziegfeld, and their colleagues at Sverdrup Technology, Inc. assisted in the preparation of this Proceedings. June Tveekrem assisted in the editing of the discussion sessions.

William V. Meyer
Workshop Organizer/Proceedings Editor
NASA Lewis Research Center

CONTENTS

LASER LIGHT SCATTERING REVIEW

Klaus Schätzel
University of Kiel
Kiel, Federal Republic of Germany

Since the development of laser light sources and fast digital electronics for signal processing, the classical discipline of light scattering on liquid systems experienced a strong revival plus an enormous expansion, mainly due to new dynamic light scattering techniques. While a large number of liquid systems can be investigated, ranging from pure liquids to multi-component microemulsions, this review will be largely restricted to applications on Brownian particles, typically in the sub-μm size range. Static light scattering, the careful recording of the angular dependence of scattered light, is a valuable tool for the analysis of particle size and shape, or of their spatial ordering due to mutual interactions. Dynamic techniques, most notably photon correlation spectroscopy, give direct access to particle motion. This may be Brownian motion, which allows the determination of particle size, or some collective motion, e.g. electrophoresis, which yields particle mobility data. Suitable optical systems as well as the necessary data processing schemes are presented in some detail. Special attention is devoted to topics of current interest, like correlation over very large lag time ranges or multiple scattering. The final sections of this review are concerned with feasibility and usefulness of laser light scattering under microgravity conditions.

Introduction

The fast progress of optics and electronics technology was a constant source of innovation for experimental work in light scattering on liquid systems, particularly over the past two decades. The development of photon correlation spectroscopy by E.R.Pike's group at Malvern is probably still the most visible of these innovations [1,2,3]. On the other hand, modern industries like macromolecular chemistry or biotechnology, created a constantly growing demand for quick, noninvasive techniques to probe liquids, emulsions, or colloids. The successful work of many people now engaged in light scattering resulted in a large number of different light scattering experiments, using different optical systems as well as signal processing algorithms [4,5]. A brief overview of the major techniques will be the central topic addressed by this review.

Because of the author's personal inclination, special attention is given to signal processing details as well as to some topics of current interest, like problems associated with the simultaneous calculation of correlograms over very large lag time ranges or multiple scattering.

Now most light scattering experiments tend to be rather bulky due to the use of large ion laser sources and big photomultiplier tubes, both needing high power or high voltage supplies, and typically accomodated on a heavy optical table. The recent development of semiconductor lasers and photon counting avalanche photo diodes now promises a dramatic reduction in size and weight for typical optical setups. Furthermore, digital correlators - the most popular signal processing hardware for dynamic light scattering - shrank in size from a full rack to a single box over the past 20 years. Progress in LSI technology now allows powerful correlators to be built on a single board, and size reduction to a single chip must be expected in the future, if sufficient demand can be stimulated. These technological advances promise to create a large number of new applications for light scattering techniques, essentially the full spread from the research lab to the monitoring of industrial production. Less important, economically, but certainly of large scientific promise, will be the use of modern light scattering as a research tool on spacecraft, as is currently being prepared both in the U.S. and in West Germany. A discussion of suitable light scattering components, systems, and experiments for microgravity environments closes this paper.

1. Optical Techniques

Laser light scattering experiments are performed with many different optical setups. While static light scattering experiments typically use a single laser beam to illuminate the sample, dynamic light scattering may be classified into (i) experiments with a single illuminating laser beam and (ii) experiments with two interfering beams in the measurement volume or at the detector. Further differences arise due to the use of coherent and incoherent detection schemes. Finally we may discuss scattering of a single particle or of a large number of particles or even the complications arising from multiple scattering processes.

1.1. Static Light Scattering

1.1.1. Single Particle Scattering

Illumination of a point-like particle by a focused laser beam is commonly (and quite well) approximated as plane-wave illumination characterized by an initial wave vector $\mathbf{k_i}$. A small detector in the far field selects a single direction of the scattered light field to be described by a final wave vector $\mathbf{k_f}$. The assumption of *quasi elastic light scattering* (QELS) corresponds to neglection of the very small length difference between $\mathbf{k_i}$ and $\mathbf{k_f}$ as it is generally caused by motion of the scattering particle.

If $\mathrm{a}(\mathbf{x})$ denotes the amplitude of the light scattered by the particle at location $\mathbf{x}$ in the illuminating beam, we obtain a complex amplitude at the detector

$$u_D(t) = a(\mathbf{x}(t)) \exp\Big[-i(\mathbf{k_i} - \mathbf{k_f})\mathbf{x}(t)\Big], \tag{1}$$

which depends on the scattering geometry through the difference of the initial and final wave vectors only. This difference is the *scattering vector* commonly denoted by

$$\mathbf{q} = \mathbf{k_i} - \mathbf{k_f}. \tag{2}$$

Its magnitude depends on the wavelength λ and the scattering angle θ between $\mathbf{k_i}$ and $\mathbf{k_f}$,

$$|\mathbf{q}| = \Big(\frac{4\pi}{\lambda}\Big) \sin\Big(\frac{\theta}{2}\Big), \tag{3}$$

and may vary between 0 and $\frac{4\pi}{\lambda}$, corresponding to virtual fringe separations down to one half of the illuminating wave length. In practice it is often difficult to obtain good signals at very small scattering angles and values below some 10° typically require specially designed light scattering experiments.

While $\mathrm{a}(\mathbf{x})$ reflects just the iluminating amplitude for point particles, it will show additional dependence on $\mathbf{q}$ for any finite size scattering particle. Within the context of static light scattering, we are interested in the temporal averages of scattered intensities only, i.e. time averages of the squared modulus of eq.(1). Neglecting polarization effects, the angular dependence of the intensity of light scattered by one particle may be expressed as a scalar function $\mathrm{P}(\mathrm{q})$, where q is the absolute magnitude of the scattering vector $\mathbf{q}$. $\mathrm{P}(\mathrm{q})$ is commonly known as the particle's form factor. It is related to the illuminating intensity $I_\circ$ and the detected intensity I_D by

$$I_D = I_\circ \, P(q). \tag{4}$$

Single particle light scattering is most interesting - and most complicated - if the particle size equals the wavelength of the scattered light or exceeds it. The full Mie theory is required for theoretical calculations, and - given sufficiently monodisperse particles - high resolution particle sizing is feasible from a static light scattering experiment. Simplified

treatments are possible for near forward or "low angle" scattering, and commercial particle sizers have been designed along these lines.

For smaller particles, especially if their refractive index varies only slightly from that of the surrounding medium, changes of the illuminating field due to the particle may be neglected, and the approximate Rayleigh-Gans theory may be applied to compute the static light scattering pattern. These patterns change from strongly forward peaked for particles not much smaller than the wavelength to the uniform Rayleigh scattering by much smaller particles. Again, particle sizing applications are possible. But knowledge of the refractive indices is generally required, and resolution degrades with decreasing particle size.

1.1.2. Many Particle Scattering

Working with coherent illumination, the complex amplitudes scattered by all the particles in the measurement volume add up at the detector and we obtain the resultant amplitude

$$u_D = \sum_{j=1}^{N} a(\mathbf{x}_j(t)) \exp\Big[-i\mathbf{q}\mathbf{x}_j(t)\Big]. \tag{5}$$

where j labels the individual scattering particles. (5) may be interpreted as a random walk problem in the complex plane and for independent stochastic particle positions (noninteracting particles) the central limit theorem predicts Gaussian statistics for the detector amplitude in the large N or many particle limit.

Upon temporal averaging of the detector signal we obtain an angular intensity pattern that is again proportional to P(q), if the particles do not interact with each other, i.e. in highly diluted samples. For more concentrated samples, however, the particles will generally show some interaction like hard core repulsion, van der Waals attraction, electrostatic repulsion due to surface charges, or hydrodynamic interactions. These interactions are responsible for a short range order of particle positions, and such order shows up in the static light scattering pattern. Let g(r) denote the conditional probability to find a particle at a position r given, there is another particle at position 0, a quantity known as the *pair distribution function* or *pair correlation*, which is normalized such that it approaches 1 at large separations. Then the mean light intensity scattered from an initial beam of intensity $I_\circ$ by a particle system of mean density ρ from a scattering volume V into the direction corresponding to a scattering vector q is

$$\Big\langle I(\mathbf{q})\Big\rangle = I_\circ P(q)\, V\, \rho\Big\{1 + \rho \int [g(\mathbf{r}) - 1]\, \exp(i\mathbf{q}\mathbf{r}) d^3r\Big\}. \tag{6}$$

The term in curly brackets is commonly designated as *static structure factor*. Fourier transform techniques can be applied to calculate pair correlations from measured structure factors, in order to investigate particle ordering or interaction potentials [6] - very much like neutron or x-ray techniques used to probe liquid structures on atomic scales.

While in the past most static scatttering was measured one angle at a time, present efforts are directed towards simultaneous multi-angle measurements, which present obvious advantages in terms of efficiency as well as the opportunity to study temporal changes of samples down to time scales of order 1s.

1.2. Dynamic Light Scattering

While for static light scattering, fluctuations of the detected intensity due to motion of the scattering particles are merely a nuisance and large aperture *incoherent detection* [5] is often applied to reduce their effect on statistical accuracy, these fluctuations constitute the starting point for dynamic light scattering experiments.

For a single scattering particle in the illuminating beam, the detection of intensities means a loss of phase information. Hence only slow fluctuations due to particle motion over distances comparable to the beam diameter are present in the signal. Such fluctuations are used in *number fluctuation spectroscopy* [6,7] as well as *single beam rate correlation* [8].

As for a single scattering particle, we are unable to measure a small collective particle motion with the single beam setup using many particles in the measurement volume. Identical phase changes of each particle's complex amplitude result in a pure phase change of u_D - a simple rotation of the random walk graph in the complex plane corresponding to eq.(5).

However, particle motions relative to each other will produce phase as well as amplitude changes in u_D, the latter resulting in measurable intensity fluctuations. The single beam setup is hence suitable to determine *velocity gradients* [9] or - a particularly important application - *Brownian motion*. In this context, the single beam setup is commonly referred to as homodyne scattering experiment.

The narrow bandwidth associated with diffusive particle motion (typ. in the kHz range), makes direct time domain processing possible, i.e. the temporal correlation analysis of the detected intensity, sometimes denoted as *intensity interferometry*. The Gaussian character of a many-particle scattering signal allows the reduction of fourth order moments like the intensity correlation to second order moments, here the amplitude correlation

$$G^{(1)}(t) = \Big\langle u(0)u^*(t)\Big\rangle = \sum_{j=1}^{N}\sum_{l=1}^{N}\Big\langle a_j a_l^* \exp\Big[i\mathbf{q}(\mathbf{x}_j(0) - \mathbf{x}_l(t))\Big]\Big\rangle. \qquad (7)$$

The relation between intensity and amplitude - or second and first order - correlations is known as *Siegert relation* and dates back to early radar work. If β is used to denote the reduction in coherence due to a finite detector aperture, the *intercept* of the correlogram, we obtain

$$G^{(2)}(t) = G^{(1)}(0)^2 + \beta|G^{(1)}(t)|^2. \qquad (8)$$

1.2.1. Noninteracting Particles

The most common application of dynamic light scattering is sub-μm particle sizing. For this purpose, the sample is typically diluted such that particle interactions may be ignored but particle scattering still clearly dominates the Rayleigh background of the solvent.

For independent particles, all non-diagonal terms in the double sum of eq.(7) are averaged to zero, and the diagonal terms result in

$$G^{(1)}(t) = N\Big\langle |a|^2 \Big\rangle \Big\langle \exp[i\mathbf{q}\,\mathbf{x}(t)] \Big\rangle, \tag{9}$$

where N denotes the average number of particles present in the scattering volume and x(t) is the particle displacement during a time interval t. Einstein's famous treatment of Brownian motion yields a Gaussian distribution for x(t) with a width of 2Dt in each spatial dimension. Hence the last expectation in eq.(9) equals the Fourier transform of a Gaussian in x-space, which is a Gaussian in q-space with a width of 1/2Dt.. If we recognize $\langle |a|^2 \rangle$ as the mean intensity scattered by a particle inside the measurement volume, we obtain

$$G^{(1)}(t) = \Big\langle |u|^2 \Big\rangle \exp\Big[-q^2 D t\Big]. \tag{10}$$

The time constant of this single exponential is typically extracted from the second order correlation function

$$G^{(2)}(t) = \Big\langle |u|^2 \Big\rangle^2 \Big[1 + \beta \exp(-2\, q^2 D\, t)\Big] \tag{11}$$

after normalization by the mean intensity to

$$g^{(2)}(t) = \frac{G^{(2)}(t)}{\Big\langle |u|^2 \Big\rangle^2} = 1 + \beta \exp(-2\, q^2\, D\, t), \tag{12}$$

by baseline subtraction and a linear fit to a semi-log plot of the data. It yields the *hydrodynamic particle radius* R if we apply the Stokes-Einstein relation for the diffusion coefficient D,

$$D = \frac{k_B T}{6\pi\eta R}. \tag{13}$$

Please note that knowledge of the Boltzmann constant k_B, the absolute temperature T, the viscosity η of the solvent, and the magnitude of the scattering vector q, which are all easily available, suffices to extract absolute particle sizes from measured decay times. There is no dependence on particle composition or any need for a calibration procedure. Typical sizes, which are easily accessed by the technique, range from about 10nm to several μm. The lower limit is set by the rapidly decreasing intensity of scattered light for particles much smaller than the wavelength. The upper limit is due to severe sedimentation problems

which occur for larger particles that are not density matched to the solvent under ordinary gravity.

While 1% relative accuracies may be achieved in particle size measurements of monodisperse particles as well as for (intensity weighted -) mean sizes of polydisperse samples, the implicit averaging over many particles in the typical dynamic light scattering experiment tends to cover details of particle size distributions. In essence, an inverse Laplace transform is required to extract a distribution of D from measured correlation functions. Much effort has been devoted to solve this ill posed problem [10], but for realistic noise levels a bimodal size distribution is rarely resolved unless both peaks are separated by more than a factor of 2 [11] or additional information like angular dependences is available.

In conclusion, dynamic light scattering from dilute samples offers precise average particle size information, but little detail as to size distributions, unless these distributions are very wide. Applications are numerous and range from suspensions of solids to macromolecular solutions and amphiphilic systems.

1.2.2. Interacting Particles

For concentrated samples, we must consider particle interactions, which tend to slow down diffusive particle motion as well as to cause dependence of the motions of two distinct particles. Starting back at eq.(7), we must now consider both, diagonal and nondiagonal terms in the double sum over all particle pairs. After normalization, we obtain a first order correlation function

$$g^{(1)}(t) = \frac{G^{(1)}(t)}{\left\langle |u|^2 \right\rangle} = \left\langle \exp\left[i\mathbf{q}\,\mathbf{x}(t) \right] \right\rangle + N \left\langle \exp\left\{ i\mathbf{q}\left[\mathbf{x}_j(0) - \mathbf{x}_l(t) \right] \right\} \right\rangle, \qquad (14)$$

which is a sum of the *self-scattering function* characterizing single particle diffusion and the *distinct scattering function* representing interaction of particle j at time 0 on particle l at time t.

For strongly interacting systems like charged latex spheres at volume fractions of some 10^{-4} in very pure water or neutral particles at much higher concentrations, the correlation functions measured by dynamic light scattering show strong departures from the single exponential decay found in the absence of interactions [12]. The observed time constants may spread several decades for one single measurement. A large range of simultaneous lag times must be used for such experiments.

Even though the computation of self and distinct scattering functions is a difficult task for concentrated particle systems, such measurements are the most important scientific effort in dynamic light scattering at present. This importance is based upon the obvious desire to investigate concentrated samples throughout the chemical industry as well as upon the possible use of colloidal systems as easily accessible models for fundamental fluid physics.

1.2.3. Dual Beam Setups

In order to detect absolute phase fluctuations in the scattered light, we need an interferometer. The simplest possible change of the single beam arrangement discussed up to now, is the addition of two beam splitting mirrors to create a reference beam with a wave vector identical to $\mathbf{k_f}$. The same result may be achieved by a single beam splitter plus a mirror, which sends a reference beam through the sample volume directly towards the detector. The latter is a more commonly used setup that provides easier alignment.

If u_{Ref} denotes the fixed complex amplitude of the reference beam at the detector, we obtain a detector intensity

$$I_D(t) = |u_D(t)|^2 = |u_{Ref}|^2 + 2\,Re\,u^*_{Ref} \sum_{j=1}^{N} a(\mathrm{x}_j(t)) \exp\Big[i\,\mathrm{q}\,\mathrm{x}_j(t)\Big], \tag{15}$$

where we already neglected a term of order a^2, as it is commonly done for reference amplitudes that are large compared to the scattered amplitude, i.e. if the cross term dominates the dynamic part of the detected signal.

Using this approximation, we obtain a second order correlation

$$G^{(2)}_R(t) = |u_{Ref}|^4 + 2|u_{Ref}|^2\,Re\,G^{(1)}(t), \tag{16}$$

which contains the real part of the first order autocorrelation introduced above rather than its modulus squared. Hence this reference beam or *heterodyne* setup provides high sensitivity to collective as well as relative particle motions.

Free Brownian particles in constant average motion characterized by a velocity v yield

$$Re\,G^{(1)}(t) = \exp\Big[-q^2\,Dt\Big]\cos[\mathrm{qv}t], \tag{17}$$

a damped cosine. The *Doppler frequency* qv can be extracted by correlation as well as by several analog techniques and serves to measure Cartesian velocity components in *laser Doppler velocimetry* [4].

While the exponential damping in eq.(17) due to diffusion is rarely ever noticeable in velocimetry applications with flow velocities ranging from some cm/s to several 100m/s, it becomes a major obstacle if very small velocities are to be determined, say in the μm/s range. Such small velocities occur in mobility studies of biological specimens or in the measurement of electrophoretic mobilities, the *micro electrophoresis* of charged particles in an external electric field [13]. Alternative signal processing techniques may be required for such measurements, as we will show in section 2.4.

1.2.4. Multiple Scattering

A topic of particular importance to all measurements on concentrated particle systems is multiple scattering, i.e. the scattering of a single photon by more than one particle. Since for Brownian particles every scattering event is the cause of additional spectral broadening, we observe correlation functions with additional components at small lag times.

Since the computation of such components becomes exceedingly difficult for higher orders of multiple scattering, experimental techniques are desired to reduce or possibly eliminate their effect on measured correlograms. The simplest technique is the use of a smaller probe volume like a very thin sample. Disadvantages of this approach are flare problems which restrict the accessible angular range and the increasing importance of particle-wall interactions.

G.Phillies introduced a dual 90° homodyne experiment, where two antiparallel laser beams illuminate the sample with wave vectors $\mathbf{k_i}$ and $-\mathbf{k_i}$, and two detectors collect scattered radiation in directions $\mathbf{k_f}$ and $-\mathbf{k_f}$. Since the two scattering vectors are antiparallel and of equal magnitudes, cross correlation of the two detector signals yields the same correlogram for singly scattered light as auto correlation of a single detector signal. The presence of one or more additional particles in the scattering process, however, breaks the symmetry of the setup and generally does not contribute any correlated fluctuations to both detector signals. Hence, multiple scattering contributions are practically eliminated from the measured cross correlation function [14].

Problems of G.Phillies' technique are difficulty of alignment and the restriction to 90° scattering which is due to the fact, that no provisions were taken to prevent light scattered from both laser beams from entering both detectors simultaneously.

The recent development of a two color cross correlation scheme by my collaborator M.Drewel overcomes the latter limitation [15]. Color coding is used to separate the two scattering processes. The different magnitudes of the **k**-vectors in both color channels, however, require more complicated illumination and detection schemes. A carefully adjusted angular separation of both, the illuminating beams as well as the detection directions can achieve perfect coincidence of the scattering vectors for both colors over a large range of scattering angles. This range increases with decreasing separation of the two wavelengths used in the experiment, while the suppression of multiple scattering tends to decrease.

Use of the argon lines at 488nm and 514nm provides a suitable compromise. With a very stable goniometer and careful initial alignment, the scattering vector may be changed over almost a decade within a few seconds. Suppression of double and higher order scattering was estimated to be better than 10^3, typically.

While computations of double, triple, and higher order scattering tend to become more complicated with increasing order of scattering, much simpler treatments are possible in the event of very high orders of multiple scattering. In this limit, the scattering process

may be treated as a *diffusion of light*. Static features like the *coherent backscattering peak* [16] as well as some dynamic features (*diffusing wave spectroscopy* [17]) can be obtained, at least for noninteracting particles.

2. Signal Processing

Throughout section 1 we used the concept of intensity and amplitude correlation functions. In this section attention will be focused on technical problems associated with the measurement of correlograms as well as an alternative signal processing scheme based on phase rather than intensity statistics.

2.1. Photon Correlation

2.1.1. Single Photon Counting

The low intensity of light scattered by small particles into small apertures (coherent detection) often requires photon counting techniques in order to obtain maximum detection sensitivity as well as sufficient temporal resolution. At present, a typical setup includes a photomultiplier tube with a large gain and low dark count, followed by a fast amplifier and pulse discriminator electronics.

The resulting sequence of photon detection pulses is then counted over sample time intervals, say of duration T, which are labelled by an index j. For a given signal intensity I(t), the counted number of pulses n_j is Poisson distributed about a mean value equal to the time integrated intensity over the sample interval times some quantum efficiency of the detector, which we will set equal to unity here. This well known relation is the *Mandel formula*. For our purposes we will need little more than just the mean count number

$$\left\langle n_j \right\rangle = \int_{jT}^{jT+T} I(t)dt \tag{18}$$

plus the knowledge, that for nonoverlapping sampling intervals j and j+k the photon counts are statistically independent for a given intensitiy I(t) [5].

It should be noted, that real photon counting systems always show some artifacts like dark count, after-pulsing, and dead time, which lead to violations of eq.(18) for very weak signals, very short delay times, or very strong signals, respectively. As a consequence, photon counting is typically limited to a dynamic range from some 10^2 to some 10^6 counts/s and special attention is required for delay times smaller than several 100ns.

2.1.2. Photon Correlation Algorithm

The digital nature of single photon counting signals is ideally suited for digital signal processing. The most popular processing scheme for the extraction of spectral information is digital correlation, the calculation of

$$\left\langle n_j n_{j+k} \right\rangle = \lim_{M\to\infty} \sum_{j=1}^{M} \frac{n_j n_{j+k}}{M}$$
$$= \int_{jT}^{jT+T} \int_{(j+k)T}^{(j+k+1)T} \left\langle I(t)\ I(t') \right\rangle dt\ dt'$$
$$= \int_{(k-1)T}^{(k+1)T} \left\langle I(0)\ I(t) \right\rangle (T - |t - kT|) dt, \qquad (19)$$

of course approximated by a sum over a finite number of samples M. The slight *triangular smoothing* over lag times ranging from $(k-1)T$ to $(k+1)T$ is often ignored, which is justified for intensity signals with little change over a single sample interval T, only.

The triangular smoothing is insensitive to the slope of the intensity correlation, but sensitive to its curvature. Exponential contributions to the correlogram are characterized by a proportionality of all derivatives to each other, particularly the second derivative and the exponential itself. Hence for a given sample time T, the effect of triangular smoothing is just a multiplicative factor, which is easily computed as

$$\frac{\left[2\cosh(\Gamma T) - 2\right]}{\Gamma^2} = T^2 \left[1 + \frac{\Gamma^2 T^2}{12} + O(\Gamma^4 T^4)\right] \qquad (20)$$

for an exponential $\exp[-\Gamma t]$ instead of the small T limit T^2. For singly exponential correlograms, T is generally chosen much smaller than the decay time. A value of $\Gamma T = 0.1$ is typical and leads to less than 0.1% amplitude change due to triangular smoothing.

If different exponential contributions occur with very different decay times, as it is often the case for Brownian motion studies on concentrated samples, much larger values of ΓT may be obtained for the faster components at a single sample time. Hence eq.(20) should be taken into account, explicitly.

While the triangular smoothing due to intensity integration over the sampling time may seem to call for a choice of small sample times T, such a choice has two possible disadvantages as well. The first one is the obvious limit on the range of available lag times for a given number of channels at equally spaced lags. Generally, a precise knowledge of the long time tail of a correlogram is highly desirable, in order to improve the stability of evaluation algorithms.

If the lag time spacing is increased over the sample time interval, say to some integer multiple of T, a larger lag range may be covered. But in this situation a second disadvantage will show up, which is a loss in signal-to-noise ratio. The triangular smoothing tends to average noise on time scales smaller than T quite efficiently. If we decrease T, more and more high frequency noise components will be picked up in the correlogram, most notably

photon shot noise, but - if present - short lived intensity fluctuations as well. The increasing number of samples which can be obtained within the same total measurement time for a smaller sample time T counteracts the loss in signal-to-noise, but cannot make up for it, since this increase in signal-to-noise only grows like the square root of the decrease due to shrinking T.

In essence, the signal-to-noise of a particular channel of a correlation function obtained at some sample time T equals that of the average over L channels located in the same lag time range, which were measured at a sample time $\frac{T}{L}$ using identical total measurement times. A single channel obtained at the shorter sample time $\frac{T}{L}$ will always be inferior in terms of noise.

2.1.3. Multiple Sample Time Correlation

Whereas noise considerations do not favor any particular sample time if an arbitrary number of channels is available, economic considerations call for as small a number of channels as possible. Furthermore, the theoretical analysis of the Laplace inversion problem proved, that a fairly small number of channels suffices for stable analysis, if lag times can be spaced linearly in log time, i.e. if the lag times form a geometric series rather than an arithmetic one [10]. Finally, such a scheme can easily be used with etremely large lag time ranges, say 4 or 6 or even 8 decades.

From our discussion in the previous section it should be clear that in parallel to the lag time, we should increase the sample time interval, if losses in signal-to-noise are to be minimized. If the lag times cover many decades, the difference between a fixed sample time scheme and a geometric sample time scheme becomes very noticeable, and significantly shorter total measurement times are possible with the latter scheme for a given statistical accuracy [5].

The channel dependent triangular smoothing due to the variation in T must be explicitly accounted for, if a very coarse channel spacing is desired. An alternative approach is the use of a finer channel spacing. For a given ratio of sample time T to lag time t, the maximum absolute distortion of an exponential $\exp[-\Gamma T]$ at any lag time is easily computed as

$$\text{max.error} = \frac{T^2}{(3e^2t^2)}, \tag{21}$$

which is well below 10^{-3} for $\frac{T}{t} = \frac{1}{8}$. In order to obtain eq.(21), we use the first two terms in the power series of eq.(20) and determine the maximum of $\frac{T^2 \exp(-t)}{12}$ for constant $\frac{T}{t}$.

In conclusion, the use of e.g. 8 channels per octave, which is equivalent to some 27 channels per decade, keeps absolute distortions of the correlogram due to the triangular smoothing much smaller than typical noise levels. The total number of channels necessary

to cover say 6 decades of lag times is 160, still a number well manageable in terms of data storage and time required for Laplace inversion.

2.1.4. Digital Correlators

The computational tasks of a digital correlator are (i) counting of input pulses, (ii) delay of these data, (iii) multiplication of delayed and direct data, and (iv) accumulation of these products in a summing store. For maximum efficiency, steps (ii) through (iv) should be performed for many lags in parallel and at real time speed.

The classical instrument of photon correlation spectroscopy used to be the *single bit correlator* which was first introduced by Malvern Instruments as the "K7023" around 1970. The instrument uses a single bit shift register for signal delay. These delayed data are then multiplied with direct data. With single bit delayed data, the multiplication can simply be done by gating the direct data to a counting store, on a pulse by pulse basis. Hence, this type of machine may be termed a $1 \times N$ *bit correlator*, in order to stress the fact that data reduction to a single bit is necessary for the delayed data only. The direct channel can accept as many pulses as there are operational cycles (typ. 50ns) in one sample time interval.

Data reduction to one bit is most simply done by *clipping*, i.e. binary thresholding at some clip level [18]. For Gaussian input signals (more precisely: Gaussian complex amplitudes), this clipping procedure does not distort the correlogram. Furthermore, if the clipping level is chosen close to the mean count per sample time interval, there is no significant change in signal-to-noise. As the majority of dynamic light scattering measurements are performed on many particles, the Gaussian assumption is acceptable for most experiments.

If non Gaussian signals are to be expected, as in number fluctuation spectroscopy, *random clipping* or *scaling* must be applied to avoid distortions of the correlation function. However, these procedures do degrade signal-to-noise, and may significantly increase total measurement times [19].

Mainly for this reason, *multibit correlators* were introduced in the late 1970's, first by Langley-Ford and later by Malvern and Brookhaven Instruments, to name just a few. Most of these machines are of the $4 \times N$ bit type, i.e. they use a 4 bit shift register for data delay and the multiplications are broken down to a series of additions of these 4 bit numbers to the accumulating store, again triggered by the direct data on a pulse by pulse basis.

While these instruments generally avoid the need for clipping and scaling, if necessary, and introduce much less loss in signal-to-noise, their more complex structure causes a slight decrease in speed. Their maximum input count rate is typically limited to 10MHz. In order to obtain full scale 4 bit signals, a sample time of $1.5\mu s$ or more must be used. The latest variant of this type of correlator was recently introduced by Malvern Instruments and uses

an $8 \times N$ bit structure at a cycle time of 50ns, corresponding to 20MHz peak count rates in real time operation.

A different correlator concept was developed during the early 1980's at my laboratory to process digital data into structure functions (sum of squares of $n_j - n_l$) as well as correlation functions. Structure functions are less sensitive to low frequency noise or drifts. Their algorithm is not easily broken into a sequence of single pulse steps. Hence a fully parallel approach was used, resulting in a 4×4 *bit structurator/correlator*. This means more complicated (and more expensive) logic, but also a significant increase in speed. Parallel operation completes the multiplication and accumulation to the store within a single machine cycle for full 4 bit data in both channels, delayed as well as direct. With a fast pulse counter in the input, peak count rates in excess of 100Mhz may be processed, using sample time intervals from 100ns up.

A second, less obvious advantage is related to full parallel data processing. A typical photon counting signal constitutes a very irregular pulse sequence. Even for constant detector intensity, Poisson fluctuations result in an exponential distribution of waiting times. Any signal fluctuation produces even wider waiting time distributions. To avoid dead time distortion, average count rates must be kept very small as compared to the peak count rate of the correlator. Factors of about 100 are commonly used. Consequently, the fast (and expensive) correlator electronics, e.g. a $4 \times N$ bit machine, actually processes data only a tiny fraction of the time, 1% is typical.

For a 4×4 bit correlator, processing is no longer tied to single pulse arrivals. Instead there is exactly one active computation cycle for every sample time interval. However, at a typical sample time of say $10\mu s$ and an internal clock of 100ns, the same low 1% duty cycle arises. There is, however, a subtle but important difference between both situations. While for the $4 \times N$ bit correlator, randomness of the input signal makes it impossible to predict which are the active machine cycles, for the 4×4 bit device we know the location of the active cycles by design.

To take advantage of this fact, we must decouple data sampling and processing, e.g. by storing all data in a fast dual port memory first. After a certain block of data is available in memory, we start its processing, of course at maximum speed. For sample times in excess of the internal processing time, processing will be done before another block of data has been sampled and we can use the available time for a second round of processing. This time we read the same set of data for the direct channel as before, but use a time displaced set of delayed data, resulting in a different range of lag times to be computed.

In this fashion, a small number of hardware channels are time multiplexed to obtain the performance of a larger number of real time channels in the correlogram. The factor by which the number of channels is increased essentially equals the ratio of sample time and internal processing cycle time. For the first commercial instrument of this type, the ALV-3000, this cycle time is about 60ns and 16 hardware channels are typically installed. For our earlier example of a $10\mu s$ sample time, more than 1000 real time channels result!

Even more useful for dynamic light scattering is the opportunity, to implement a *quasi geometric lag time and sample time* pattern in such a 4×4 bit correlator. Such a scheme, where both the lag time increment as well as the sample time are doubled every m channels, becomes prohibitively expensive if implemented in traditional $4 \times N$ bit hardware, if many decades of lag time are to be covered [20].

With data buffering, simply add pairs of adjacent data and store these sums in place of the old data between each two rounds of processing of a particular block of data. The required hardware is minimal and can operate in parallel to the processing without requiring extra computation time. Doubling of the sample time naturally implies a halved number of samples. Hence the necessary computation time decreases like a geometric series. Due to some overhead, the ALV-3000 achieves real time operation in this quasi geometric or multiple tau fashion at an initial sample time of about $1\mu s$ for 8 channels per octave (m=8) and 8 additional channels to fill the lag time range from 0 to $7\mu s$. 4×4 bit hardware is used for sample times up to about 1ms. Larger lags are processed on a separate 16 bit microprocessor using a full 16×16 bit data format. In this manner, simultaneous lag times from $1\mu s$ to some 60s are covered at real time in a single measurement.

As the next logical step in correlator development, the performance of these *multiple tau* machines will be improved by 8×8 bit parallel hardware processing for the small sample times and, again, 16×16 bit processing at large sample times. The increase in bit format allows quantization errors to be kept below photon noise levels for all lags. The ALV-5000, which will be commercially available in early 1989, covers a simultaneous lag time range from 200ns to an essentially unlimited upper bound with 8 channels per octave, to avoid significant triangular smoothing distortion. Increase of sample time with lag time and full real time operation ensure optimum statistical accuracy over the whole lag time range.

Consequently, multiple tau is the only mode of operation, and sample time setting is no longer necessary. The only user setting is a choice of auto or cross correlation (a second pulse input is included) and of single or dual auto correlation mode. The latter allows the simultaneous calculation of two independent correlograms, both at a 400ns initial sample time. This simplicity plus the heavy use of LSI technology allows the correlator to fit onto a single board.

The increasing power of microprocessors stimulated the design of *pure software correlators* at several laboratories (including my own). While this approach is succesful at large sample times, say on the order of 1 ms, or if sufficient experimental time is available to work in non real time at a low duty cycle, typical dynamic light scattering experiments with sample times in the μs region still profit from hardware machines with fast real time operation.

In order to give a comparison of the relative computational powers achieved, we may use the number of elementary operations (multiply and add to store) completed in one second - for short designated as Op/s. A typical 16 bit microprocessor (e.g. 68000) achieves

some 2×10^5 Op/s, this number is essentially doubled for 32 bit processors. Another factor of two is available through the use of the fastest available versions of the processor with fast memories. Programmable signal processors achieve some 10^6 Op/s (2×10^6 Op/s for 32 bit processors) due to their faster memory cycle and separate data and program access. However, the parallel hardware of the ALV-5000, to give an example of current hardware technology, runs at 2×10^8 Ops/s, about a factor of 100 faster than the fastest current "pure software" approach.

An extension of the multiplexing to more than just two simultaneous correlograms, which is easily added to a hardware correlator with data buffering like the ALV-5000, seems to be more promising than the use of a large number of lower performance software correlators run in parallel, if many correlograms are to be measured at the same time with maximum efficiency. This is true both in terms of cost as well as in terms of space and power requirements. The development of dedicated powerful *single chip correlators* could, however, be a superior third alternative. While such a development seems feasible today, the high cost of custom LSI design will probably discourage commercial companies, unless the photon correlation market expands rather significantly.

2.1.5. Dead Time Correction

Before leaving the topic of photon correlation, I want to point out some special problems that should be considered at very small or very large lag times, respectively. At small lags, photon noise generally dominates and a large count rate is very desirable. The count rate is, however, limited by detector and correlator dead times, typically ranging between 10ns and 100ns.

While this limitation had been realized in the early days of photon correlation, not much beyond a simple first order approximation was available to estimate dead time distortions in correlograms until our recent work on correction algorithms for arbitrary signals with complex joint Gamma amplitude statistics as they occur by spatial or temporal averaging of Gaussian or many particle scattered amplitudes.

Dead time behavior may be classified according to whether or not a skipped pulse extends the dead period of the detection or counting system. If such an extension occurs, the system will be completely blocked at very large input event rates and is hence called *paralyzable*. If skipped pulses are just completely ignored, the output rate will saturate at the inverse dead time at very large input rates. This type of dead time behavior is known as *non paralyzable*. Unfortunately, some real photon counting systems fall in between both cases and some *mixed model* is required.

An exact algebraic expression for dead time distortion in correlation functions of Gamma signals is available for the *paralyzable* system. Approximations, which are accurate for input rates up to about 40% of the inverse dead time, have been computed for the *non paralyzable* and *mixed* cases. They may be used in an *iterative correction procedure* for correlograms, which removes essentially all nonlinear distortions due to dead time.

This algorithm is stable beyond 40% dead time effects, thus greatly increasing the useful dynamic range of photon correlation spectroscopy [21,22].

As a side effect, our computations may be used to estimate the "safe range" of count rates, where no correction of dead time distortion is required. In fact, almost 10% dead time effects are necessary to produce severe deviations in time constants extracted from photon correlograms.

2.1.6. Bias and Symmetric Normalization

At large lag times, the common assumption of having a large number of samples, about 10^6, is violated, unless exceedingly long total measurement times are being used. A first consequence of this fact is the appearance of some bias in the normalized correlogram [23].

While this bias problem has long been recognized, a signal-to-noise problem related to the common procedure of normalization was not realized until our recent work, which was stimulated by an investigation of the superior immunity of structure functions against the use of a short total measurement time. We discovered, that a novel symmetric normalization scheme may be used, to achieve a similar improvement in the signal-to-noise ratio of correlograms [24].

Symmetric normalization takes into account the difference between the delayed and the direct data sets by using separate monitor channels for each of them and normalizing raw corralation data by their product rather than the usual square of the number of counts measured in the direct channel, only. It should be noticed, however, that this scheme requires a separate monitor channel for each lag time. This information is so far not available in existing hardware correlators, except for the ALV *multiple tau* machines.

The effect on signal-to-noise can become quite enormous if the sample time becomes a significant fraction of the total measurement time and the signal shows a very small relative variance on this time scale as is typically the case with dynamic light scattering data. Reductions in signal-to-noise of more than a decade have been observed [24]. This corresponds to a decrease in the total measurement time required to achieve a given statistical accuracy in the long time tail in excess of 100 - i.e. minutes instead of hours.

Even for experiments where no long time components are expected in the photon correlation function, the accurate measurement of the long time tail will yield an improved baseline plus the opportunity to detect distortion due to the passage of slow dust particles close to the measurement volume. With symmetric normalization, such measurements are feasible without an increase in the total measurement time.

2.2. Phase Processing

Photon correlation analyzes temporal intensity fluctuations of scattered light. While this technique is certainly the most popular signal processing scheme in dynamic light

scattering, it should be noted that there are alternatives that may be superior in special situations. As an example, we will discuss a processing scheme based upon analog measurements of the optical phase of a scattered light signal.

As discussed earlier in the context of dual beam dynamic light scattering, the measurement of small collective particle velocities by photon correlation velocimetry is limited in terms of resolution by line broadening due to random Brownian particle motion. Many experiments undertaken to measure electrophoretic mobilities have to apply high electric fields in order to create measurable particle velocities. High fields tend to destroy the sample by heating and electrolysis. The latter problem is usually avoided by the use of alternating fields [13]. In an ac-field, particles show a collective periodic motion plus the superimposed Brownian random walk motion.

To apply standard laser Doppler techniques, the periodic motion must have an amplitude that exceeds both the rms Brownian motion over one field period as well as the effective fringe spacing, i.e. the inverse length of the scattering vector times 2π. If phase processing is being used, collective particle oscillations may already be detected at much smaller amplitudes.

The technique is most easily explained by discussing the scattering from a single particle. Here, the optical phase in some kind of heterodyne experiment is directly given as the scalar product of wave vector and particle position. Hence the mean squared phase change - *the phase structure function* - is proportional to the mean square particle displacement, in our case the sum of a linear term with slope 2D for diffusion plus a (1 - cos) term for an electrophoretic motion in a sinusoidal field. The amplitudes of both terms are easily fitted to measured data with good accuracy over a large range of relative magnitudes, especially if the Brownian motion strongly exceeds the field motion on the time scale of a field period. Furthermore, the field induced motion may well be just a small fraction of a single fringe separation.

For many particle scattering, the simple phase processing scheme breaks down. A complex signal as in eq.(5) has a phase difference distribution without a finite second moment. Occasional destructive interference of the single particle scattering amplitudes is responsible for this divergence. Hence the problem is best removed by including an amplitude weighting in the measured phase differences. The structure function of this *amplitude weighted phase (AWPS)* may be computed and turns out to be very similar to the single particle phase structure function. The difference is essentially an additional factor equal to the mean square amplitude, which is removed prior to further analysis by division with a suitable monitor channel [25].

The *AWPS-technique* was successfully applied to a number of colloids and emulsions. An early measurement on 300nm diameter emulsion droplets with a zeta potential of some 40mV detected a 10nm peak-to-peak motion in a 0.6V/cm ac-field at 50Hz. This motion was less than 1/200th of the effective fringe separation and of course very much smaller than rms particle diffusion over 20ms [25,26]. AWPS measurements to check the effects of

retardation and relaxation, which complicate the theoretical derivation of surface potentials from mobilities, are underway as well as a large number of pharmaceutical applications.

3. Microgravity Considerations

The suitability of laser light scattering for microgravity experimentation largely depends on our ability to replace full size optical table experiments with small, lightweight, rugged setups. We will discuss this issue first on the level of the necessary components, then proceed to discuss an example of a particular setup, and finally address the question of worthwhile experiments.

3.1. Components

Key components of the optical setups used in laser light scattering in terms of size are the laser and the detector. Many current experiments use small or large ion lasers, which are extremely inefficient devices, when comparing their power consumption with the optical output produced.

The obvious alternative for space experiments are *semiconductor laser diodes*. Such lasers are both, small and power efficient. Their wavelengths are at present limited to the far red and the near infrared. Powers of some 100mW may be obtained near 800nm with decent single transverse mode beams. Several mW are available at 670nm, just inside the visible region of the spectrum where alignment is considerably easier.

The diode laser power supply is a simple current source driving some 100mA at only about 2V. But for stable operation, thermal control, e.g. by a Peltier cooler, is necessary.

The large *beam divergence* and *astigmatism* of laser diodes must be corrected with special optics, including large aperture lenses plus cylinder lenses or anamorphic prisms. Single mode optical fibers may prove useful for beam delivery and spatial filtering.

If shorter wavelengths are required, *hybrid lasers* like the diode-pumped frequency-doubled YAG with up to 5mW at 532nm and excellent beam properties may be used.

The standard detector in present day laser light scattering is a photomultiplier tube, typically 1.5" in diameter and accompanied by a space consuming high voltage power supply. Again, semiconductor technology must supply us with an alternative. Static light scattering is already easily performed with ordinary small *photo diodes*, which offer high quantum efficiency and low noise at small bandwidth. Multi element detectors like *line arrays* are available, too.

For dynamic light scattering, the *avalanche photo diode* (APD) has just been improved to produce about 100Hz dark count rates at high quantum efficiencies in Geiger mode. Active quenching reduces dead times to less than 50ns [26]. Some afterpulsing problems

remain, but may be circumvented by cross correlation techniques if small lag times are important.

APDs need a moderately high supply voltage of some 200V plus thermal control, usually slight cooling by a very small Peltier device, which may be mounted right underneath the diode's substrate. Their spectral range matches that of laser diodes extremely well with the highest quantum efficiency being obtained at about 800nm.

The application of avalanche diodes for photon counting will be greatly eased if commercial modules, including the necessary thermal control and active quenching electronics, become available.

As a second alternative to photomultipliers for photon counting, we may consider micro channel plate detectors. While these devices still need high supply voltages, their size is typically smaller than ordinary photomultipliers, though still much larger than that of photo diodes. Compared to photomultipliers, micro channel multipliers offer faster response and less sensitivity to magnetic or mechanical disturbances. Multi-anode detectors are available, that use the imaging properties of micro channel plates.

Optical components of typical light scattering setups like lenses, mirrors, and apertures, are replaced by smaller components with relative ease, such components are now becoming readily available mainly for light wave communications. The most difficult aspect of miniature optics like *graded index lenses* or *fibers* is their mechanical alignment, if bulky mechanical components are to be avoided.

The decreasing size of digital correlators was already mentioned in section 2.1.4. Present state-of-the-art are single board correlators with the possibility of future single chip machines in the air.

3.2. Systems

A large number of light scattering exeriments may be performed using the new miniature components. To illustrate the possibilities, I will sketch a setup that I recently proposed for a critical light scattering experiment in space.

Very close to the critical temperature - a region generally not accessible except under microgravity due to the divergence of the isothermal compressibility - the critical opalescence of single component liquids becomes so strong that severe multiple scattering occurs, unless extremely small sample volumes are being used. For dynamic light scattering, the decorrelation of multiple scattering seems an obvious choice. The dual color technique may be directly applied, e.g. based on two diode lasers operating at suitably spaced wavelengths.

However, the required complicated alignment for a change of the scattering angle and the large number of necessary optical components do not look very attractive for an

experiment that must be small as well as rugged. Instead, I propose a setup very close to G. Phillies' original idea. There are just two diode lasers - selected to yield identical wavelengths - illuminating the measurement volume with counterpropagating beams and two detectors looking at exactly opposite scattered wave vectors.

Semiconductor lasers show a fast output response to the driving current (only about 1ns delay). This allows for an extremely simple way of separating the two desired propagation paths from the two undesired ones, which were always present as well in Phillies' experiment. We divide each sample time interval into two non overlapping time intervals of equal length and switch on just one of the two lasers for every sub-interval. The detector signals are gated synchronously, and in this way time-multiplexing serves to select the desired combinations of laser and detector only. Arbitrary scattering angles may now be accessed by a single common rotation either of the two lasers, or the two detectors, whichever is simpler.

A point to be illustrated by the sketch of this "time slotted cross correlation experiment" is, that in addition to the use of small modern optical components, new ideas for simple novel setups are required if optimum instrumentation for microgravity environments is desired.

3.3. Experiments

Many of the current suggestions for the use of laser light scattering in space are related to critical fluid experiments. The need for microgravity for close approaches to the critical temperature in single component fluids was already mentioned. Experiments which have been performed in Germany include holographic interferometry on SF_6 during the D-1 mission and a static light scattering measurement using a camera detector to observe spinodal decomposition during a TEXUS flight. A dynamic light scattering experiment is prepared on ground to investigate spherical particles in a near critical fluid. My own proposal for the use of dynamic light scattering on critical fluids aims at the study of equilibration effects close to the critical point, about which there seems to be surprisingly little theoretical understanding, and where the absence of gravity induced convection is a major prerequisite.

As for other experiments, there is some demand for the exclusion of sedimentation or convection in aggregation and crystal growth and light scattering is being discussed as a useful analytic technique. But to my knowledge no specific light scattering experiments along those lines are currently underway in Germany.

Conclusions

Current technology certainly allows the construction of compact rugged laser light scattering experiments for, both static and dynamic light scattering. In addition to the use of micro components like diode lasers, micro lenses, APDs, and single board correlators, we should put considerable effort into the design of the simplest possible setups to perform

a successful light scattering measurement under the essentially hostile environment on spacecraft with a high level of vibration and stringent requirements for small and light weight equipment.

Before the design of such a specific experiment, we need answers to two important questions: First, who are the users and what are their experiments (possibly other than just critical light scattering)? Second, what quantities should we measure at what precision and what environment is required for the sample?

Only with clearly stated answers to these questions should we proceed into the extremely time consuming task of preparing a light scattering system to go on board a spacecraft. Only on the basis of these answers can we attempt to design an optimal experiment with a high probability of successful performance in space.

If we proceed to develop multi-purpose light scattering equipment prior to sufficient answers - possibly motivated by the desire to attract new users by the actual availability of some instrumentation - we should not forget about our questions for exact experimental requirements. There is always a certain danger for projects to keep on running just by their own inertia (though not always to their disadvantage)!

However, just the use of compact light scattering setups on the ground may be sufficient stimulus as well as reward for their design. While this may be regarded as another spin-off from space technology, it is at the same time certainly beneficial for future micro gravity instrumentation if suitable systems have already been used thoroughly on earth. And - one way or the other - laser light scattering will become a more powerful experimental tool in the end.

References

1 H.Z.Cummins, E.R.Pike (eds.): *Photon Correlation and Light Beating Spectroscopy*, Plenum Press, New York (1974).

2 B.J.Berne, R.Pecora: *Dynamic Light Scattering*, John Wiley, New York (1976).

3 H.Z.Cummins, E.R.Pike (eds.): *Photon Correlation Spectroscopy and Velocimetry*, Plenum Press, New York (1977).

4 E.O.Schulz-DuBois (ed.): *Photon Correlation Techniques in Fluid Mechanics*, Springer, Berlin, Heidelberg, New York (1983).

5 K.Schätzel: *Correlation Techniques in Dynamic Light Scattering*, Appl.Phys. B 42, 193-213 (1987).

6 K.Schätzel, M.Drewel: *Laser Light Scattering and Correlation Techniques for Characterization of Colloidal Suspensions*, Z.Phys. B 68, 229-232 (1987).

7 P.N.Pusey: *Number Fluctuation of Interacting Particles*, J.Phys. A 12, 1805-1818 (1979).

8 J.C.Erdmann, R.P.Gellert: *Recurrence Rate Correlation in Scattered Light Intensity*, J.Opt.Soc. Am. 68, 787 (1878).

9 C.Keveloh, W.Staude: *Determination of Velocity Gradients with Scattered Light Cross Correlation Measurements*, Appl.Opt. 22, 333-338 (1982).
10 J.G.McWhirter, E.R.Pike: *On the Numerical Inversion of the Laplace Transform and Similar Fredholm Integral Equations of the First Kind*, J.Phys. A 11, 1729-1745 (1978).
11 R.S.Stock, W.H.Ray: *Interpretation of Photon Correlation Spectroscopy Data: A Comparision of Analysis Methods*, J.Polymer Sci. Polymer Phys. 23, 1393-1447, (1985).
12 W.van Megen, S.M.Underwood, R.H.Ottewill, N.Williams, P.N.Pusey, in Faraday Discuss. Chem. Soc. 83, paper 16 (1987).
13 A.J.Bennet, E.E.Uzgiris: *Laser Doppler Spectroscopy in an Oscillating Electric Field*, Phys.Rev. A 8, 2662-2669 (1973).
14 G.Phillies: *Suppression of Multiple Scattering Effects in Quasielastic Light Scattering by Homodyne Cross-Correlation Techniques*, J.Chem.Phys. 74, 260-262 (1981).
15 M.Drewel, J.Ahrens, U.Podschus: *Decorrelation of Multiple Scattering for Arbitrary Scattering Angle*, subm. to J.Opt.Soc.Am. A (1988).
16 P.E.Wolf, G.Maret: *Weak Localization and Coherent Backscattering of Photons in Disordered Media*, Phys.Rev.Lett. 55, 2696-2699 (1985).
17 G.Maret, P.E.Wolf: *Multiple Light Scattering from Disordered Media. The Effect of Brownian Motion of the Scatterers*, Z.Phys. B 65, 409-413 (1987).
18 E. Jakeman, C.J.Oliver, E.R.Pike: *Clipped Correlation of Integrated Intensity Fluctuations of Gaussian Light*, J.Phys. A 4, 827-835 (1971).
19 K.Schätzel: *Signal Preprocessing for Digital Correlators*, Appl.Phys. 22, 251-256 (1980).
20 K.Schätzel: *New Concepts in Correlator Design*, Inst.Phys.Conf.Ser. 77, 175-184 (1985).
21 K.Schätzel: *Dead Time Correction of Photon Correlation Functions*, Appl.Phys. B 41, 95-102 (1986).
22 K.Schätzel, R.Kalstroem, B.Stampa, J.Ahrens: *Correction of Detection System Dead Time Effects on Photon Correlation Functions*, J.Opt.Soc.Am. B (May 1989).
23 E.Jakeman, E.R.Pike, S.Swain: *Statistical Accuracy in the Digital Autocorrelation of Photon Counting Fluctuations*, J.Phys. A 4, 517-534 (1971).
24 K.Schätzel, M.Drewel, S.Stimac: *Photon Correlation Measurements at Large Lag Times: Improving Statistical Accuracy*, J.Mod.Optics 35, 711-718 (1988).
25 K.Schätzel,J.Merz: *Measurement of Small Electrophoretic Mobilities by Light Scattering and Analysis of the Amplitude Weighted Phase Structure Function*, J.Chem.Phys. 81, 2482-2488 (1984).
26 K.Schätzel, M.Drewel, J.Merz, S.Schroder: *Simultaneous Measurement of Small Electrophoretic, Convectional, and Diffusional Motions by Amplitude Weighted Phase Structure Functions*, Inst.Phys.Conf.Ser. 77, 185-190 (1985).
27 R.G.W.Brown, R.Jones, J.G.Rarity, K.D.Ridley: *Characterization of Silicon Avalanche Diodes for Photon Correlation Measurements*, 2: Active Quenching, Appl.Opt. 26, 2383-2389 (1987).

CRITICAL FLUID LIGHT SCATTERING*

Robert W. Gammon
Institute for Physical Science and Technology
University of Maryland
College Park, Maryland

The objective is to measure the decay rates of critical density fluctuations in a simple fluid (xenon) very near its liquid-vapor critical point using laser light scattering and photon correlation spectroscopy. Such experiments have been severely limited on earth by the presence of gravity which causes large density gradients in the sample when the compressibility diverges approaching the critical point. The goal is to measure fluctuation decay rates at least two decades closer to the critical point than is possible on earth, with a resolution of 3 μK. This will require loading the sample to 0.1% of the critical density and taking data as close as 100 μK to the critical temperature (T_c = 289.72 K). The minimum mission time of 100 hours will allow a complete range of temperature points to be covered, limited by the thermal response of the sample. Other technical problems have to be addressed such as multiple scattering and the effect of wetting layers.

We have demonstrated the ability to avoid multiple scattering by using a thin sample (100 microns), and a temperature history which can avoid wetting layers, a fast optical thermostat with satisfactory microcomputer temperature control and measurement, and accurate sample loading. With the questions of experimental art solved, there remain the important engineering tasks of mounting the experiment to maintain alignment during flight and using vibration isolation to prevent Shuttle motions from distorting the sample.

The experiment entails measurement of the scattering intensity fluctuation decay rate at two angles for each temperature and simultaneously recording the scattering intensities and sample turbidity (from the transmission). The analyzed intensity and turbidity data gives the correlation length at each temperature and locates the critical temperature.

The fluctuation decay rate data set from these measurements will provide a severe test of the generalized hydrodynamics theories of transport coefficients in the critical region. When compared to equivalent data from binary liquid critical mixtures they will test the universality of critical dynamics.

*Work was funded by NASA Lewis Research Center under grant NAG-727 (Project Manager; Richard Lauver). This work was previously presented at a Program Review requested by Code EN (Microgravity Science and Applications Division).

1 Introduction

Near a critical point it is possible to approach a macroscopic instability continuously through equilibrium states. This instability is the source of a continuous symmetry breaking or *ordering*. The key to understanding the anomalous phenomena observed in the critical region is the thermodynamic fluctuations. Approaching the critical point the fluctuations in the order parameter become extremely large in amplitude, show long range correlations, and decay exceedingly slowly. The large amplitude and extent of the fluctuations means that they can not longer be neglected and are truly dominating the properties of the system. This dominance of the order parameter fluctuations leads to a universality of the behavior, an independence from the details of the molecular interactions, so that descriptions of the anomalies only depends on the dimensionality of the system and the number of components of the order parameter. The prediction of asymptotic static properties near critical points is now more precise than experiments.

We now know that there are many examples of critical transitions: liquid-vapor critical points, magnetic transitions such as Curie ferromagnetic points or Neel anti-ferromagnetic points, superconductivity, the helium lambda transition, binary mixture miscibility critical points, ferroelectric Curie points, etc. All these continuous transitions share in having divergent thermodynamic fluctuations. It is the study theoretically and experimentally of these fluctuations that marks this current era of critical phenomena research.

Thermodynamic fluctuations are the variations in space and time of a thermodynamic variable from its equilibrium value. The fluctuations reflect the underlying heat modes (thermally excited microscopic material modes) of the material. From condensed matter physics point of view the divergence of fluctuations is the result of the instability of a heat mode. The eigenfrequency goes to zero, at the critical point and its thermal population diverges. The energy stored in this mode diverges and this is seen in the divergence of the heat capacity. In a liquid-vapor critical point the relevant modes can be described by generalized hydrodynamics. For each wavevector $\vec{q}$ there are five modes, two sound modes, two shear modes, and a thermal diffusion mode. At the liquid-vapor critical point the diffusive density fluctuation is unstable and through couplings to the other modes from the non-linearities of hydrodynamics, the other modes are affected leading to anomalies in sound propagation and shear viscosity. These modes can be used as a basis for describing the static and dynamic properties of a material and are the fundamental excitations of the material.

Experimentally it is often possible to look directly at the microscopic excitations. Most commonly this is done with a scattering measurement where one can measure either the static or dynamic structure factors of the modes. Such measurements probe modes having wavevector magnitude q, with

$$q = 2k\sin(\theta/2) \quad ,$$

where k is the wavevector magnitude of the incident radiation and θ is the scattering angle. Measurements of the intensity versus angle gives the correlation length ξ of the fluctuations and spectroscopy of the scattered light gives the spectrum or time correlation of the modes. For liquid-vapor transitions light scattering has furnished the best method. The techniques are now highly developed and by using photon correlation measurements of the scattered laser light intensity it is possible to have accurate measurements of the space and time correlations of the critical fluid density fluctuations.

In what follows we describe the context for the proposed experiment on critical fluid light scattering named Zeno, give the Zeno Science Requirements which will produce a

significant data set during a Shuttle flight, and describe the Zeno apparatus conceptual design to meet the Science Requirements.

2 The Context for Zeno

2.1 Critical Exponents and Universality

The theory of critical phenomena is overseen by an experimental fact: thermodynamic response functions are singular at a critical point; and a conjecture: the principle of universality. The theoretical approach to critical phenomena has matured in the past decade to the point where its predictive success is rivaled only by quantum electrodynamics.

The singularity of response functions suggests that they be described simply near a critical point. Measuring the distance from the critical point by the reduced temperature $t \equiv (T - T_c)/T_c$, where T_c is the critical temperature, one expects the response function $f(t)$ to satisfy a power law $f(t) \sim t^{\varsigma}$ as $t \to 0$. The value of the critical exponent ς depends on the particular function $f(t)$. Examples for a liquid-vapor critical point are:

$$\begin{aligned} \text{specific heat,} \quad & C_v \sim t^{-\alpha}, \quad \alpha = 0.110; \\ \text{correlation length,} \quad & \xi \sim t^{-\nu}, \quad \nu = 0.630; \\ \text{isothermal compressibility,} \quad & \kappa_T \sim t^{-\gamma}, \quad \gamma = 1.241. \end{aligned}$$

The universality principle makes critical exponents more than just a mathematical curiosity. Separate all critical points into universality classes, where each universality class has two unique properties: the spatial dimension of the system in question (3 for a fluid), and the degree of the order parameter for the critical point (1 for a liquid-gas critical point since the order parameter, the difference between liquid and gas densities $\rho_L - \rho_G$, is a scalar). Then, within a universality class, the critical exponents of all static properties should be universal, unvarying from system to system.

Critical exponents are a powerful way to characterize critical phenomena, but they provide a challenge for experiment. Since they are defined from the limiting, or asymptotic, behavior of the thermodynamic functions, the exponent of a particular function will not be clearly revealed unless an experiment reaches the so-called asymptotic region. The challenge is that critical behavior is often not manifestly evident before reduced temperatures less than 10^{-6} are reached. Thus, experiments in critical phenomena are usually very concerned with penetrating ever closer to the critical point.

2.2 Critical Dynamics in Fluids

The critical fluctuations in a liquid-vapor system correspond to density fluctuations which decay isobarically by thermal diffusion. The mean square fluctuation in density is proportional to the isothermal compressibility and hence diverges with exponent $\gamma = 1.241$. From the thermal conduction equation it follows that the density fluctuation with wavevector $\vec{q}$ (its qth Fourier component) decays with a rate given by

$$\Gamma = Dq^2 \quad ,$$

with D the thermal diffusivity, which in the hydrodynamic limit $q \to 0$, is given by

$$D_0 = \frac{\Lambda}{\rho C_p} \quad ,$$

with Λ the thermal conductivity, ρ the density, and C_p the heat capacity at constant pressure. The thermal conductivity diverges approximately like ξ and C_p diverges with exponent γ. The result is that as the critical point is approached, D_0 goes to zero about like ξ^{-1}. For finite q, Γ and D approach finite limits with a strong q dependence. One of the principle results of dynamic scaling is the prediction that

$$\lim_{t \to 0} D_t = q^{(1+x_\eta)} \quad ,$$

where x_η is the correlation range exponent of the viscosity divergence.

2.3 The Need for Low Gravity

The techniques of temperature control in the laboratory are sufficiently advanced that it is possible to begin penetrating deeply into the critical region. However, once there it is impossible to obtain the desired result of measuring critical anomalies. The problem is gravity.

The compressibility of a fluid system diverges at the critical point: $\kappa_T \sim t^{-\gamma}$. The compressibility expresses the response of the fluid's density to pressure on the fluid. Across any fluid container, there is of course a pressure differential caused by the weight of the fluid itself: $\Delta P = \rho g h$. In normal circumstances, when a fluid is nearly incompressible, this is barely noticeable; near the critical point, the effects of the pressure differential are greatly magnified by diverging compressibility.

Under the influence of its weight, the fluid develops a density gradient; that is, fluid at the bottom of a container is more dense than fluid at the top. As the critical point is approached, the density gradient increases. What happens is that the fluid density at the extremes of the container deviates more from the critical density, and the regions of deviation grow toward each other. The net result is that only a thin layer of fluid near the center of the container is close enough to the critical density to show critical behavior; as t is reduced, the thickness of the layer decreases. This is a severe limitation for measurements on macroscopic samples.

In a light scattering experiment the laser beam used to probe the sample can only be usefully focused to a diameter of about 100 μm. When the thickness of the layer of critical fluid drops approaches this size, the light is no longer sampling a homogeneous critical system. In effect, the density gradients limit the useful range of t which can be explored. This is shown in figure 1, which gives the acceleration dependence of the limiting temperature at which the density of xenon varies by more than 1% over a 100 μm distance. At 1 g the critical point may be approached to within 14.5 mK, while at 10^{-3} g the limit is 145 μK.

This result is disappointing. At $t = 5 \times 10^{-5}$, the asymptotic region for these fluctuation wavelengths is just being reached. The decay rate for any finite wavevector will saturate at a finite, lowest value as the critical point is approached. This is shown in figure 2 for the wavevectors corresponding to the 12° and 168° scattering angles planned for Zeno. At the 1 g limit, the small angle decay rates have not yet really begun to saturate. By going to at least the 10^{-3} g limit the asymptotic behavior at both angles will be reached. This then sets the minimal requirement for reduced gravity for critical fluid light scattering. The Zeno instrument flown on the Shuttle provides a solution to this problem.

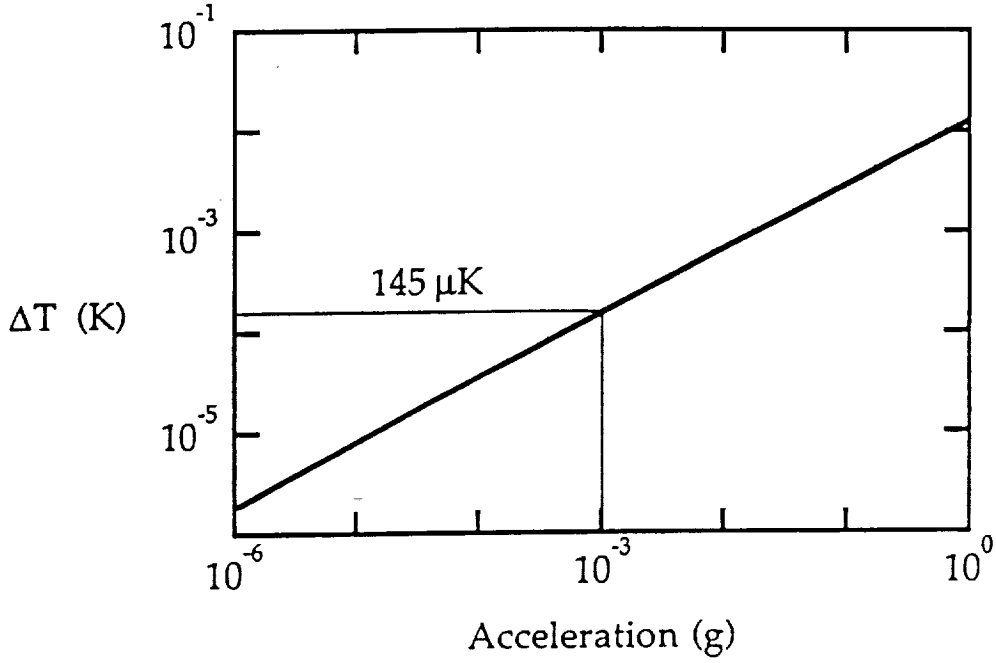

Figure 1. ΔT limit set by acceleration for 100 μm height and 1% precision.

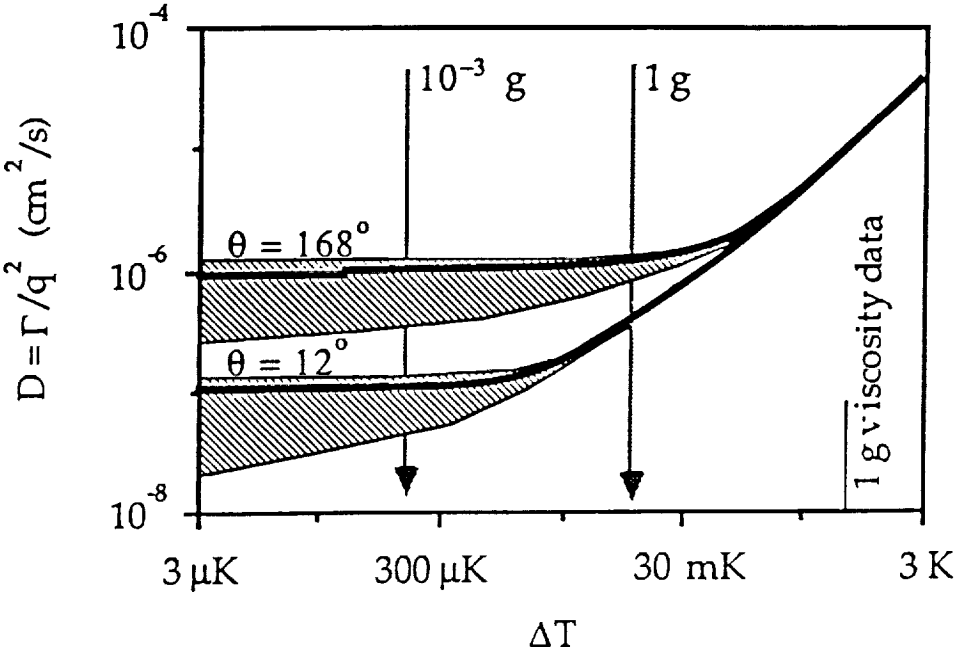

Figure 2. Calculated Xenon Diffusivity

2.4 Previous Work

Progress in understanding critical phenomena has been substantial in the past decade since the methods of the renormalization group theory, first developed to solve problems in high-energy physics, have been applied to calculating the critical exponents of static divergent quantities. This theoretical work has given a computational base to the ideas of universality classes and two-scale universality, as well as accurate estimates of many critical exponents (Sengers, 1982).

In contrast, the theory of critical fluctuation dynamics and transport phenomena, although actively pursued, leaves many questions unanswered. The questions are both theoretical, because the calculations have proved difficult to perform; and experimental, because of limitations imposed by gravity as well as experimental problems with multiple scattering in light scattering experiments.

The general state of experiment and comparison with current theory has been left at about the state of the experiments by Swinney and Henry (Swinney and Henry, 1973). Figure 3 is taken from their paper and shows the level of agreement. The quantity Γ^* is

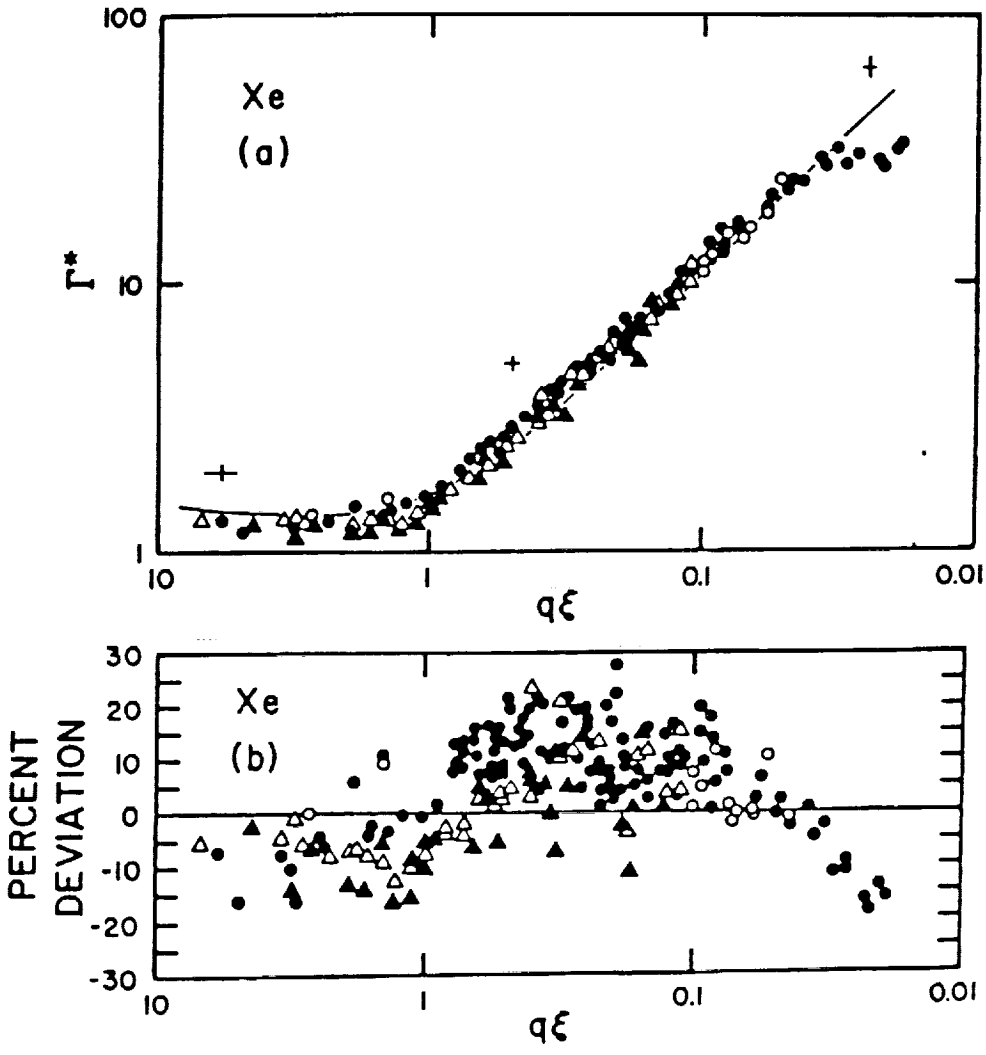

Figure 3. Reduced decay rate vs. scaled wavevector (from Swinney and Henry, 1973).

a scaled decay rate from which viscosity and angular dependence has been divided out, plotted as a function of scattering wavevectors scaled by the correlation length: $x = q\xi$. The range in x of 0.01 to 8.0 corresponds to a temperature range of 5.8 K to 3 mK from the critical temperature. The most recent and only other work on xenon was by Güttinger and Cannell (Güttinger and Cannell, 1980). They covered the same range in x with fitting errors of $\pm 5\%$ using more accurate values for ξ.

Other efforts have included work to account for multiple scattering (Bray and Chang, 1975; Reith and Swinney, 1975; Sorenson *et al.*, 1977; Beysens and Zalczer, 1977), or to avoid it altogether (Chang, Burstyn and Sengers, 1979). Particularly notable is the work by Burstyn and Sengers (1982) on the index-matched, weakly scattering binary liquid mixture 3-methylpentane-nitroethane. Excellent, precise results to 0.3 mK from its critical temperature were obtained. No significantly improved light scattering studies of the fluctuation decay rates for single component fluids have been possible.

2.5 Xenon: A Simple Fluid

Theory presumes that the liquid-gas critical point of simple fluids and the component-separation critical point of binary liquid mixtures belong to the same universality class; more specifically, that they belong to the same *static* universality class. Hence, they should exhibit the same critical behavior, at least for the static properties.

As an example of a simple fluid, xenon is without competition. The molecule is monatomic, spherically symmetric, and has no dipole moment; one expects the inter-atomic forces to be as simple as possible. While this would be the case for any of the noble gases, xenon wins as a choice for experimental use because it has a convenient critical temperature (16 °C), and many of its properties have been studied extensively. Nevertheless, if density-matched binary fluids, with their greater insensitivity to gravity, could apparently provide the same results on earth as a space experiment on xenon, why use xenon?

Studying critical point dynamics at a simple fluid, liquid-vapor critical point can yield better critical point measurements than in any mixture. We present the following reasons.

1. A simple fluid can be more accurately loaded to its critical density than can a mixture to its critical concentration.

2. A simple fluid reaches equilibrium more quickly after crossing the phase boundary since no time is taken for molecular diffusion to readjust the concentration profile.

3. Simple fluid systems have smaller viscosity and correlation ranges so that the order parameter relaxation time, ξ^2 / D (D is the thermal diffusivity), is 100 times shorter than for the most favorable density-matched mixtures. This allows the measuring of viscosity one decade close to the critical temperature than for any mixture.

4. The viscosity background is smaller in the pure fluid while the amplitude of the critical part of the viscosity is about the same, making it easier to analyze the critical part.

5. A simple fluid is less susceptible to a drifting critical temperature.

6. A simple fluid has no diffusion controlled, surface wetting, sample segregation processes.

7. The order parameter in a simple fluid is identified with greater ease and certainty.

8. Additional thermodynamic measurements necessary for analyzing the dynamics into background and critical contributions exist in sufficient detail only for pure fluids.

9. Only by studying both systems can one experimentally answer the question: Do both of these fluid systems belong to the same *dynamical* universality class?

As mentioned previously, for static properties, universality classes of critical points are characterized completely by the spatial dimension of the system under study and the symmetry of its order parameter; all other properties of the system are assumed to be irrelevant. However, for dynamical properties, the static universality classes must be subdivided according to whether the order parameter is conserved in the system's dynamics. Conservation laws for other hydrodynamic variables may further subdivide universality classes (Hohenberg, 1977; Bhattacharjee and Ferrell, 1983). In contrast to pure fluids, binary liquid mixtures contain an extra hydrodynamic variable which is conserved. This is thought to be irrelevant asymptotically close to the critical temperature, although it can be relevant in the temperature range experimentally accessible on earth.

The complications that can occur when an extra degree of freedom is introduced are illustrated by the recent measurements of transport properties by Meyer and co-workers (Cohen, 1982; Cohen, 1983) near the critical point of mixtures of ^{3}He and ^{4}He. Meyer did not observe distinct composition and density fluctuations. He did observe the thermal conductivity and thermo-diffusion ratio diverging as ξ and ξ^2 respectively. To interpret Meyer's data, it was necessary to introduce the concept of the "degree of azeotropy" and to argue that the asymptotic behavior of transport properties would only become evident at reduced temperatures smaller than 10^{-5}.

Since the very careful work by Swinney and Henry and the refinement by Güttinger and Cannell on xenon, it has been clear that to apply the theories which attempt to calculate the modification of dynamic properties due to divergent fluctuations in a critical system, one needs to know the "bare" properties (without the effects of critical fluctuations) in particular of the thermal conductivity, heat capacity at constant volume, and pressure coefficient on the isochore. Then, accurate measurements of the correlation range, viscosity, and fluctuation decay rates for several wavevectors can be used to explore solutions of the coupled equations for the critical enhancements of the fluctuation lifetimes and the viscosity. Most systems do not have a large enough data base of critically evaluated properties to allow crucial comparisons. As Swinney discussed, for those systems with enough of the properties known (CO_2, SF_6, and Xe), the crucial uncertainties entering the comparison with theoretical forms are from the correlation range and the viscosity. Except for the correlation range, we still depend on the properties gathered and evaluated by Swinney and Henry in 1973.

Meanwhile, the theoretical developments of the renormalization group calculations and universality have established the static critical exponents reliably. This requires that the old data be refitted to modern forms and exponents. But, when one is finished, the fact remains that we are still extrapolating old measurements well beyond their range to provide a "test" of the new and accurate decay rate measurements. New measurements taken closer to the critical point are needed for anyone who wishes to evaluate current theoretical ideas.

2.6 Experiment and Theory at their Limit

The current theoretical treatments of dynamic critical fluctuations can be reduced to the form from generalized hydrodynamics which shows that the wavevector dependent, fluctuation corrections to the viscosity and fluctuation decay rate are coupled in a pair of integral equations over particular functions of the static structure factor (Kawasaki, 1976). Various iterative approximations to these equations have lead to several estimates for the viscosity anomaly and decay rates which differ depending on where the iteration is stopped. Bhattacharjee and Ferrell (1983) have clarified the calculation of the critical viscosity exponent, Bhattacharjee, Ferrell, Basu and Sengers (1981) showed how to treat the cross-over region of viscosity data, and Burstyn, Sengers, Bhattacharjee and Ferrell (1983) applied the calculations of the dynamic scaling function to classical fluids. Of particular interest is the prediction (Bhattacharjee and Ferrell, 1983) for the dynamic scaling exponent, i.e. the exponent, as ξ diverges, for the wavevector dependence of the decay rate, which has only been tested on binary liquid mixtures. The results for the decay rates differ from earlier estimates when the scaled wavevector becomes greater than 10. The experiment described in this document should reach scaled wavevectors of 1000.

The form suggested by Ferrell (Burstyn, 1983) for the critical part of the diffusivity is

$$D_c = \frac{\Gamma_c}{q^2} = \mathrm{R}\,\frac{kT}{6\pi\eta\xi}\,\Omega(x)\,(1 + b^2x^2)^{x_\eta/2} \quad ,$$

where R is the amplitude factor, η the shear viscosity, ξ the correlation range, $x = q\xi$ the scaled wavevector, $\Omega(x) = \mathrm{K}(x)/x^2$ with $\mathrm{K}(x)$ the Kawasaki function, b the amplitude of the dynamical correction, and x_η the exponent of the correlation range in the viscosity.

The real tension between theory and experiment at present is over the viscosity exponent x_η. Siggia *et al.* (1976) suggested that $x_\eta = 0.065$ and that the amplitude, R, of the Stokes-Einstein-Kawasaki form of the decay rate was 1.20 rather than 1.00. Experiments have been rather convincing that the amplitude is 1.00, but they are not independent of the method used to estimate the correct extrapolation of the viscosity into the temperature range of the light scattering measurements. Measurements of the viscosity seem to show that the binary mixtures are best described by $x_\eta = 0.065$ (Burstyn *et al.*, 1983), but recent fitting of the available data for liquid-vapor critical systems favors the value $x_\eta = 0.054$. This is in agreement with the suggestion of Ferrell that the Siggia calculation had missed a cancellation of corrections and that the exponent is nearer the original estimate (Bhatacharjee and Ferrell, 1983).

Because the viscosity exponent is not established, the predicted values of the decay rates close to the critical temperature are very uncertain. Figure 4 shows the scaled decay rate calculated with two fits to the Strumpf xenon viscosity data (using the exponents 0.065 and 0.054) extrapolated into the temperature range of the space experiment which we are discussing. The difference grows to 10% and illustrates why we must measure the decay rates in this region. They simply cannot be calculated with the limited viscosity data available: even with improvements to viscosity data from a low-gravity experiment, they would still need to be extrapolated into the temperatures reached in this scattering experiment. We do not know whether the equations used for binary mixtures (Burstyn and Sengers, 1982; Kopelman, 1983) will work for a liquid-vapor system. The only way to determine this is to have measurements close to the critical point *without the distortions in the density of the sample induced by gravity*.

We see this experiment as a means to probe the fundamental dynamics of a critical system, specifically that of a simple fluid, by accurately measuring the critical fluctuation

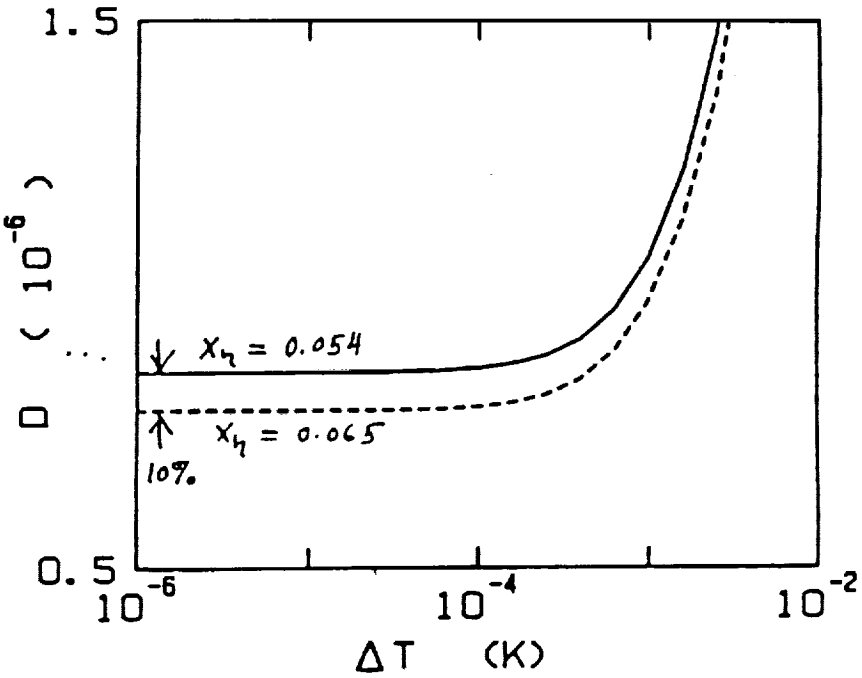

Figure 4. Calculated diffusivity of xenon at a scattering angle of 12°.

decay rates closer to the critical point than is possible in any earth-bound experiment. We expect to measure the actual limiting decay rates at finite wavevector and determine their wavevector dependence. In addition, we will measure the correlation length of the fluctuations. As discussed above, it is not possible at present to calculate the decay rates to the accuracy with which they can be measured in this experiment. Thus, it is a worthy goal to make such a set of measurements on a carefully chosen, simple fluid system like xenon. This *data set* will have a lasting value as a testing ground for any ideas about transport properties and dynamics in thermodynamic systems with large fluctuations.

3 Zeno Science Requirements

The list of science requirements distills the experiment into its barest essentials, to provide a foundation on which to build engineering requirements. The list derives from two principle considerations.

First, there are two major measurement goals of the experiment, namely decay rates and correlations lengths of critical fluctuations. Further, the decay rate measurements are to be performed at two angles to fix their dependence on the scattering wavevector. The associated science requirements specify the conditions that must be met to accomplish the precision and range of the measurements that will lead to a satisfactory data set.

1. Determine the decay rates of critical fluctuations in xenon.

    1.1. Measure to $\pm 1\%$ from correlation functions.

    1.2. Measure at two angles, θ and $\pi - \theta$ ($\theta \cong 12°$), with angles known to $\pm 0.03°$.

1.3. Maintain the multiple scattering below 1% of the scattered intensity.

1.4. Measure over a temperature range of 1 K to 100 μK from the critical point, with at least two values per decade.

2. Determine the correlation length of critical fluctuations in xenon.

2.1. Measure to $\pm 3\%$ from transmission and intensity data.

2.2. Measure time-averaged transmission continuously, to $\pm 0.1\%$.

2.3. Measure the scattered intensity continuously, to $\pm 0.1\%$.

2.4. Measure over a temperature range of 1 K to 100 μK from the critical point, with at least two values per decade.

3. Establish the thermodynamic trajectory towards the critical point of xenon.

3.1. Measure and control the temperature of the sample to ± 3 μK for periods of at least 3 hours.

3.2. Locate the critical temperature of the sample to ± 20 μK.

3.3. Establish the absolute temperature of the critical point to ± 10 mK.

3.4. Load the sample cell to within $\pm 0.1\%$ of the critical density of pure xenon.

3.5. Allow no temperature gradients across the sample larger than 1 μK/cm.

3.6. Limit residual and vibrational accelerations to $\leq 10^{-3}$ g.

3.7. Limit radiation heating of the sample to < 1 μW.

4 The Zeno Experiment

The instrument which performs the experiment divides easily into two subsystems. The optics subsystem includes the xenon sample under study, the means to maintain its thermodynamic state, the light source to probe its fluctuations, and the optical, thermal, and mechanical transducers which monitor its environment and collect the results of the interaction between light and critical fluid. The electronics subsystem oversees the control of the sample's environment, collects information from the transducers, and processes, reports, and stores the information. The operating of the subsystems are coordinated by the control software which manipulates the components of the optics subsystem, supervises the components of the electronics subsystem, and directs the experiment so that it can meet its science goals within the mission timeline.

4.1 Optics

4.1.1 Sample Cell

The xenon sample cell, shown schematically in figure 5, contains the sample at its critical temperature of 289 K and critical pressure of 58 atmospheres, while providing optical access for the light scattering measurements. The primary design constraint, to meet the science requirement of less than 1% multiple scattering, is that the laser beam have a 100 μm path length through the fluid, accomplished simply by having the windows of the sample cell separated by this amount. However, this would create such a small total volume of sample that meeting the science requirement that the cell be loaded

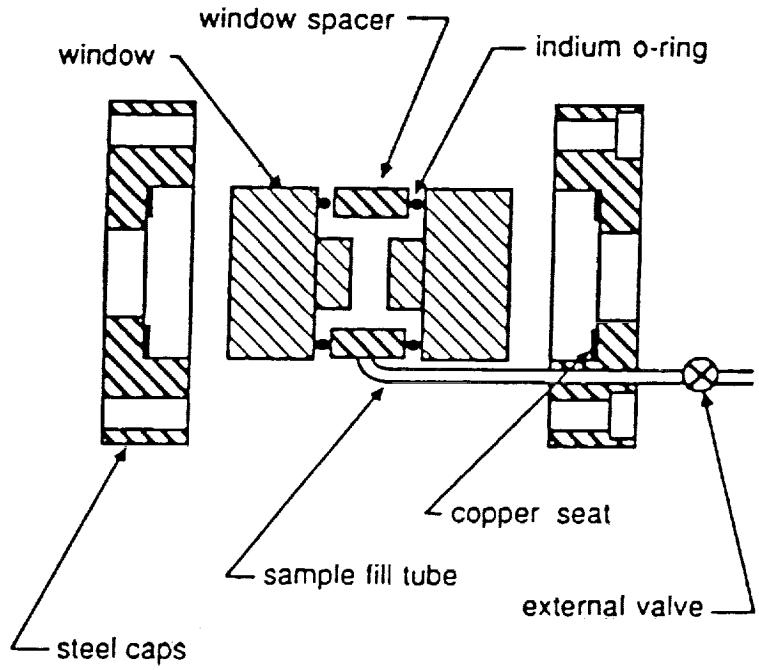

Figure 5. Xenon sample cell with 100 μm optical path length.

to within 0.1% of the critical density would be difficult. Thus, the 100 μm sample space is surrounded by a reservoir of xenon sample, but the reservoir must be designed carefully. If its volume is too large, the heat capacity of the xenon would begin to slow the response of the thermostat. If its surface to volume ratio is too small, the divergent thermal conductivity of xenon at its critical point would lead to unacceptably long thermal relaxation times.

4.1.2 Thermostat

The only parameter controlling the thermodynamic state of the xenon sample is temperature; this is the responsibility of the thermostat. To achieve the goals of the experiment, the requirements that it must satisfy are severe: controlling and measuring the temperature of the sample to $\pm$ 3 μK (near a temperature of 298 K), and preventing temperature gradients across the sample larger than 1 μK/cm. Furthermore, for its trip into space, the thermostat must be small, lightweight, and able to change temperature quickly to meet accommodation and mission time restrictions.

The thermostat shown schematically in cross section in figure 6 satisfies these goals, assuming an ambient environment stable only to $\pm$ 1 K. It is constructed of four co-axial cylindrical shells (numbered 1 through 4, innermost to outermost), with the sample cell contained within shell 1. The thermal coupling between shells is radiant, with 15 minute time constants. Optical access to the interior is provided by windows mounted on the ends of each shell. The overall size is 16 cm by 7 cm diameter, and the mass is less than 1.5 kg.

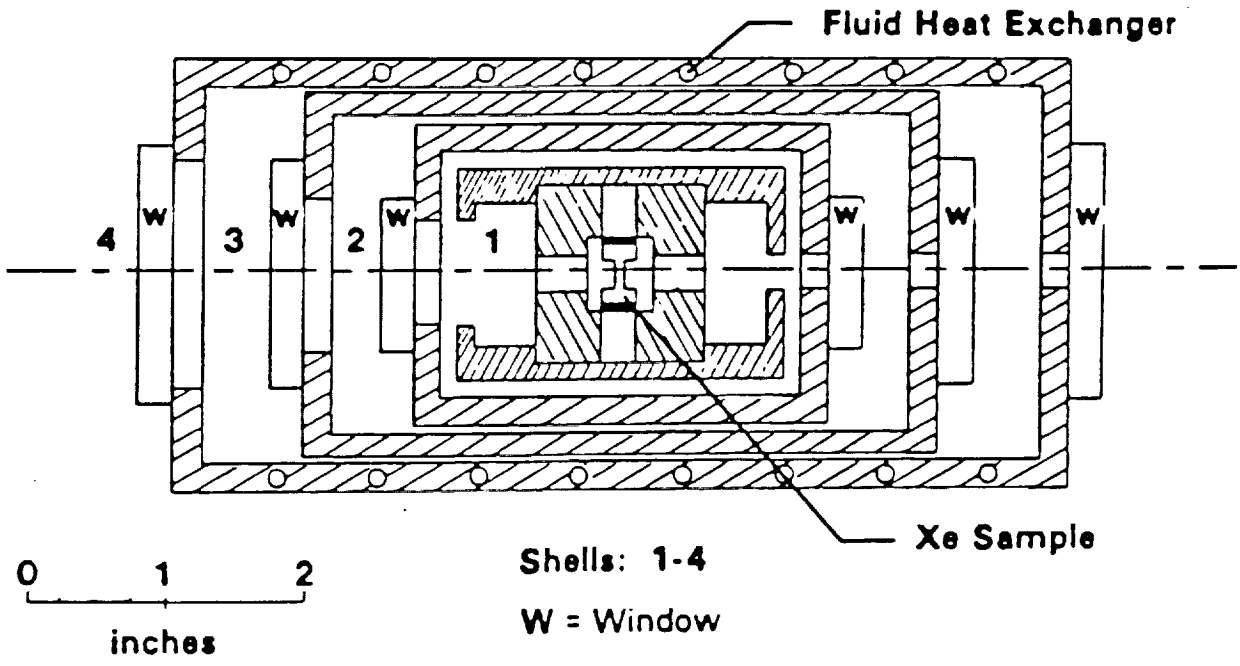

Figure 6. Thermostat

Mounted on shell 1 is a platinum resistance thermometer, used for absolute temperature calibrations; in operation, temperature sensing is done with thermistors. Each shell has at least one thermistor mounted on its surface to monitor temperature. On each of the outer three shells, the thermistor is part of a feedback circuit, which includes surface-mounted heaters on the shell, to control the temperature of the shell. Proceeding inward, each shell reduces temperature gradients by a factor of 100.

4.1.3 Optical Paths

A schematic layout of the optical configuration is shown in figure 7. The layout satisfies the science requirements for measuring fluctuation decay rates at two scattering angles and the correlation length of the fluctuations.

The beam from the low-power (5 mW) Helium-Neon laser can take one of two paths through the xenon sample; the path is chosen by the shutters, only one of which is open at a time. In the forward scattering configuration (top of figure 7), part of the beam is deflected into a photodiode to provide a reference for turbidity measurement. The remainder, focused by a lens, passes through the thermostated sample. The light which is scattered by fluctuations in the sample into a small solid angle (defined by the pinholes) at angle θ is collected for decay rate analysis by the photomultiplier tube. That light which survives its trip through the sample unscattered is directed to a second photodiode.

In the backscattering configuration (bottom of figure 7), the beam follows in reverse the path of the forward scattering beam. Again, part of the beam is deflected into a photodiode for turbidity reference. The remainder is focused and passes through the sample. That which makes it through unscattered is collected by another photodiode. The light scattered by the fluctuations in the sample is still collected by the photomultiplier tube, but the scattering angle is now $\pi - \theta$, the supplement of the forward scattering angle.

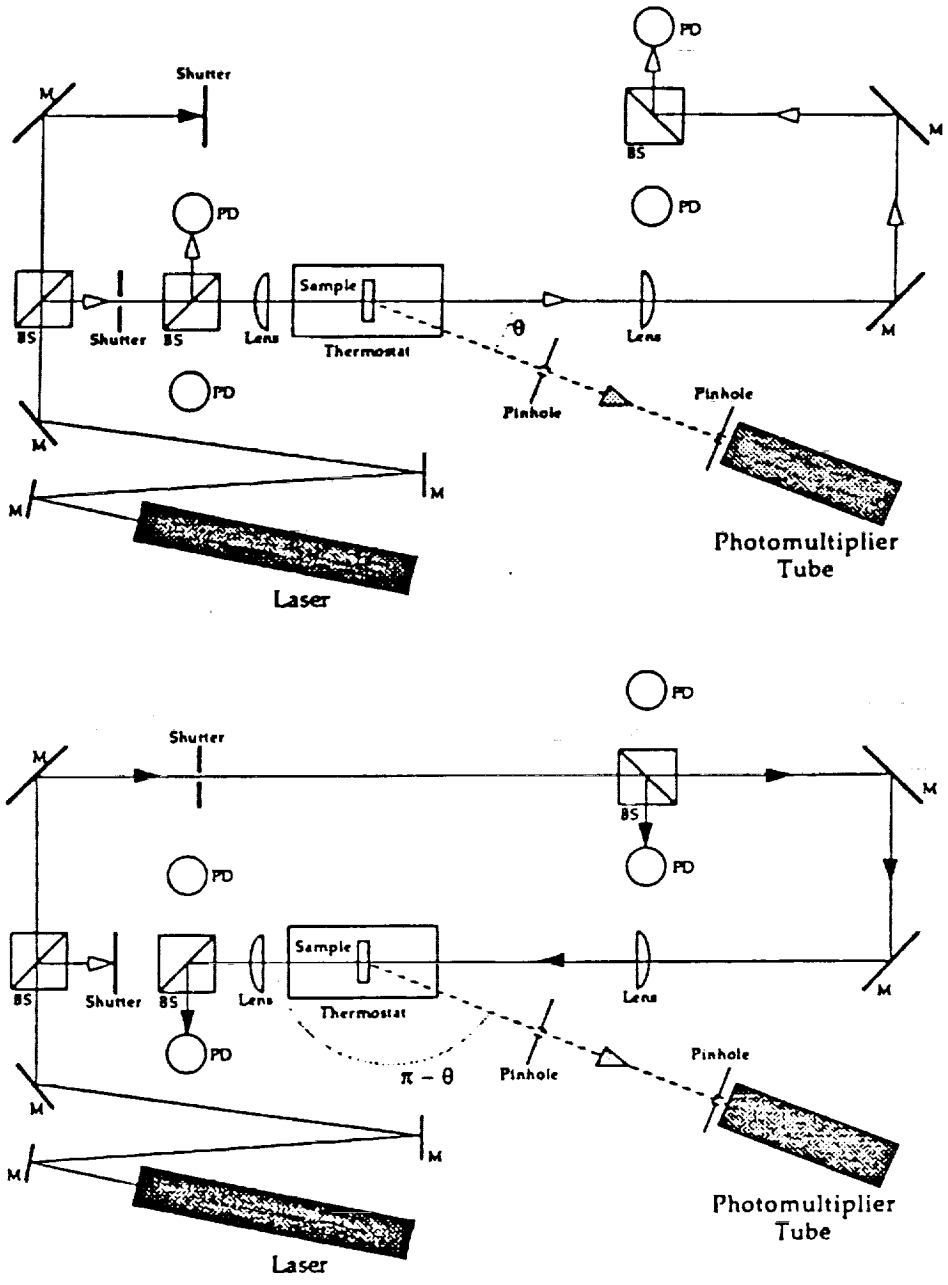

Figure 7. Optical layouts: forward scattering (top) and backscattering (bottom)

4.1.4 Mechanical Environment

The degree to which the experiment achieves its scientific goals increases in proportion to the degree to which it is isolated from vibrations on the STS. Thus the table on which the optics are mounted, beyond providing a stable surface to prevent distortion of the optical paths, is a component of a vibration isolation system to protect the optics subsystem.

Adjunct to the isolation system is the means for real-time monitoring of disturbances passes to the table from the STS. A high dynamic-range triaxial accelerometer is mounted on the surface of the optical table to inform the operating software of vibrational disturbances, also providing information on the size and duration of the disturbance.

4.2 Electronics

The electronics which support the experiment provide five basic functions: thermometry and temperature control, processing of the light scattering signal, processing of the turbidity signal, processing of the accelerometer signal, and opening and closing the shutters which set the scattering configuration. These operations are under the control of a microcomputer which coordinates them and effectively runs the experiment. The system is shown in figure 8.

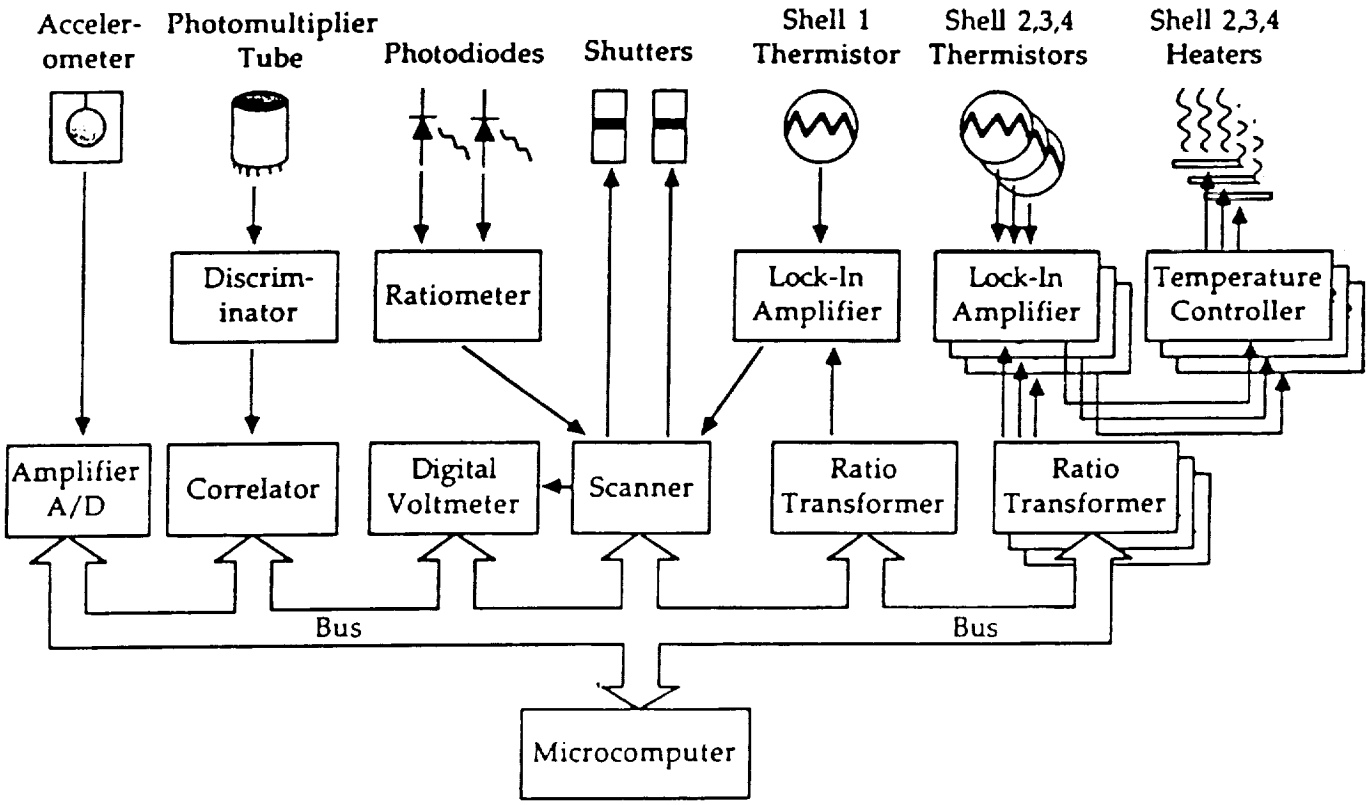

Figure 8. Control and Data Acquisition System

4.2.1 Temperature Measurement and Control

Thermometry is done using AC bridge circuitry, where one of the bridge is formed by a thermistor and reference resistor (located on each of the thermostat shells), and the other arm is provided by a ratio transformer. The bridge is nulled (i.e. temperature is measured) by changing the tap position in the ratio transformer; null detection is accomplished with a phase sensitive, lock-in amplifier. Using AC signals to excite the bridge with lock-in signal recovery is necessary to achieve the temperature resolution required by the experiment. The output of the lock-in amplifier is a DC voltage representing the amount by which the bridge is out of balance. In the case of the shell 1 thermometer, this error signal represents the temperature of the sample. in the case of the outer shells (2, 3, and 4) the error signal is processed by the temperature controller, which drives heaters mounted on the shells to maintain their temperature, which is set by the ratio transformers. The ratio transformers are in turn set by the microcomputer, in this way determining the temperature profile across the thermostat and monitoring the temperature of the sample via the shell 1 thermometer.

4.2.2 Transducer Signals

The light scattering signal is collected on the optical table by a high-gain, high quantum efficiency photomultiplier tube. The output of the tube is converted by the preamplifier/discriminator into a high-frequency (order MHz) stream of TTL pulses, with the pulse count rate proportional to the intensity of the scattered light. The programmable correlator calculates in real-time the autocorrelation function of the pulse stream as well as the average intensity, then makes the results available to the microcomputer after a pre-determined time. From these data the microcomputer calculates decay rates of the fluctuations, and some of the correlation length information.

In each of the two light path configurations, there is a pair of photodiodes which produce the raw signals for the turbidity measurements. In each case, one photodiode produces a current proportional to the intensity of the test beam to use as an amplitude reference, and a second photodiode produces a current proportional to the intensity of the light transmitted by the sample. The output of the ratiometer circuit is the logarithm of the ratio of transmitted to reference current, which is proportional to the turbidity of the sample. This signal is averaged by a digital voltmeter and passed to the microcomputer.

The signal from the accelerometer mounted on the optical table is processed by its amplifier, and the results passed to the microcomputer when safe levels of acceleration, determined by the current operating temperature of the experiment, are exceeded. With information about the level and duration of the detected disturbances, the control software can choose the proper strategy for accumulating data during the disturbance that takes best advantage of the limited mission time.

4.3 Timeline and Control Software

The software which controls the experiment is responsible for the operation of the electronics, and for coordinating them in the most efficient way to accomplish the science goals. Figure 9 shows a hierarchy of functions to be performed by the control software. Coordination of experimental activity is the primary responsibility of the experiment scheduling program, which decides the optimal approach to data taking, subject to programmmed information from the planned mission schedule and real-time information

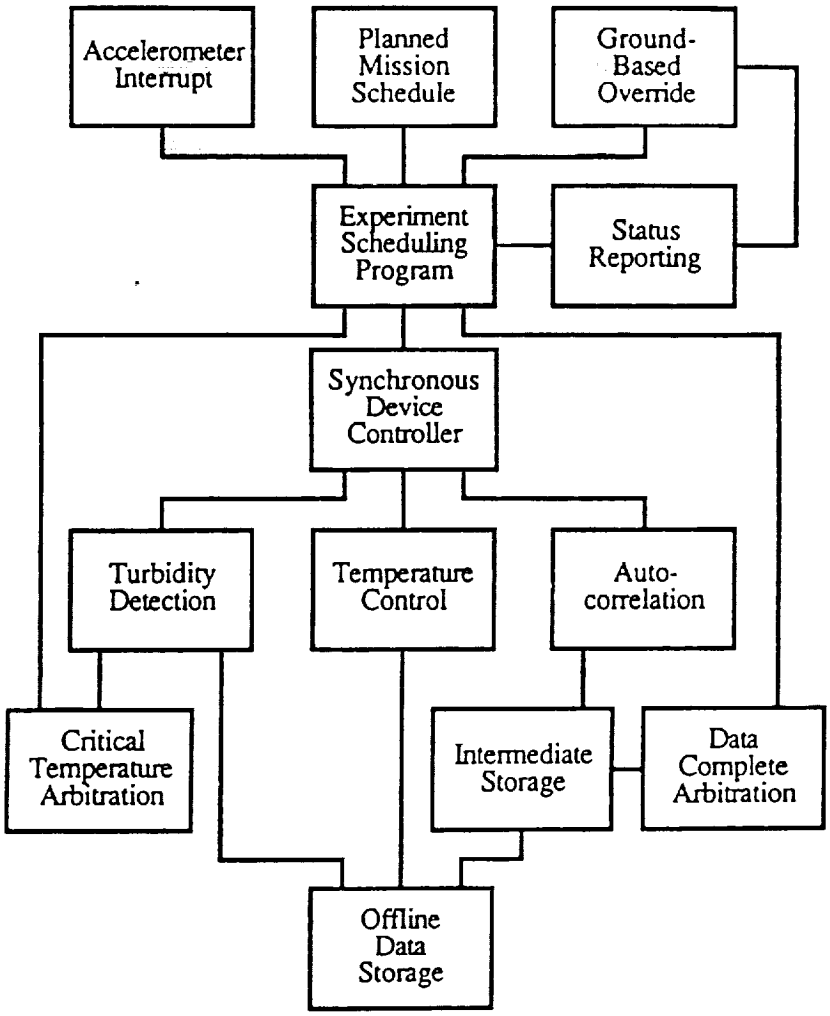

Figure 9. Experiment Control Hierarchy

from the accelerometers located on the optics table. This schedule is passed to the synchronous device controller which is responsible for overseeing the actual operation of the electronics, as well as handling data storage. Some results of the lower lever operations are made known to the scheduling program to inform it of progress. With this feedback the scheduler is able to report both its decisions and the progress of the experiment based on those decisions to a ground-based monitor which can override its decision process.

The time line for the experiment breaks down into four parts:

1. Turn-on, initialize, and establish stating conditions.
2. Locate the critical temperature of the sample.
3. Measure decay rates and turbidity at temperature sequence.
4. Verify the critical temperature of the sample.

The turn-on of the instrument proceeds automatically after being actuated by the STS crew. The xenon sample must be put at a known, equilibrium state at a determined temperature, in order that it be homogeneously mixed and ready for operations. Given intershell time constants in the thermostat of 15 minutes, and an overall time constant of 45 minutes, reaching the initial temperature would take several hours. To allow the sample to equilibrate thoroughly, we allow 6 hours for the initialization procedure.

Locating the critical temperature of the sample is done by first cooling the sample quickly to a temperature near the critical temperature (typically within 100 μK); distance from the critical temperature can be inferred from the turbidity of the xenon sample. Once near the critical point, the thermostat alternately cools and warms the sample, looking for hysterisis in the turbidity signal which marks the beginning of the irreversible spinodal decomposition of the fluid which marks the critical point. The final steps in the cooling and warming are made at the temperature resolution of the thermostat, establishing the critical temperature of the sample to 100 μK. At present, the most length searches performed in the laboratory take from 4 to 6 hours; for the mission, we allow 8 hours as an upper bound and expect the actual time needed to be shorter.

The turbidity and fluctuation decay rates of the xenon sample are to be measured throughout the temperature range of 1 K to 100 μK from its critical point. Depending on the severity of the vibration environment encountered by the experiment, this range could be extended from 1 K to 3 μK. We plan to take measurements at a sequence of temperatures of two per decade, at temperature differences of 1 K, 0.3 K, 0.1 K,..., 3×10^{-5}K, 10^{-6}K, 3×10^{-6}K. The last points will be more difficult than the first and may require extra attention. Thus, the sequence will have about 12 temperature points as a minimum set. At each temperature a sequence of forward ($\theta = 12°$) and backward ($\theta = 168°$) scattering fluctuation decay rates will be taken automatically by the correlator and analyzed, alternating between forward and backscattering configurations. Fitted correlation functions give the experimentally determined decay rate. These are compared as they accumulate; when the prescribed statistical accuracy is achieved, that determination is considered complete and the microcomputer moves the experiment on to the remaining temperatures.

Each correlation takes about 15 minutes for reasonable statistics and 10 points at each angle should reduce the statistical uncertainty of the decay rates to the required accuracy of 1%. The switch between forward and backscattering configurations is accomplished by the shutters on the optical table in less than 1 second. During the time that correlation functions are accumulating (in either configuration), the turbidity of the sample is logged continuously at the rate of approximately 1 sample/second. Thus the time for accumulating the correlation functions sets the time scale of the experiment at 6 hours per temperature point or a total of 78 hours.

If more time is available to the experiment during this phase, then the control program would concentrate on obtaining additional information in the temperature range from 3 mK to 3 μK from the critical point, the range in which earthbound measurements are impossible. Note that, for the self-consistency and integrity of the data set for post-flight analysis, we do take time to measure the turbidity and decay rates rather far from the critical temperature.

Finally, to check for possible (but unexpected) drifts in the thermometry, the experiment will verify its earlier determination of the critical temperature. We expect again that this will take no longer than 8 hours.

Thus, the total time line is made up of 6 hours to establish initial operating conditions, 8 hours for locating the critical temperature of the xenon sample, 78 hours for

completing the turbidity and decay rate data set, and a final 6 hours for verifying the critical temperature, for a total mission time of 100 hours. We expect that some of the start-up time and time for locating the critical temperature can be eliminated. If more time is available for data taking, the measurements can be made in a smaller temperature sequence concentrating on the smaller temperature differences.

5 Acknowledgements

This project is currently funded under NASA grant NAG3-727 through NASA/Lewis Research Center. The Lewis project manager is Dr. R. Lauver. The project has been named Zeno after the Greek philosopher famous for his paradoxes about limits.

The principal investigator wishes to acknowledge his many collaborators in this project. The principal scientist for the the project is Dr. J. Shaumeyer, who has made major contributions to all phases of the work and particularly to the automation of the present laboratory prototype of the experiment. The NASA project scientist is R. A. Wilkinson. University of Maryland graduate students M. Briggs and H. Boukari have each taken on portions of the lab work. Many of the design ideas have been developed and refined with the help of our design subcontractor Ball Aerospace Systems Division, with the team under project manager Dr. R. Reinker.

6 References

Beysens, D. and G. Zalczer (1977), Phys. Rev. **A15**, 765.

Bhattacharjee, J. K., R. A. Ferrell, R. S. Basu, and J. V. Sengers (1981), Phys. Rev. **A24**, 1469.

Bhattacharjee, J. K., and R. A. Ferrell (1983), Phys. Rev. **A28**, 2363.

Bray, A. J. and R. F. Chang (1975), Phys. Rev. **A12**, 2594.

Burstyn, H. C., J. V. Sengers, J. K. Bhattacharjee, and R. A. Ferrell (1983), Phys. Rev. **A28**, 1567.

Burstyn, H. C. and J. V. Sengers (1982), Phys. Rev. **A25**, 448.

Chang, R. F., H. Burstyn and J. V. Sengers (1979), Phys. Rev. **A19**, 866.

Cohen, L. H., M. L. Dingus and H. Meyer (1982), J. Low Temp. Phys. **A49**, 545.

Cohen, L. H., M. L. Dingus and H. Meyer (1983), Phys. Rev. Lett. **50**, 1058.

Güttinger, H. and D. S. Cannell (1980), Phys. Rev. **A22**, 285.

Kawasaki, K. (1976), in *Phase Transitions and Critical Phenomena* ed. C. Domb and M. S. Green (Academic, New York, 1976), Vol. 5A, p. 165.

Kopelman, R. B. (1983), Ph. D. thesis, University of Maryland, "Light Scattering Measurements of Critical Fluctuations in an Optically Thin Binary Liquid Sample".

Reith, L. A. and H. L. Swinney (1975), Phys. Rev. **A12**, 1094.

Sengers, J. V. (1982), from *Phase Transitions: Cargese 1980*, ed. Maurice Levy, Jean-Claude Le Guillou, and Jean Zinn-Justin (New York: Plenum Publishing Corporation).

Siggia, E. D., B. I. Halperin and P. C. Hohenberg (1976), Phys. Rev. **B13**, 2110.

Sorenson, C. M., R. C. Mockler and W. J. O'Sullivan (1977), Phys. Rev. **A16**, 365.

Swinney, H. L. and D. L. Henry (1973), Phys. Rev. **A8**, 2586.

MINIATURE INSTRUMENTATION FOR LASER LIGHT SCATTERING EXPERIMENTS

Robert G.W. Brown
Royal Signals and Radar Establishment
Malvern, Worchestershire, United Kingdom

Traditional optical systems for photon correlation spectroscopy and laser anemometry have relied upon physically large and fairly expensive lasers, "bulk-optics" such as lenses of a few inches diameter, large mechanical mounts and carefully selected, fragile and bulky photon-counting photomultiplier detectors. In some cases experimental fluid dynamics at a desired position in a flow, perhaps deep inside complex machinery, is physically impossible or very difficult. Similar problems exist with photon correlation spectroscopy, eg., remote and heterodyne experiments. We have investigated and characterized various optical and electro-optical components with the aim of replacing existing photon correlation laser spectroscopy and anemometry techniques in miniaturized form, and with significant cost reduction.

Very recently we have constructed a range of miniature, modular light scattering systems from little solid-state optical and electro-optical components, and experimentally verified measurement performance comparable to (and in some cases better than) standard laboratory photon correlation spectroscopy and laser anemometry equipment.

Introduction

Throughout the development of photon correlation techniques [1,2] the experimental equipment has been of a considerable size and expense, often occupying a volume of approx a cubic metre and at a cost of approx $20,000 - $100,000. These values have limited more widespread application of photon correlation procedures eg, to industrial applications such as process control.

Recent commercially available electronics includes photon correlators and structurators constructed on a single circuit board together with microprocessor or desk-top computer control and data processing.

Also, recently, photon correlators useful for study of low velocities and large macromolecules have been constructed at greatly reduced costs, eg, in Uncommitted Logic Array chips [3] and within small desktop microcomputers [3,4,5], both at a cost of <= $1000. Current developments in systolic array correlators [6,7] may also impact on their size and cost.

However, it is the purpose of this paper to concentrate on recent developments in the optical and electro-optical aspects of photon correlation experiments, solid-state lasers, monomode optical fibres and solid-state detectors. These new, commercially available devices offer the potential for construction of new photon correlation systems at reduced size, cost and complexity. Opto-electronic systems occupying volumes of only a few cubic centimentres and costing $500 - $2000 in components are possible, and are described later.

New Solid-State Lasers

Traditional lasers for photon correlation experiments have been gas lasers of the HeNe or Argon-ion variety, the size of an arm or a leg and costing $2000 - $20,000. These lasers output nominally TEM_{00} cw visible light of between a few milliwatts and a few hundred milliwatts power in a single line. For photon correlation applications the chosen laser must be of sufficient power stability and lacking in spurious noise and light correlations that it does not contribute significantly to and distort the correlation function of the scattered-light process being observed [8].

Recently, we have characterized some solid-state, visible laser diodes for photon correlation applications [9]. These Sharp lasers output at 750nm to 780nm wavelength, with power levels of some milliwatts to 30+ milliwatts in a single longitudinal and transverse TEM_{00} mode whose linewidth is approx 80 MHz, i.e. having a coherence length of ~ 3.75m. They cost only a few hundred dollars and together with their simple drive circuitry can occupy a volume of just a few cubic centimetres. The other principal differences between these lasers and conventional gas lasers are twofold. First, the drive currents are typically 40 - 100 mA at approx 2 Volts and second, the output laser beam is of elliptic cross-section and requires a correction lens before use.

In our investigations, in order to prevent longitudinal mode hopping we used a simple temperature control circuit utilizing a thermistor placed

close to the laser diode and a miniature Peltier heat pump to maintain a preset temperature.

Power output stability was checked using a standard photon counting arrangement with a count rate of 400KHz, and found to be stable to within 1% over 30 minutes after a brief warm-up period.

We compared the laser diodes directly to various HeNe lasers often used for light scattering in terms of factorial moment and photon correlation performance, both parameters being of importance in a full assessment. We used a carefully selected EMI9863 photomultiplier to detect laser photons and supply the photodetection signal to a Malvern Instruments K7025, 10 nanosecond sample-time photon-correlator.

Experimental verification of the expected value of Factorial moments of a coherent laser source (unity) and departure from that value in excess of the calculated experimental error is an excellent test of the quality of the laser and its drive circuit in terms of small instabilities. We examined up to the fourth moment, finding agreement to within experimental error for sample times chosen between 10^{-6} and 10^{-2} seconds, ie, performance comparable with our often used SP120/124 gas lasers.

Correlation measurements were conducted on time-scales equal to and greater than 10 nanoseconds. The measure of degree of excess correlation was the usual after-pulsing expression, $\alpha = (g^{(2)}(\tau)-1).\ \bar{n}$, where α is the excess correlation probability, g the normalized correlation function value and $\bar{n}$ the average photon-count rate.

In 47 experiments, photon correlation functions of constant magnitude to within an excess of 0.01% - 0.02% were recorded, and up to timescales of 0.5 seconds. This is negligible, as required.

Thus we concluded that it is possible to construct simple laser diode circuitry and achieve basic photon correlation performance similar to and in some respects better than traditional gas lasers used in photon correlation experiments at a fraction of the size and cost and with significantly less fragility. Our experimental apparatus is shown in Figure 1.

New Optics

Traditional photon correlation optical systems have been large, cumbersome structures containing an array of lenses, prisms, pinholes and filters together with their mechanical adjustments. The alignment procedure is lengthy, the cost some thousands of dollars and the capability is only a single measurement point at a time.

In recent years a variety of optical fibre laser anemometry schemes have been constructed [10,11] and tested. Mostly they involve delivery of laser power to small optical heads via monomode optical fibre(s) and direction of collected scattered light to a remote detector via multimode fibre. Opto-mechanical multiplexing is available to allow construction of arrays of measurement sites. Monomode optical fibres also allow a very simple method of creating self-aligning coherently-detected LDA and spectroscopy

geometries useful for observing flows containing high concentrations of particles or solid surfaces, albeit with Doppler shifts of approx 10MHz/m/s for the measured component.

Recently we have described basic monomode optical fibre components (fibre coupled to microlenses) for photon correlation use [12], paying close attention to their design and manufacturing problems. An example monomode fibre and microlens assembly is shown in Figure 2. In design and manufacture the major problem areas are inachieving tolerances at the micron level and eliminating contamination of the fibre endfaces. Testing of the laser beam parameters produced by monomode optical-fibre components is especially easy using boiling speckle and photon correlation techniques. Special problems that must be considered in photon correlation experiments include the requirement for close similarity of the gaussian beam waist dimension in the two orthogonal transverse directions to the laser beam propagation direction. Monomode optical fibre systems will be discussed shortly.

New Solid-State Detectors

Traditional detectors for photon correlation experiments have been single photon counting photomultiplier tubes specially selected for very low noise (20 - 100 cts/sec) and afterpulsing performance (<= 0.04%) [8]. Such devices are often the size of a forearm, costing $1000 - $4000 and rather fragile. Operating quantum efficiencies of a few percent and supply voltages in excess of 1600 V are typical.

Recently we have characterized silicon avalanche photodiodes (APD) as replacements for photomultipliers used for photon correlation experments [13,14]. In particular the RCA C30921S reach-through style APD has proved useful in both passive and actively quench modes of operation. In both cases the APD is operated in reverse bias beyond breakdown to achieve photon-counting or "Geiger" operation, and cooling by mini-Peltier devices to approximately 0°C is used to reduce dark counts to acceptable levels. Whilst voltage stabilities at the millivolt level are needed and easily achieved, temperature stabilities of order 1/20°C are also required but can be fairly easily accomplished by suitable APD encapsulation and active control.

In passive quenching the APD is placed in series with a ballast resistor through which it recharges following a photodetection. Combination of the series resistance and APD capacitance leads to a typical dead time of approx 1 or 2 microseconds and a maximum counting rate of approx 250,000 cts/sec before distortions are excessive. Recent device modifications by RCA should allow significant improvements in these figures.

In active quenching, photodetection by the APD is detected by a high sensitivity, low noise, very fast comparator which is used to reduce the APD bias voltage and thus stop the current-flow and build-up of afterpulses. After a few nano-seconds the APD has recharged and so the bias voltage is restored to allow the next photodetection. In this manner we have achieved dead-times of 20-30 nanoseconds and count-rate capability up to 1MHz before excessive distortions are apparent. Again, recent device

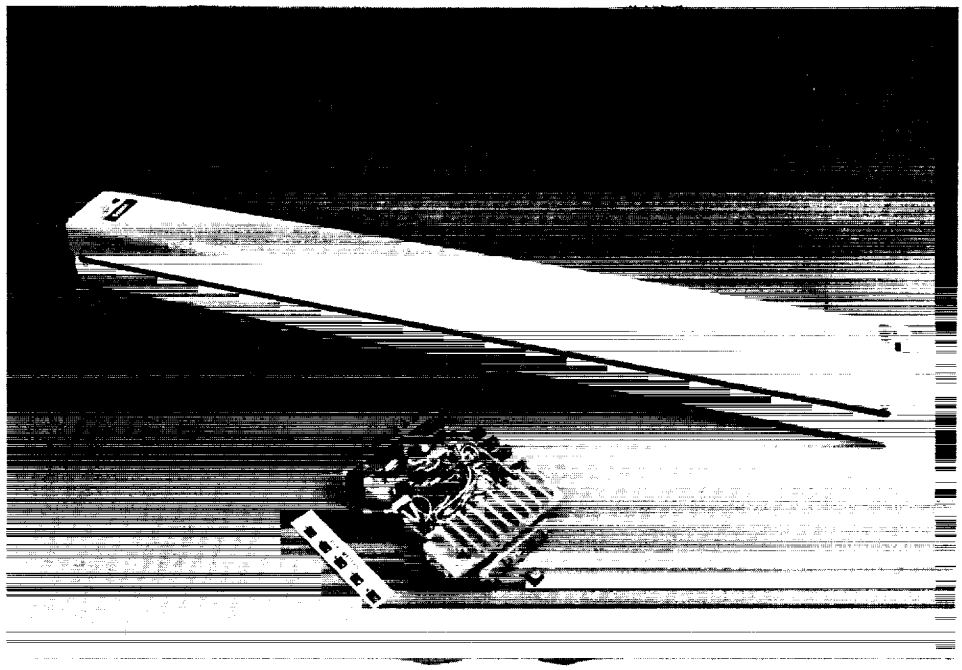

Figure 1- A 25 mW HeNe gas laser (upper box) compared to a 30 mW semiconductor laser (lowest item) and its drive circuitry (middle box)

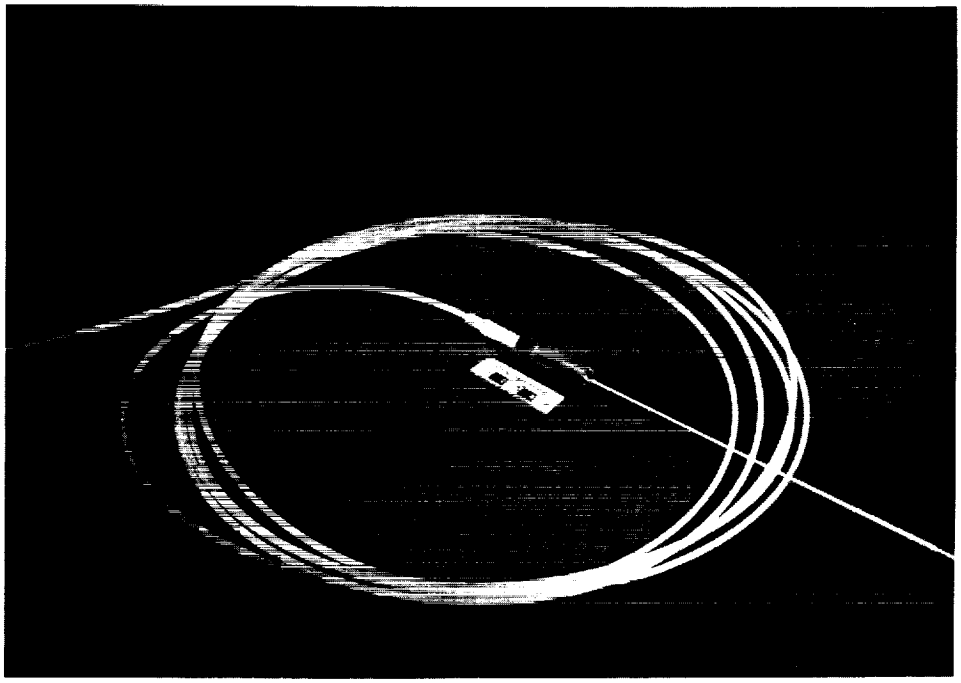

Figure 2- A 10m protected length of monomode optical fibre transmitting a few hundred milliwatts of 5145A^{o} light from an Argon ion laser and focused via a 1mm focal length microlens.

modifications by RCA, such as direct Peltier cooling, should allow major improvements in count-rate capability.

Notable features of APD performance of significance to photon correlation experiments are that afterpulsing levels of only 0.006% (passive) and 0.04% (active) are achievable, together with quantum efficiency exceeding 9% at 633nm. In fact the quantum efficiency may be set at a much higher value by increase in the reverse-bias voltage so long as the cooling is increased to remove the corresponding increase in dark-count rate and maintain the overall dynamic range of the detector. A photograph of our experimental apparatus compared to a standard Malvern Instruments photon-counting photomultiplier assembly is shown in Figure 3.

A photograph of a modular, fully engineered, twin APD system incorporating active cooling and active quenching circuitry is shown in Fig 4. The APD's stabilized bias voltage is supplied by a one cubic inch power-supply cube ($1.64 \times 10^{-5} m^3$).

These APD's are available with optical fibre input leads, making them more compatible with optical fibre anemometry and spectroscopy than photomultipliers.

Figure 5 shows an example of photon correlation LDA functions and data analysis using both a conventional photomultiplier and an APD viewing the identical Doppler-difference LDA measurement-volume placed in an axi-symmetric air jet. The upper traces show the correlograms with a fitted gaussian velocity probability density function, in which mis-fit because of negative skewness in the flow velocity statistics is clearly evident. The middle traces show the same correlogram data fitted by a spline procedure in which no Gaussian assumptions are made about the form of the flow velocity distribution [15]. The lower traces show the velocity probability density functions obtained from information-theoretic transformation [15] of the spline fits shown in the middle traces. The results from the APD are seen to be very similar to those from the photomultiplier except for minor artefacts caused by the transform procedure. Agreement between the first two calculated moments of these distributions was better than 0.5%, and is typical of a set of data so-treated.

Figure 6 shows an example of photon correlation spectroscopy functions using the same suspension of latex spheres in the same scattering geometry and using the same laser power, but varying the detector from a photo-multiplier to an APD. The curves are displaced vertically for clarity and show essentially identical slope-behaviour, as required.

The solid-state APD's have a component cost of $150-$500 including circuitry and occupy a total volume of a few cubic centimetres. We concluded that they may be suitable replacements for larger, more costly and fragile photon-counting photomultipliers in photon correlation experiments.

Combinations of the new technologies

The construction of a series of prototype photon correlation instruments has been undertaken to demonstrate the feasibility of combining the new-

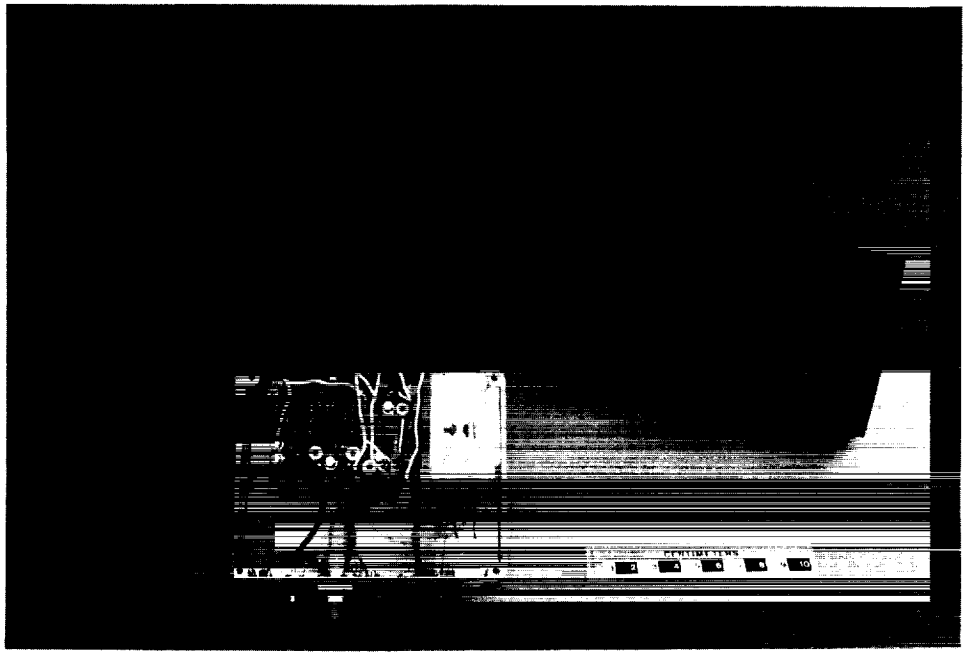

Figure 3- A standard photon-counting photomultiplier for photon correlation experiments (upper box) compared to our APD circuitry (lower box). The APD is at the centre of the white part of the unit.

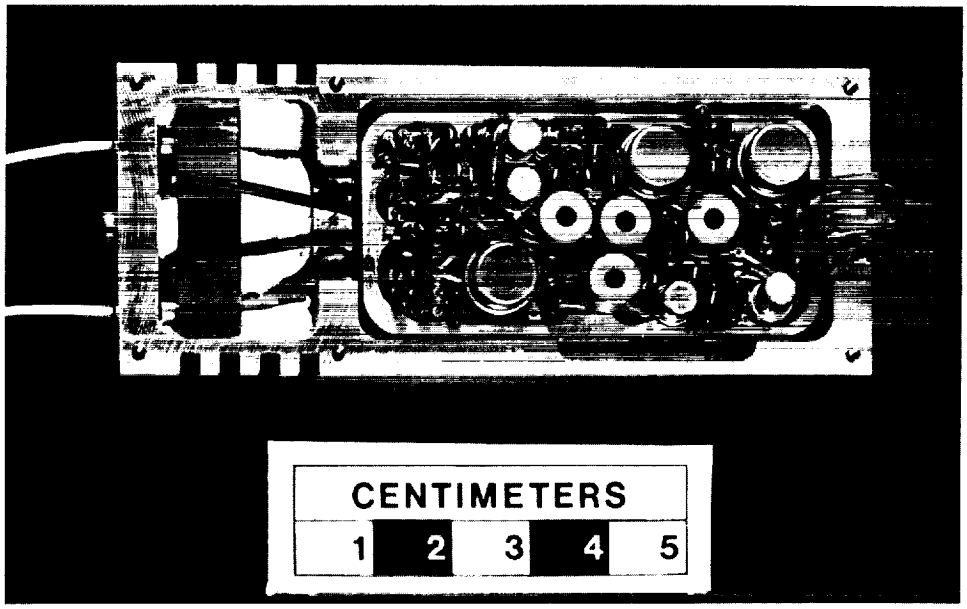

Figure 4- A fully engineered twin APD system with active quenching circuitry and active temperature control. Light enters the APD compartment via two optical fibres to the left hand side of the figure. The left hand compartment contains two fibre-coupled APD's mounted adjacent to two Peltier coolers and surrounded with insulation. The right hand compartment contains the active quenching circuitry and temperature control. Bias and supply voltages are supplied by the wires to the right hand side of the figure.

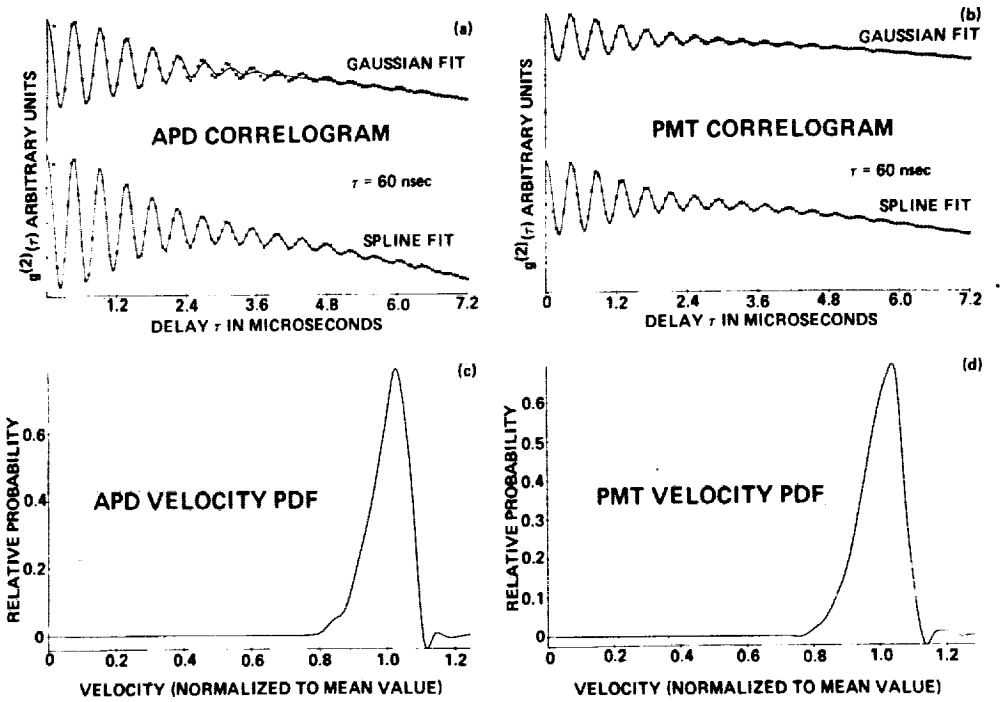

Figure 5- Photon correlation LDA results;- (a) Gaussian (upper) and spline (lower) fits to APD correlogram data; (b) Gaussian (upper) and spline (lower) fits to photomultiplier correlogram data; (c) APD velocity probability density function (pdf) derived from the spline fit in (a); and (d) photomultiplier velocity pdf derived from the spline fit in (d).

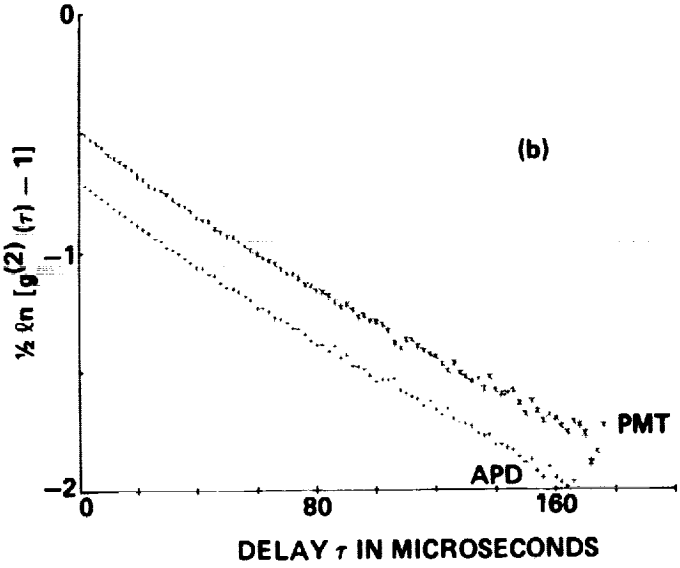

Figure 6- Photon correlation spectroscopy results, APD (lower) and photomultiplier (upper) correlogram data at 2 μ sec sample time. Mean size and polydispersity estimates from cumulants analysis are the same to within experimental errors.

technology devices just described into usable miniature systems. We will now briefly review a series of new photon correlation spectroscopy and anemometry instruments.

(i) Monomode-optical-fibre photon correlation spectroscopy

The use of optical fibres in dynamic light scattering experiments is well known [16] and usually employs multimode optical fibres. Recently, we have shown [17] how to employ monomode optical fibres to advantage in such experiments, allowing some substantial gain in correlogram intercept value at the slight expense of signal power. The use of such fibres with micro-optics allows major miniaturization of the standard experimental configuration for photon correlation spectroscopy, as can be seen from the photograph of our experimental arrangement shown in Figure 7.

A basic test of the monomode-fibre photon-correlation spectroscopy (PCS) arrangement was direct comparison with a conventional dynamic light scattering apparatus observing the same suspension of particles at 90° and using single-coherence-area detection and the same suspension temperature.

Comparative correlograms with a Malvern Instruments 4700 Spectrometer, integrated for the same length of time, are plotted in Figure 8. Significant intercept differences are observed as expected (1.985 monomode PCS: 1.62 standard 4700 PCS) but close correspondence of correlogram slopes (and slight curvature) is obvious, as also expected and required. Estimates of mean size and polydispersity from these data agreed to better than 0.5%, typical of a set of such data.

Apart from standard PCS replacement, there are a variety of potential additional advantages to be gained from employing monomode fibres in PCS experiments, e.g., possible flare rejection advantages at low scattering angles, TEM_{01}^{*} mode-effects removal, multi-angle and multi-sample geometries, and particularly simple heterodyne-PCS implementation using a fibre-coupler. These are detailed elsewhere [17].

Monomode optical fibre PCS is already finding uses in Biotechnology measurements, e.g., the measurement of proteins eluting from a liquid chromatography column as described in detail elsewhere [18]. An example result is shown in Figure 9. Many other potential applications exist within the general area of Downstream processing and we are pursuing a number of these in collaboration with the Public Health Laboratory Service, Porton Down. The key features here are miniaturized, low cost, multiplexable, remote measurement potential.

(ii) Monomode fibre-optic probes for laser anemometry

Whilst optical fibre LDA's are now becoming common [10,11], the construction of all-solid-state LDA's has created new challenges and problems. Recently, we have collaborated with the University of Kent in the creation of an all-solid-state LDA using the new electro-optic components discussed above [19]. This R and D programme has yielded a laser diode driven (780nm and 850nm), two-component full-backscatter LDA constructed in a cylindrical head of 25.4mm diameter and approx 80mm length. Lens-ended monomode optical fibres are used to deliver the laser

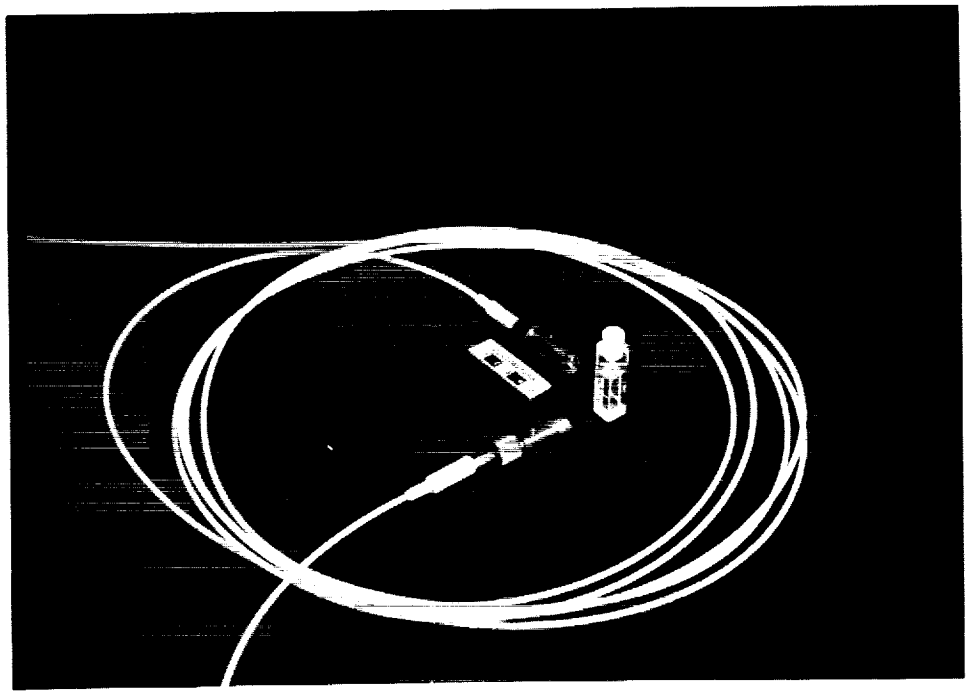

Figure 7- Monomode-optical-fibre photon correlation spectroscopy experiment. The particulate suspension is held in the square cell at the centre of the photograph and illuminated from the upper lens-ended fibre. Scattered light is collected by the lower lens-ended fibre at 90^{0} scattering angle.

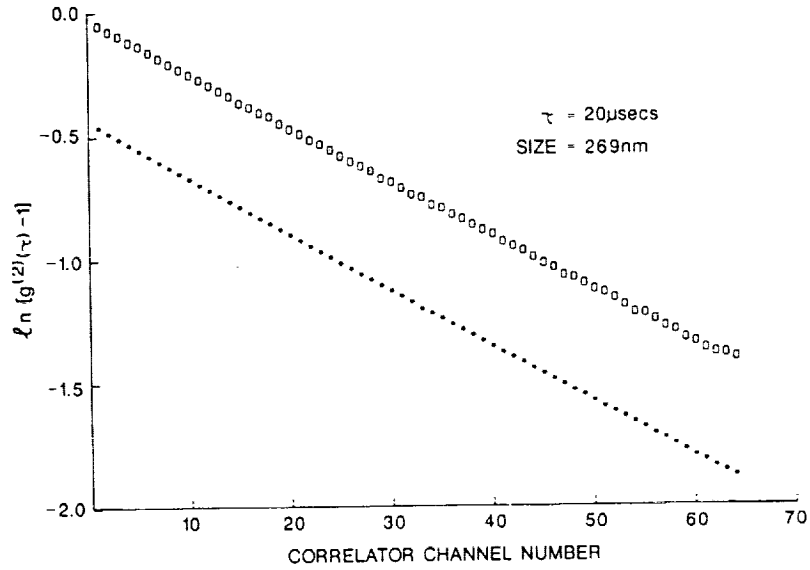

Figure 8- Comparative photon correlation spectroscopy correlograms, plotted semi-logarithmically. The upper data are from monomode-optical-fibre photon correlation spectroscopy, and the lower data are from a standard photon-correlation spectrometer with approximately single coherence area observation.

beams to the measurement volume at 100mm range, and a multimode optical fibre delivers collected scattered light to APD's for photo-detection. The electro-optical system has been designed specially to operate with photon-correlation signal and data processing with velocities up to 500 ms^{-1}. Computer simulations of signal levels indicate the feasibility of such performance, and detailed testing is currently in progress.

(iii) A miniature, battery operated laser Doppler anemometer

Because of the small size, high efficiency and low power consumption of diode lasers, we have recently been able to construct a hand-held, portable, lithium battery operated, 30 mW laser diode, backscatter LDA constructed in a tube of 30 mm diameter and 250 mm length. The tube also contains micro-optical beam collimation, a miniature galilean telescope, miniature beamsplitter and prism, spatial filtering, solid state detector, electronic amplifier, bandpass filter, discriminator and either (1) telemetry to transmit Doppler (analogue or digital) signals to a remote signal processor or (2) integral frequency analysis of analogue signals and LCD display of single component velocity. All components are mounted on micro optical benching. The velocity range is up to a few metres per second; the system operates for a few hours before battery replacement is necessary. The component cost was eight hundred UK pounds. Full details are reported elsewhere [20]. A picture of the completed system is shown in Figure 10.

(iv) Modularized, miniature photon correlation spectroscopy and laser anemometry

The principles of miniaturization outlined in the previous section are being taken forward into prototype, fully-engineered, modular light-scattering systems for photon correlation spectroscopy, laser Doppler and laser transit (time-of-flight or L2F) anemometry [2]. The aim is to open-up a new range of applications to industrial monitoring and process-control, as well as making possible new research experiments.

Recently we have designed a range of modular units that can be "plugged" together in various geometries to form quite different light scattering experiments. The basic modules are (i) laser, (ii) optics and (iii) detector(s). These modules are designed for manufacture on numerically-controlled engineering facilities, with high-tolerance, cheaper, small, lightweight, fairly rugged "mass" produced output. The laser module contains the laser and its power stabilization and supply circuitry together with collimation and beam diameter control. It outputs a beam of known size, divergence and pointing error. This unit is positioned at one of many possible sites on a baseplate using dowel-location techniques. Similar descriptions apply to the optics and detector modules.

Whichever configuration is chosen, the overall dimensions of the entire photon correlation light scattering system is 36 mm width by 200 mm length by 40 mm height. The detector unit contains all the electronics necessary to operate 2 APD detectors in active-quenching mode for high speed (short sample time) photon correlation measurements.

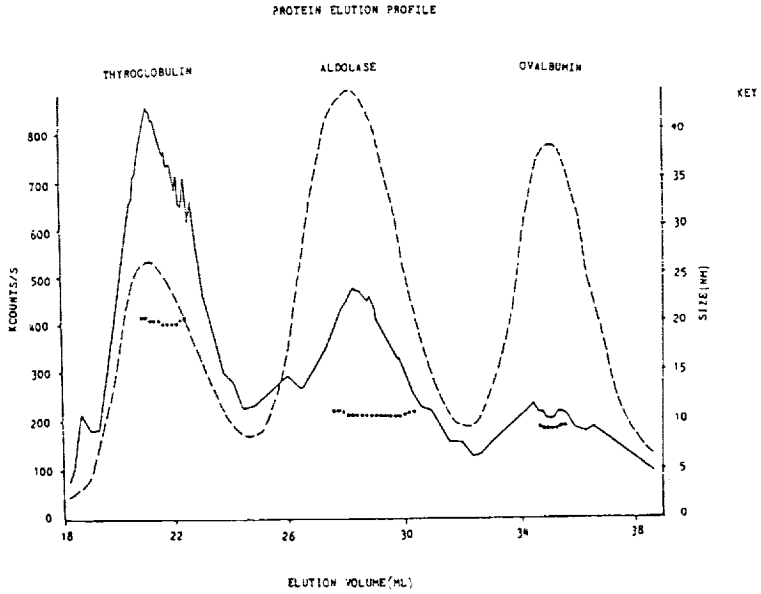

Figure 9- Protein elution profile from a liquid chromatography column measured by photon correlation spectroscopy; ----:UV trace 280; _____: photon counts per second x 1000; .....: size in nanometres.

ORIGINAL PAGE
BLACK AND WHITE PHOTOGRAPH

Figure 10- Photograph of the constructed battery-driven LDA.

Fig 11 shows the miniature, modular laser Doppler anemometer (LDA) corresponding to the prototype battery-operated instrument shown in Fig 10. The laser and collimating optics is contained in the fore-most right-hand-side rectangular metal block, the prisms for beamsplitting and separation are seen centrally and the focussing lens to intersect the two laser beams of the LDA is at the left hand side of the device. Scattered light is imaged back through this lens onto a multimode optical fibre and directed to an APD detector and electronics housing in the rear-most rectangular metal block. Internal details of the APD unit are shown in Fig 4. Voltage supplies and signal connection to the processor are provided by the ribbon-cable to the right hand side of the figure. The distance of the measurement volume from the end (lens) of the instrument can be varied from 5 cms upwards via interchangeable lenses. A clearer understanding of the laser beam paths is gained from study of the corresponding original artist's impression shown in Fig 12.

Continuing in the manner of Figs 11 and 12, we have used the same detector module with two, simpler laser diode modules (using different wavelengths to avoid crosstalk in the receiver) and a transit-anemometer optics-module (incorporating a Wollaston prism and quarter-wave plate) to create a miniature modular laser-transit anemometer system where two parallel laser beams are formed in the measurement region [2]. The constructed system is shown in Fig 13. In Fig 13, the two laser diode modules in the fore-most right hand side direct light through two polarization-preserving monomode fibres to a Wollaston prism and transit anemometer optics module. The beams are imaged by the left-hand-side lens to form the parallel beam pair of the measurement volume. The same lens collects scattered light and directs it back through the Wollaston prism and to two multimode optical fibres and thence to the two APD's mounted in the detector module. The velocity dynamic range is from near zero to potentially thousands of metres per second with present day processor bandwidths; at 60 mm operating range from the output lens the measurement volume comprises two parallel ten micron beam waists spaced by approximately 300 microns.

The miniature modular photon correlation spectroscopy or dynamic light scattering system is shown in Figs 14 and 15. The laser and APD modules are positioned as described for Fig 11. The laser beam is directed via a 50 mm focal length lens to form a 50 micron diameter laser beam waist inside the Hellma sample cell seen to the left hand side of the figure. At the extreme left hand side of the figure is a simple triangular beam stop with highly absorbing painted surfaces. Fig 12 shows more clearly how scattered light at 90° (in this instance) is directed via a small prism to a lens-ended monomode fibre (as described earlier) and onward transmission to the APD module for detection. Using this system with a 30 mW, 780 nm laser and a suspension of nominally monodisperse 8.5 nm diameter particles (at a concentration of $\sim 0.5\ \mu g/m\ell$) we have acquired high quality correlograms in approx 30 seconds when using the APD detector with a quantum efficiency of approx 15-20%.

One of the major advantages of the modular approach with high accuracy machining is the lack of adjustments in aligning the optics. The LDA in Fig 11 requires three small (one angular, two lateral) minor adjustments, the transit anemometer has two simple slide-to-focus-and-lock adjustments and the photon correlation spectrometer has only one lateral adjustment of

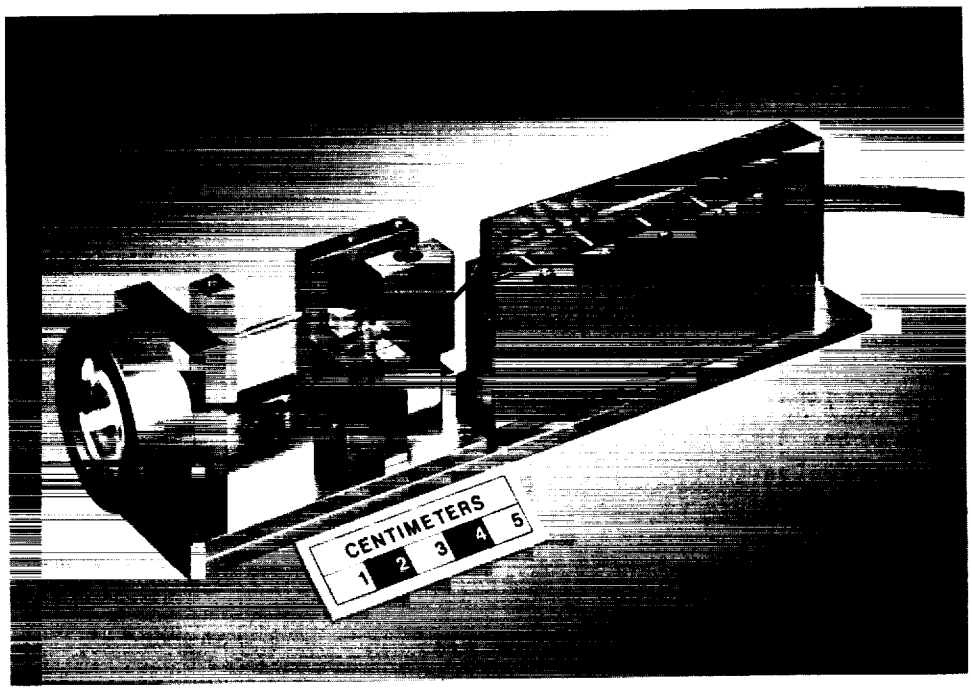

Figure 11- A modular miniature laser Doppler anemometer.

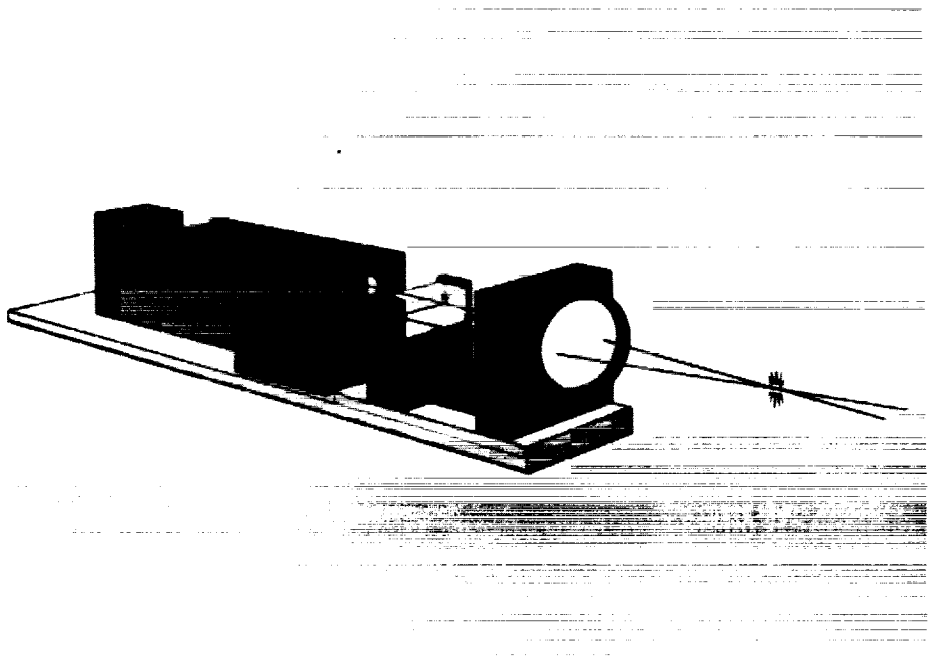

Figure 12- The original artist's impression of Figure 11, showing the laser beam paths.

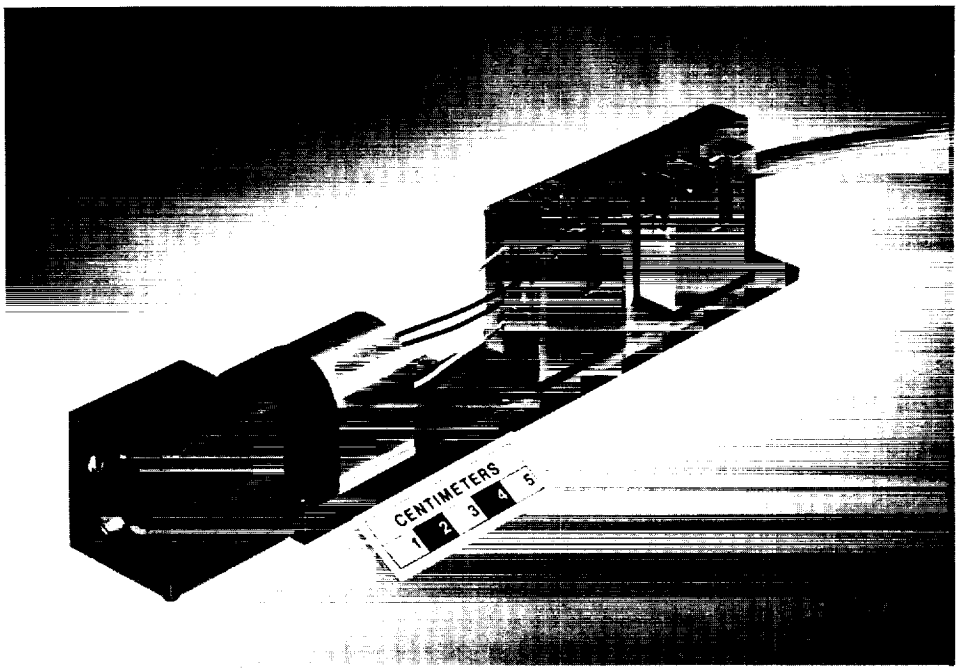

Figure 13- A modular miniature laser transit anemometer.

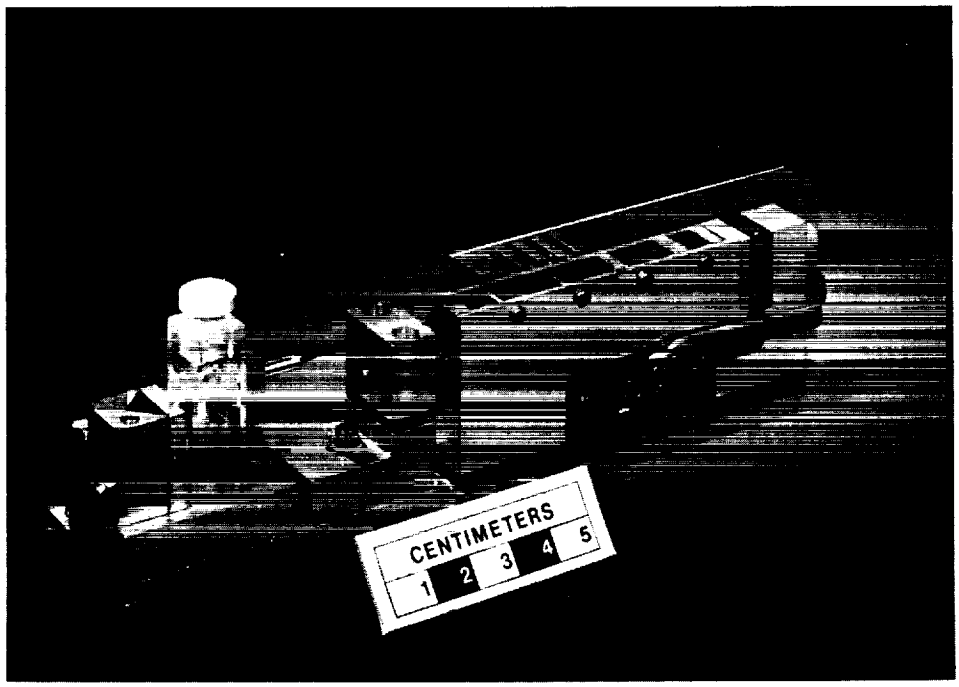

Figure 14- A modular miniature photon correlation spectroscopy system.

the laser beam to ensure intersection with the receiver's field-of-view. Finally, Fig 16 shows some of the family of new light scattering instruments created from the new technologies, and here the commonality of modules is obvious. Further light scattering instruments are planned, based on the same components.

By now it will be clear that all of these systems could have been made even smaller than already achieved; there is a considerable amount of metal and space around the components used. Furthermore, although lightweight through use of duraluminium throughout, improvements in this area may be made by using high-stability plastics and ceramics, especially for quantity production.

Concluding Remarks

We have briefly reviewed developments in the miniaturization of photon correlation instrumentation that have occurred during the last three years. Prototype, small new photon correlation spectroscopy and laser anemometry systems have been constructed and successfully demonstrated.

We confidently expect to see a new range of photon correlation instrumentation constructed from the solid-state technologies outlined here. It is possible to replace some previous photon correlation-instrumentation at an order-of-magnitude smaller size and (perhaps) cost. Significant advantages are possible, in parameter measurement-capability, ease of system adjustment, detection efficiency and ruggedness.

Developments in integrated electro-optic devices will lead to further size and cost reductions. Semiconductor laser diodes output powers are steadily increasing ($\gtrsim$ 100 mw) and their availability ready-coupled to beam-forming optics or directly into monomode fibres will steadily improve. APD performance also continues to improve and we expect to see in the near-future the commercial availability of devices with noise performance at $\geqslant$ 0°C suitable for photon correlation experiments. Further in the near-term we expect to see APD's packaged with integral temperature control and active-quenching circuitry as modular units with which to construct photon correlation experiments.

Finally, we note that these miniaturized components for photon correlation measurements are presently being incorporated into a new range of instruments for research and industrial environments, notably for process-control. The exploitation procedure is being co-ordinated by Defence Technology Enterprises. We anticipate the commercial availability of some of the devices discussed here in 1989 and beyond.

Acknowledgements

The author is grateful to many colleagues for continuing, fruitful collaboration in connection with the miniaturization research and development described here, notably those at RSRE, the Universities of Kent and Southampton, the Public Health Laboratory Service at Porton Down, York VSOP Ltd, RCA at Vaudreuil, Canada and DTE Ltd.

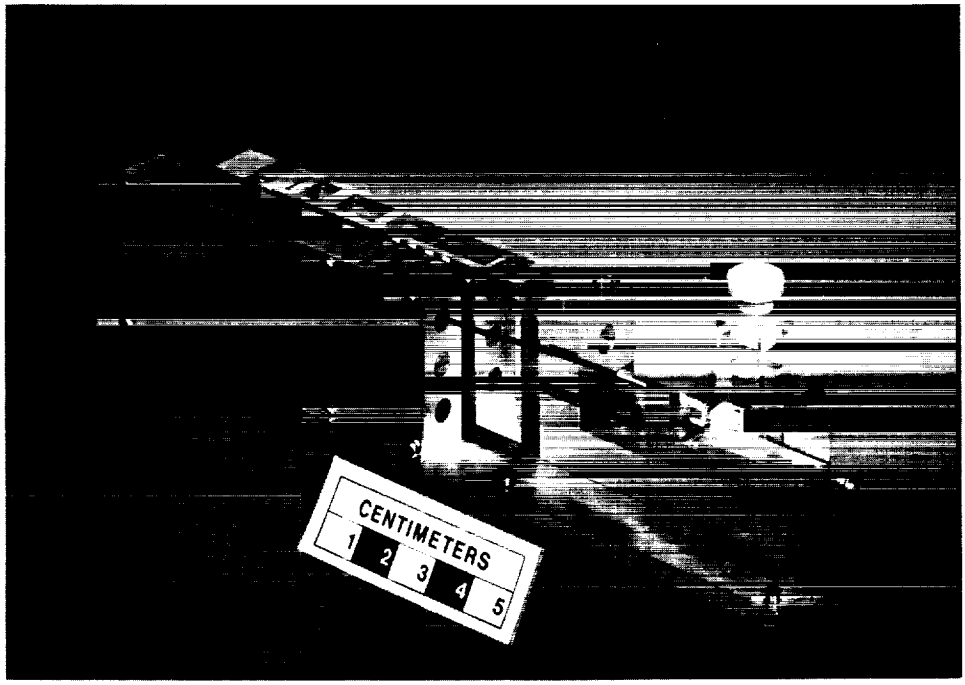

Figure 15- As per Figure 14, but from a different viewpoint to show 90^{o} scattering via a small prism into a lens-ended monomode optical fibre that connects to the APD housing.

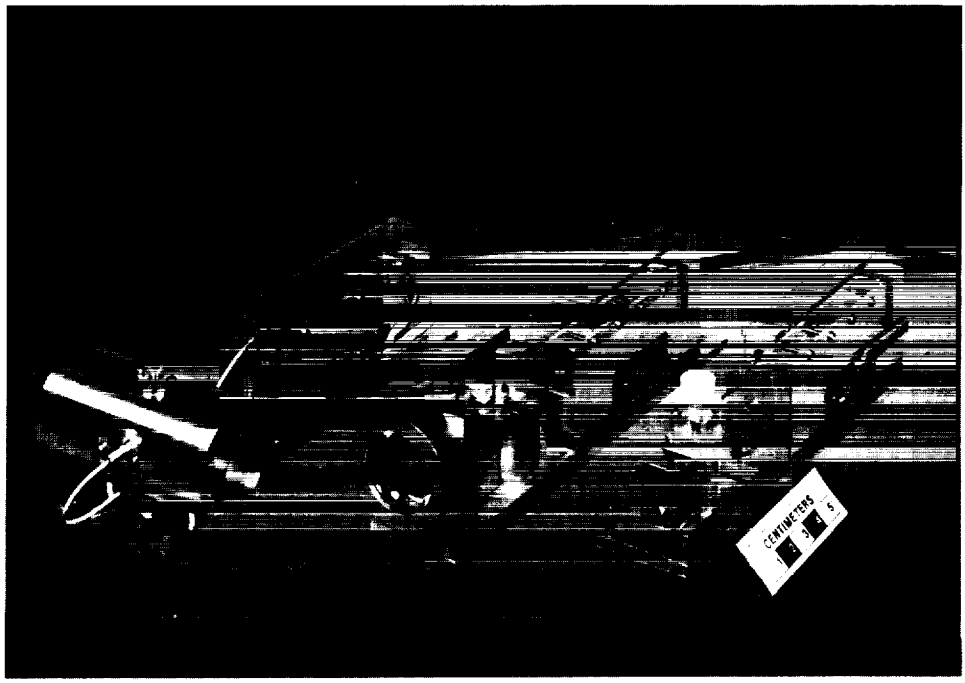

Figure 16- Three of the family of four new modular light scattering systems constructed from semiconductor laser, monomode fibre, microlens and APD technologies. From left to right: a flowing-aerosol photon correlation spectroscopy particle sizer, the laser Doppler anemometer, and the photon correlation spectrometer, showing commonality.

References

1 H. Z. Cummins and E. R. Pike, (Eds), Photon Correlation Spectroscopy and Velocimetry, Plenum press, New York., (1977).

2 E. O. Schulz-DuBois, (Ed), Photon Correlation Techniques in Fluid Mechanics, Springer-Verlag, Berlin, (1983).

3 R. Jones, RSRE, Private communication.

4 A. Noullez and J-P Boon, "Microprocessor-based photon correlator", Rev. Sci. Instrum. Vol 57, 2523-2528, (1986).

5 RSRE and Kings College, London, joint project. A 100ns sample time, 16 bit, 12-16 channel log-log correlator with no prescaling on a single ½-Eurocard has been demonstrated. Realtime correlation at 6μ secs sample time, 50% efficiency at 2 μsec has been achieved. 5W power consumption.

6. J. G. McWhirter, J. V. McCanny and K. W. Wood, "A novel multi-bit convolver/correlator chip design based on systolic array principles", SPIE, Vol 341, paper 8, (1982).

7. R. A. Leaver, P. Mars and M. Sarhadi, "Application of a stochastic systolic array to photon correlation and LDA techniques", Proc. 2nd Int. Conf. on Laser Anemometry: Advances and Applications, 21-23 Sept 1987, Glasgow, UK.

8. C. J. Oliver, "Correlation techniques", in H. Z. Cummins and E. R. Pike, (Eds) Photon Correlation and Light Beating Spectroscopy, Plenum press, New York, pp 151-223, (1974).

9. R. G. W Brown and R. Grant, "Photon statistical properties of visible laser diodes", Rev. Sci. Instrum, Vol 58, 928-931, (1987).

10. J. Knuhtsen, E. Olldag and P. Buchhave, "Fibre optic laser Doppler anemometer with Bragg frequency shift utilizing polarization-preserving single-mode fibre", Journal of Physics E (Sci Instrum), Vol 15, 1188, (1982).

11. D. A. Jackson and J. D. C. Jones "Extrinsic fibre-optic sensors for remote measurement", Optics and Laser Technology, Vol 18, 243-252 (Part 1) and 299-307 (part 2) (1986).

12. R. G. W. Brown and A. P. Jackson, "Monomode fibre components for dynamic light scattering", Journal of Physics E (Sci Instrum), Vol 20, 1503-1507, (1987).

13. R. G. W. Brown, K. D. Ridley and J. G. Rarity, "Characterization of silicon avalanche photodiodes for photon correlation measurements. I:Passive quenching", Applied Optics, Vol 25, 4122-4126, (1986).

14. R. G. W. Brown, R. Jones, J. G. Rarity and K. D. Ridley. "Characterization of silicon avalanche photodiodes for photon correlation measurements. II:Active quenching", Applied Optics, Vol 26, 2383-2389, (1987).

15. J. G. McWhirter, "A well-conditioned cubic B spline model for processing laser anemometry data", Optica Acta, Vol 28, 1453-1475, (1981).

16. H. Auweter and D. Horn, "Fibre-optical, quasi-elastic light scattering of concentrated dispersions", J. Colloid Interface Sci, Vol 105, 399 (1985).

17. R. G. W. Brown, "Dynamic light scattering using monomode optical fibres", Applied Optics, Vol 26, 4846-4851 (1987).

18. R. J. G. Carr, J. G. Rarity, A. G. Stansfield, D. J. Clarke and R. G. W. Brown, "Determination of protein size in chromatography column eluant by on-line photon correlation spectroscopy", Anal. Biochem, 1988, in press.

19. P. W. Forder, C. N. Pannell, J. D. C. Jones, D. A. Jackson and R. G. W. Brown. "Designs of fibre-optic probes for laser anemometry", Proc. 2nd Int. Conf. on Laser Anemometry: Advances and Applications, 21-23 Sept 1987, Strathclyde, UK.

20. R. G. W. Brown, J. G. Burnett and N. Hackney, "A miniature, battery operated laser Doppler anemometer", Proc. Fourth Int. Conf. on Applications of Laser Anemometry to Fluid Mechanics, Lisbon, Portugal, July 1988; also J. Phys. D (Applied Physics) 1988, in press.

PHOTON COUNTING MODULES USING RCA SILICON AVALANCHE PHOTODIODES

Alexander W. Lightstone, Andrew D. MacGregor, Darlene E. MacSween,
Robert J. McIntyre, Claude Trottier, and Paul P. Webb
RCA Incorporated, Electro Optics
Vaudreuil, Quebec, Canada

Avalanche photodiodes are excellent small-area, solid-state detectors for photon counting. Performance possibilities include: photon detection efficiency in excess of 50%; wavelength response from 400 to 1000 nm; count rates to 10^7 counts per second and higher; dark count rates well below 100 counts per second; afterpulsing at negligible levels, $< 10^{-2}$%; timing resolution better than 1 ns. Unfortunately these performance levels are not simultaneously available in a single detector-amplifier configuration. By considering theoretical performance predictions and previous and new measurements of APD performance, this paper derives the anticipated performance of a range of proposed APD-based photon counting modules.

1.0 INTRODUCTION

Silicon avalanche photodiodes (APD's) offer a practical approach to photon counting. This paper considers proposed APD module performance in terms of:

Available performance - what RCA can offer today (Fall 1988).

Target performance - what RCA could offer within twelve months ..... given sufficient funding and market incentive.

Possible performance - how good an APD module could be.

An APD is a solid-state photodiode which operates at a reverse bias voltage which is high enough to cause avalance multiplication in the vicinity of the p-n junction. Since the avalanche process is statistical in nature, the resultant gain is statistical. The gain increases with voltage until the "Breakdown Voltage" is reached, at which point the average gain is statistically infinite. Appendix I considers the gain probability distribution as a function of voltage in greater depth.

RCA has been manufacturing silicon APD's commercially for over fifteen years. Typical applications include optical rangefinding, target designation and optical communication receivers; such applications reflect the APD's system advantages of compact device size, high internal gain and high quantum efficiency.

For photon counting, specialized APD's and receiver circuitry are required. In this paper we discuss so called "Linear mode" and "Geiger mode" photon counting, defined in more detail in Sections 2 and 3 respectively. In both cases it is necessary to make a clear distinction between the following quantities:

QE (Quantum Efficiency) - The probability that an incident photon generates a primary electron.

P_e (Photo-Electron Detection Efficiency) - The probability that the primary electron gain gives a pulse height that exceeds the receiver threshold.

and

P_d (Photon Detection Efficiency) - equals (QE x P_e).

Historically, and currently, PMT's have been the main detector for photon counting. Recent publications [1 to 4] and on-going work reported here, indicate that APD's can offer competitive or better performance in a more compact package. It is therefore important to be aware of the basic differences between APD's and PMT's for photon counting; typical parameters are summarized in Table 1.

TABLE 1	APD	PMT
Quantum Efficiency (QE)	High > 80%	Low 25% (max.)
Photon Detection Efficiency (P_d)	Up to 60% x QE [1]	< Q.E. Not normally quoted for PMT's
Wavelength Range	<400 to 1000 nm [2]	200 nm to 700 nm [2]
Active Diameter	< 1 mm	< 50 mm
Dark Count @ 22°C	10's to 1000's cps	1's to 1000's cps
Maximum Count	See discussion	Few x 10^6 cps
After Pulsing	Few x 10^{-2} to <10^{-4}%	Few x 10^{-4}%
Timing Resolution	100ns to 1ns: < 1ns?	Few hundred pS
Lifetime	> 100,000 hours	5,000 to 20,000 hrs.
Ease of Use	APD modules will be easy	Familiarity a factor

[1] Depends on the particular configuration, preamplifiers, etc.
[2] Defined at a QE of approximately 10% minimum. Assumes an APD or PMT optimized for the wavelength and for photon counting.

2.0 LINEAR MODE PHOTON COUNTING

2.1 Technique

In a previous publication, operation of the APD for photon counting below the breakdown voltage was described theoretically and experi-

mentally [Ref. 4]. Appendix I highlights the theoretical background to this technique and includes new calculations on P_e.

In this mode, the diode is operated close to but below the breakdown voltage, at a voltage such that the average gain is large but finite. It is connected to a low-noise, charge-sensitive preamplifier. A threshold is set sufficiently high (6 to 10 times the rms noise level) to reduce amplifier noise to an acceptable level. Any thermally or optically generated electron which undergoes a gain greater than the threshold setting is then counted. Amplifier or thermal noise pulses which exceed the threshold are dark counts.

A hybrid prototype version of the circuit of Figure 1 has been developed. An integrating front end preamplifier is followed by a pulse shaping circuit and a threshold discriminator circuit. In such a preamplifier, low input capacitance is essential. Currently the total input capacitance with an 0.5 mm active diameter C30902S APD chip is 2.0 pF; the equivalent input noise charge of the hybrid amplifier is ≈ 180 electrons rms. Ongoing developments will reduce total capacitance below 1.0 pF to give a noise below 100 electrons rms.

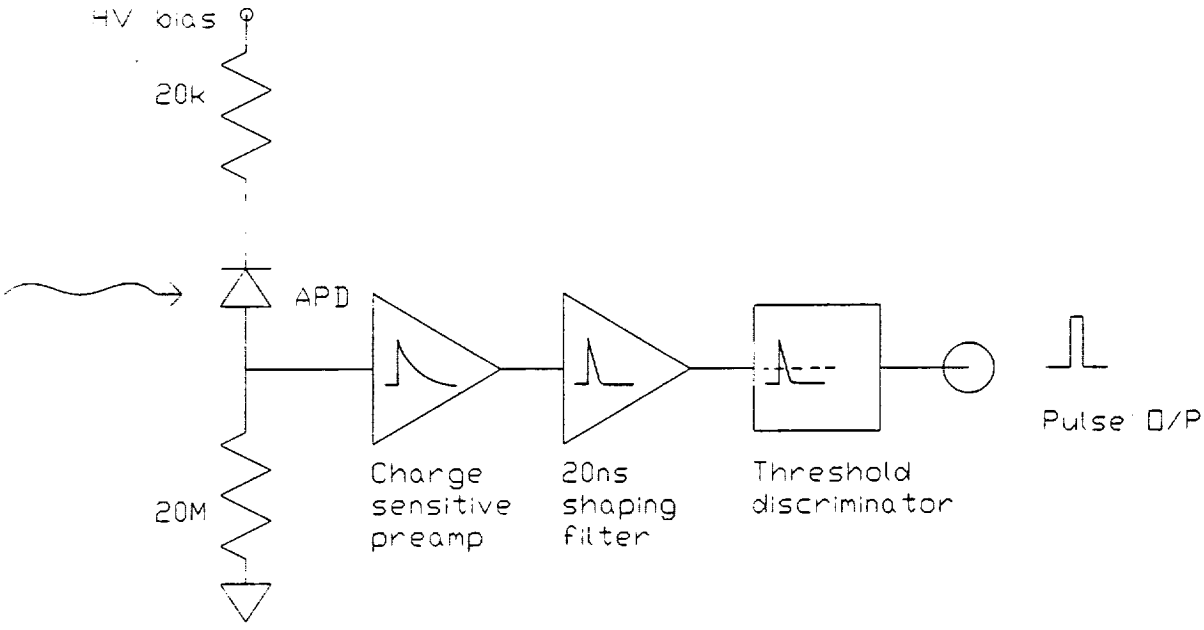

FIGURE 1. Linear mode photon-counting preamplifier

2.2 Results

Initial results achieved very recently are illustrated in Figures 2, 3 and 4.

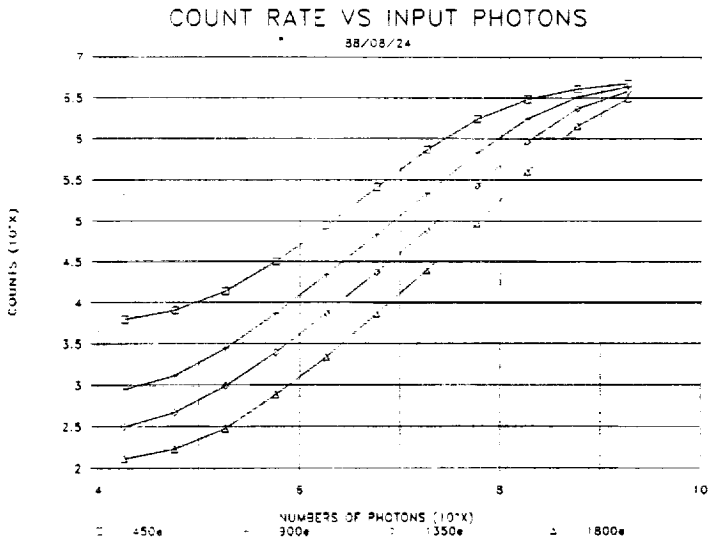

FIGURE 2

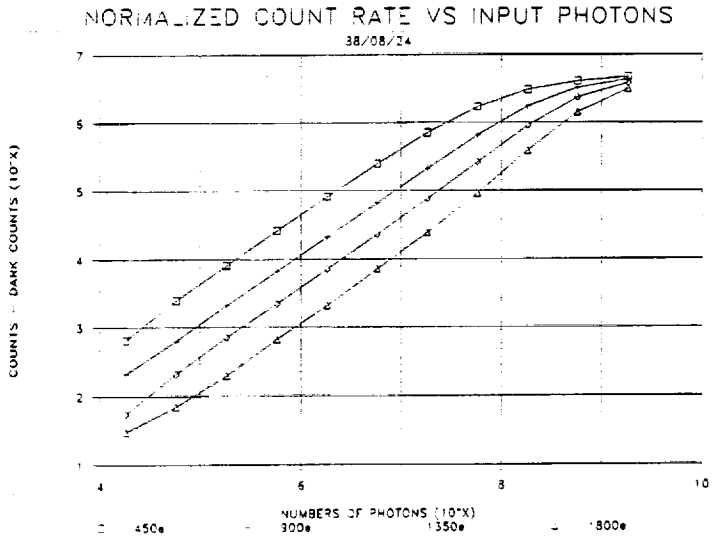

FIGURE 3

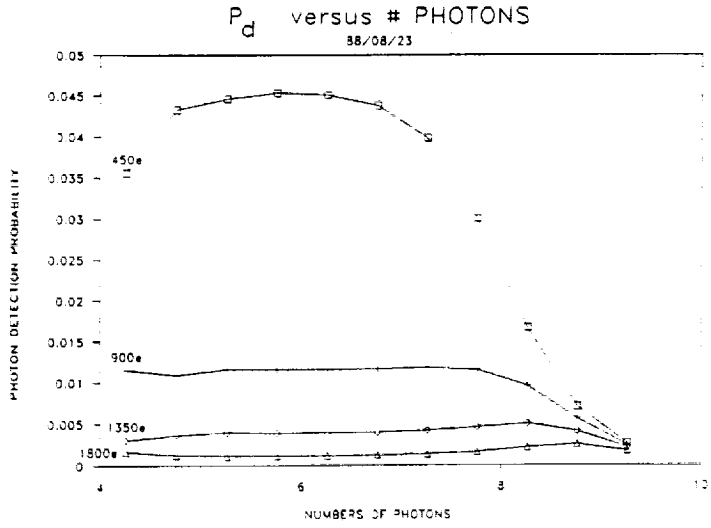

FIGURE 4

Figure 2 shows raw count rate versus number of input photons for various threshold settings. Subtracting an estimate of the the "dark count" gives the normalized curves of Figure 3. Converting these to photon detection efficiency gives the results of Figure 4. The P_d of about 4.5% was achieved a few volts below breakdown at a maximum count rate around 10^6 cps. By comparison, Ref. 4 reported a P_d of 10% at a few x 10^5 cps.

3.0 GEIGER MODE PHOTON COUNTING

3.1 Breakdown Process

Above the breakdown voltage, an optically or thermally generated electron initiates a chain of ionization which either peters out with a current pulse amplitude which does not exceed an external threshold setting (self-quenching), or causes a huge breakdown pulse containing $>10^6$ electrons which is detected as a count. The pulse must then be actively or passively quenched by reducing the bias voltage below the breakdown voltage; the detector bias is then reset in order to detect the next optically or thermally generated electron.

Once a breakdown has started, the breakdown ignition spreads through the APD. Unless it is self-quenched due to space charge, it must then be quenched by an active or passive circuit which reduces the bias voltage to below the breakdown voltage.

During a breakdown, two other things occur which can be of significance:

(a) The leading edge of the breakdown pulse exhibits step-like fluctuations with a timescale of nanoseconds between steps - this affects timing resolution. However, by arranging to trigger on the first step ($< 10^5$ electrons), subnanosecond timing should be possible, and 1 ns FWHM timing resolution has already been reported [Ref. 4].

(b) Photons generated by the breakdown process can be absorbed elsewhere in the APD structure. Some of the resulting photoelectrons are trapped, leading to afterpulsing when the trap empties some time later. If this afterpulsing becomes excessive, it results in either distortion of the correlation function, or a limit on the maximum count rate due to the requirement for a "dead" time after each pulse. (By operating below the breakdown, in the linear mode, such afterpulsing is virtually eliminated.)

3.2 Passive Quenching

Once a breakdown has been initiated, the current in the diode rises in a timescale which is subnanosecond. This current is drawn through the load resistor and the APD series resistance, causing the bias voltage across the APD to decrease. Since the instantaneous number of carriers in the pulse is time and bias dependent and fluctuates wildly, this decrease in bias voltage increases the

probability that the number of carriers can fall to zero, quenching the pulse. For a C30902S, a "critical current" of ≈50 μA may be defined, implying that for a starting bias voltage 10V above the breakdown voltage and a load resistor of 200 kΩ, all breakdown pulses will be quenched within a few nanoseconds. This type of pulse quenching is referred to as "passive quenching".

The bias regains its original value by exponential charging of the APD capacitance, C, via the load resistor, R_L, giving a time constant given by $\tau = R_L C$. For R_L = 200 kΩ, C = 1.6 pF (packaged C30902S). τ = 0.32 μs.

The count rate limitation is a consequence of both the sensitivity of P_d to $(V-V_{BR})$, and therefore to recharge time, (see Figure 5) and the degree of acceptable non-linearity.

For a non-linearity specification of (e.g.) 5% at maximum count rate, the P_d must approach its original value within 5%. This occurs after a period of about 3τ. For randomly spaced photons, the maximum mean count rate is substantially lower, and may be calculated in terms of photon arrival rate probability statistics.

This limits the linear count rate region to a few hundred thousand counts per second. New small area APD's are under development; packaged with integral resistors they may achieve C of around 0.3 pF, reducing τ to around 60 ns, and allowing count rates of around 1 Mcps. R_L itself cannot be reduced below the value at which the breakdown is self-sustaining, about 200 kΩ for a C30902S biased 6V above breakdown (allowing a x2 safety factor). However, after-pulsing must also be considered.

Afterpulsing and Maximum Count Rate

The probability of afterpulsing is a complex function of device structure, breakdown pulse shape, temperature and bias voltage [Ref. 4]. Since it is a trapping problem, increasing R_L to reduce the total charge dissipated will reduce the afterpulsing probability, but only at the expense of increasing τ and lowering the maximum count rate.

Ref. 4 reports results using an active quench circuit (see 3.3) designed by RCA specifically to evaluate afterpulsing characteristics. At ambient temperatures, the characteristic afterpulse delay time was 65 ±10 ns for a random selection of C30921S APD's from various wafers. The actual afterpulsing magnitude in a given 10 ns period varied by nearly an order of magnitude between different devices. Cooling the APD to -25°C, a low probability afterpulse phenomena with a characteristic delay time of 500 ns appears.

For the C30902S, at a P_d of 5%, afterpulsing is quoted at 2% maximum for pulses occurring 1 μs to 60s after a signal pulse or a dark count pulse.

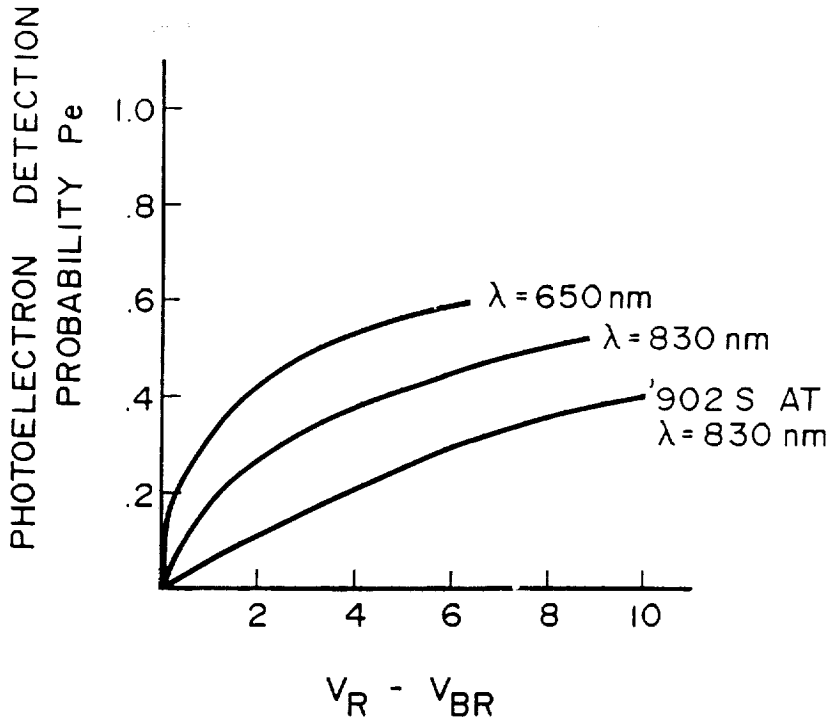

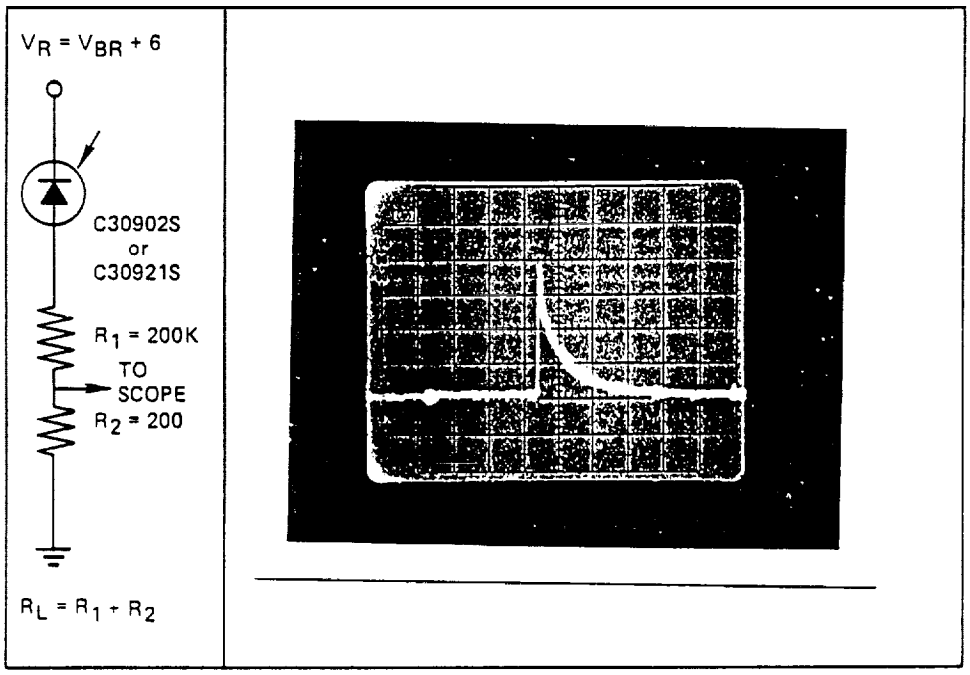

HORIZONTAL – 500 ns/DIVISION
VERTICAL – 1 mV/DIVISION

FIGURE 5

Results on New Low-k APD's for Commercial Modules

Figure 5 plots measured P_e versus V_R-V_{BR} for some new k = 0.004 (at 650 nm) APD's, together with the 830 nm results and, for comparison, the data sheet values for a C30902S.

Three things are apparent:

(i) Higher P_e's are achieved at lower excess voltages. At λ = 830 nm the low-k APD has substantially higher P_e than a C30902S; 0.22 instead of 0.11 at 2V above breakdown. (Ideal situation with a focussed spot.)

(ii) The P_e is more wavelength dependent in the newer devices.

(iii) The voltage dependence of relative P_e is greater at low $(V-V_{BR})$ and less at high $(V-V_{BR})$.

These, very recent, results are close to the theoretical predictions. In essence, it is now possible to achieve either higher P_e than a C30902S with the same degree of afterpulsing, or the same P_e with less afterpulsing than a C30902S.

Figure 6 plots P_e against position for the APD of Figure 5. High P_e is achieved over a 150 µm wide FWHM. Very good P_e uniformity is evident over the central 80 µm.

3.3 Active Quenching

In order to count at faster rates than is possible with passive quenching, it is necessary to threshold detect the breakdown pulse and then immediately quench the breakdown by reducing the bias voltage to below V_{BR}. After a suitable delay to allow the traps to empty, the bias voltage is reset.

Currently no active quench APD module is commercially available. An optimized active quench module would use a sensitive first stage to trigger the thresholding circuit and quench circuitry after only 10^4 to 10^5 electrons had appeared in the pulse. This might give a timing resolution of around 1 ns or better, and substantially reduced afterpulsing. Such a module might achieve count rates of 10's to 100's of Mcps.

Reported Results on RCA Devices

Currently the circuitry for actively quenched modules is still being optimized. Ref. 3 reports the use of a quench delay time of 6 ns on a C30902S and a dead time of 40 ns to achieve afterpulsing of around 0.04% at a photon detection efficiency of 9% at 633 nm. Improvements in chip heatsinking should improve the linear range of operation over the ≈ 1 Mc/s observed.

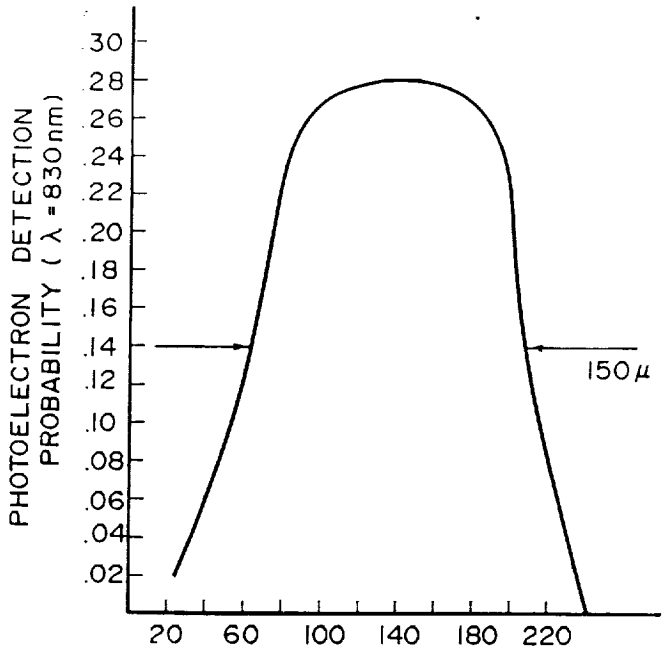

SPOT SIZE $\lesssim 20\mu$ $V_{BR}+2.5\,V$

DARK COUNT = 3,500 COUNTS/SEC.
AT ROOM TEMP. (22°C)

FIGURE 6

Ref. 4 reports an active quench circuit which gave similar results. Such circuits will form the basis of actively-quenched photon counting modules which will achieve higher maximum count rates than passive quench circuits, but at the expense of circuit complexity and perhaps afterpulsing.

4.0 PERFORMANCE SUMMARY FOR PHOTON COUNTING MODULES

RCA is currently developing modules and detectors to satisfy the "Target" performance for counting below breakdown and for passive quenching. Module development for active quenching will recommence shortly.

An essential feature of all modules will be "Photons In - Pulses Out". Voltage bias and APD temperature will be internally factory set to achieve the design performance for photon counting. Modules for all three modes will be optomechanically identical, implying identical optical and mechanical interfaces, and hence interchangeability. Power supply requirements will be low voltage only. The bias voltage (200V to 500V) will be generated internally.

The modules will incorporate the following subassemblies:

APD Chip
Thermoelectric Cooler
APD High Voltage Power Supply (DC to DC Converter)
Thermoelectric Cooler Driver Circuit
Preamplifier (as appropriate)
TTL Output Buffer

4.1 Linear Mode, Counting Below the Breakdown

	Available Now	Target < 12 Months	"Possible"
P_d (%)	-	30% to 50% (λ dep)	Same
Max count rate*	-	> 1 Mcps	10 Mcps?
Dark count @ 22°C	-	≈ 100 cps	< 100 cps
Timing Resolution	-	≈ 20 ns	< 20 ns
Active Diameters	-	200 µm	10's to 500 µm
Afterpulsing	-	< 0.01%	< 0.01%

* (5% non-linearity at max. count rate)

4.2 Geiger Mode, Passive Quenching**

	Available Now (C30902S)	Target < 12 Months	"Possible"
P_d (%)	0 to 50%	0 to 60%	> 60%
Max count rate	Few 100's kcps	≈ 1 Mcps	> 1 Mcps?
Dark count @ 22°C	1.5×10^4 cps	Few x 10 cps	?
@ -5°C	$< 10^3$ cps (Note 1)		
Timing Resolution	< 10 ns	Few ns	< 1 ns?
Active Diameters	500 µm	200 to 500 µm	10's to 1000 µm
Afterpulsing	< few % to 10's%	< 1% to 10's%	< 0.01%

** Actual values depend on the bias above breakdown. Not all parameters are available simultaneously at the same bias.

Note 1: Custom package incorporating C30902S on thermoelectric cooler is available now.

4.3 Geiger Mode, Active Quenching**

	Available Now	Target < 12 Months	"Possible"
P_d (%)	-	0% to 60%	> 60%
Max count rate	-	Tens of Mcps	100 Mcps?
Dark count @ 22°C	-	Few 10^2 cps	?
Timing Resolution	-	Few ns	< 1 ns
Active Diameters	-	200 to 500 µm	10's to 1000 µm
Afterpulsing	-	< 1%	<< 0.01%

** Actual values depend on the bias above breakdown. Not all parameters are available simultaneously at the same bias.

5.0 ACKNOWLEDGEMENTS

This work was partially supported by an Industrial Regional Development Program grant from the Canadian government.

APPENDIX I

A.1 GAIN PROBABILITY DISTRIBUTION

The theory of photon detection using silicon APD's is described in Refs. 1, 4, 5 and 6. This Appendix summarizes the derivation of photoelectron detection efficiency from the theory, and how this impacts the optimum attainable performance of photon counting modules.

For photon counting, the output pulse height must be sufficient to exceed the threshold set in an external amplifier. The pulse is a current pulse resulting from a single photoelectron which has undergone an avalanche gain "m".

Both below and above the breakdown voltage, the gain probability distribution P(m), is highly dependent on the "effective k" of the APD design and on the applied field. k is the ratio of the electron and hole ionization coefficients. Subsequent discussions use a "constant k" assumption, which involves some degree of approximation over real device structures.

It is possible to calculate both P(m) and the average gain <m> for any given effective k at any given electric field with respect to the breakdown field [Ref. 5].

Figure A-1 [from Ref. 1] shows P(m) for a k = 0.02 APD for three cases:

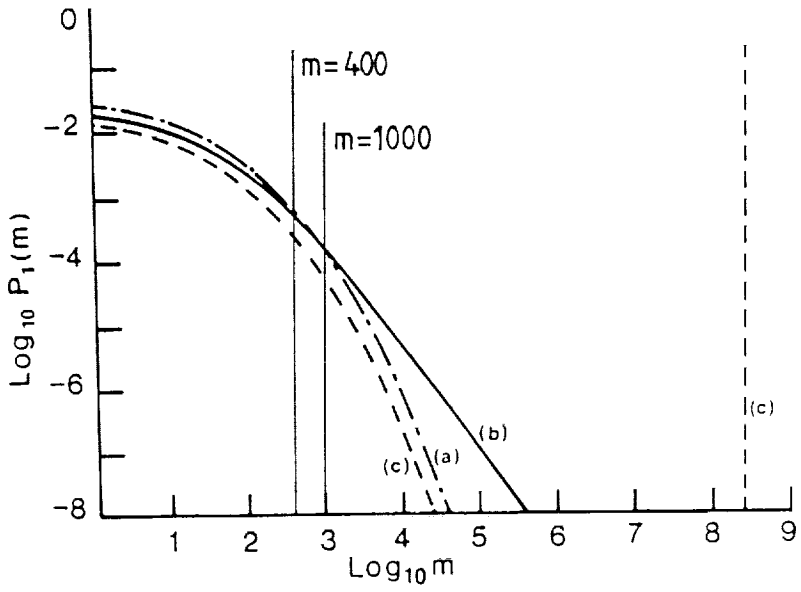

FIGURE A-1

(a) $E = E_B - 1{,}000$ V/cm

(b) $E = E_B$ = The breakdown field

(c) $E = E_B + 1{,}000$ V/cm

In case (a), $\langle m \rangle = 400$, but only 15% of photoelectrons have $m > 400$. In case (b), $\langle m \rangle = \infty$ ($>10^8$), because the tail goes to infinity, but even so, only 20% of photoelectrons have $m > 400$. In case (c), $\langle m \rangle = \infty$, and some 15% of photoelectrons lead to breakdown pulses, $m > 10^6$.

For a lower k diode at the same fields (relative to E_B), all these percentages can be substantially increased.

The allowable threshold setting depends on the amplifier noise. With low capacitance diodes (< 1.5 pF), it is possible to fabricate low-noise charge-sensitive preamplifiers with response times in the 10 ns range and equivalent noise charges (ENC's)of the order of 100 to 200 electrons (rms). Noise from the amplifier can be suppressed by setting the threshold at a level of five to eight times the rms level. Any photon which generates a pulse greater than the threshold setting can be detected. For example, refering to figure A-1, if the amplifier threshold has been set at 1000 electrons, all the distributions in the case of (a), (b) and (c) to the right of this threshold will be detected.

A.2 PHOTOELECTRON DETECTION EFFICIENCY

If the gain is sufficiently high, the output pulse height due to the absorption of a single photon will be sufficient to exceed the threshold set in an external circuit.

Figures A-2 and A-3 plot photoelectron detection efficiency, P_e, versus δ/δ_{BR} above and below the breakdown for effective k values of 0.02, 0.004 and 0.002, and for thresholds of 500 and 1000 electrons. Decreasing k increases P(m) at a given m, and hence P_e at any given δ/δ_{BR} value. δ is defined as:

$$\delta = \int_0^w \alpha(E).dx \quad \text{[Ref. 5]}$$

which integrates the electric field dependent electron ionization coefficient $\alpha(E)$ through the device depletion width w at a particular applied voltage V. The gain is related to δ and k by:

$$M = (1-k)/(k^{\delta(V)/\delta(V_{BR})}-k) \quad \text{[Ref. 5]}$$

leading to: $\delta_{BR} = -(\ln(k))/(1-k)$

Figures A-2 and A-3 may best be considered in terms of the breakdown uniformity of the APD. Performance is dominated by the first part of the active diameter to breakdown. Since the silicon doping

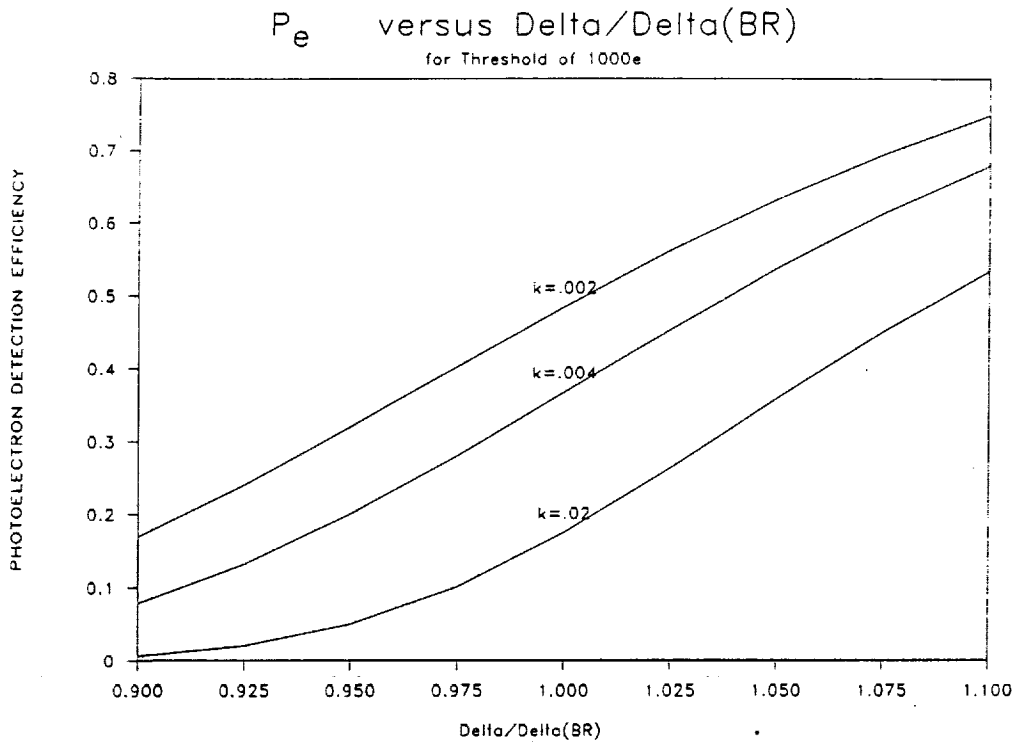

FIGURE A-2

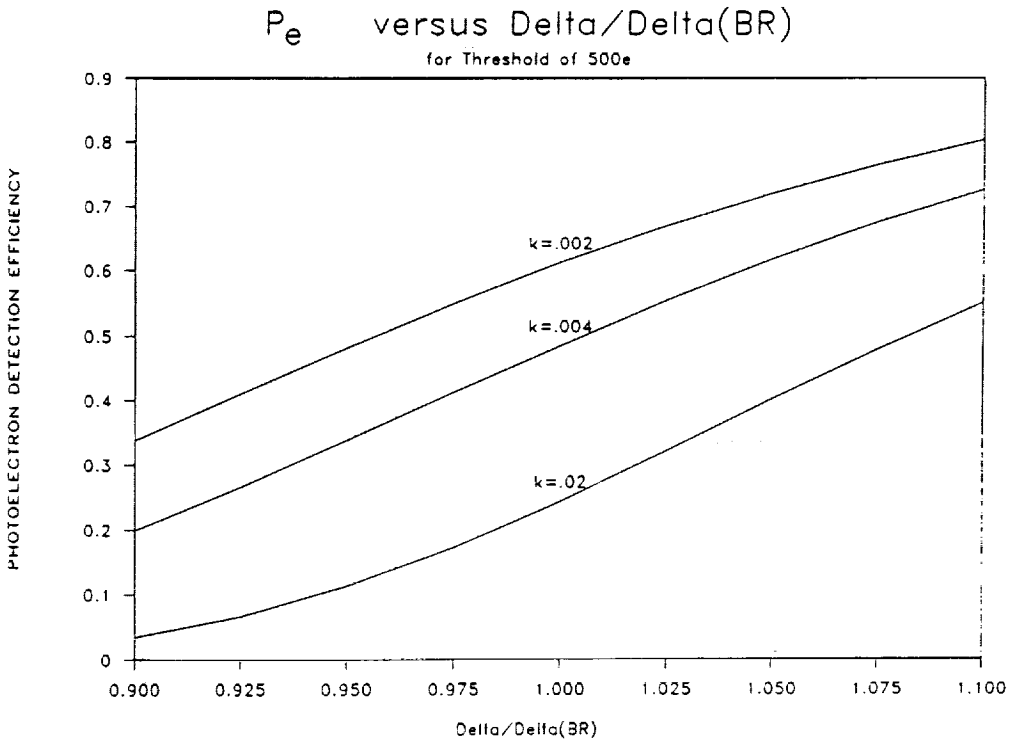

FIGURE A-3

process cannot be perfectly controlled, actual APD's vary on a chip-to-chip basis, even for chips from the same wafer. On Figures A-2 and A-3, any given APD will actually cover a band of δ/δ_B values; the width of the band reflects the processing uniformity on the actual device. A very uniform device is required if it is to be operated close to the breakdown. It is apparent that "low-k" APD's give significantly better P_e, and that working close to or above the breakdown is desirable.

At a 500 electron threshold, a perfectly uniform k = 0.002 APD working at just below V_{BR} would give a PDE of 0.61, substantially above the 0.24 predicted for a k = 0.02 APD of similar uniformity.

A.3 ACHIEVABLE APD PERFORMANCE

Effective k. To date, standard product (e.g. C30902S) has had an effective k of 0.02. Novel devices have recently been fabricated with theoretical k values of around 0.002 at visible wavelengths and measured values of k = 0.005 at 633 nm. Lower k may be possible but only for very high bias voltage APD's.

Dark Current. Improved gettering has reduced dark count levels by an order of magnitude [Ref. 4]. Room temperature dark currents of a few fA (approximately 10^4 "dark" electrons per sec) have been achieved on 0.5 mm active diameters. Actual dark counts will depend on the APD bias and temperature and on the threshold setting.

The dark count rate decreases by a factor of approximately five for a 20°C decrease in operating temperature, and can be mathematically described as proportional to exp(-0.55eV/kT).

REFERENCES

[1] R. J. McIntyre, "Recent Developments in Silicon Avalanche Photodiodes", Measurement 3, 146-152 (1985).

[2] R. G. W. Brown, K. D. Ridley, and J. G. Rarity, "Characterization of Silicon Avalanche Photodiodes for Photon Correlation Measurements. 1: Passive Quenching", Appl. Opt. 25, 4122-4126 (1986).

[3] R. G. W. Brown, R. Jones, J. G. Rarity, and K. D. Ridley, "Characterization of Silicon Avalanche Photodiodes for Photon Correlation Measurements. 2: Active Quenching", Appl. Opt. 26, 2383-2389 (1987).

[4] A. W. Lightstone and R. J. McIntyre, "Photon Counting Silicon Avalanche Photodiodes for Photon Correlation Spectroscopy". Proc. Photon Correlation Techniques and Applications, OSA, Washington, D.C., May 31 - June 2, 1988.

[5] R. J. McIntyre, "The Distribution of Gains in Uniformly Multiplying Avalanche Photodiodes. Theory", IEEE Trans. Electron Devices, Vol. ED-19, p. 703, June 1972.

[6] P. P. Webb, R. J. McIntyre and J. Conradi, "Properties of Avalanche Photodiodes", RCA Review, June 1974, pp 234-278.

DESIGN OF FIBER OPTIC PROBES FOR LASER LIGHT SCATTERING

Harbans S. Dhadwal* and Benjamin Chu†
State University of New York at Stony Brook
Stony Brook, New York

In this paper we present a quantitative analysis of the role of optical fibers in laser light scattering. Design of a general fiber optic/microlens probe by means of ray tracing is described. Several different geometries employing an optical fiber of the type used in lightwave communications and a graded index microlens are considered. Experimental results using a non-imaging fiber optic detector probe show that due to geometrical (numerical aperture and core diameter) limitations of single-mode fibers a probe using a multi-mode optical fiber has better performance, for both static and dynamic measurements of the scattered light intensity, compared with a probe using a single-mode fiber. Fiber optic detector probes are shown to be more efficient at data collection when compared with conventional approaches to measurements of the scattered laser light. Integration of fiber optic detector probes into a fiber optic spectrometer offers considerable miniaturization of conventional light scattering spectrometers, which can be made arbitrarily small. In addition static and dynamic measurements of scattered light can be made within the scattering cell and consequently very close to the scattering center.

1. INTRODUCTION

Over the past year we have seen a dramatic and new use of optical fibers in laser light scattering (LLS)[1-6]. Up until recently the use of multi-mode and single-mode fibers of the type used in lightwave communications was restricted to back-scatter anemometers of Dyott[7] and of Auweter and Horn[3]. Optical fibers used in spectrometers of the type described by Haller et al.[8] use fibers which are made from a single piece of glass or polymer and are typically 1 mm in diameter. In order to perform dynamic light scattering measurements fibers of the latter type are used in combination with lenses and aperture stops. In this paper we present a detailed design procedure for a general fiber optic

*Department of Electrical Engineering.
†Department of Chemistry and Department of Materials Science and Engineering.

probe which uses an optical fiber and a graded index microlens but no additional apertures are required. The resulting probe is typically 2 mm in diameter and no longer than 15 mm. Experimental results confirm the important role these miniature probes will play in future LLS systems.

2. THEORY AND DESIGN OF FIBER OPTIC PROBES

2.1. An optical fiber

Optical fibers used in fiber optic probes comprise two similar coaxial cylinders of silica. The inner cylinder, called the core, is usually doped with germanium and has a refractive index, n_1. The outer region, called the cladding, has a refractive index, n_2, which is usually slightly lower than n_1. Light is transmitted along the optical fiber by means of total internal reflection at the core/cladding interface. Current state of the art optical fibers are almost at the theoretical limit of performance and typically have an attenuation loss of less than 0.2 dB/km, corresponding to a 5% reduction in intensity over 1 km length of fiber. An optical fiber, which is a cylindrical dielectric waveguide has a critical acceptance angle, θ_c beyond which light is not guided along the length of the optical fiber. The sine of the critical acceptance angle in air defines the numerical aperture of the optical fiber $\left[(NA)_f = \sin(\theta_c) = \sqrt{n_1^2 - n_2^2}\right]$ [9]

Note that the light always exits from the tip of the optical fiber at the full numerical aperture, independent of the launching conditions. If the tip of the optical fiber is embedded in an arbitrary medium of refractive index, n_{em}, then the numerical aperture is accordingly reduced. Waveguiding properties of optical fibers are well understood and numerous textbooks are available on the subject. For our application in LLS instrumentation we are primarily interested in the numerical aperture, $(NA)_f$ and core diameter, D_f of the optical fiber. Optical fibers can usually support a large number of discrete modes in the guiding region, each mode being characterized by a particular cut-off fre-

quency. The normalized frequency, $V = \left[\frac{\pi D_f (n_1^2 - n_2^2)^{\frac{1}{2}}}{\lambda_o} \right]$ with λ_o being the free space wavelength, determines the cut-off between singie-mode and multi-mode fibers. For a single-mode fiber, that is, propagation of HE_{11} mode[9], V should be less than 2.405. An optical fiber with $n_1 \approx n_2 = 1.46$, $\Delta n = 0.002$ and $\lambda_o = 0.85 \mu m$ requires D_f to be less than 8.5 μm for single-mode propagation. The number of modes propagating in a multi-mode fiber is $\approx \left[\frac{2V}{\pi} \right]^2$. Wave guiding properties of optical fibers become an important consideration in the design of laser delivery systems and do not play an important role in the design of fiber optic detector probes.

2.2. SELFOC[10] graded index microlenses

The SELFOC graded index microlens is a cylindrical rod of glass with a circular cross-section. The microlens typically has a radial refractive index profile, $n(r) = N_o(1 - \frac{1}{2}Ar^2)$. N_o is the refractive index on the optical axis (r=0), A is the gradient refractive index constant and r is the radial distance from the optical axis. The optical ray is guided along the length of the microlens by periodic focussing. This is particularly strong for meridional rays and somewhat weaker for skew rays. The spatial period is referred to as the the pitch, P $(= \frac{2\pi}{\sqrt{A}})$ of the microlens. The length z of the microlens is normally specified as a fractional multiple of the pitch. The focal length, f, is given by $[N_o \sqrt{A} \sin(\frac{\sqrt{A}\, z}{2})]^{-1}$. The small size and parallel end surfaces makes the microlens a very attractive component for mating with optical fibers in order to make miniature fiber optic probes suitable for a wide variety of applications.

2.3. A general fiber optic probe

A fiber optic probe, whether to be used as a transmitter of incident optical radiation into the scattering cell or as a receiver of the scattered light from within the cell, must go through the same design criterion. A general fiber optic probe comprises an optical fiber of the type used in lightwave communications and a SELFOC graded index microlens. Careful matching of the two components gives the desired properties of the subsequent probe, which can be used either in an imaging configuration or in a non-imaging mode. The latter being more appropriate for dynamic and/or static light scattering and is a special case of the former type.

Geometrical optics, by means of ray tracing using transfer matrices[11], is employed as the design tool for describing the propagation of the laser light emanating from the tip of an optical fiber as it propagates through arbitrary stratified media. The propagating ray is defined by two parameters: , Fig. 1, its height, r at the point of intersection with a reference plane; and angle $\dot{r}$ which a particular ray makes with the optical axis. In order to make the governing equations independent of the refractive index, n, of isotropic and homogeneous media, bounded by parallel planes perpendicular to the direction of propagation, a normalized angle $v = n\dot{r}$ is used to specify the optical direction cosine of a particular ray. With this notation propagation of a ray through a series of P different media, bounded by parallel planes, can be expressed through a matrix relation

$$\begin{bmatrix} r_{p+1} \\ v_{p+1} \end{bmatrix} = \begin{bmatrix} R_p \end{bmatrix} \cdot \begin{bmatrix} R_{p-1} \end{bmatrix} \cdots \begin{bmatrix} R_1 \end{bmatrix} \begin{bmatrix} r_1 \\ v_1 \end{bmatrix} \tag{1}$$

where $[R_p]$ is a ray transfer (or ABCD) matrices for the P'th medium, $[r_1, v_1]$ and $[r_{p+1}, v_{p+1}]$ define the ray parameters in the input and output reference planes, respectively. With knowledge of the transfer matrices for different types of media the imaging conditions for an arbitrary optical system can be quickly derived. Versatility is introduced in the design stage by having an arbitrary coupling medium between the optical

fiber and the microlens, and by allowing the output face of the microlens to be embedded into an arbitrary scattering medium. The coupling and scattering media are assumed to be isotropic and homogeneous with refractive indices n_{cm} and n_{sm} respectively. The ABCD matrix for such a medium is given by[11]

$$\begin{bmatrix} 1 & \hat{l} \\ 0 & 1 \end{bmatrix} \tag{2}$$

where $\hat{l}$ is the optical path length in the medium. The microlens, a distributed lens-like medium, described in section 2.2 has a ABCD matrix[11] given by,

$$\begin{bmatrix} \cos(\sqrt{A}\,z) & \frac{1}{N_o\sqrt{A}}\sin(\sqrt{A}\,z) \\ -N_o\sqrt{A}\sin(\sqrt{A}\,z) & \cos(\sqrt{A}\,z) \end{bmatrix} \tag{3}$$

Thus for a general fiber optic probe shown in Fig. 1 the output ray parameters $[r_1, v_1]$ can be related to the input ray $[r_o, v_o]$ through the relation

$$\begin{bmatrix} r_1 \\ v_1 \end{bmatrix} = \begin{bmatrix} A & C \\ B & D \end{bmatrix} \cdot \begin{bmatrix} r_o \\ v_o \end{bmatrix} \tag{4}$$

where

$$A = \cos(\sqrt{A}\,z) - \hat{T}N_o\sqrt{A}\sin(\sqrt{A}\,z) \tag{5a}$$

$$B = \frac{1}{N_o\sqrt{A}}\sin(\sqrt{A}\,z) + \hat{l}\cos(\sqrt{A}\,z) + \hat{T}\cos(\sqrt{A}\,z) - \hat{T}\hat{l}N_o\sqrt{A}\sin(\sqrt{A}\,z) \tag{5b}$$

$$C = -N_o\sqrt{A}\sin(\sqrt{A}\,z) \tag{5c}$$

$$D = \cos(\sqrt{A}\,z) - \hat{l}N_o\sqrt{A}\sin(\sqrt{A}\,z) \tag{5d}$$

where $\hat{l} = \frac{l}{n_{cm}}$, $\hat{T} = \frac{T}{n_{sm}}$.

2.3.1. The imaging probe

The imaging condition is obtained by considering a point source in the object reference plane RP_o, that is r_o=0. The image of a point source will be another point , that is,

r_i=0 - requiring that B=0. Re-ordering Eq. (5b) gives

$$\hat{T} = \frac{\hat{t}N_o\sqrt{A}\cos(\sqrt{A}z) + \sin(\sqrt{A}z)}{[\hat{t}N_o\sqrt{A}\sin(\sqrt{A}z) - \cos(\sqrt{A}z)]N_o\sqrt{A}} \tag{6}$$

and the magnification, m ($=\frac{r_i}{r_o}$) is given by

$$m = \frac{-(N_o\sqrt{A})^2\sin(\sqrt{A}z)}{N_o\sqrt{A}\,\hat{t} - \cot(\sqrt{A}z)} \tag{7}$$

Eqs. (6) and (7) can be used to determine the position and magnification of the image for any optical fiber, microlens, coupling and scattering medium combination. Note, by replacing t by (d_o-h_1) and T by (d_i-h_2) it can be easily shown that Eq. (6) is consistent with the usual lens formula associated with spherical lenses ($n_{cm} = n_{sm} = 1.0$). h_1 and h_2 are the positions of the principal planes of the microlens as measured from the front and back surfaces, respectively. In Fig. 1, $h_1 = h_2 = \frac{1}{N_o\sqrt{A}}\tan(\sqrt{A}z)$.

2.3.2. The non-imaging probe

A fiber optic probe suitable for light scattering may have a non-imaging configuration, that is the image is at infinity ($\hat{T} = \infty$). This condition produces a collimated beam from a point source located in the front focal plane. Under the non-imaging condition Eq. (6) gives

$$\hat{t} = \frac{1}{N_o\sqrt{A}\tan(\sqrt{A}z)} \tag{8}$$

Substituting Eq. (8) into Eq. (5) and using Eq. (4) we can express the diameter, $(D_A)_p$ and divergence, $(\Delta\theta)_p$ of the collimated beam, Fig. 2, at any plane parallel to the output face of the microlens as follows

$$(D_A)_p = 2r_1 = 2\left[r_o \cos(\sqrt{A}\,z) - r_o \hat{T} N_o \sqrt{A} \sin(\sqrt{A}\,z) + \frac{v_o}{N_o \sqrt{A} \sin(\sqrt{A}\,z)}\right] \quad (9)$$

and

$$(\Delta\theta)_p = \left|\frac{v_1}{n_{sm}}\right| = \frac{r_o N_o \sqrt{A} \sin(\sqrt{A}\,z)}{n_{sm}} \quad (10)$$

Eqs. (9) and (10) can be simplified considerably if a quarter-pitch microlens is used (z=0.25P) - the equations reduce to

$$(D_A)_p = \frac{2v_o}{N_o \sqrt{A}} \quad (11)$$

$$(\Delta\theta)_p = \frac{r_o N_o \sqrt{A}}{n_{sm}} \quad (12)$$

Note that v_o is equivalent to the numerical aperture of the optical fiber in the coupling medium and $r_o = \frac{D_f}{2}$.

The collimated transmission probe, suitable for LLS, is obtained when an optical fiber is excited by a spatially coherent and quasi-monochromatic source, typically a laser, and the output end of the optical fiber is positioned in the front focal plane of the microlens. The spatial coherence and polarization of the source are preserved by using a single-mode polarization maintaining optical fiber. The disadvantage of such a delivery system is the critical alignment which has to be maintained and launching efficiencies of greater than 60% are not practically achievable.

The requirements for a non-imaging fiber optic detector probe are somewhat different from those required for the transmission probe. In this instance the fiber optic probe is illuminated by a three dimensional spatially incoherent source - that is the scattering region. For efficient dynamic light scattering (DLS) we require, according to Lastovka[12], that collection of the scattered light intensity be confined to within a small spread in the scattering vector, ensuring that the magnitude of the normalized mutual coherence function seen by the observer is significantly greater than zero. This condition usually

translates into a stringent requirement of the angle over which the detector probe should collect light from the scattering region. The maximum divergence angle, $(\Delta\theta)_p$ of the fiber optic detector probe must be less than the coherence angle $(\Delta\theta)_{coh}$, which is determined by the size of the scattering volume and is a function of the scattering angle. For a scattering volume having the shape of a parallelepiped, the coherence angle decreases from a maximum value at a scattering angle $\theta = 90^o$ to zero at $\theta = 0^o$ [1]. Note that this dependence is significantly different from that given by Lastovka for a rectangular parallelepiped scattering region of fixed volume[12]. The angular dependence of $(\Delta\theta)_{coh}$ suggests that there will be an optimum fiber optic detector probe at each scattering angle. However, as discussed by Dhadwal and Chu[1] commercially available optical fibers and graded index microlenses cannot take advantage of this optimization.

It should, however, be noted that for the non-imaging detection configuration the optical fiber provides a spatial filtering of the angular spectrum of the light wavefield. Thus spatial coherence properties of the optical fiber are of no consequence as far as the performance' of the detector probe is concerned. According to Eqs. (11) and (12) the core diameter and the numerical aperture of the optical fiber dictate the properties of the composite probe.

Three fiber optic detector probes using single-mode and multi-mode optical fibers were constructed. The three probes had aperture diameters of 1.3 mm, 0.410 mm and 0.410 mm and divergence angles (in air) of 0.3 mrad, 5.0 mrad and 25 mrad respectively.

In this section we have outlined a generalized approach to the design of fiber optic probes. The accuracy between the predicted and measured characteristics, of course, depends upon the accuracy of the governing constants and input parameters. In particular, the optical fiber has been assumed to be a planar extended source whose near field radiation pattern is adequately defined by its core diameter and numerical aperture. The approximation is generally very good for multimode optical fibers but for single-

mode fibers the $(NA)_f$, as defined by $\sqrt{n_1^2 - n_2^2}$ [9], is an overestimation. However, the near field radiation pattern may be measured for a more precise estimate [13]. Other configurations, using different values of z for the microlens, may also be employed to design fiber optic detector probes. On occasion it may be advantageous to use a 0.23P microlens - allowing possible use of a coupling medium.

3. EXPERIMENTAL RESULTS

3.1. Performance of fiber optic detector probes

A laser beam from a Spectra Physics He-Ne laser (#SP124B) was focussed into an aqueous suspension of 0.176 μm nominal diameter latex spheres. The focussed spot had a beam waist of $\approx 168 \mu m$ diameter. The concentration of the sample was $\approx 10^{-8}$ g/ml. The same sample was used for all of the measurements reported in this paper. Each of the detector probes described in the previous section was mounted on the rotation arm of a goniometer in a conventional laser light scattering spectrometer as shown in Fig. 3. In all cases the scattered light intensity was detected by the same photomultipler (EMI 9863B/350) and electronic processing of the signal was identical. A Brookhaven Instruments 4-bit digital correlator (#BI2030) was used to measure the intensity-intensity correlation function. In addition an Hewlett-Packard photon counter (#5316A) was used to record the signal count rate.

Measurements of the un-normalized intensity-intensity correlation function, $G^2(\tau)$ $(=A\,[1 + \beta\,|\,g^{(1)}(\tau)\,|\,^2])$[14] were made at several scattering angles for each of the detector probes described in section 2.3.2. A is the baseline, β is the spatial coherence factor, τ is the delay time and $g^{(1)}(\tau)$ is the normalized first order electric field correlation function. Fig. 4 shows a plot of the normalized correlograms, $\left[\frac{G^{(2)}(\tau)}{A} - 1\right]$ at a scattering angle of 30 ^{o}. Curves I, II and III correspond to measurements made with probes 1, 2

C-2

and 3 respectively. The intercept of the ordinate axis in Fig. 4 indicates the value of β, which as expected is the largest for the single-mode fiber optic detector probe.

In order to obtain a quantitative assessment of the accuracy of the measurements each data set was analyzed using an established non-linear least squares curve fitting procedure based on the method of cumulants[14,15]. The function $g^{(1)}(\tau)$ can be related to the normalized linewidth distribution function $G(\Gamma)$ by a Laplace transform

$$g^{(1)}(\tau) = \int_{\Gamma_{min}}^{\Gamma_{max}} G(\Gamma)\exp(-\Gamma\tau)d\Gamma \tag{13}$$

where $G(\Gamma) = 0$ for $\Gamma<\Gamma_{min}$ and $\Gamma>\Gamma_{max}$. The curve fitting procedure gives values of β, $\bar{\Gamma}$ and $\frac{\mu_2}{\bar{\Gamma}^2}$, with

$$\bar{\Gamma} = \int_{\Gamma_{min}}^{\Gamma_{max}} \Gamma G(\Gamma)d\Gamma \tag{14a}$$

$$\mu_2 = \int_{\Gamma_{min}}^{\Gamma_{max}} (\Gamma - \bar{\Gamma})^2 G(\Gamma)d\Gamma \tag{14b}$$

Estimates of $\bar{\Gamma}$ were within 1% of the expected value for probes 1 and 2 and within 2% for probe 3. The spatial coherence factor β, which is a measure of the efficiency of the probe for DLS was also computed from the least squares curve fitting. We note from Fig. 4 that probes 1,2 and 3 have β values of 0.78, 0.21 and 0.004 respectively.

Performance of the fiber optic detector probes was compared with a detection arrangement used in a conventional spectrometer described by Chu et al.[16] - they used an eyepiece detector made by Gamma Scientific to measure the static and dynamic properties of the scattered light. This arrangement has been described by Dhadwal et al.[2] in connection with the fiber optic detector probes and will not be elaborated upon in this paper, except to note that the eyepiece detector has an effective divergence angle of 0.6 mrad and a beam diameter of 1.4 mm. Fig. 5a shows a semi-log plot of the normalized

correlograms, $\left[\frac{G^{(2)}(\tau)}{A} - 1\right]$ at a scattering angle of 60^{o}. For this plot and Figs. 6 and 7 triangles, squares and diamonds represent measurements made with the eyepiece detector and fiber optic detector probes 1 and 2, respectively. Fig. 5b shows the percentage of relative deviations obtained from a second order cumulant fit to the data shown in Fig. 5a. Efficiency of the various detector probes was determined by computing the accumulation times required to achieve a baseline and a net count of one million in the intensity-intensity correlation function. The two respective times being defined by $t_{base} = \frac{A}{\bar{n}^2 \Delta t}$ and $t_{net} = \frac{1}{\beta} t_{base}$, respectively[2]. $\bar{n}$ is mean signal count rate (counts/second), Δt is the sample time in seconds. Figs. 6 and 7 show a plot of t_{base} and t_{net} for probes 1, 2 and the eyepiece detector. From Figs. 6 and 7 it can be ascertained that probe 2 is the best choice for both static and dynamic measurements of the scattered light intensity. This is contrary to what might have been expected based on β values only. It should be noted that light from the eyepiece was coupled to a photomultiplier by means a fairly lossy optical fiber, which if replaced or removed, could result in an improvement in the accumulation times by an additional factor of 4.

3.2. Evaluation of a fiber optic light scattering spectrometer

As described by Dhadwal and Chu[1] the fiber optic probes described above were integrated into a light scattering spectrometer which had no moving parts and the detector probes were inserted directly into the scattering cell at various fixed scattering angles, Fig. 8. Fig. 9a shows a plot of the normalized intensity-intensity correlation function with probe 1 inserted into the 90^{o} scattering port. Fig. 9b shows a relative deviations plot indicating an extremely good third order cumulants fit to the data. Again estimates of $\bar{\Gamma}$ were within 1% of the expected values and a variance value of 0.03 was well within the expected range for an aqueous suspension of latex spheres.

4. SUMMARY

In this paper we have quantitatively shown the important role that fiber optic/microlens detector probes will play in future LLS systems. The probe is no more than 2.0 mm in diameter and has a typical length of 15 mm. The performance of the multi-mode fiber optic detector probe is far superior than both the existing conventional light scattering detection geometries as well as the single-mode fiber optic detector probe. The fiber optic detector probes can be integrated into existing light scattering spectrometers or form an integral part of new spectrometers. These new developments will truly make LLS a far more versatile tool to be used in an industrial environment as well as in a research laboratory.

5. ACKNOWLEDGEMENTS

We wish to thank Dr. C. Wu, who helped with some of the experiments described here.

REFERENCES

1 H.S.Dhadwal and B.Chu,*A Fiber Optic Light Scattering Spectrometer*, Rev. Sci. Instrum., in press

2 H.S.Dhadwal, C.Wu and B.Chu,*Fiber Optic Probes For Laser Light Scattering*, submitted for publication App. Opt.

3 H. Auweter and D. Horn, J. Colloid and Interface Sci., **105**, 399 (1985)

4 R.G.W.Brown, App. Opt., **26**, 4846 (1987)

5 R.G.W.Brown, J.Phys. E:Sci. Instrum., **20**, 1503 (1987)

6 H.S.Dhadwal and B.Chu, J. Colloid and Interface Sci., **115**, 561 (1987)

7 R.B. Dyott, Microwave Opt. Acoust., **2**, 13 (1978)

8 H.R.Haller, C.Destor and D.S.Cannell, Rev. Sci. Instrum., **54**, 973 (1983)

9 T.Okoshi, *Optical Fibers*, (Academic Press, New York, 1982)

10 SELFOC - trademark of NSG America Inc., 28 Worlds Fair Drive, Somerset, New Jersey 08873

11 A. Gerrard and J.M.Burch, *Introduction to Matriz Methods in Optics*, (John Wiley and sons, London, 1975)

12 J.B.Lastovka, *Light Mixing Spectroscopy and the spectrum of light scattered by thermal fluctuations in liquids*, Ph.D thesis , M.I.T. (1967)

13 D. Marcuse, *Principles of Optical Fiber Measurements*, (Academic Press, London,

14 B.Chu, J.R.Ford and H.S.Dhadwal in *Methods of Enzymology. vol 117*, eds. S.Collowick and N.O.Kaplan (Academic Press, Orlando, Florida, 1985)

15 D.E.Koppel, J. Chem. Phys., **57**, 4814 (1972)

16 B.Chu ans C.Wu, Macromolecules, **19**, 1285 (1986)

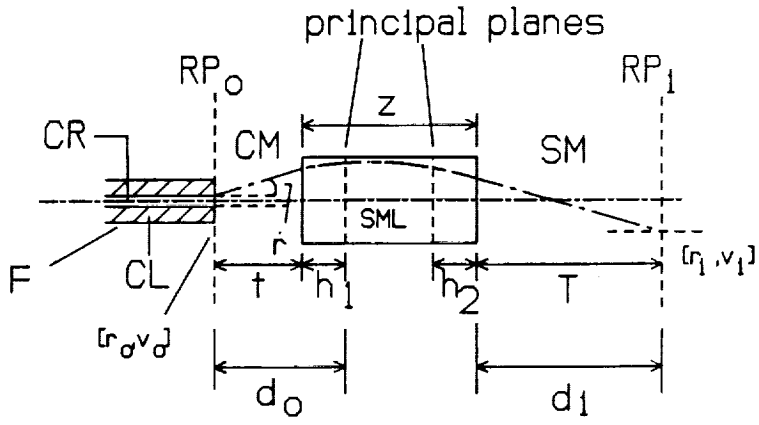

Figure 1 - Schematic of a fiber optic probe. SML- SELFOC[10] graded index microlens; RP_0 and RP_i are the object and image reference planes; h_1 and h_2 are the principal planes of the microlens measured from the two end faces; CL and CR are cladding and core regions of the optical fiber (F) respectively; d_o and d_i are the object and image distances measured from the principal planes; n_{cm} - refractive index of coupling medium; n_{sm} - refractive index of scattering medium. The dash-long dash line indicates a typical ray path through the optical system.

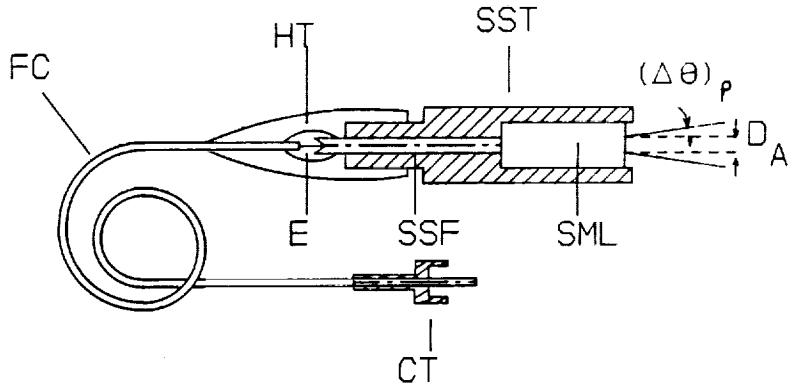

Figure 2 - Schematic of a typical fiber optic detector probe. SST - a machined piece of cylindrical stainless steel; SML - SELFOC[10] microlens; SSF - a stainless steel or ceramic ferrule used for mounting the bare optical fiber; E - epoxy used for holding fiber in ferrule; HT - heat shrink tubing; FC - fiber cable; and CT -SMA type II male connector. $(D_A)_p$ and $(\Delta\theta)_p$ are the effective detector aperture and divergence angle, respectively, as defined in Eqs. (11) and (12).

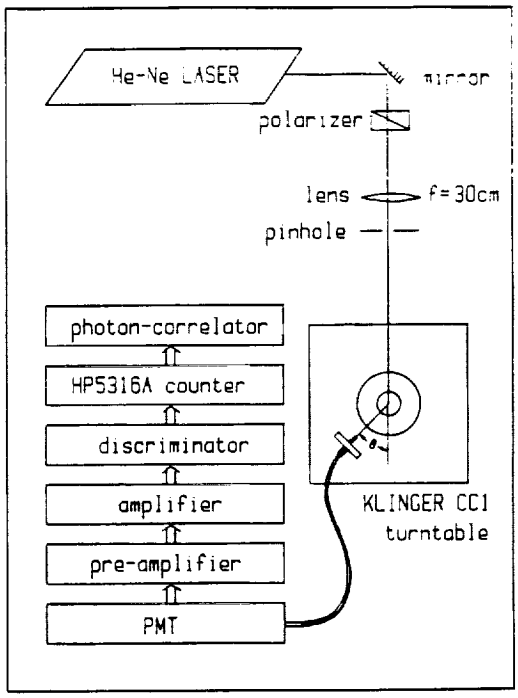

Figure 3 - Schematic layout of the optical spectrometer used to obtain the static and dynamic measurements of the scattered laser light.

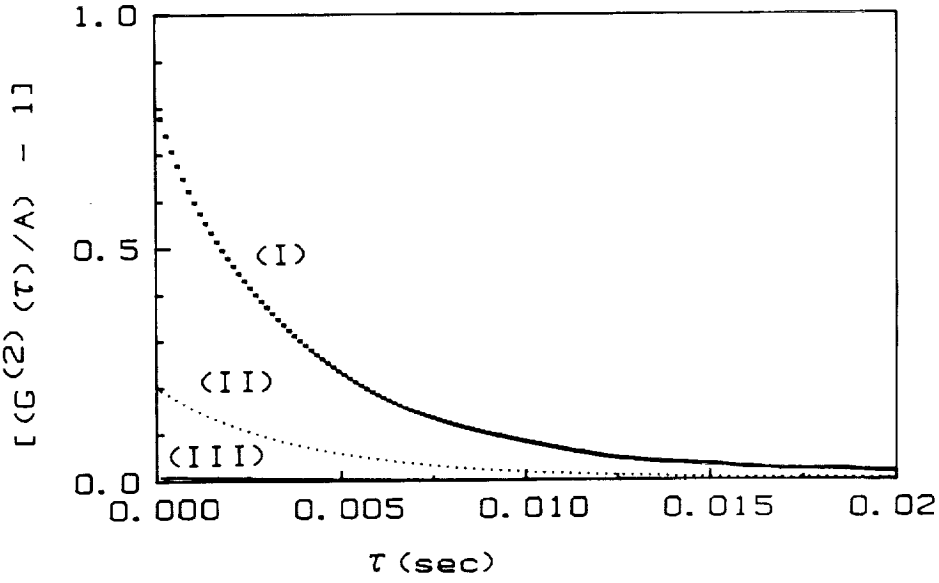

Figure 4 - Normalized intensity-intensity correlation data obtained from a dilute ($C \approx 10^{-8}$g/ml) aqueous suspension of polystyrene latex spheres of nominal diameter 176 nm. Measurements were made at $\theta = 30°$ using a modified conventional spectrometer[16]. Curves I, II and III are the corresponding correlograms obtained, under identical conditions, for probes 1, 2 and 3, respectively. The $[(D_A)_p, (\Delta\theta)_p]$ values of the probes were [1.29 mm, 0.3 mrad], [0.41 mm, 5 mrad] and [0.41 mm, 25 mrad], respectively. Third order cumulants analysis of the three data sets gave β values of 0.78, 0.20, and 0.01; $\overline{\Gamma}(sec^{-1})$ values of 128, 130, 132; and variance values of 0.10, 0.05 and 0.08 for the three probes, respectively. ($\overline{\Gamma} = \int_{\Gamma_{min}}^{\Gamma_{max}} \Gamma G(\Gamma) d\Gamma$ and the variance is defined by $\frac{\mu_2}{\overline{\Gamma}^2}$ with $\mu^2 = \int_{\Gamma_{min}}^{\Gamma_{max}} (\Gamma - \overline{\Gamma})^2 G(\Gamma) d\Gamma$).

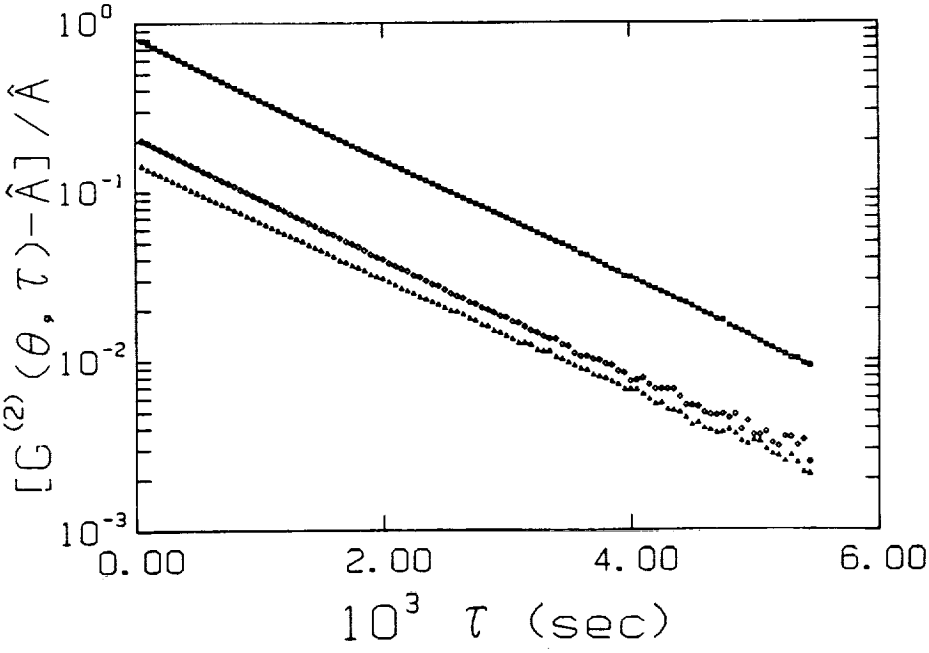

(a) - A semi-log plot of the normalized intensity-intensity correlation function at a scattering angle of 60°. τ is the delay time increment. Triangles, squares and diamonds correspond to measurements made with eyepiece, probe 1 and probe 2, respectively;

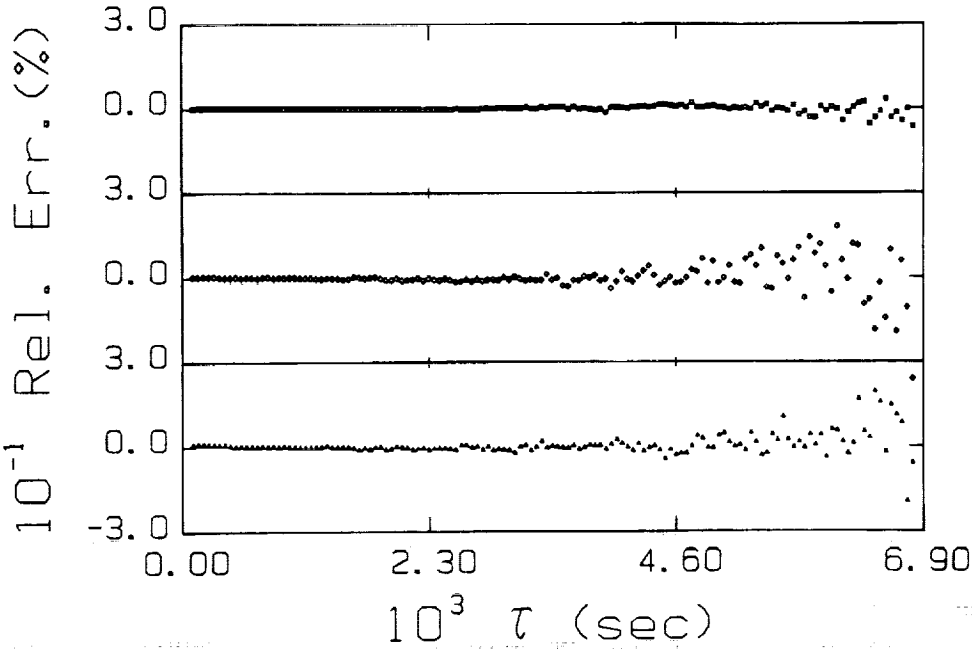

(b) - A plot of the percentage of relative deviations obtained from a non-linear least squares fit to the data shown in Fig. 4.

Figure 5 - Comparison of the dynamic light scattering measurements made with probes 1 and 2 and the eyepiece detector. The sample under investigation was as described in Fig. 4.

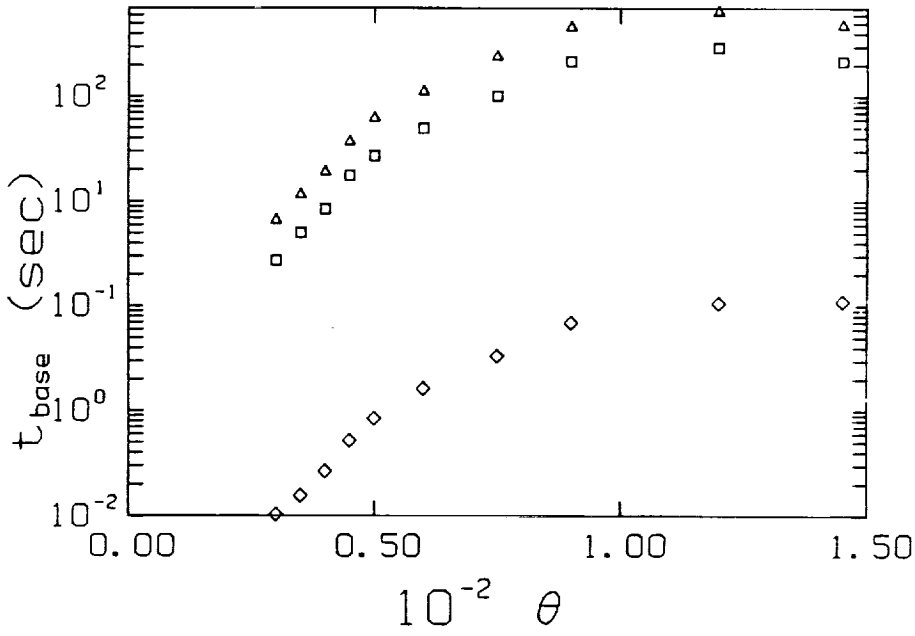

Figure 6 - A plot of the accumulation time, $t_{base} = \frac{A}{\bar{n}^2 \Delta t}$, required to achieve a baseline count A, of say, one million. Note there is an arbitrary scaling factor 16 which is internal to the Brookhaven digital correlator. $\bar{n}$ is the mean signal count rate and Δt is the sample time.

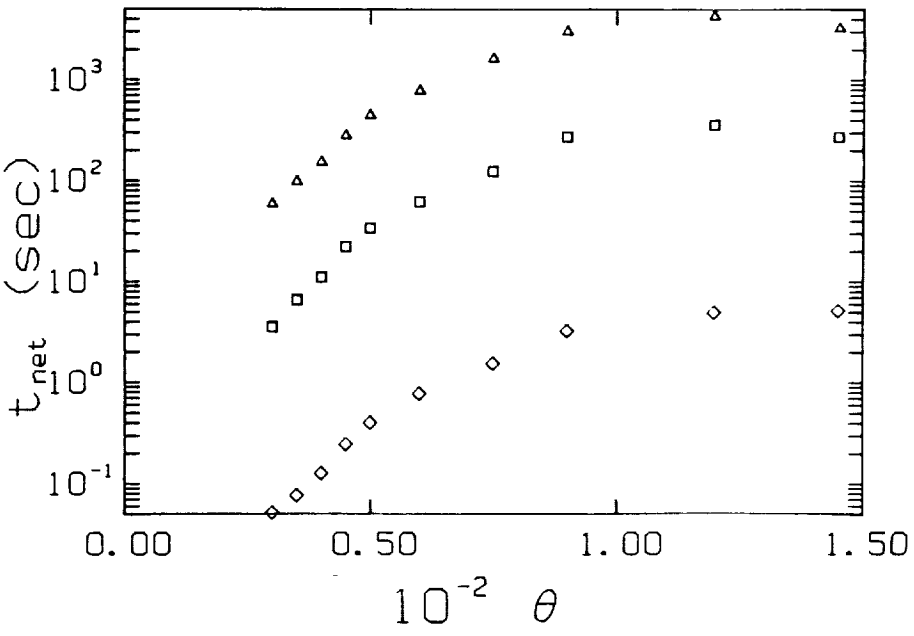

Figure 7 - A plot of the net accumulation time, $t_{net} = \frac{t_{base}}{\beta}$, required to achieve a net count Aβ, of say, one million. β is the spatial coherence factor.

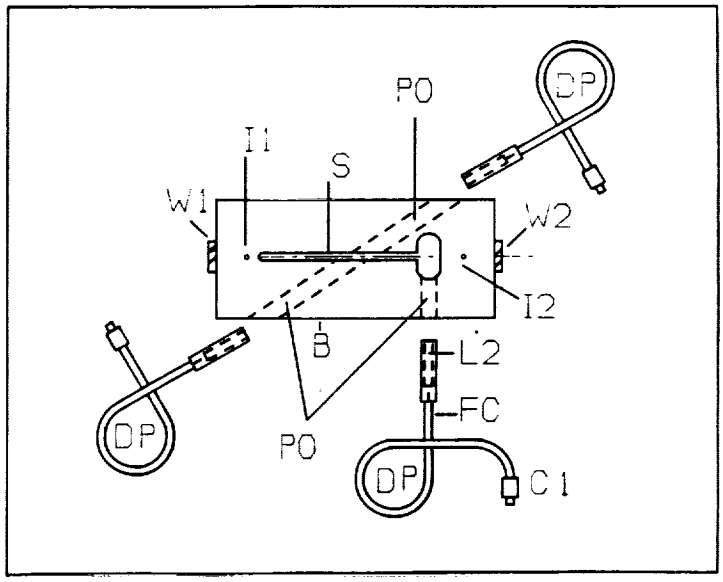

Figure 8 - Schematic of the fiber optic light scattering spectrometer. B - the lower stainless steel block; PO - three of the possible 14 detector probe ports (not shown); S - scattering cell of total volume 0.3 ml; I1 and I2 are input and output ports for use as a flow cell respectively; W1 and W2 are entrance and exit windows respectively; DP - detector probes; L2 - microlens; FC - fiber cable; C1 - SMA type II male connector. The small dash-long dash line indicates the path of the incident laser beam.

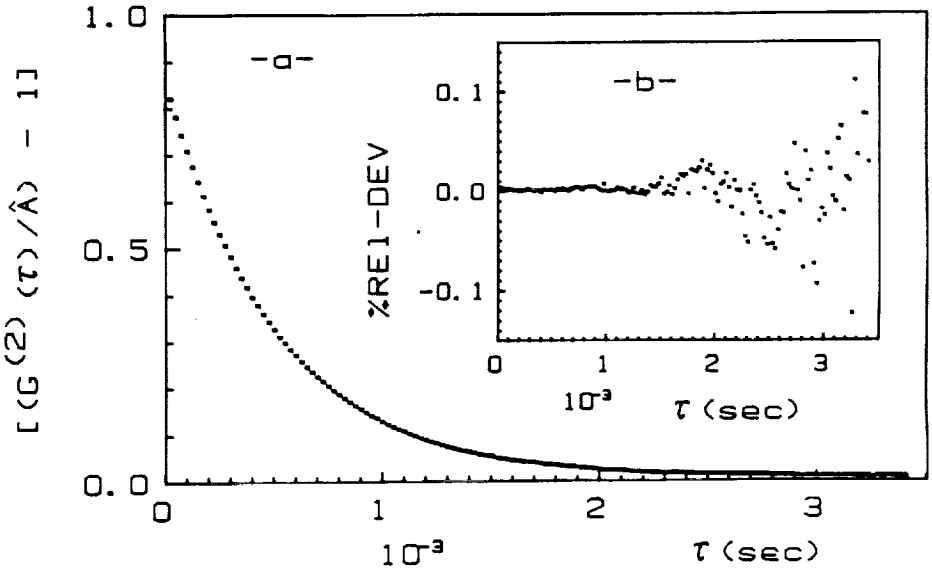

Figure 9 - Dynamic light scattering measurements using the fiber optic spectrometer described by Dhadwal and Chu[1]. Curve (a) is the normalized intensity-intensity correlation function $\left[\frac{(G^{(2)}(\tau))}{\hat{A}} - 1\right]$ obtained using probe 1 positioned in the 90° detector port, Fig. 8. A third order cumulants fit gave values of 0.83, 963, 0.03 for β, $\overline{\Gamma}$ and $\frac{\mu_2}{\overline{\Gamma}^2}$, respectively. Curve (b) shows the percentage of relative deviations, [(date-fit)/fit] × 100.

MAXIMUM LIKELIHOOD TECHNIQUES IN QELS

Robert V. Edwards
Chemical Engineering Department
Case Western Reserve University
Cleveland, Ohio

A framework for the analysis of QELS experiments designed to be used in micro–gravity environment is derived. Example calculations of the type to be used to design the QELS system are given.

0.0 Introduction

Since the announcement [1] of dynamic laser light scattering as a method of measuring the size statistics of small particles suspended in solution, many have looked for an efficient method of extracting the statistics. The methodology's initial appeal was that it could be very fast compared to competing methods such as electron microscopy and that it was non–obtrusive. Indeed, mean particle sizes could be obtained with an accuracy of 3% in less than five minutes. However, getting other moments of the particle size distribution proved to be a daunting challenge.

For almost ten years, attempts were made to generate algorithms for extraction of the particle size statistics with little regard to the possible resolution of the methodologies. Measurement times expanded from five minutes to days. Finally, in 1978, McWhirter and Pike [2] published a seminal paper that demonstrated that the possible resolution of the particle size distribution was directly related to the noise on the measured correlogram and thus to the averaging time. Roughly, the resolution is inversely proportional to the square root of the averaging time.

McWhirter and Pike also made some shrewd guesses that the resolution would not be the same for every size particle. They consequently recommended logarithmic and geometric ratio distributions of intervals with which to represent the particle size histogram. Several computer programs based on their work are available.

Recently, Cummins and Staples [3] published a paper where they incorporated the above mentioned concepts, but added the concept of using the data from several different angles at the same time. It takes advantage of the fact that the Mie coefficients for the scattering power of each size can be computed *a priori*. The additional information obtained by this technique appears to greatly increase the obtainable resolution. Even more resolution may be obtained using *a posteriori* classical light scattering data.

Like many mature experimental techniques, QELS has a well developed set of methodologies. Some of them are based on established basic research, others are based on what could be called the "mythology" of the experienced users of the technique. This mythology is loosely based on basic research, but has usually never been subjected to rigorous analysis or testing under the conditions that obtain in a given experiment. Let me hasten to add that I am not questioning the truth of these myths. It is simply that their rigor and applicability under all conditions has never been checked. Example statements of this type are: "You need 1 million counts to get a good correlation function". You only need 16 points in the correlogram, if you space them right." ...

As is well known, any experiment with noise in it is incompletely specified until some method of dealing with the noise is specified. Otherwise, there are an infinity of solutions that will satisfy the experimental requirements equally well. Usually, the problem specification is completed by using a form of least–squares procedure to solve for the desired experimental parameters. As I will show below, greater care than is typically shown should be given to this part of the problem specification. Failure to do this may result in algorithms for extracting the experimental parameters that are intrinsically biased.

The framework for the analysis here will be based on the concepts of parameter estimation typified by Maximum Likelihood Estimation (MLE) methods. There are other parameter estimation schemes in the literature. However, the essential attributes of the methods are all contained in MLE. These methods not only serve as the template for parameter estimation algorithms, but can also be used for optimal design of the experiments. Optimal design of experiments is facilitated by the fact that these methods not only give procedures for parameter estimation, but also estimates of the errors associated with the parameter estimation.

Since the technique is not that well known, I will include a brief tutorial on MLE.

1.0 PARAMETER ESTIMATION

1.0 Maximum Likelihood Estimation

Suppose you have a model of what a data set should look like – a model function $f(n,\alpha)$. The independent variable is denoted n and α represents the set of parameters of the model function. For instance, in a QELS experiment for a monodispersed sample, f( ) would be given by

$$f(n,\alpha) = \alpha_0 \exp(-\alpha_1 \Delta t n)$$

where α_0 is the initial point, α_1 is the decay rate and Δt is the time interval for each measurement count. The parameters to be estimated are α_0 and α_1.

You could try to obtain the parameters α by simply varying α_0 and α_1 until you match the data exactly. Of course, you can never do it that easily for the simple reason that the data always has "noise" in it. In practice, you vary the coefficients α until you have obtained a "best" fit. Least Squares is a popular method for doing this.

Before going into the formal structure of paramenter estimation schemes, I will give an

example of a typical problem and an example of how not to solve the problem. Consider the simple QELS experiment outlined above.

Engineers are usually taught that the way to do this problem is to take the log of the data and plot it against t. The resulting plot should be a straight line which is then usually fit using a least squares procedure. That procedure made some sense in the days before computers and handheld calculators. I will show here that this procedure is incorrect and guaranteed to give the wrong answers! In the following, I assume that the data were taken by sampling at regular time intervals, so that the time will be identified by the variable n, n= 0,1,2,3 ...

In any experiment, there will be "noise" on the data. I will assume for purposes of illustration that the noise here is solely due to photon shot noise. Such errors are approximatedly Gaussian with a constant variance. i.e.

$$d(n) = \alpha_0 \exp(-\alpha_1 n) + \epsilon_n,$$

where ϵ_n is the error at each point. Saying that the statistics are Gaussian is to say the the pdf for ϵ_n is given by

$$p(\epsilon) = \frac{1}{\sqrt{2\pi\sigma^2}} \exp(-\frac{\epsilon^2}{2\sigma^2}). \qquad 1.0.2$$

The variance of the error is independent of the time n. The pdf for the log of the data can be derived, however here I will use an approximate model here to demonstrate the problem with using the logarithm.

Take the log of the data.

$$\log(f(n)) = \log(\alpha_0 \exp(-\alpha_1 n) + \epsilon_n) = \log((\alpha_0 \exp(-\alpha_1 n)(1 + (\epsilon_n/\alpha_0)\exp(\alpha_1 n)))$$

$$= \log(\alpha_0) - \alpha_1 n + \log(1 + (\epsilon_n/\alpha_0)\exp(\alpha_1 n)). \qquad 1.0.3$$

The noise term for the log of the data, $\log(1 + (\epsilon_n/\alpha_0)\exp(\alpha_1 n))$, is clearly a function of time, n, and does not have a constant variance. Note that for large values of n, the term $(\epsilon_n/\alpha_0)\exp(\alpha_1 n)$ can approach ± 1. For a +1 variation, nothing extraordinary happens, but for a fluctuation of the size −1, one has an error term of the order log(0) ($=-\infty$)! In other

words, negative fluctuations are heavily emphasized over positive fluctuations. Further, the fluctuations can make f(n) negative, whereupon you can not take the logarithm. You are forced to eliminate all negative points or truncate the data at the first occurence of a negative point. I object to either option, since experience shows that taking data is very expensive and to throw out data points is unnecessarily costly. Further, it will bias the results of the experiment. The bias of the data toward emphasizing negative fluctuations will always bias the results toward overestimating the magnitude of α_1 and α_0.

To illustrate this, I will do a simulated experiment. The model function is

$f(n) = 100\exp(-.3n)$.

Then zero mean Gaussian noise of expected variance 16 was added to the data. Figure 1.1 shows a plot of the log of the data truncated at the first negative point.

Using a least squares on the log of the data, I obtained values for the parameters

$\alpha_0 = 127,\ \alpha_1 = 0.3595.$

Not bad, but it suggests the bias I mentioned above. The values for α_0 and α_1 are on the high side.

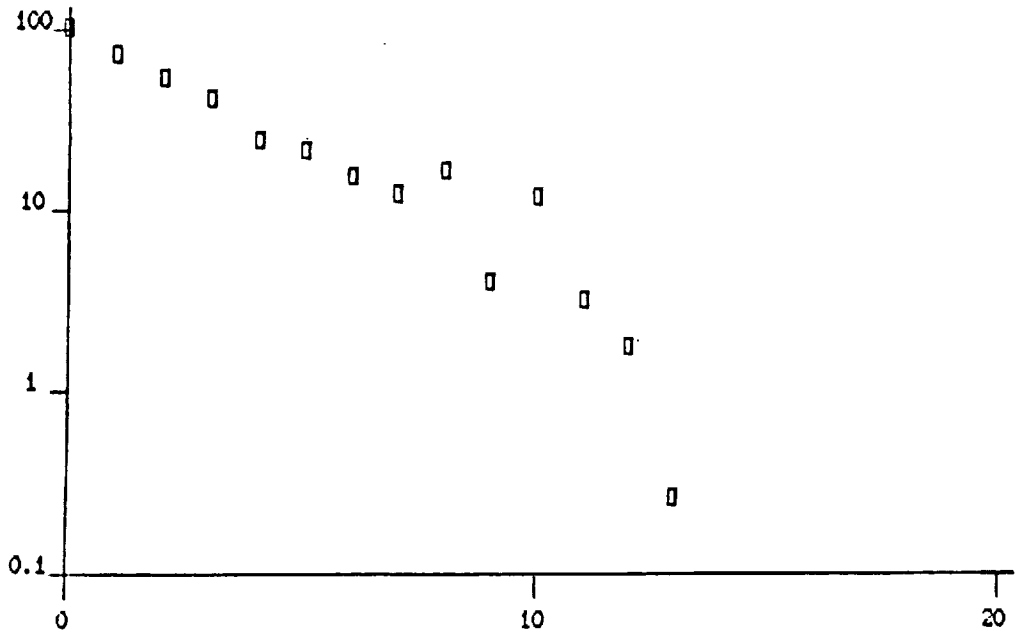

Figure 1.1

There are really two problems to deal with here. It is possible to still use a least squares procedure, but it will be a nonlinear one since it will have to deal with the nonlinear coefficient α_1. Second, it is not obvious that least squares is the correct procedure to use. At this point, all we know is that least squares is popular and software to do it is readily available. In what follows, a plausible framework to arrive at the correct procedure to handle problems of this sort will be derived. Later, procedures for dealing with the nonlinear equations derived will be discussed.

A formal method of extracting parameters from noisy data is the so–called Maximum Likelihood Estimation process. Let $p(\{d_n\} \mid \boldsymbol{\alpha})$ be the probability of a data set $\{d_n\}$ given the set of parameters $\boldsymbol{\alpha}$. In other words, a procedure for calculating the probability of the data set, if you know $\boldsymbol{\alpha}$. The MLE method consists of varying $\boldsymbol{\alpha}$ until the probability of the data set is maximized. The trick is to find an expression for the probability of the data set. The rest is purely numerical analysis.

The secret to finding the probability of a data set is to have a model for the measured fluctuations in the data, i.e. the noise. In the QELS experiment described above the errors ϵ has a Gaussian pdf. In that example, $p(d_n \mid \boldsymbol{\alpha})$ is given by

$$p(d_n \mid \boldsymbol{\alpha}) = p(\epsilon) = \frac{1}{\sqrt{2\pi\sigma^2}} \exp\left(-\frac{(d_n - f(n,\boldsymbol{\alpha}))^2}{2\sigma^2}\right), \qquad 1.0.4$$

where $f(n,\boldsymbol{\alpha}) = \alpha_0 \exp(-\alpha_1 n)$.

Often, the data at each measurement point is statistically independent of the data in every other interval, thus the errors are independent random variables. Then using the formula for the joint probability of multiple independent random variables, we get the probability of the data set given $\boldsymbol{\alpha}$ as

$$p(\{d_n\} \mid \boldsymbol{\alpha}) = p(d_1 \mid \boldsymbol{\alpha}) p(d_2 \mid \boldsymbol{\alpha}) p(d_3 \mid \boldsymbol{\alpha}) \ldots = \prod_n p(d_n \mid \boldsymbol{\alpha}). \qquad 1.0.5$$

Since the log of a function is a maximum when the function is a maximum, most users prefer to use the log of the probability. The log of the probability of the data set is given by

$$\log p(\{d_n\} \mid \boldsymbol{\alpha}) = \sum_n \log p(d_n \mid \boldsymbol{\alpha}). \qquad 1.0.6$$

Finding the set of parameters α that will maximize the probability of the data set is done by solving the set of equations

$$\frac{\partial \log\ p(\{d_n\}\,|\,\alpha)}{\partial \alpha_i} = 0.\ \ i = 1,2,3,\ \ldots \qquad 1.0.7$$

subject to the usual constraints that the second derivatives be negative. These are called The Maximum Likelihood Equations [4]. Since we have the data set $\{d_n\}$ and the model function $f(n,\alpha)$, and an explicit function for $p(\{d_n\}\,|\,\alpha)$, the problem is now completely specified.

1.1 Gaussian Processes

Let us see what the explicit equations look like for the simplified QELS experiment.

$$\log p(d_n\,|\,\alpha) = -\frac{(d_n - f(n,\alpha))^2}{2\sigma^2} - 0.5\log 2\pi\sigma^2.$$

$$\log p(\{d_n\}\,|\,\alpha) = -\sum_n \frac{(d_n - f(n,\alpha))^2}{2\sigma^2} - 0.5\sum_n \log 2\pi\sigma^2. \qquad 1.1.1$$

Since in this example σ is not a function of α, this problem is solved by maximizing the first sum in the expression above, or minimizing minus the expression. This is exactly a least squares procedure. We have shown that for a measurement process with constant Gaussian errors, the MLE method is identical to a least squares procedure.

If the variance of the measurements, σ^2 was a function of α and/or n, the method would be a weighted least squares procedure. In that case, the terms involving derivatives of σ^2 would have been kept.

1.2 Residuals

A question that often arises is how you tell if you used the correct model function and statistics. That question can be answered by examining the so–called weighted residuals.

$$\text{Let } w_n = \frac{(d_n - f(n,\alpha))}{\sigma(n,\alpha)}. \qquad 1.2.1$$

It is the difference between your measured data point and the model function weighted by the function $\sigma(n,\alpha)$, the expected standard deviation at that point. The calculation of the

standard deviation changes depending on what kind of statistics you think you have. Here, we have assumed Gaussian statistics.

$$\langle w_n \rangle = \left\langle \frac{(d_n - f(n,\alpha))}{\sigma} \right\rangle = 0.$$

$$\langle w_n^2 \rangle = \left\langle \frac{(d_n - f(n,\alpha))^2}{\sigma^2} \right\rangle = \frac{1}{\sigma^2} \langle (d_n - f(n,\alpha))^2 \rangle = \frac{\sigma^2}{\sigma^2} = 1.$$

The mean is zero and the expected variance is 1.

The weighted residuals should be a set of random numbers with a mean of zero and a variance of one. Further, since a critical assumption in the analysis to this point is that the residuals are independent of each other, the weighted residuals should also be independent of each other. A plot of the weighted residuals should appear to be featureless. There should be no apparent pattern in it.

If there is a pattern in the residuals plot or if the mean or vaiance are incorrect, then the model function or the statistics are wrong.

Figure 1.2.1 shows a plot of the residuals for the QELS example where the fit was done using a non–linear least squares (MLE) procedure. Note the lack of an apparent pattern. However, note also that the variance is not 1. It is fairly typical when you are doing a problem with Gaussian statistics that you don't know the variance. All you know is that the variance is constant. In that case, you get the same information about the goodness of the fit fron a weighted residuals plot as you do from an unweighted one. In fact, the variance can be estimated from the residuals data. In this example, it was calculated to be 14.4.

Figure 1.2.2 is a plot of the residuals for the same simulated data, but using the fit obtained by taking the logarithm of the data. Notice how large the residuals are at the beginning of the data set. This is fairly typical of fits made to the log of the data. As predicted, the fit tended to emphasize the smaller values in the data. This residuals plot obviously has structure in it. Structure in the residuals is a sure clue that the assumed statistics or the model function is incorrect.

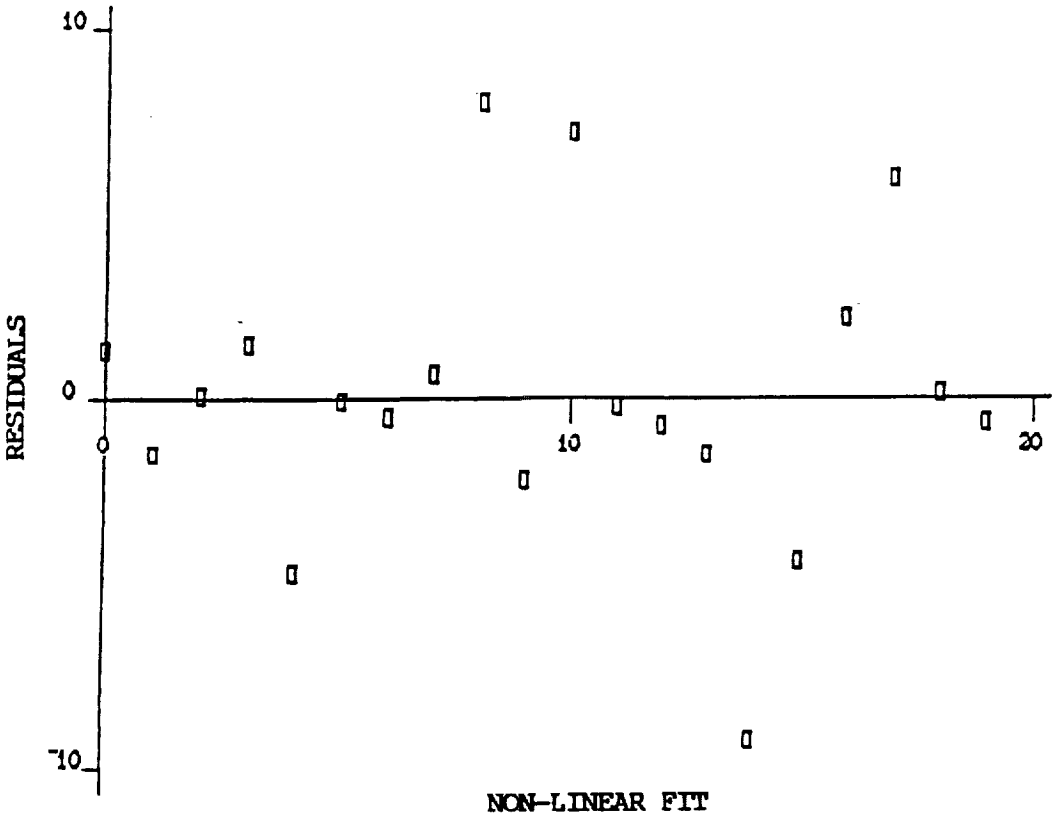

NON-LINEAR FIT

FIGURE 1.2.1

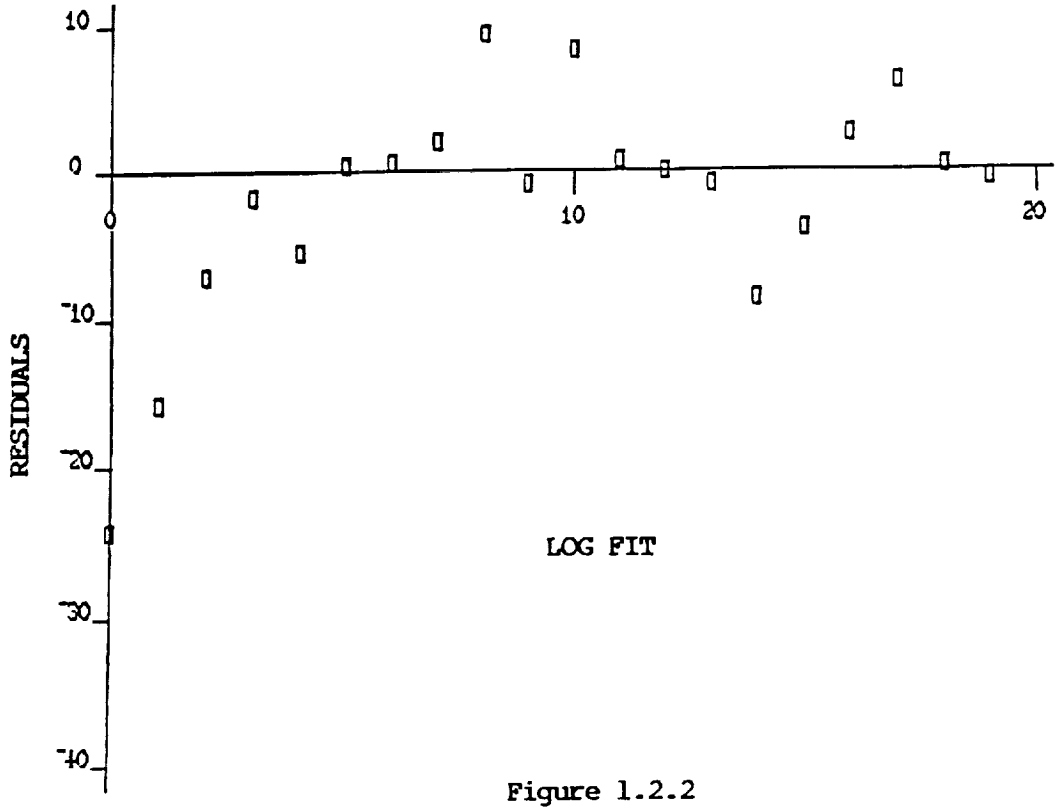

LOG FIT

Figure 1.2.2

1.3 Error Estimates

A question that is not asked enough, is how good the estimates of the parameters α are. Until now, we have merely told how to get the best estimates of the parameters. We have given no hint as to how good the estimates are. We should always keep in mind that the procedure for deriving the parameters is really an elaborate procedure for making a new random variable. If we do an identical parameter estimation scheme with two different sets of data from the same experiment, I guarantee that you will get two different sets of answers. This section is devoted to deriving expressions that give an estimate of the variation in the answers.

The method for getting the error estimates is based on examining the sharpness of the peak in the log of the probability of the data set as a function of α_i. If the peak is very sharp, the error in the estimation of α_i is expected to be small. The measure of the sharpness of the peaked used is the second derivative of the log of the probability taken with respect to the estimated parameter.

The procedure is as follows...

Let the matrix F_{ij} be computed by

$$F_{ij} = < - \frac{\partial^2 \log\ p(\{d_n\}|\alpha)}{\partial\alpha_i \partial\alpha_j} >, \qquad 1.3.1$$

where $< >$ denotes expected value. Then the estimate of the variance in the measurement of α_i from the expected value $<\alpha_i>$, σ_i^2 is given by

$$\sigma_i^2 \simeq F_{ii}^{-1}. \qquad 1.3.2$$

F_{ii}^{-1} is the i^{th} diagonal element of the matrix inverse of F_{ij}. The matrix F is referred to as the Fisher matrix.

In principle this calculation gives a lower bound on the expected error for the i^{th} parameter and is the estimate only for a problem with Gaussian distribution. However, in my experience, it does a good job as an error estimate.

1.4 Expected Errors for Gaussian Statistics.

Recall that for Gaussian statistics

$$\log p(\{d_n\}\,|\,\alpha) = -\sum_n \frac{(d_n - f(n,\alpha))^2}{2\sigma^2} - \frac{1}{2}\sum_n \log 2\pi\sigma^2.$$

Thus

$$\frac{\partial \log p(\{d_n\}\,|\,\alpha)}{\partial \alpha_i} = \sum_n \frac{1}{\sigma^2}\frac{\partial f}{\partial \alpha_i}(d_n - f) + \frac{(d_n - f)^2}{2(\sigma^2)^2}\frac{\partial \sigma^2}{\partial \alpha_i} - 0.5\,\frac{\partial \sigma^2}{\sigma^2 \partial \alpha_i}.$$

$$\frac{\partial^2 \log p(\{d_n\}\,|\,\alpha)}{\partial \alpha_i\, \partial \alpha_j} = \sum_n \frac{1}{\sigma^2}\frac{\partial^2 f}{\partial \alpha_i \partial \alpha_j}(d_n - f) - \frac{1}{\sigma^2}\frac{\partial f}{\partial \alpha_i}\frac{\partial f}{\partial \alpha_j} - \frac{(d_n - f)}{(\sigma^2)^2}\frac{\partial f}{\partial \alpha_i}\frac{\partial \sigma^2}{\partial \alpha_j}$$
$$- \frac{(d_n - f)}{(\sigma^2)^2}\frac{\partial f}{\partial \alpha_j}\frac{\partial \sigma^2}{\partial \alpha_i} - \frac{(d_n - f)^2}{(\sigma^2)^3}\frac{\partial \sigma^2}{\partial \alpha_i}\frac{\partial \sigma^2}{\partial \alpha_j} + \frac{(d_n - f)^2}{2(\sigma^2)^2}\frac{\partial^2 \sigma^2}{\partial \alpha_i \partial \alpha_j}$$
$$- \frac{1}{2}\frac{1}{\sigma^2}\frac{\partial^2 \sigma^2}{\partial \alpha_i \partial \alpha_j} + \frac{1}{2}\frac{1}{(\sigma^2)^2}\frac{\partial \sigma^2}{\partial \alpha_i}\frac{\partial \sigma^2}{\partial \alpha_j}.$$

Fortunately, this formidable expression simplifies greatly when we take the expected value. Recalling that

$$\langle (d_n - f) \rangle = 0 \text{ and}$$

$$\langle (d_n - f)^2 \rangle = \sigma^2,$$

we get

$$\left\langle -\frac{\partial^2 \log p(\{d_n\}\,|\,\alpha)}{\partial \alpha_i \partial \alpha_j} \right\rangle = \sum_n \frac{1}{\sigma^2}\frac{\partial f}{\partial \alpha_i}\frac{\partial f}{\partial \alpha_j} + \frac{1}{2(\sigma^2)^2}\frac{\partial \sigma^2}{\partial \alpha_i}\frac{\partial \sigma^2}{\partial \alpha_j}. \qquad 1.4.1$$

For the QELS problem demonstrated here,

$$F_{00} = \frac{1}{\sigma^2}\sum \exp(-2\alpha_1 n),\ F_{01} = F_{10} = \frac{1}{\sigma^2}\sum \alpha_0\, n \exp(-2\alpha_1 n),$$

$$F_{11} = \frac{1}{\sigma^2}\sum \alpha_0^2\, n^2 \exp(-2\alpha_1 n)$$

In order to evaluate this expression, you use the values for α obtained in the parameter estimation process. Recall that the variance was not known at the beginning of the fitting process, although we did know that the statistics were Gaussian. The measured variance was 14.4. The values of F_{ij} are found to be

$$F_{00} = .15\ ,\ F_{01} = F_{10} = 17.7,\ F_{11} = 5981.$$

The inverse matrix containing the error estimates is thus,

$$F^{-1}_{00} = 10.23,\ F^{-1}_{01} = F^{-1}_{10} = .0305,\ F^{-1}_{11} = 2.57\times10^{-4}.$$

The computed error estimates of the estimation procedure are

$$\sigma_0 \simeq 3.2, \text{ and } \sigma_1 \simeq 0.016.$$

The computed numbers are the estimated standard deviation of the parameters derived. There is an implied assumption here that the statistics of the estimates are Gaussian. Given that, there is a 67% chance that the expected value lies within $\pm \sigma$ of the derived parameter.

The off diagonal terms in the matrix are the crosscorrelation coefficients. They are a measure of how the error in the i^{th} parameter estimate affects the error in the j^{th} parameter estimate.

1.5 A Priori Error Estimation

Note that data is not needed to evaluate the error estimates. All you need is some preknowledge about approximately what value the parameters may have. It is always true that you have some idea of the range of the possible answers from an experiment. If you claim to have no idea of what the possible answers are, you don't have any idea of the size and range of the instruments you need to do the experiment. Besides, computer experiments are cheap. You can check the error estimates for large ranges of possible answers.

The point is that the MLE error estimates can be used ahead of time to set up the optimal experimental conditions. Suppose you were only able to take 4 equally spaced data points in the heat transfer experiment. Where should they be to give the best possible results?

The procedure is to evaluate the F matrix and its inverse using the approximate values of the parameters and varying the placement of the data points to find the placement that will give the smallest variance in the most important parameter. In this particular experiment, we are interested in the decay rate coefficient, so we want to minimize the measurement variance of α_1.

A good way to proceed here is to define a time "stretch" factor β. The model function is thus written

$$f(n,\alpha) = \alpha_0 \exp(-\alpha_1 \beta n).$$

Time is stretched by the factor β. The equations for the Fisher Matrix are now

$$F_{00} = \frac{1}{\sigma^2}\sum \exp(-2\alpha_1\beta n),\ F_{01} = F_{10} = \frac{\beta}{\sigma^2}\sum \alpha_0\, n \exp(-2\alpha_1\beta n)\ ,$$
$$F_{11} = \frac{\beta^2}{\sigma^2}\sum \alpha_0^2\, n^2 \exp(-2\alpha_1\beta n)$$

Figure 1.5.1 is a plot of the expected standard deviation in the estimate of α_0 as a function of the stretch factor. Note that there is a minimum in the error at a stretch factor of approximately 1.9. This gives a minimum expected error of .023. Not bad for only 4 measurements. Recall that before we had an expected error of .016 with 20 measurements.

2.0 QELS PARAMETER ESTIMATION

The situation for processing real QELS correlograms is similar to the procedure outlined above, although more complex. In this section, the analysis will still be simplified

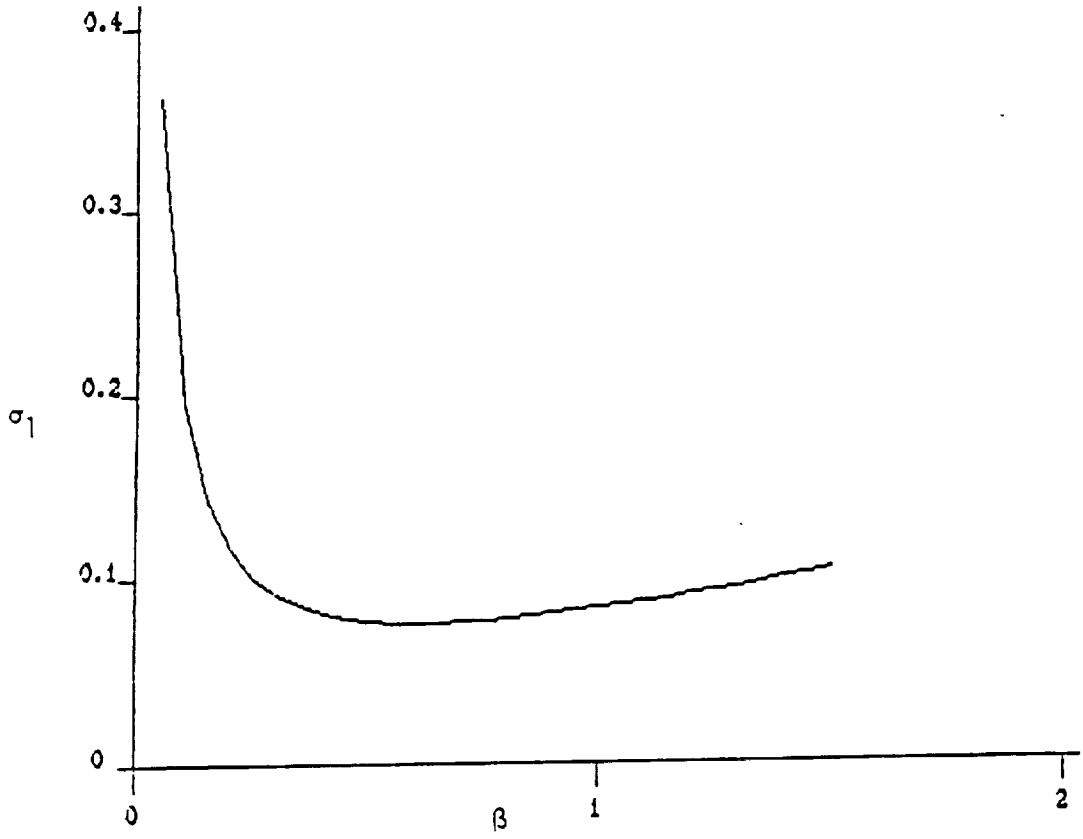

Figure 1.5.1

σ_1 vs. stretch factor β for the example with Gaussian statistics.

somewhat in order to illustrate the essential concepts. Let R(n) be a measured correlogram and let <R(n)> denote the expected correlogram at that point. If we use the typical multiple exponential approach to fitting the correlogram, the model function is given by

$$<R(n)> = \sum_k \alpha_k \exp(-b_k n),$$

where the b_k are preselected decay rates. The closer spaced these coefficients can be, the higher the possible resolution of the particle size distribution. If the correlogram is to be measured at different scattering angles, the correlogram model is better written

$$<R(n,\Theta)> = \sum_k \alpha_k M(b_k,\Theta) \exp(-\beta_k \sin^2(\Theta/2) n),$$

where M() is the Mie coefficient for the scattering cross–section at angle Θ and at the particle size specified by b_k.

In the previous section, I assumed that the errors were given by an independent Gaussian process. However, correlograms obtained from QELS experiments do not have that type of statistics. In fact it can be shown that the errors in a correlogram are correlated with each other. If the error in the n^{th} point is positive, it is likely that the error in the $n+1^{th}$ point is also positive. The covariance Λ_{mn} between data points on a correlogram is approximately given by (see appendix 1)

$$\Lambda_{nm} = <(R(n) - <R(n)>)(R(m) - <R(m)>)>$$
$$\simeq \frac{<R(0)><R(n-m)> \; + \; <R(n)><R(m)>}{N} + S\delta_{nm},$$

where N is the total number of products involved in the estimation of each point of the correlogram, and S is the shot noise contribution to the correlogram.

Since estimation of the correlogram involves the addition of a large number of points, it seems reasonable to invoke the Central Limit theorem and assume Gaussian statistics for the correlogram. This can be true, even if the process whose correlogram we are estimating does not have Gaussian statistics. The model for the errors in the measured correlograms is thus given by a joint Gaussian expression. Ignoring terms that are not a function of α,

$$\log p(\{d_n\} \mid \alpha) = -\sum_m \sum_n \Lambda_{mn}^{-1} (R(n) - <R(n)>)(R(m) - <R(m)>).$$

Thus the MLE equations are given by

$$\frac{\partial \log p}{\partial \alpha_i} = \sum_n \sum_m \Lambda^{-1}_{mn} (R(m) - \langle R(m) \rangle) \frac{\partial \langle R(n) \rangle}{\partial \alpha_i} = 0, \; i = 1,2,3 \ldots$$

The matrix F_{ij} used to calculate the errors in the estimates of α is given by

$$F_{ij} = \sum_n \sum_m \Lambda^{-1}_{nm} \frac{\partial \langle R(n) \rangle}{\partial \alpha_i} \frac{\partial \langle R(m) \rangle}{\partial \alpha_j}. \qquad 2.1$$

Elucidation of time sampling scheme and particle histogram resolution.

The MLE expressions for the measurement variance can be used to examine the effect of various time lag schemes in the correlator and of various spacings of the histogram intervals. For instance, the b_k's can be selected and the error estimates of the α performed. The errors can be examined to see if any are as large as the expected coefficients. If such errors are found, the algorithm clearly cannot tell those b_k apart, thus fewer will be selected and the procedure redone until the errors are acceptably small. Alternatively, the procedure could be set up to estimate the b_k given a known α distribution. The procedure would be used to see which b_k are distinguishable from one another.

Effect of Multiple Angle Measurements.

This problem can be explored both theoretically and experimentally. The MLE equations can easily be modified to include multiple angle experiments. Again, the various controllable parameters can be varied to find optimal operating conditions.

Efficient algorithms.

It is well known that the numerical problem associated with parameter estimation in QELS is very difficult. The fundamental reason for this was clearly shown by McWhirter and Pike [2]. They were able to solve the associated Fredholm eigenvector problem and showed that the eigenvalue distribution was such that small errors in the measurements would be magnified into large errors in the estimated particle size distribution.

A more immediate manifestation of the numerical difficulties of the problem can be obtained by examining the Fisher matrix derived from the MLE equations (Equation 2.1). The inverse matrix, F_{ij}^{-1}, gives two thing: 1) the error estimates on the measured parameters, and 2) an estimate of the condition number for the numerical problem. Recall that the condition number is roughly given by the ratio of the largest diagonal element to the smallest diagonal element of the inverse matrix. It is a measure of the numerical stiffness of the problem. It can be shown that condition numbers for QELS problems for a single scattering angle are of the order of magnitude of 10^8 or larger. Further the diagonal elements can be on the order of 10^{13} or larger. All of this means that the minimum in the least squares problem (or the maximum in the MLE problem) is very shallow indeed. Very large changes in the estimates of the parameters can result in a very small change in the object function. With this in mind, a perusal of the literature may lead one to be puzzled as to which results are due to the particle statistics and which are due to the fitting algorithm. For instance, some investigators claim to be able to resolve bimodal distributions with correlograms computed over a few minutes, whereas other investigators claim that hours of averaging are necssary.

Figure 3.1 is a plot of a histogram fit to exp(−.5n) with independent Gaussian noise of standard deviation .05 added to it. Figure 3.2 is a plot of the residuals from that fit. Note that the best fit is grossly in error although there is no noticeable pattern in the residuals. Under the circumstances, this false solution is indeed the best fit.

Another test of the histogram fit procedure was made by fitting exp (−.55n) plus Gaussian noise. The values of the exponentials in the fit were .1,.2,.3,.4,... , 1.0. Note that the plot of the residuals (figure 3.3) does have a noticeable structure. This structure comes about because the fitting function is wrong. There is no term exp(−.55n) in the fit.

The stiffness of the problem can be mitigated somewhat by adding some pre–knowledge to the problem. A common method of doing this is by so–called regularization schemes. For the histogram method in QELS this means forcing a smoothness condition on the distribution of sizes. The main problem with this method is that the result

is strongly determined by the degree of regularity forced on the solution and the "correct" amount of smoothness is not known *a priori*.

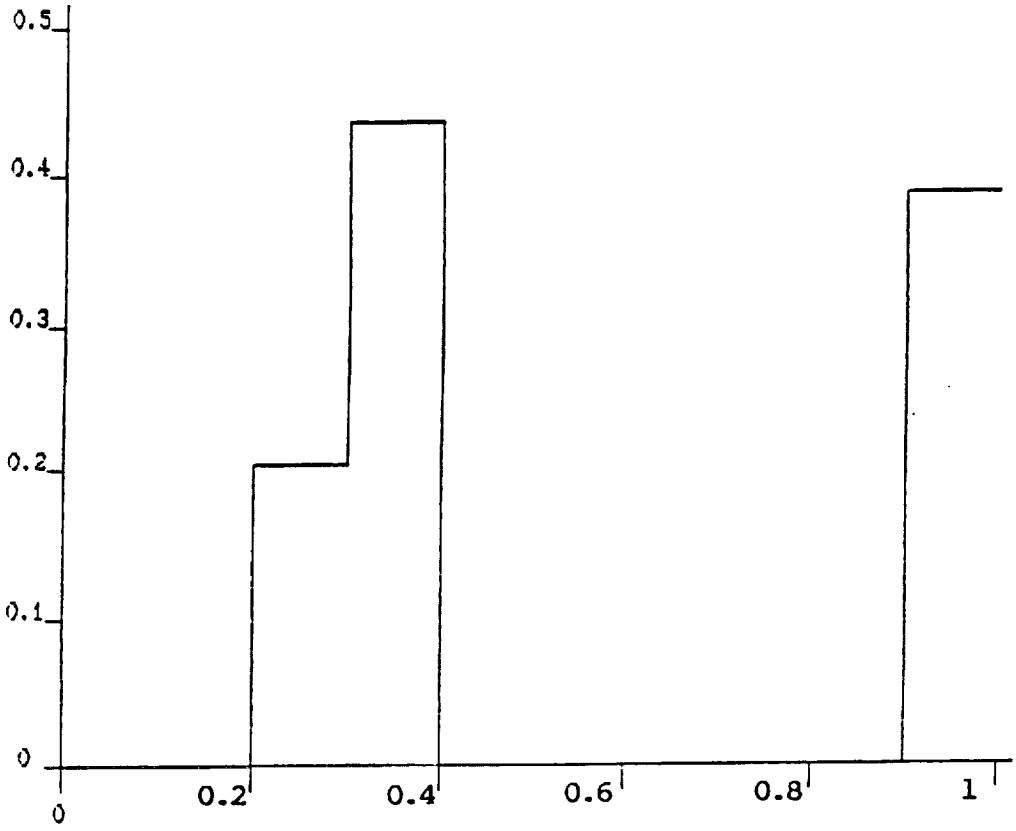

Figure 3.1

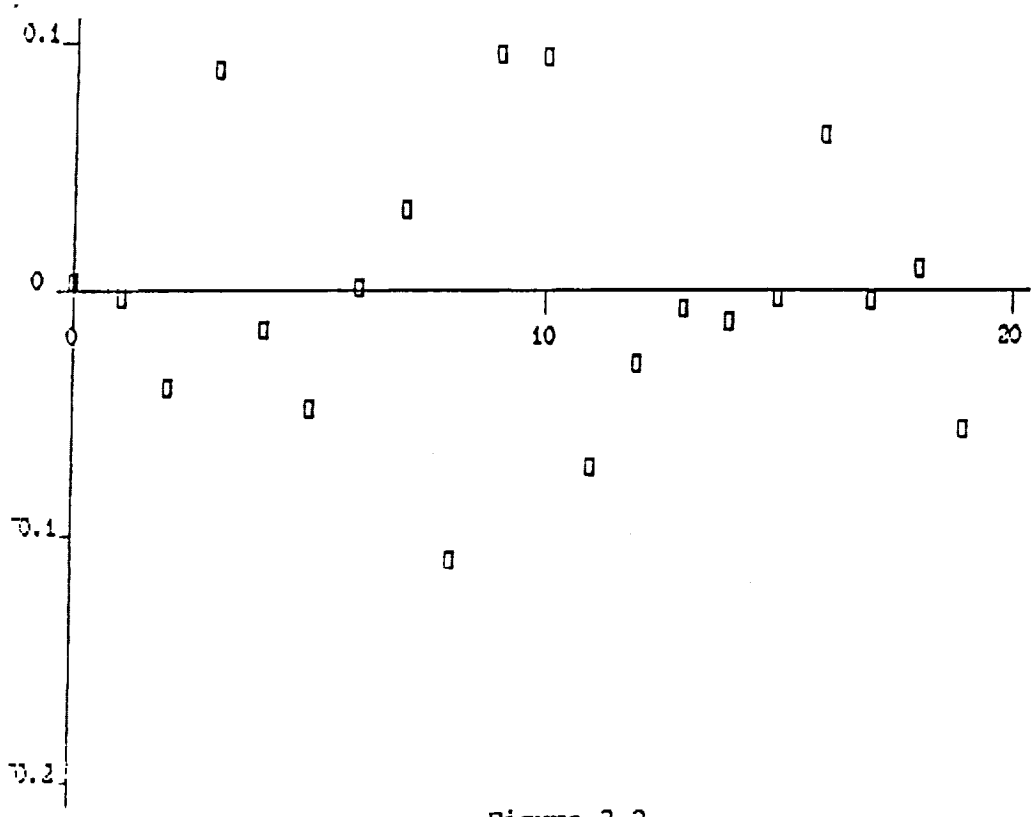

Figure 3.2

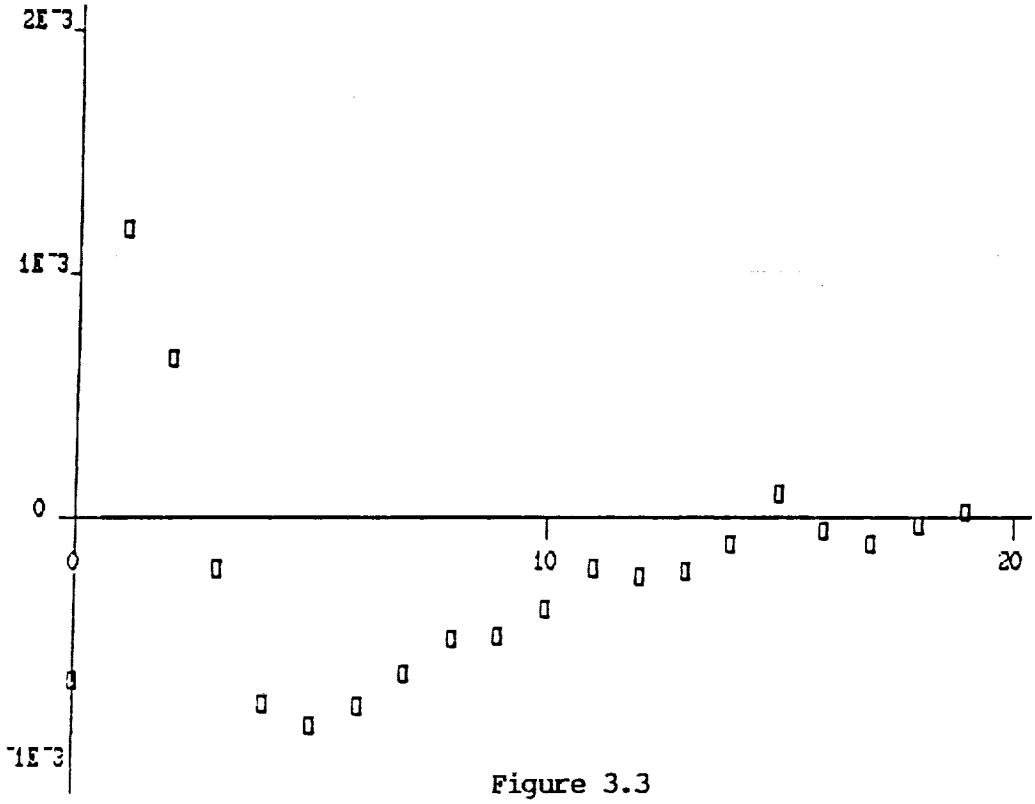

Figure 3.3

CONCLUSIONS

It has been shown that a MLE framework can be used to design and analyze QELS experiments. Further, the framework can be used to design software that can monitor experiments and by examining such outputs as the residuals, decide on the optimal experimental conditions.

Appendix I

Covariance of Noise on Correlograms

Consider the covariance of the correlogram of the measured photon count f(n).

$$\Lambda_{nm} = \langle (R(n) - \langle R(n) \rangle)(R(m) - \langle R(m) \rangle) \rangle$$

$$\Lambda_{nm} = \langle (\frac{1}{N}\sum_{k} f(k)f(k+m) - \langle R(m) \rangle)(\frac{1}{N}\sum_{p} f(p)f(p+n) - \langle R(n) \rangle) \rangle$$

$$\Lambda_{nm} = (\frac{1}{N^2}\sum_{k}\sum_{p} \langle f(k)f(k+m)f(p)f(p+n) \rangle - \langle R(n) \rangle \langle R(m) \rangle$$

Evaluation of the expression for the covariance requires evaluation of the expected fourth order moment $\langle f(k)f(k+m)f(p)f(p+n) \rangle$. There is no general expression to compute this term as the variable f(n) is not necessarily Gaussian and the details of the correlator algorithm can vary. In order to get a feel for how this term behaves, assume:

1. f(n) is a Gaussian random variable.

2. The correlation computer operates in the so–called batch mode. i.e. If $k \neq p$, the data sets do not overlap and thus

$$\langle f(k)f(k+m)f(p)f(p+n) \rangle = \langle f(k)f(k+m) \rangle \langle f(p)f(p+n) \rangle .$$

Thus,

$$\Lambda_{nm} = \frac{1}{N^2}(N \langle f(k)^2 f(k+m)f(k+n) \rangle + N(N-1) \langle R(n) \rangle \langle R(m) \rangle) - \langle R(n) \rangle \langle R(m) \rangle .$$

$$\Lambda_{nm} = \frac{1}{N} \langle f(k)^2 f(k+m)f(k+n) \rangle + (1-1/N) \langle R(n) \rangle \langle R(m) \rangle - \langle R(n) \rangle \langle R(m) \rangle .$$

$$\Lambda_{nm} = \frac{1}{N} \langle f(k)^2 f(k+m)f(k+n) \rangle - \frac{1}{N} \langle R(n) \rangle \langle R(m) \rangle .$$

Now, invoking Gaussian statistics for $n \neq m$, we get

$$\langle f(k)^2 f(k+m) f(k+n) \rangle = \langle f(k)^2 \rangle \langle f(k+m) f(k+n) \rangle + 2 \langle f(k) f(k+m) \rangle \langle f(k) f(k+n) \rangle$$

$$\langle f(k)^2 f(k+m) f(k+n) \rangle = \langle R(0) \rangle \langle R(m-n) \rangle + 2 \langle R(m) \rangle \langle R(n) \rangle$$

For $n = m$, the situation is complicated by the fact that $f(n)$ is a measured photon count rate. (See Saleh [5].)

$$\langle f(k)^2 f(k+m)^2 \rangle = \langle f(k)^2 \rangle \langle f(k+m)^2 \rangle + \langle f(k) \rangle \langle f(k+m)^2 \rangle + \langle f(k+m) \rangle \langle f(k)^2 \rangle + \langle f(k) \rangle \langle f(k+m) \rangle .$$

$$= \langle R(0) \rangle^2 + 2 \langle R(0) \langle f \rangle + \langle f \rangle^2$$

Finally,

$$\Lambda_{nm} = \frac{1}{N} (\langle R(0) \rangle \langle R(m-n) \rangle + \langle R(m) \rangle \langle R(n) \rangle + (2 \langle R(0) \rangle \langle f \rangle + \langle f \rangle^2) \delta_{nm}).$$

Literature Cited

1. Cummins, H.Z., Knable, N., Yeh, Y., *Phys. Rev. Lett.* 12, 150 (1964)
2. McWhirter, J. C., Pike, E. R., *J Phys. A: Math. Gen.*, 11, 1729 (1978)
3. Cummins, P. G., Staples, E. J., *Langmuir*, 3, 1109, (1987)
4. Van Trees, H. L., Detection, Estimation, and Modulation Theory, John Wiley and Sons, (1968)
5. Saleh, B. , Photoelectron Statistics , Springer–Verlag, (1978)

IMPROVED OPTICS FOR LASER LIGHT SCATTERING

H. Michael Cheung
Department of Chemical Engineering
The University of Akron
Akron, Ohio

Laser light scattering experiments contemplated for use in a microgravity environment must conform to a number of operational constraints which do not apply on Earth. In particular, the use of index matching fluid to control flare is unacceptable. This paper describes work in progress to eliminate index matching fluids by the use of high spatial resolution receiving optics. By increasing on-axis spatial resolution flare from the sample cell walls (both the cell/sample and cell/air interfaces) can be effectively prevented from reaching the photodetector. In general, improving the on-axis discrimination degrades the angular resolution of a receiving optical train. Several different possible configurations of receiving optics are compared for their spatial resolution and angular resolution. For cylinder symmetric optics, the dual lens, fourier transform pair, receiving train with a center mask located between the lenses gives the best on axis spatial resolution. Future work will focus on optimizing this configuration as well as some non-cylinder symmetric configurations which may decrease the angular resolution "cost" of the dual lens, center mask arrangement.

INTRODUCTION

A number of experiments using laser light scattering are contemplated for future space shuttle missions. As part of an effort to develop a suitable instrument, this work is examining the use of high spatial resolution receiving optics to eliminate the need for index matching fluids. Often Earth based light scattering instruments utilize index matching fluids to control flare from the interfaces between the sample cell, the air surrounding the sample cell, and the sample itself. It is very desirable to eliminate the need for these fluids in any instrument destined for use in microgravity as they constitute both an engineering problem and a potential hazard.

There are a large number of potential configurations for the receiving optical train, see for instance Chu[1], Ford[2], and numerous other papers in the literature. However, most fall into the categories of dual pinhole, single imaging lens, or dual imaging lens (with many variations on the theme). These configurations can be compared in terms of three optical system performance parameters:

Δx - cross axis resolution
Δz - on axis resolution
σ_θ - angular uncertainty

The cross axis resolution, Δx, describes the spatial selectivity of the optical train on the axis perpendicular to the axis which passes down the center of the optical system. The on axis resolution, Δz, describes the spatial selectivity on the axis passing down the center of the optical system. The angular uncertainty, σ_θ, describes the contribution to measurement error induced by the optical system subtending a finite angle (and hence not measuring one and only one K-vector).

Today's paper will compare several base case receiving optical systems with the intent of illustrating the relative merit (and "price") of using a center mask to achieve on axis spatial resolution. The systems to be examined are:

1. Double Pinhole
2. Single Lens and Pinhole
3. Center Mask, Lens, and Pinhole
4. Dual Lens and Pinhole
5. Lens, Mask, Lens, and Pinhole

---

[1]Chu, B. "Laser Light Scattering"; Academic Press: New York, 1974; Chapter VII.

[2]Ford, N.C. In "Measurement of Suspended Particles by Quasielastic Light Scattering"; Dahneke, B.E., Ed.; John Wiley & Sons: New York, 1983; Chapter 2.

The spatial resolution parameters, Δx and Δz, are configuration dependent. The angular uncertainty, however, can be described by

$$\sigma_\theta = \frac{4}{3\pi L} \cdot \frac{R_L^3 - R_M^3}{R_L^2 - R_M^2} \tag{1}$$

where L is the distance from the center of the sample volume to the first optical element in the receiving train, R_L is the radius of the first optical element in the train, and R_M is the radius of the center mask ($R_M = 0$ if no center mask is present). This expression overestimates σ_θ for the double pinhole case, but it is so small anyway that it this of no practical concern. This angular uncertainty leads to the following relative error in the measured diffusion coefficient

$$\left[\frac{\sigma_D}{D}\right]_\theta \cong \sigma_\theta \cot \frac{\theta}{2} \tag{2}$$

where the subscript indicates that this is an error contribution due to the angular uncertainty. Since this scales as the cotangent the errors become increasingly severe as the scattering angle is decreased.

DOUBLE PINHOLE

The double pinhole configuration is diagramed in Figure 1. Ray tracing yields the following expression for the cross axis resolution:

$$\Delta x = R_{A_1} + \frac{L_1}{L_2}\left[R_{A_1} + R_{A_2}\right] \tag{3}$$

where R_{A_1} is the radius of the first pinhole, R_{A_2} is the radius of the second pinhole, L_1 is the distance from the center of the sample volume to the first pinhole, and L_2 is the distance between the two pinholes. For the base case considered $R_{A_1} = R_{A_2} = 50\ \mu$, $L_1 = 75$ mm, and $L_2 = 150$ mm. From equation 3 $\Delta x = 0.1$ mm and from equation 1 $\sigma_\theta = 0.29 \times 10^{-3}$.

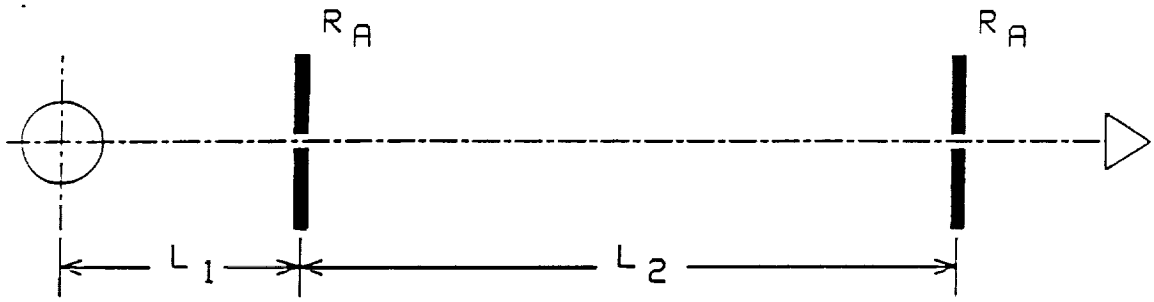

$$\Delta x = R_{A_1} + \frac{L_1}{L_2}\left[R_{A_1} + R_{A_2}\right] \quad \& \quad \Delta Z \rightarrow \infty$$

BASE CASE: $R_{A_1} = R_{A_2} = 50\ \mu$

$L_1 = 75$ mm

$L_2 = 150$ mm

$\Delta x = 0.1$ mm & $\sigma_\theta = 0.29 \times 10^{-3}$

FIGURE 1 Diagram of Double Pinhole Receiving System

Raytracing software was implemented in APL to better illustrate the spatial resolution characteristics of the receiving optical systems compared in this paper. Figure 2 shows both a surface plot and a two dimensional representation of the fraction of light originating at grid points in the vicinity of the sample volume center which reach the photodetector (through the receiving train). In the two dimensional plot the circled asterisk is the "brightest" point detected, "8" indicates points which are at least 80% as bright as the maximum, "6" indicates points which are 60% as bright as the maximum, and so forth for "4" and "2". The small dot indicates points which are nonzero, but less than 20% as bright as the maximum. The "-" indicates points which are not detected at all. It is clear that the dual pinhole setup has no on axis resolution. Light can always get into the detector from straight down the optical axis. In these figures the span on the cross (x) axis is 0.25 mm and the span on the optical axis (z axis) is 5 mm.

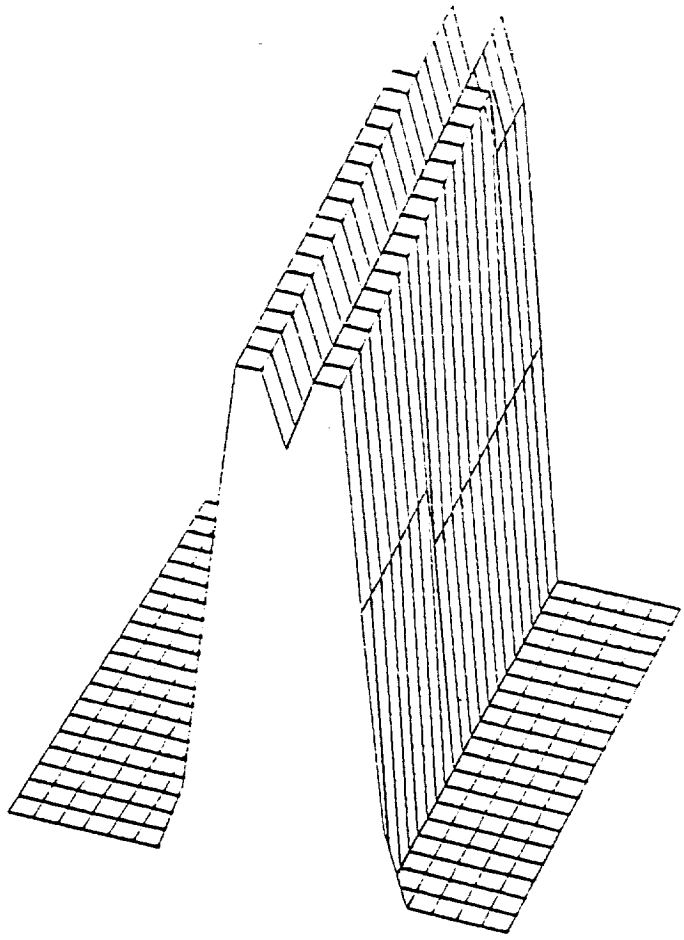

FIGURE 2 Spatial Resolution Plots for the Double Pinhole System

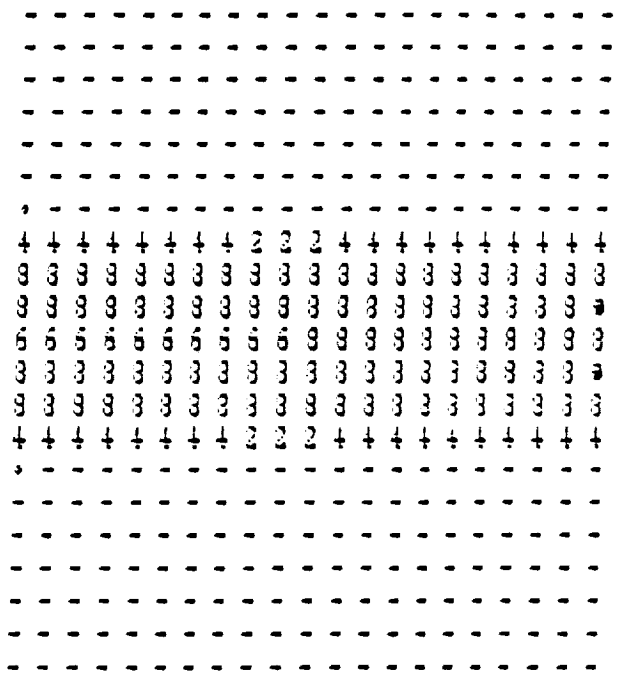

The dual pinhole system has angular resolution which cannot be matched by any of the lens based receiving systems. However it leaves a great deal to be desired in terms of on axis spatial resolution.

SINGLE LENS SYSTEMS

Figure 3 depicts the single (imaging) lens base case examined. A single lens is placed such that it forms an image of the sample volume on an aperture in from of the photodetector. The system was considered with and without a center mask placed just in front of the lens. In the figure L_1 is the distance from the sample volume to the mask, R_M is the radius of the mask, R_L is the lens radius, and R_A is the pinhole radius. The cross axis spatial resolution, Δx, is equal to the radius of the pinhole, R_A.

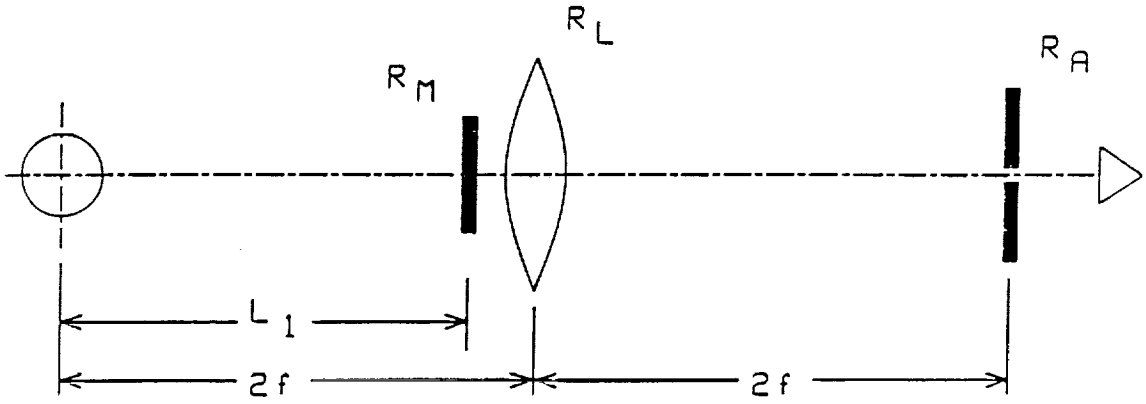

$$\Delta x = R_A \quad \& \quad \Delta z \rightarrow \infty \quad \text{(w/o mask)}$$

with mask,

$$\Delta z = \frac{R_A . L_1}{R_M} \quad , \quad L_1 > \frac{2 f R_M}{R_L}$$

FIGURE 3 Diagram of the Single Lens Base Case

Without the mask the system has no on axis resolution in the sense of excluding light absolutely. With a center mask the on axis resolution is given by

$$\Delta z = \frac{R_A \cdot L_1}{R_M} \quad , \quad L_1 > \frac{2fR_M}{R_L} \tag{4}$$

The specific parameters used in the single lens base case were: R_L = 2.5 mm, f = 75 mm, R_A = 50 μ, R_M = 1.5 mm, and L_1 = 140 mm. The cross axis resolution in both cases is Δx = 0.05 mm. Without the mask the angular uncertainty is $\sigma_\theta = 7.1 \times 10^{-3}$. With the center mask the on axis resolution is Δz = 4.7 mm and the angular uncertainty is $\sigma_\theta = 9.3 \times 10^{-3}$. The addition of the center mask increases the angular uncertainty, but not to a great extent. Figures 4 and 5 depict the spatial resolution in surface plots and two dimensional plots. The x and z axis ranges spanned and the significance of the symbols are the same as for Figure 2. Notice that the addition of the lens does provide some on axis resolution even without the center mask. There is a definite peak near the sample volume center. The angular spread induced by adding the lens is also clearly apparent. In Figure 5 the cleft in the received intensities caused by the center mask is easily seen. The on axis dead space created is quite small for this configuration and mask size.

DUAL LENS SYSTEMS

Figure 6 depicts the dual lens base case examined. The nomenclature is consistent with the prior figures. Again the cross axis resolution, Δx, is equal to the pinhole radius, R_A. With the mask there is an on axis dead zone created with

$$\Delta z = \frac{R_A \, f}{R_M} \tag{5}$$

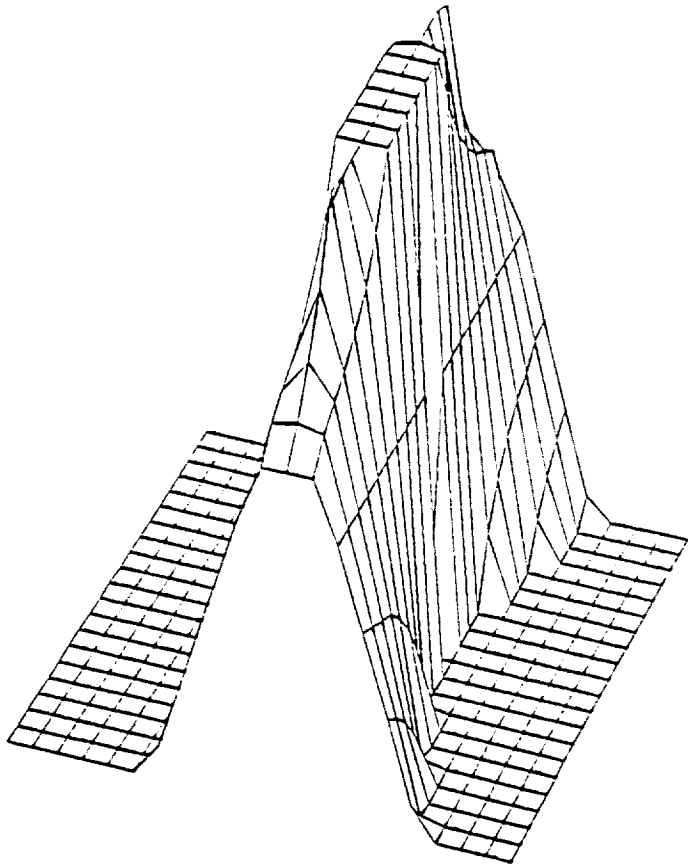

FIGURE 4 Spatial Resolution Plots for Single Lens System with no Mask

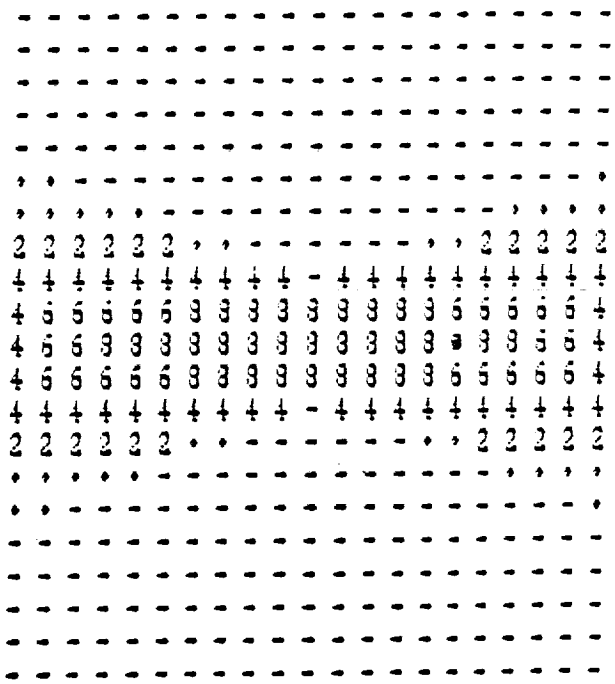

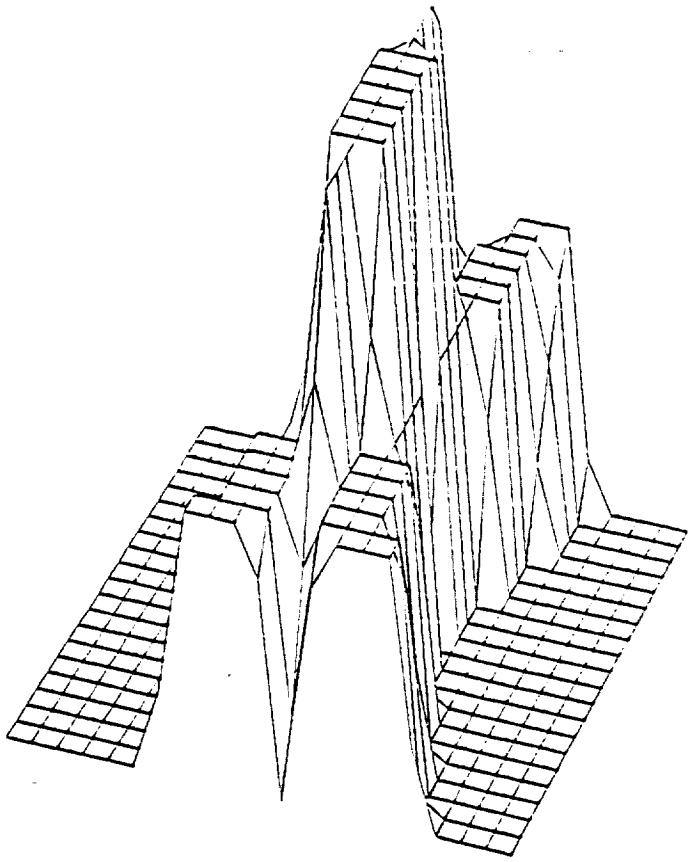

FIGURE 5 Spatial Resolution Plots for Single Lens System with Mask

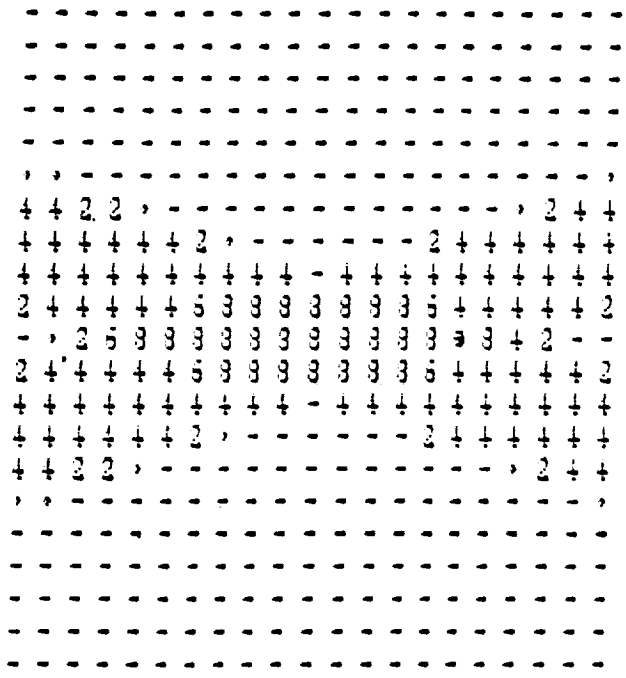

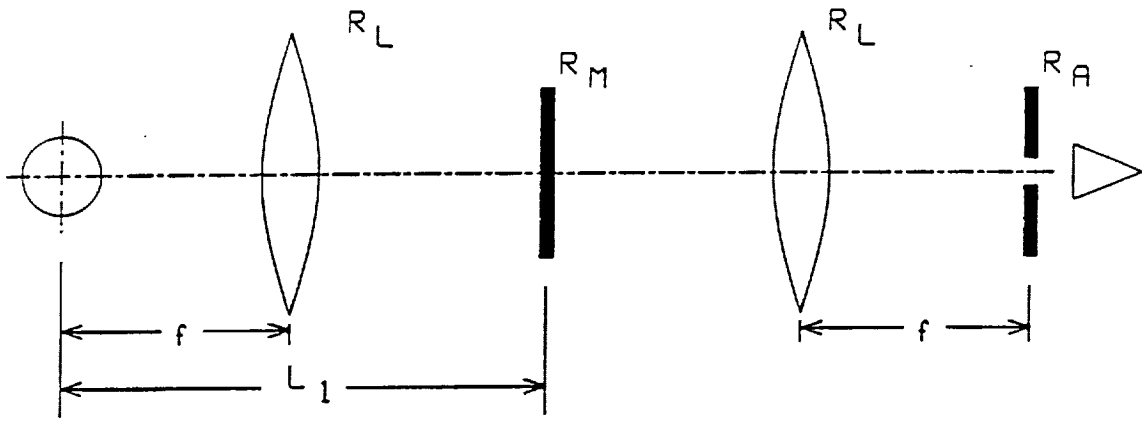

$$\Delta x = R_A \ , \quad \Delta z \rightarrow \infty \quad \text{(w/o mask)}$$

$$\text{with mask} \ , \quad \Delta z = \frac{R_A \ f}{R_M}$$

FIGURE 6 Double Lens Receiving System Base Case

The specific parameters used in the dual lens base case calculations are: R_L = 2.5 mm, f = 75 mm, R_A = 50 μ, R_M = 1.5 mm, and L_1 = 150 mm. Without the mask the angular uncertainy is $\sigma_\theta = 14 \times 10^{-3}$. With the mask there is on axis spatial resolution of Δz = 2.5 mm and an angular uncertainty of $\sigma_\theta = 17 \times 10^{-3}$. The dual lens system has much poorer angular uncertainty values than any of the other, yet offers the best on axis spatial resolution. In fact, this type of receiving optical train has been applied in the study of strongly scattering oil-in-water microemulsion samples in which it was necessary not only to control flare from the entrance and exit of the laser beam from the sample cell but also to reduce the amount of light reflected from the cylindrical cell wall, see Cheung et al[3]. Figures 7 and 8 depict the spatial resolution without and with a center mask ,respectively, using the same format as for earlier plots. Without a

[3]Cheung, H.M.; Qutubuddin, S.; Edwards, R.V.; Mann, J.A., Jr. *Langmuir* 1987, 3, 744-752.

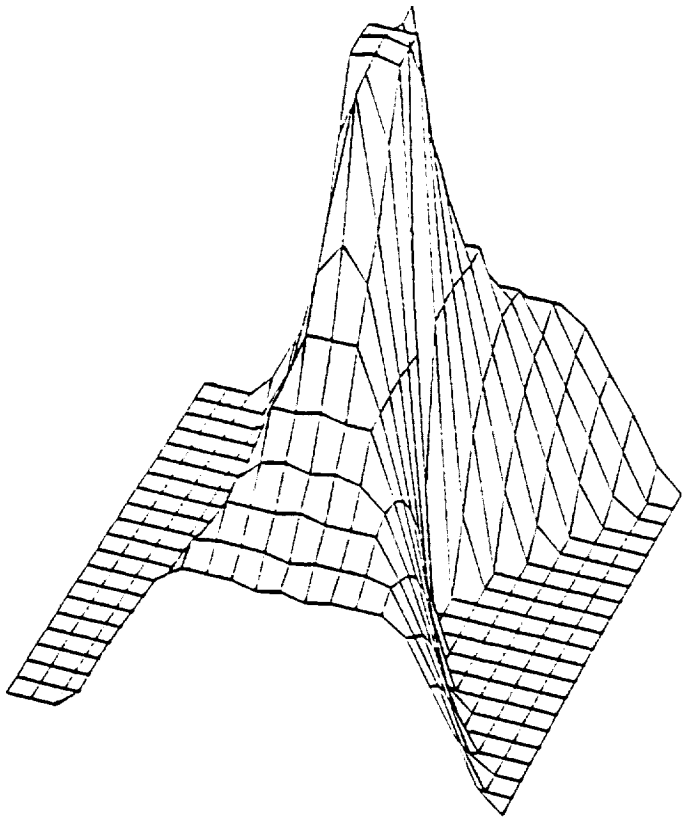

FIGURE 7 Spatial Resolution for Dual Lens System without Mask

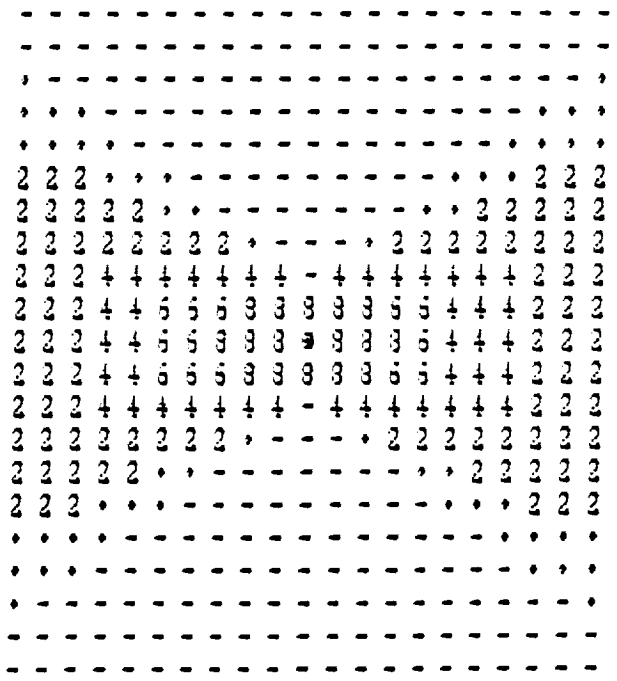

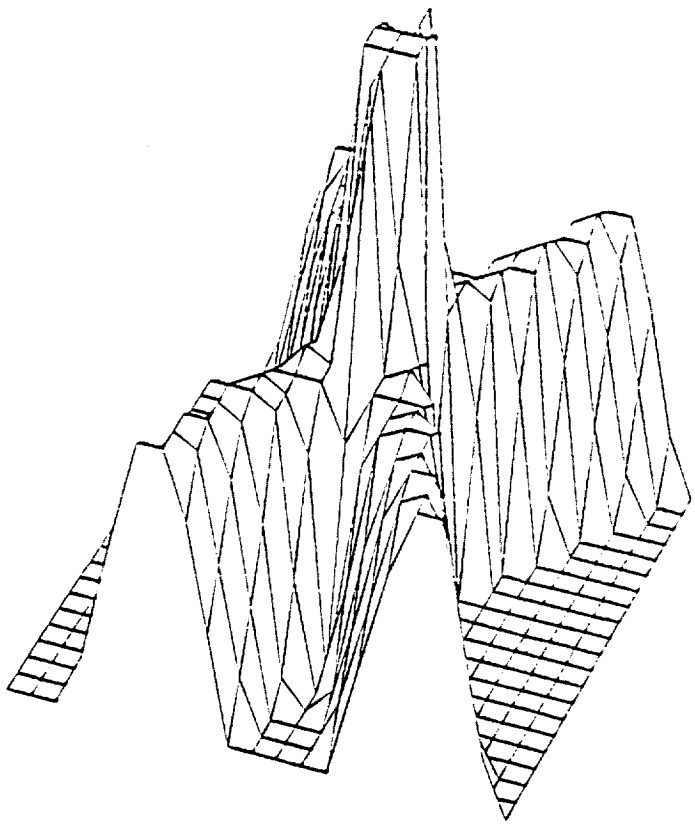

FIGURE 8 Spatial Resolution for Dual Lens System with Mask

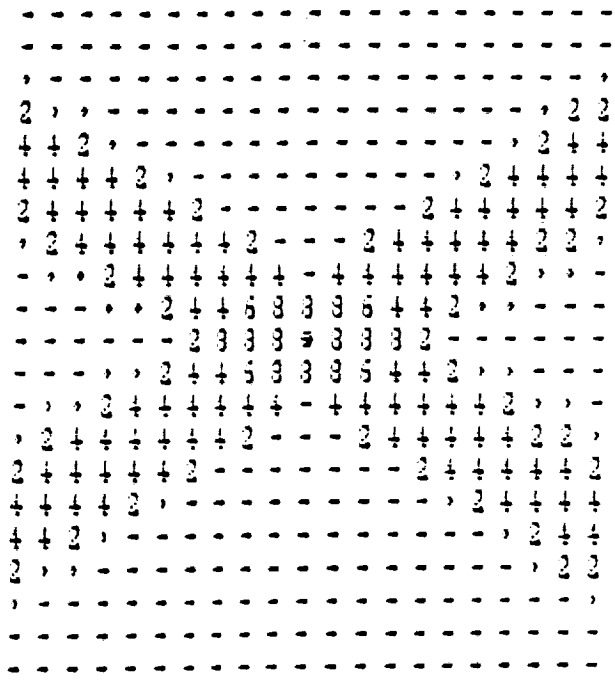

center mask, the dual lens system demonstrates increased selectivity on the optical axis. This is essentially an f-number effect, the f-number of the dual lens system is half that of the single lens system for the same focal length lenses. In Figure 8 the increased on axis resolution is apparent. There is a dead zone on the optical axis (which is cone shaped in three space) from which no light can reach the photodetector. The size of this zone is dependent on the focal length of the lenses, the radius of the pinhole, and the radius of the mask. Figure 9 depicts the spatial resolution of the same optical system except with a much larger center mask, $R_M = 0.8\ R_L$. The dead zone is considerably enlarged.

The dual lens system with a center mask also provides the opportunity to incorporate a second detector train based on the dual pinhole design directly into the receiving train. This co-linear receiving train would then provide both high spatial and high angular resolution in one device. The second (dual pinhole) train may be desirable for making total intensity measurements in parallel with the QELS measurements. There may be computational advantages to having both sets of data available, especially for multi-angle based fitting schemes, see for instance Cummins and Staples [4]. This configuration is depicted in Figure 10 and will be the base case configuration implemented for the NASA instrument. It is expected that at angles above 30 degrees this configuration will be adequate. For lower angles (and possibly for the entire instrument) designs which incorporate the high spatial selectivity of the dual lens, center mask scheme, but which address the angular resolution problem will need to be investigated and developed.

DISCUSSION

The dual lens, center mask design for receiving optics offers high spatial resolution and the opportunity to cleanly incorporate high angular resolution total intensity measurements. While the comparisons made in this paper are not exhaustive, it is probably the best cylinder symmetric option available. The design will be used as the starting point for a QELS

[4]Cummins, P.G.; Staples, E.J. *Langmuir* 1987, 3, 1109-1113.

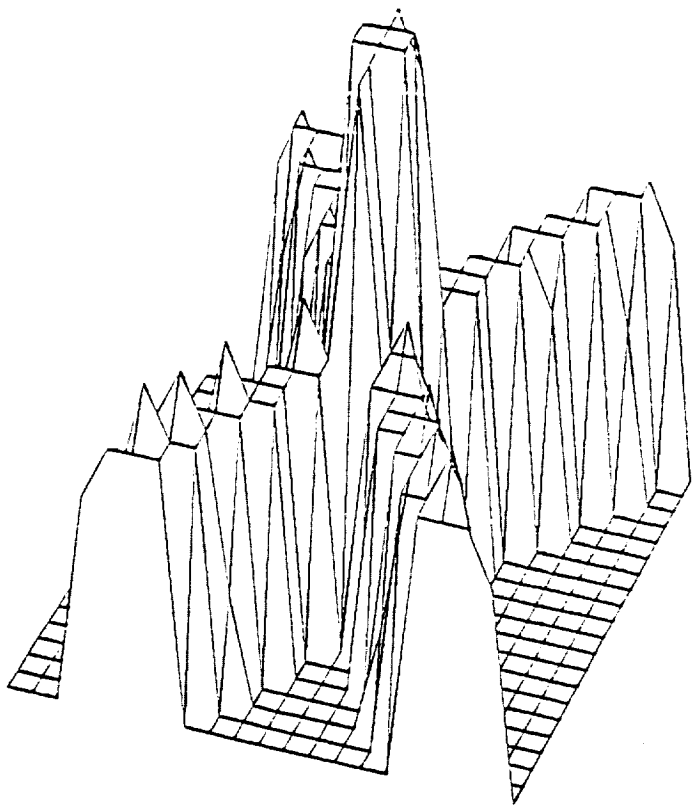

FIGURE 9 Spatial Resolution with $R_M = 0.8\ R_L$, Dual Lens System

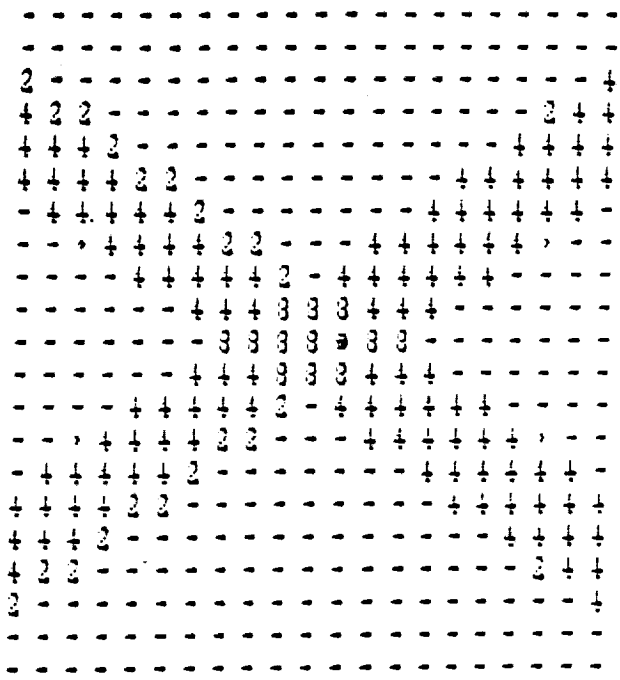

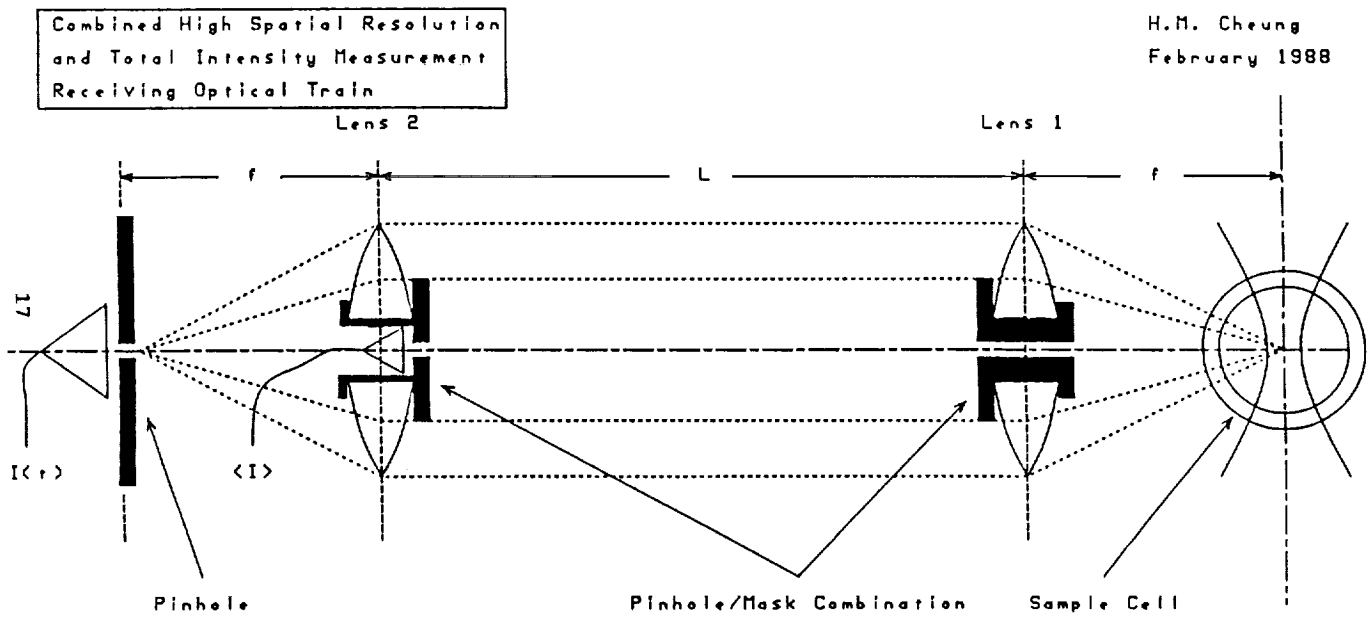

FIGURE 10 Proposed Starting Configuration for NASA Instrument

instrument which does not require index matching fluid. To overcome the angular resolution problem several non-cylinder symmetric options, which are modifications to the dual lens, center mask design will be investigated. The aim of these modifications will be to increase the angular resolution (decrease σ_θ) while preserving the high on axis spatial selectivity.

Testing will be performed at The University of Akron using single and multi-angle techniques on standard polystyrene latex samples.

ADVANCED INSTRUMENTATION FOR QELS EXPERIMENTS

Walther Tscharnuter, Bruce Weiner, and John Thomas
Brookhaven Instruments Corporation
Holtsville, New York

Abstract: Quasi Elastic Light Scattering experiments have become an important tool in both research and quality control applications during the past 25 years. From the crude beginnings employing mechanically driven spectrum analyzers, an impressive array of general purpose digital correlators and special purpose particle sizers is now commercially available. In this article the principles of QELS experiments are reviewed, their advantages and disadvantages are discussed and new instrumentation is described.

Theory:

The determination of molecular weights by means of static light scattering measurements is well known. Here the average ("static") scattered intensity at several scattering angles and concentrations is recorded. In QELS experiments the **intensity fluctuations** are investigated. These fluctuations arise from the random movement of the particles in a suspending liquid (Brownian motion). The particles form secondary oscillators that are induced by the laser light electromagnetic field. Thus the resulting amplitude is proportional to the polarizibility, which in turn is proportional to the mass of the particle. Any photometer can only measure the **intensity**, which is proportional to the square of the superposition of the amplitudes of the scattered light from all contributing particles. As a result the intensity of the scattered light has the following mathematical form:

$$I_S = M^2 P(\theta, \lambda, r) B(c)$$

I_S is the scattered intensity at the scattering angle θ
M is the mass of the particle
$P(\theta, \lambda, r)$ is the Mie-factor, which approaches 1 for $\theta = 0$ or $r << \lambda$, λ being the wavelength of the laser light in the suspending liquid. This factor also depends on the shape and composition of the particles. In most cases spheres, solid or hollow, are assumed.

B(c) is the concentration factor, which also approaches 1 for c=0.

The power spectral density of a randomly excited oscillator (in this case the concentration fluctuations) has the form of a Lorentzian. In the time domain the autocorrelation function is an exponential. These 2 functions form a Fourier transform pair where the half-width frequency Γ at half height relates to the time τ at the 1/e point as $\Gamma = 1/\tau$. Smaller particles yield faster decaying autocorrelation functions than larger ones.

At any scattering angle the following equation holds

$$\Gamma = Dk^2 \qquad (1)$$

where Γ = half-width at half-height in rad/sec
D = diffusion coefficient in cm^2/sec
$k = (2\pi n/\lambda) * 2\sin(\theta/2)$ momentum transfer vector
n = refractive index of the suspending liquid
λ = wavelength of the laser in vacuo (cm)
θ = scattering angle

By assuming spheres and applying the Stokes-Einstein equation a radius may be calculated

$$r = k_b T/(6\pi D \eta(T)) \qquad (2)$$

where r = radius (cm)
k_b = Boltzmann constant (erg/degree)
T = Temperature (Kelvin)
η = viscosity of the suspension liquid (poise)

Similar equations exist for other particle shapes.
The autocorrelation function is of the form

$$C(t) = B + A*\exp(-2\Gamma t) \qquad (3)$$

where B = measured or calculated base, = $(\langle n^2 \rangle)$
A = pre-exponential factor which is a function of the optical setup and, more importantly, of Γ .
n = Photon counts/sample time

The normalized form of (3) for a monodisperse system (a system that contains only one size) may be written as

$$g(t) = G(\Gamma) * \exp(-\Gamma t) \qquad (4)$$

For more than one size the right side of (4) changes into a sum of exponentials. Finally, for a continuous distribution of sizes, the equation becomes an integral

$$g(t) = \int_0^\infty G(\Gamma) * \exp(-\Gamma t)\, d\Gamma \qquad (5)$$

This integral equation is known to be ill-conditioned, which

means that for any measured function g(t) a number of equally valid solutions G(Γ) exist. It is of utmost importance to determine a correlation function g(t) as noise free as possible. Also, the time axis should be as long as practicable. Due to the statistical nature of the measurement the random errors become smaller as the experiment duration is increased. However, contaminations (dust), laser drift, chemical reactions, sedimentation, agglomerization and simply operational time constraints will form an upper limit in any given particle sizing problem. Thus it is very important to gather the available data as efficiently as possible. For example, the Brookhaven Instruments Corp. BI-90 submicron particle sizer eliminates overflows at any useable count rate without prescaling or other electronic means. The time axis is equivalent to several thousand linearly spaced channels and the baseline is determined exactly by passing the data through an electronic dustfilter. The BI-90 features fully automated operation including automatic sample time selection and thus achieves an unprecedented repeatability. No operator intervention is required.

The limits of the particle size resolution obtainable from light scattering were first investigated by R.Pike et al [1][2][3]. They showed the rapid decay of the amplitudes of the singular functions. For a typical noise level of .001 the third singular value is already below this noise and thus cannot be extracted from the autocorrelation function. Thus more than 2 peaks can rarely be resolved. Even for 2 peaks the size ratio cannot be lower than 1:2 in most cases.

The authors also showed that only a small number of data points are required to extract G(Γ) from the time correlation function, provided that the data points cover the full time range. Specifically, only 5 exponentially spaced and properly placed data points are neccessary to resolve a bimodal distribution. In fact, correlation data that are obtained at delay times with a **constant ratio** always yield better distributions than those obtained with a **constant difference**.

It can be seen from the above discussion that it is crucial to decrease the experiment noise as much as possible. Once the data are stored the resolution limits can only be improved through additional operator input (a priori knowledge of a distribution), selection of reasonable solutions out of a set of possible solutions and, in some cases, constraining the set of solutions by using data from several scattering angles. Although in theory multi-angle experiments should yield higher resolutions, the results are also more suspect due to the unavoidable dust in most real world samples and the Mie corrections.

Instrumentation: Brookhaven Instruments Corp. has been involved in the design of correlators since 1971. All efforts have been directed to the goal of achieving the lowest possible noise level in the raw correlation data.

1. The most important experimental parameter in equation (3) and

is the base line, because all raw data must be normalized before any subsequent data reduction.

2. The correlation length (time axis) must be sufficiently long to cover all fluctuations, but should not include many points on the base line.

3. Integration effects should be avoided at long delay channels.

4. Prescaling should be avoided to obtain the highest data collection efficiency and avoid distortions in the correlation function.

5. Data should be taken with a constant ratio in delay times.

6. The number of channels and the delay time ratio should be fully programmable.

The new BI-8000AT digital correlator was designed with these goals in mind. It is a single card correlator with a IBM-AT form factor. However, any other bus structure may be easily accomodated since all communications with the main processor are handled through I/O space. No memory conflicts are possible.

All the goals were achieved by separating the **sampling time** and the **sample (=delay) time**. The BI-8000AT for the first time enables the build-up of a correlation function according to the definition of the function: $C(\tau)= \sum n(t) * n(t-\tau)$. The summation is performed over the product of **differences** with **no** summation of the photo-electron pulses within the time difference. The samples are taken at very small time intervals and stored. The special hardware, using custom high speed integrated circuits, rapidly multiplies and adds the difference values. Although this has been done in the past by software alone, real time operation in the BI-8000AT was achieved by parallel processing and pipe-lining.
At present the total time range is 5 decades. (Min delay time = 1 microsec, max. 165 millisec, measured baseline at 320 millisec). Work is in progress to achieve a minimum and maximum delay time of 10 nanosec and 10 sec. respectively (9 decades).

The correlation function that is used for the size distribution calculations is the sum of many short measurements, each of which may be automatically checked for total counts and rejected, if they exceed an (operator specified) multiple of the expected standard deviation of the total intensity. This method allows discrimination against "dust" and yields excellent baselines. The relatively short individual functions also prevent drift of the baseline due to laser fluctuations or other long term drifts. This also facilitates longer experiment durations for a further reduction in random noise.

Applications: Aside from the usual applications of correlators the BI-8000AT for the first time allows the design of light scattering systems where data may be obtained at several angles

simultaneously without the need to install a large amount of hardware. This is particularly important in space based applications where low power and high reliability are of utmost concern. In addition, the software can be designed such, that the input signals from several photo detectors can be switched to any single card, thus providing full redundancy in case of a hardware failure in one card. In this respect the BI-8000AT is also the first fault-tolerant correlator. Other advantages are the reduction in total experiment time making the data less susceptible to long term changes in temperature, chemical reactions, agglomerizations etc.

In critical point experiments, e.g., scattered light must be measured at a low and a high angle. Again, the use of 2 correlator cards, combined with the proper optical configuration, reduces the total experiment time by a factor of 2.

The BI-8000AT is also programmable to measure the structure function $S(\tau) = \sum [n(t)-n(t-\tau)^2]^2$ with the same delay time modes (constant distance or constant ratio) as when used to measure the correlation function.

Conclusion: A new digital correlator has been introduced to complement the existing multiple sample time correlator (BI-2030AT) and the industrial particle sizer (BI-90). This new instrument provides for a significant reduction in hardware and will lead to the design of new QELS systems in research and industrial quality control applications.

References:

1. On the recovery and resolution of exponential relaxation rates from experimental data: a singular-value analysis of the Laplace transform inversion in the presence of noise.
M.Bertero, P.Boccacci, E.R. Pike, Proc. R. Soc. London, A 383, 15-29 (1982)

2. On the recovery and resolution of exponential relaxation rates from experimental data. II. The optimum choice of experimental sampling points for Laplace transform inversion.
M. Bertero, P.Boccaci, E.R. Pike, Proc. R. Soc. London, A 393, 51-65 (1984)

3. Light scattering polydispersity analysis of molecular diffusion by Laplace transform inversion in weighted spaces.
M.Bertero, P.Brianzi, E.R. Pike, G. de Villiers, K.H. Lan, N.Ostrowsky
J. Chem. Physics Vol 82, No. 3, 1 Feb. 1985

ENHANCED RESOLUTION PARTICLE SIZE DISTRIBUTIONS BY MULTIPLE ANGLE PHOTON CORRELATION SPECTROSCOPY

Steven E. Bott
Coulter Electronics, Inc.
Langley Ford Instruments
Amherst, Massachusetts

Abstract Photon correlation spectroscopy has become a method of choice for measuring submicrometer particles. It is capable of rapid, accurate measurements of mean particle size. Since the measurements are nonperturbing, it is ideal for monitoring systems undergoing dynamic changes. Despite its widespread acceptance, the information content of PCS measurements for particle size distributions is low and provides limited resolution.

A method is presented whereby PCS measurements made at several scattering angles plus the angular distribution of light scattered from the particles are combined in a single simultaneous analysis to effect an enhanced resolution particle size distribution. The efficacy of the method is assessed by recovering size distributions from computer simulated data and by comparisons of conventional PCS measurements of polystyrene spheres with those made by the new method.

• Single Angle PCS Measurements

Introduction

In a dynamic light scattering measurement, a sample comprising a group of diffusing particles or molecules are illuminated by a beam of coherent light. Light scattered into a small solid angle in one well defined direction is collected and directed onto a detector. The intensity of light sensed by the detector is the result of the interference at the detector of the light scattered from every illuminated particle in the part of the sample viewed by the collection optics.

As the particles randomly diffuse through the solution, the interference pattern at the fixed detector is modulated by the particle motion. In the simplest terms, smaller, faster diffusing particles cause more rapid changes in intensity at the detector than do larger particles, which diffuse more slowly. Since diffusion is a random phenomenon, the changes in light intensity at the detector are random fluctuations, not periodic oscillations. Thus the intensity recorded at the detector is a random function of time, i.e. a noise signal.

That the size of particles in a PCS measurement is coded in a noise signal is at the heart of the underlying reason for the limited resolution of which the

technique is capable. Unlike other techniques which more directly measure the size of, for example, individual particles, PCS measures an indirect property of a large ensemble of particles and must from this indirect, convoluted information extract a particle size distribution. The ensemble measurement is necessary because signals from individual particles in this size range are too small to be directly detected.

Inverse Laplace Transform

Noise signals do not contain large quantities of information. What information is present in noise can be characterized by its power spectrum. The time domain equivalent (Fourier transform) of a power spectrum is the autocorrelation function (acf). The acf of a random noise signal has the form of a decaying exponential.

In a general system of diffusing particles or molecules, the acf can be written as a linear combination of the exponential decays:

$$g(t) = \int_0^\infty e^{-2\Gamma t}\, x(\Gamma)\, d\Gamma \qquad (1)$$

where g(t) is the acf, Γ is the decay constant of the decaying exponentials, and $x(\Gamma)$ is the distribution function of decay times.

The actual meaning of $x(\Gamma)$ and the model by which Γ is interpreted will depend on the dynamical system under study. PCS is used in characterizing a wide variety of dynamical systems, ranging from simple particle sizing to flexing of random coil polymers, etc. Although this communication will concentrate on particle sizing, the methods developed here are quite general and could be used for increasing PCS resolution on a variety of systems.

For a dilute system of diffusing spheres,

$$\Gamma = q^2 [k T / (3 \pi \eta d)] \qquad (2)$$

where k is Boltzmann's constant, T is the absolute temperature, η is the solution viscosity and d is the particle diameter. q is the magnitude of the scattering vector: $q=4\pi\sin(\theta/2)/\lambda$, where θ is the scattering angle and λ is the wavelength of the incident radiation. $X(\Gamma)$ will represent the particle size distribution: $x(d)=x(\Gamma(d))$.

Since g(t) in (1) has the form of a Laplace transform, the process of extracting the desired distribution of decay times, $x(\Gamma)$, from g(t) amounts to an inverse Laplace transform (ILT).

Data analysis

Because of the low information content of a PCS measurement, the problem of numerically inverting the Laplace transform is at least ill conditioned and often ill posed (i.e. possessing no unique solution). A raft of methods have been devised to perform the ILT. It has been shown that these methods are essentially equivalent for PCS measurements[1]. For purposes of discussion it will be assumed that the inversion can be satisfactorily accomplished by a method called regularization.

Equation (1) can be written in discrete form:

(3) $$\mathbf{g} = \mathbf{K}\,\mathbf{x}.$$

x and **g** have the same meanings as before but are now characterized by values at a discrete set of points. **K** is a matrix which includes the kernel of the transform and whatever quadrature coefficients are chosen for the numerical integration.

According to the regularization method, the best distribution of decay times, **x**, is given by

(4) $$\mathbf{x} = (\mathbf{L}^t\mathbf{L})^{-1}\,\mathbf{L}^t\,\mathbf{g}', \qquad \text{where}$$

(5) $$\mathbf{L} = \begin{bmatrix} \mathbf{K} \\ \alpha\mathbf{H} \end{bmatrix} \qquad \mathbf{g}' = \begin{bmatrix} \mathbf{g} \\ \mathbf{0} \end{bmatrix}$$

The superscript t refers to the matrix transpose, **H** is a matrix used to impose a smoothing constraint on the solution and α is a scalar which controls the degree of smoothness of the solution. **H** is conventionally taken to be a matrix such that $\mathbf{x}^t\mathbf{H}\mathbf{x}$ forms the norm of the second order differences of **x** [4].

It is essential that (4) be solved under the constraint that all components of the solution vector, **x**, be nonnegative[1]. The nonnegativitiy constraints are valid because **x** represents a probability distribution and the constraints are necessary to prevent artificial oscillations in **x** caused by the ill conditioning. An efficient algorithm for solving (4) subject to nonnegativity constraints is 'nnls' [3].

A figure of merit for testing resolution

Statistics on the repeatability or precision of measurements of bimodal distributions provide a good way to characterize the information content and resolution of particle sizing measurements. Although most systems of interest are not bimodals, response to bimodal distributions is a good predictor of general particle sizing capability.

To provide a metric by which bimodal particle sizing resolution can be assessed, the following figure of merit (fom) will be introduced:

(6) fom = sum of coefficients of variation (CVs) = $\sigma_1/\mu_1 + \sigma_2/\mu_2$

where σ_i and μ_i are, respectively, the run to run standard deviation and the mean overruns of the position of peak i. Thus the sum of CVs fom characterizes the repeatability from run to run of the measured peak positions (i.e. mean diameters) of the two modes comprising a bimodal. For all of the data presented here, twenty measurements were made of each sample to compute the σ_i and μ_i.

To give an idea of the usual sizing resolution of PCS measurements of

moderate duration (3-20 minutes) on a variety of bimodal systems of standard spherical particles (polystyrene latex spheres or PSLs) using a single scattering angle, 90°, refer to Figure 1.

Figure 1

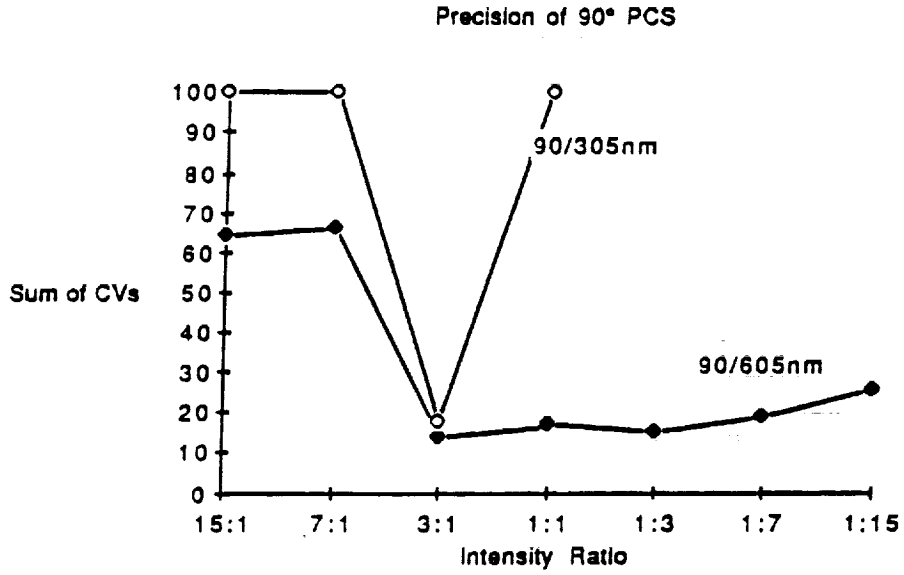

To prepare this graph, several mixtures of each of two bimodals (90nm/305nm and 90nm/605nm PSL) were prepared in proportions characterized by the ratio of scattered light intensity of the two populations of particles at a 90° scattering angle. For example, mixtures were made such that the scattered light intensity from the smaller particles divided by that from the larger were 1:15, 1:7, etc.

If a complete family of such curves were made, covering a wide range of diameter ratios (ratio of diameters of particles in the two populations comprising the bimodal) and intensity ratios, the particle sizing performance of a technique would be well specified.

There are two important conclusions which can be drawn from the data shown in the figure and other similar data not shown. First, the precision of a measurement at a given diameter ratio depends on how balanced the two peaks are in relative scattered intensities. Bimodals with intensity ratios near 1:1 are measured with greatest precision. Second, bimodals with well separated peaks are measured with higher precision than those with closely spaced peaks. Although it is not shown here, the smallest diameter ratio which can be resolved by PCS under optimal conditions (near 1:1 intensity ratio) is around 2:1.

The range of relative intensity ratios over which a bimodal of given diameter ratio can be resolved with reasonable precision is at least as important as the smallest diameter ratio which can be resolved. This is self evident because of the necessity to measure real samples of arbitrary relative mass ratios and modality.

Another, less obvious but equally important ground for the importance of the relative intensity ratio criterion, is that intensity ratios close to the ideal 1:1 often correspond to mass ratios far from 1:1. Often an extremely wide range of intensity ratios must be measurable in order to measure successfully the mass ratio range of interest.

- **Combined PCS and Classical Light Scattering**

Angular dependence of scattered light

The inverse of magnitude of the scattering vector, q, is a benchmark of the distance scale over which light scattering responds to a system under study. For particles of a size close to or exceeding 1/q (1/q ~ 50nm for λ=500nm, θ=90°), light scattered from different parts of the same particle can destructively interfere at the detector. The extent of destructive interference depends on scattering angle through q. This interference phenomenon leads to patterns of angular scattering intensity dependent on particle size, shape and composition.

For solid spheres of uniform composition (and for a few other shapes of particles) expressions exist[5,6] giving scattered light intensities as a function of scattering angle for different sized particles. For purposes here, we will concentrate on this simplest system, uniform spheres. Extensions of this work can be made straightforwardly for particles of other geometries, shapes and compositions.

Figure 2

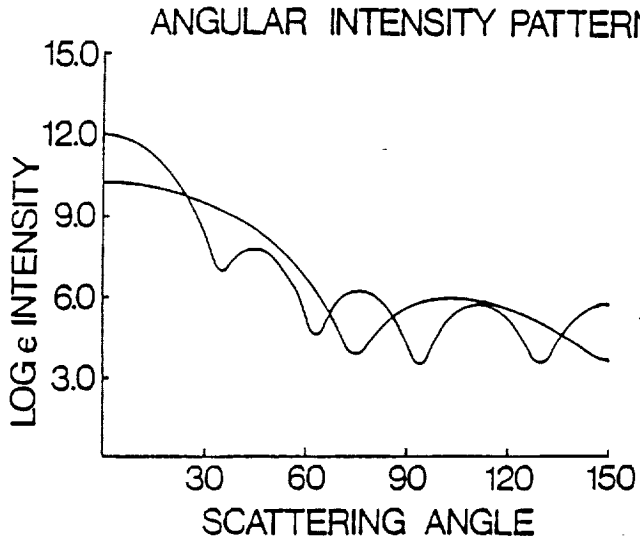

Figure 2 shows the angular dependence of scattered light for particles of 300 and 1000nm. The characteristic scattering patterns for different sized particles can be used to deduce particle size. Particle size can be related to the pattern of angular scattered light by

(7) $$\mathbf{p} = \mathbf{M}\,\mathbf{v}$$

where **p** is a vector whose components are the relative scattered light intensities at various angles, **v** is a vector volume or mass weighted particle size distribution, and **M** is a matrix relating particle sizes to the angular scattering pattern, i.e. the ith column of **M** is the vector giving the angular scattering pattern for a particle of a size corresponding to the ith component of **v**. Measurements of angular scattering patterns are called classical light scattering (CLS) measurements.

PCS measurements at different scattering angles

The angular dependence of scattered light intensity affects PCS measurements. Figure 3 shows the scattered light intensity per unit volume for spheres of a range of sizes, for 90° and 30° scattering angles. Each curve could be used to convert an angle dependent intensity weighted distribution measured by PCS to a volume distribution. Equation (3) can be rewritten to show the angle dependent part of **x**:

(8) $$\mathbf{g}(\theta) = \mathbf{K}(\theta)\,\mathbf{x}(\theta) = \mathbf{K}(\theta)\,\mathbf{C}(\theta)\,\mathbf{v}$$

where **v** is the same as in (7), and the diagonal elements of the diagonal matrix, $\mathbf{C}(\theta)$, give the volume to intensity conversion factor at the angle θ.

The explicit dependence of $\mathbf{x}(\theta)$ on θ means that intensity distributions measured at different angles will contain independent information.

Figure 3

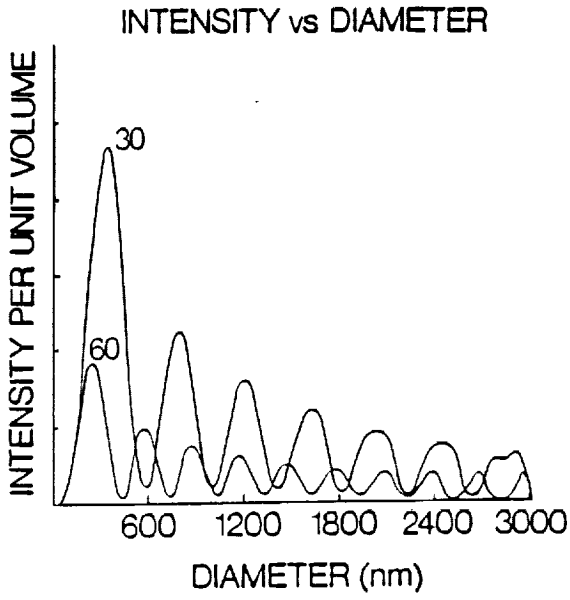

The overall light scattering picture

So far, ways to measure particle size by PCS measurements at different angles or by CLS have been presented. To picture how these two methods are related, refer to Figure 4. In the figure, the z axis represents the amplitude of the acf, the y axis represents scattering angle and the x-axis represents delay time in the acf. Thus the curves coming out of the plane of the paper are acfs, as in equation (8).

The curve in the plane of the paper (y-z plane) contains the zero time values of acfs of different scattering angles. The zero time values are directly proportional to the cls intensity: thus this curve is also the cls pattern for the distribution of particles.

Figure 4

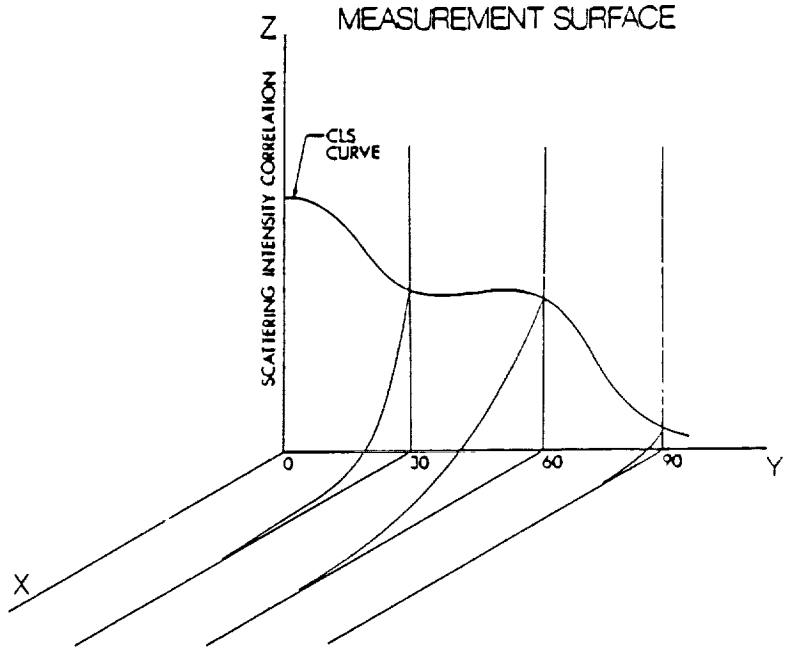

The key to enhanced particle size measurements

The surface circumscribed by the acfs and cls curve in Figure 4 represents a 'measurement surface' for a particular system of particles. This surface provides a far more sensitive characterization of particle size than any single curve on the surface. The single curves represent individual PCS or CLS measurements such as are conventionally used to measure particle size.

The measurement surface is related to the size distribution v, by

(9) $$\mathbf{s} = \mathbf{J}\,\mathbf{v},$$

where J and s are a row augmented kernel matrix and measurement vector, respectively, relating the volume weighted distribution to the various light scattering measurements comprising the measurement surface and have the forms:

$$(10) \qquad \mathbf{s} = \begin{bmatrix} g(\theta_1) \\ \cdots \\ g(\theta_n) \\ \mathbf{p} \\ \mathbf{0} \end{bmatrix} \qquad \mathbf{J} = \begin{bmatrix} K(\theta_1)\, S(\theta_1) \\ \cdots \\ K(\theta_2)\, S(\theta_n) \\ \mathbf{M} \\ \propto \mathbf{H} \end{bmatrix}$$

Equation (10) implies that an acf is measured at n angles. Since (9) has the same form as (3), the solution is found as in (4).

- **Computer simulated inversions**

Computer simulations were used to test the resolution enhancement resulting from the use of an abbreviated form of the measurement surface: two acfs measured at different scattering angles. In these simulations, the acfs corresponding to a bimodal distribution of diffusing spherical particles at the scattering angles, 90° and 20°, were calculated and the direct sum formed to comprise **s**. Gaussian noise of amplitude 10^{-3} times the acf amplitude was added to simulate a real experiment. The appropriate **J** matrix was calculated (c.f. (10)). Then, using the measured acfs, a modified form of a common PCS analysis program, CONTIN[1] was used to solve equation (9).

Figure 5 shows the true distribution (solid line) and recovered distribution using the acf at each scattering angle separately and that using both acfs together. The modes of the bimodal differed by a factor of two in size, i.e the diameter ratio is 2.0.

Figure 5

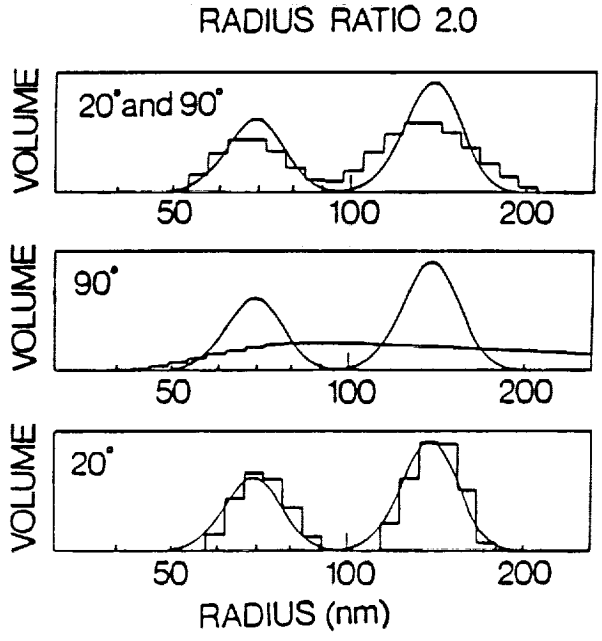

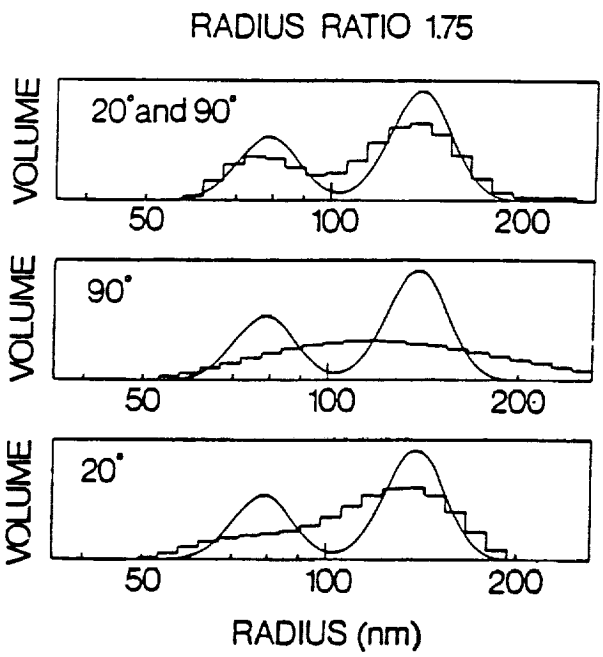

Figure 6

Figure 7

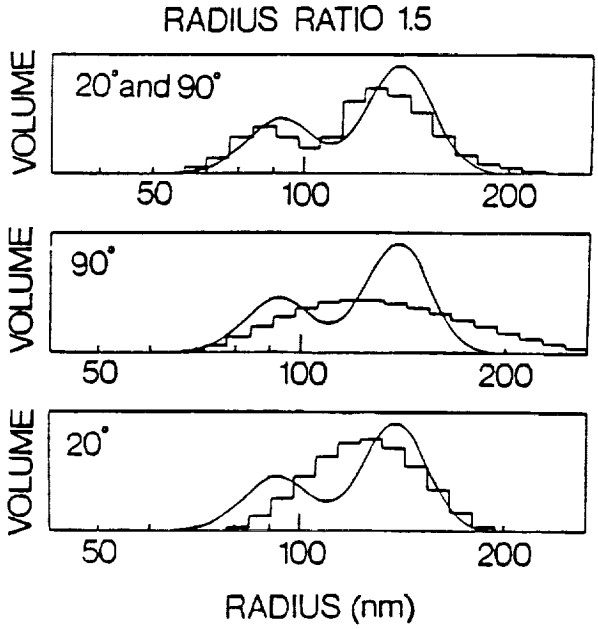

Figures 6 and 7 show the same data for bimodal populations of diameter ratios 1.75 and 1.5. The graphs show that at a diameter ratio of even 1.5, the two angle PCS measurement is able to resolve the bimodal. On the other hand, the acfs for one PCS angle alone is not able to truly resolve the bimodal even at a diameter ratio of 1.75:1.

- **Experimental Comparisons of Combined PCS/CLS vs PCS**

To test the method on real samples, three groups of bimodal samples were prepared at various intensity ratios. Samples of each bimodal were prepared to intensity ratios, measured at a 90° scattering angle, of between 15:1 and 1:15 (see Figures 8-10).

For the multi scattering angle measurements, PCS data was collected at three scattering angles: 30°, 90° and 150°. In addition, the angular scattering patters was at 50°, approximately equally spaced angles between 10° and 120°, was also used.

The measured data formed the vector **s** as in (10). The kernel, **J**, was computed assuming Mie conversions from intensity to volume distributions. The data were analyzed using a modified version of the PCS data analysis program CONTIN. The precision of the measurements was characterized according to the sum of CVs found in equation (6).

Figure 8.

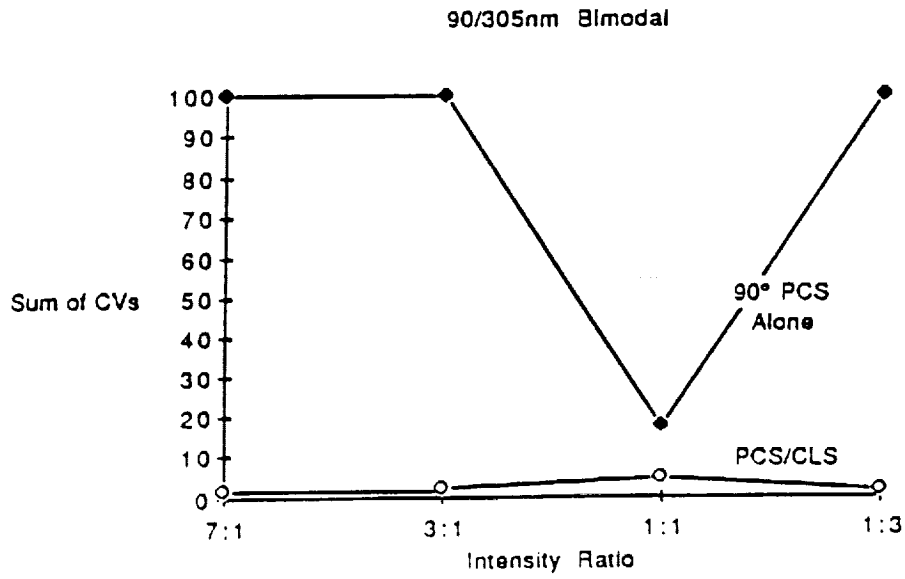

Figure 9.

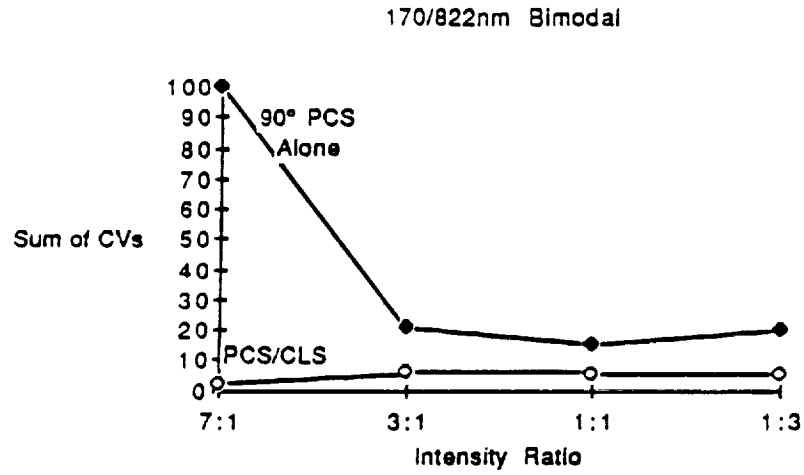

Figure 10.

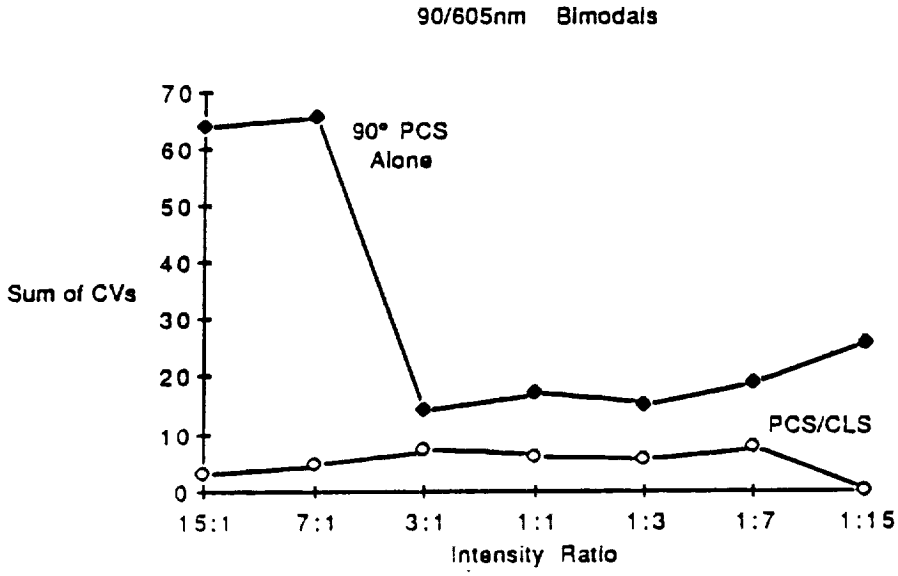

A comparison of the precision of the combined multiple angle PCS/CLS with simple 90° PCS measurements is presented in Figures 8-10. In each case, the range of intensity ratios over which a high precision (low sum of CVs fom) measurement could be made was extended considerably. In fact with unbalanced

intensity ratios, the single 90° PCS measurement often showed a fom of greater than 100% , which was rounded down to 100% in order that the much smaller foms of the combined PCS/CLS measurements could be seen on the same scale.

Not shown is a measurement of a 90nm/170nm bimodal at an intensity ratio of 1:1 at 90°. The sum of CVs fom for the combined PCS/CLS data was 16%, which is better than the precision of the 90nm/305nm 1:1 intensity ratio bimodal measured at the 90° PCS angle alone. Results with the combined measurements were thus comparable to the single angle results at a diameter ratio almost twice as great.

• Conclusion

By combining PCS measurements made at several angles with the angular scattering pattern of a distribution of particles, a particle size distribution of considerably greater resolution and precision can be measured than by current means employing a single angle PCS or single CLS measurement. The improvement in resolution is at least a factor of two over current measurements. More importantly, the mass ratio range over which the combined PCS/CLS measurements are of reasonable precision has been shown to be at least an order of magnitude greater than the range using single PCS measurements.

References

1. S. E. Bott, Doctoral Thesis (Stanford University), University Microfilms International, Ann Arbor, Michigan, 1984.
2. J. G. McWhirter and E. R. Pike, J. Phys. A: Math. Gen., 11, 1729, (1978).
3. C. L. Lawson and R. J. Hanson, Solving Least Squares Problems, Prentice Hall, New Jersey, 1974.
4. S. Twomey, J. Assoc. Comput. Mach., 10, 97 (1963).
5. M. Kerker, The Scattering of Light and Other Electromagnetic Radiation, Academic Press, New York, 1969.
6. C. E. Bohren and D. R. Huffman, Absorption and Scattering of Light by Small Particles, John Wiley and Sons, New York, 1983.
7. S. W. Provencher, Computer Physics Comm., 27, 213 (1982).

ONLINE SUBMICRON PARTICLE SIZING BY DYNAMIC LIGHT SCATTERING USING AUTODILUTION

David F. Nicoli and V.B. Elings
Particle Sizing Systems, Inc.
Santa Barbara, California

Efficient production of a wide range of commercial products based on submicron colloidal dispersions would benefit from instrumentation for online particle sizing, permitting real-time monitoring and control of the particle size distribution. Important specific examples include synthetic polymers, oil-in-water and water-in-oil emulsions, and vesicles/liposomes. Recent advances in the technology of dynamic light scattering (DLS) -- especially improvements in algorithms for inversion of the intensity autocorrelation function -- have made it ideally suited to the measurement of simple particle size distributions (i.e. unimodals and bimodals) in the difficult submicron region. Crucial to the success of an online DLS-based instrument is a simple mechanism for automatically sampling and diluting the starting concentrated sample suspension, yielding a final concentration which is optimal for the light scattering measurement. We have developed a proprietary method and apparatus for performing this needed sampling/dilution function, designed to be used with a DLS-based particle sizing instrument. For preliminary evaluation of this technology, we have used our sampler/diluter in conjunction with a NICOMP Model 370 Submicron Particle Sizer (Pacific Scientific, Instruments Div., Silver Spring, MD). A PC/AT computer is used as a smart controller for the valves in the sampler/diluter, as well as an input-output communicator, video display and data storage device for the Model 370. For simple unimodal distributions, very good run-to-run reproducibility and absolute accuracy ($\pm$2%) are achieved with periodic sampling periods of 10 to 15 minutes, in which 5 minutes is dedicated to acquisition of scattered light data and analysis, and the remaining time is devoted to the functions of sampling, dilution, temperature equilibration and system flushing. Quantitative results are presented for a latex suspension and an oil-in-water emulsion.

BRIEF THEORETICAL REVIEW

Dynamic light scattering is concerned with the time behavior of the scattered light intensity obtained from a suspension of particles in liquid. This contrasts with traditional classical light scattering, which measures only the average scattered intensity. A simplified schematic diagram of a typical DLS instrument is shown in Fig. 1.

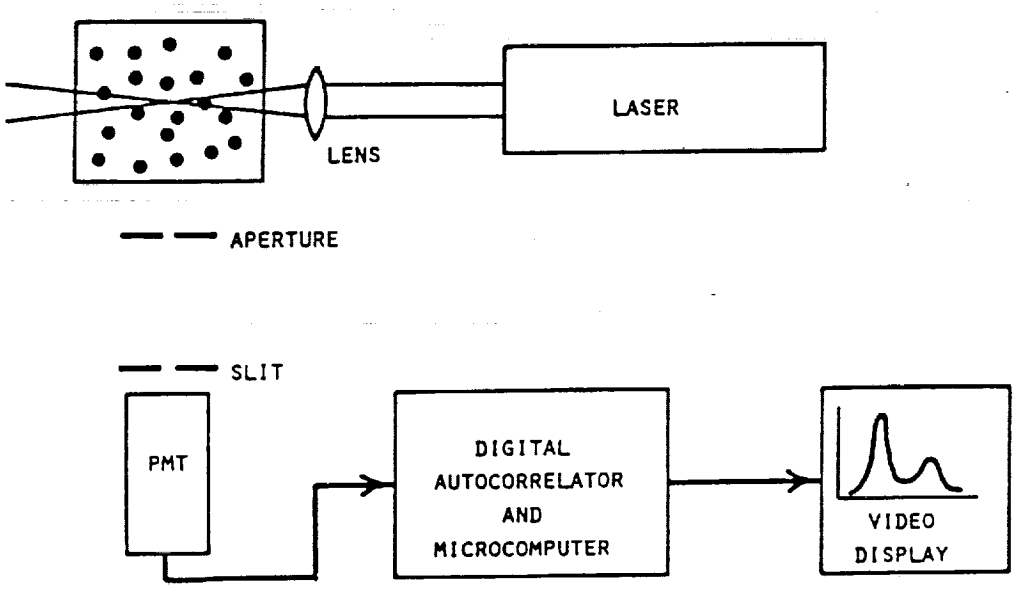

Fig. 1. Simplified schematic diagram of a typical DLS instrument.

When a colloidal dispersion is illuminated by a coherent laser light source, each particle in the suspension transmits a scattered wave whose phase at a distant detector depends on the position of the particle with respect to both the incident laser beam and the detector. These waves combine coherently, or "interfere", at the point of detection to yield a net scattered intensity, I(t). As the particles mutually diffuse in the liquid by the well-known process of Brownian motion, the scattered intensity fluctuates randomly in time due to changes in the phases of the individual scattered waves, caused by changes in the positions of the particles. The time behavior of this fluctuating intensity is related to the rate of diffusion of the suspended particles: the smaller the mean particle diameter, the faster the diffusivity D and the more rapid the rate of "flicker" of I(t).

Fluctuations in I(t) can be quantitatively related to the distribution of particle diffusivities by

computing and analyzing the intensity autocorrelation function, C(t),

$$C(t) = \langle I(t')\, I(t'-t) \rangle \tag{1}$$

where the bracket symbols < > denote an ensemble average of many such intensity products over a succession of different times t', representing different locations of the particles. In the idealized case of a monodisperse, or uniform, distribution of particle sizes, the autocorrelation function C(t) is particularly simple -- a single, decaying exponential function,

$$C(t) = A \exp(-2DK^2t) + B \tag{2}$$

where K, the "scattering wavevector", is a constant, depending on the laser wavelength, the scattering angle and the index of refraction of the suspending liquid. From the decay time constant of C(t) one easily obtains the particle diffusivity D. Finally, the particle radius R is obtained from D using the Stokes-Einstein equation,

$$R = kT/6\pi\eta D \tag{3}$$

where k is Boltzmann's constant, T the temperature (deg. K) and η the shear viscosity of the diluting solvent (usually water). A simplified representation of the fluctuating scattered intensity I(t) and the corresponding exponential autocorrelation function C(t) are shown in Fig. 2. Further details relating to the theoretical background of the DLS technique, experimental devices and methods, and applications to particle systems can be found in a number of references[1-4].

In actual practice, one rarely encounters an idealized, nearly monodisperse particle size distribution which yields a C(t) well described by a single decaying exponential function, as shown in Eq'n 2. Instead, one is often confronted with a polydisperse system whose autocorrelation function represents a combination of decaying exponential functions, each of which possesses a different decay constant, corresponding to a particular diffusivity D_i, relating to a particle radius R_i obtained from Eq'n 3. The resulting autocorrelation function C(t) obtained from the scattered intensity must be "inverted" to reveal the most likely distribution of particle diffusivities, f(D).

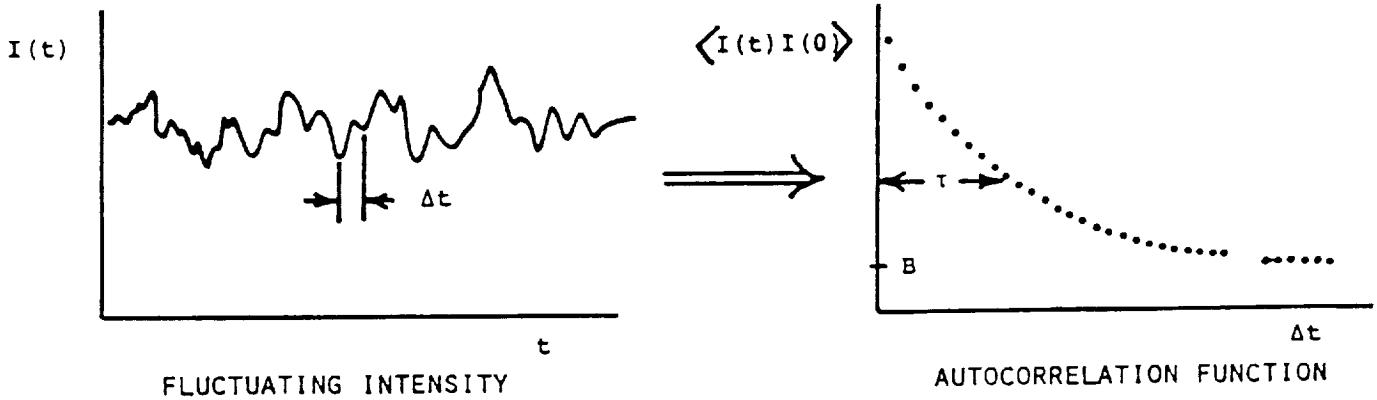

Fig. 2. Simplified representation of scattering intensity I(t) and corresponding autocorrelation function C(t).

INTRODUCTION

In recent years the technique of dynamic light scattering (DLS) (also known as photon correlation spectroscopy, PCS, or quasi-elastic light scattering, QELS) has developed into a powerful laboratory tool for characterizing submicron particle size distributions in solution. Instruments based on this technology have been used successfully to analyze a wide variety of commercial products, ranging in particle diameter from 5 or 10 nanometers to approximately 5 microns. Important specific applications include synthetic polymers (e.g. latexes) made by emulsion polymerization, colloidal silicas, pigments and dyes, phospholipid vesicles, and a wide variety of oil-in-water and water-in-oil emulsions produced by homogenization or microfluidization™.

The parameter of particle size distribution has been shown to be of considerable importance in determining important physical characteristics of an end product, as well as indicating the efficiency of the overall production process. For example, in the case of emulsions made by homogenization or microfluidization, frequent measurement of the mean particle diameter can be used to establish the optimal number of cycles (i.e. the total elapsed time) and energy input for the process. In the case of latex production, the particle size distribution has a critical influence on the physical properties -- and therefore the end use -- of the final latex dispersion. For products produced in continuous or semi-batch reactors, the particle size distribution can, in principle, be controlled by manipulating such variables as emulsifier concentration and monomer feed rate. Success with such manipulation, however, requires use of a fast, accurate and reliable method for online determination of the polymer particle size. Needless to say, the time required for a complete particle size measurement must be short enough to allow sufficient time for the appropriate control actions to be calculated and implemented.

Instrumentation based on dynamic light scattering would appear to be well suited to online particle sizing applications, owing to its characteristics of high speed, simplicity of operation, noninvasiveness, reproducibility and accuracy, and applicability over a wide size range. Thusfar, however, this technology has been confined almost exclusively to laboratory and offline quality control environments. It has yet to be integrated successfully into production facilities for submicron particles, so as to provide automatic online sizing capability suitable for real-time process monitoring and control.

The principal factor behind this obvious shortcoming is the normal requirement of significant operator intervention associated with sample preparation and introduction into the light scattering instrument. This includes the capture of a portion of concentrated sample and dilution of the latter (in a suitable solvent, typically water) to a final concentration optimal for the light scattering measurement. A simple, proprietary system for automatic sample acquisition and dilution has been developed by the authors, designed to interface with a DLS-based instrument. The results discussed herein were obtained using a modified Nicomp Model 370 Submicron Particle Sizer (Pacific Scientific, Instruments Div., Silver Spring, MD).

The determination of the full particle size distribution from DLS data for general polydisperse particle systems is an ill-conditioned problem, and therefore one which is unable to produce unique solutions. There have been a number of attempts to solve this problem[4-11] -- i.e. to improve the resolution and convergence of algorithms designed to invert C(t). A review of most of the avilable algorithms for determining unimodal and bimodal distributions can be found in Stock and Ray[12].

Two completely different mathematical approaches have evolved for analyzing C(t), based on the complexity of the underlying particle size distributions. For complex distributions, such as those containing two peaks (bimodals), or single, highly-skewed peaks (asymmetric unimodals), one must use the most general inversion algorithm appropriate for multimodal analysis -- e.g. a generalized Laplace transform inversion using a nonlinear least-squares fitting procedure, such as that developed for the Nicomp Model 370 instrument. Fortunately, however, one frequently encounters quite simple particle size distributions, such as smooth, unimodal populations, for which f(D) (after intensity weighting) is approximately Gaussian in shape. For these cases, one finds that the simpler method of cumulants analysis[1-4,13] usually yields a good fit to the autocorrelation function data.

In the cumulants procedure one fits a polynomial (in time t) to the "reduced" autocorrelation data, $R(t)=0.5\log_e[C(t)-B]$. In the trivial case of a monodisperse distribution, R(t) vs t is simply a straight line of negative slope; the particle diffusivity D is proportional to the slope. For more general polydisperse distributions, R(t) vs t acquires curvature, where the degree of curvature increases with the extent of polydispersity (i.e. the overall width of the distribution of particle diffusivities). One usually carries out a second-order cumulants analysis, using a quadratic least-squares fit to R(t). In this case, one obtains the first two moments of f(D). The first moment, or average diffusivity D_{avg}, corresponds roughly to an average particle radius R_{avg} obtained using Eq'n 3. The second moment, obtained from the curvature of the quadratic fit, yields a standard deviation, or coefficient of variation (C.V.), of f(D), which is related to the half-width of f(D).

A chi-squared fitting error parameter serves to test whether the assumed gaussian shape in diffusivities is reasonable. The cumulants fit is considered reliable if a low value of chi-squared (i.e. close to unity) is obtained after sufficient data have been accumulated in C(t) to overcome statistical noise. Such a 2-parameter cumulants fit to the intensity autocorrelation data has the advantage of being computationally fast and of settling relatively quickly with improving statistical accuracy in C(t). The calculated values of D_{avg} and C.V. are relatively accurate for those actual distributions f(D) which are: i) narrow -- having a C.V. no larger than 20-25% of D_{avg}, and ii) approximately symmetric.

The DLS technique for particle sizing contains a number of inherent advantages over competitive methods (e.g. optical turbidity), which make it ideally suited to automated, online applications. First, and most important, it is an absolute technique which, in principle, requires no calibration over time. As mentioned earlier (in connection with Eq'n 2), the scattering wavevector K connecting the absolute time scale of the intensity fluctuations with the particle diffusivity D depends on three parameters, all of which are constant (for a given choice of suspending solvent). The conversion of a given value of D into the corresponding particle radius R (Eq'n 3) depends on two additional parameters which can be held constant -- temperature T and solvent viscosity η. Hence, a DLS-based instrument should yield consistent, reproducible results over extended periods of time, requiring no calibration.

Second, the measured particle diffusivity D (and hence the calculated radius R, from Eq'n 3) is essentially independent of the concentration of suspended particles, provided the original suspension is diluted to a sufficient extent that multiple scattering and interparticle interactions (such as electrostatic repulsions between highly charged particles at low electrolyte concentrations) have no appreciable effect on the autocorrelation function C(t).

Third, the diffusivity D of suspended particles depends only on their size, and is independent of their composition -- i.e. density, molecular weight, index of refraction, etc. Although these physical properties will certainly influence the average level of the scattered light intensity, they will not affect the particle diffusivity, nor the resulting time behavior of the intensity fluctuations.

Clearly, these three characteristics of the DLS technique make it ideally suited to an online measurement, in which sample acquisition, dispersion and dilution must be performed in an automatic fashion (discussed further below). The contrast to particle size estimation based on optical turbidity is particularly striking. In the latter technique, a precisely regulated amount of starting concentrated suspension must be metered into a controlled volume of diluent. The mean particle diameter can then in principle be determined from the optical turbidity of the resulting diluted suspension, given a single-valued calibration curve of turbidity vs particle size; of course, the starting sample concentration and composition (i.e. index of refraction) will greatly influence the latter, and therefore must be known. If the dilution factor should change (due, for example, to gradual clogging of the metering valve or variabilities in other fluidics components), the measured turbidity will also change, for reasons unconnected with the particle size distribution. In addition, the presence of substantial polydispersity (e.g. bimodality) in the size distribution can result in very misleading estimates of mean particle diameter using the turbidimetric method.

REQUIREMENTS FOR THE AUTOMATIC SAMPLER/DILUTER

The crucial new ingredient required for successful online particle size analysis using DLS instrumentation is a computer- controlled mechanism capable of automatically capturing a quantity of concentrated suspension from the reactor and diluting it to an appropriate concentration. The automatic diluter must produce a final particle concentration which gives rise to a scattered intensity level that is optimal for the autocorrelator. That is, it must be sufficiently low to avoid multiple scattering and interparticle interactions, but large enough to yield a high signal-to-noise ratio in the autocorrelation function after a relatively short data acquisition time -- i.e. a few minutes.

There are at least two difficulties associated with the use of conventional dilution schemes (i.e. those employing fixed dilution factors). First, the required dilution factor is not easily calculable at the outset, even for a sample of known characteristics. Second, the optimal dilution factor can be expected to vary greatly with changes in the physical properties of the starting suspension. The scattered intensity increases linearly with the particle number density (number of particles per unit volume of latex). More importantly, it is also strongly dependent on the ratio of the refractive index of the particles to that of the diluting liquid (a function of the square of that ratio), as well as, of course, the particle size distribution. For example, in the Rayleigh region (particle diameters < ca. 50 nm), the scattered intensity goes as the square of the particle volume, or as the 6th power of the radius.

In practice, the strong dependence of the scattered intensity on the above characteristics of the

particle suspension requires that the automatic dilution system possess a very wide dynamic range. That is, it must be capable of achieving dilution factors ranging from roughly 100:1 (for very small particles and/or low concentrations) to 100,100:1 or greater. Because the particle concentration and size distribution are, at worse, completely unknown, there is no *a priori* knowledge of the correct dilution factor appropriate for a given DLS measurement.

With the above requirements and tradeoffs in mind, we have recently developed a method and apparatus (patents pending) for automatically diluting any starting concentrated suspension of particles for delivery to a light scattering cell in a DLS instrument. For the purpose of carrying out this preliminary study, an existing Nicomp 370 instrument was modified for use with an external sampler/diluter. For most routine applications, the latter utilizes three electrically controlled valves; for high pressure applications (e.g. emulsion polymerization), pneumatically controlled ball valves with electrically-operated solenoid valve actuators are substituted. The valve assembly serves to connect the three principal components of the system: i) the tank or pipe containing the concentrated particle suspension, ii) the autodilution system/flow-through scattering cell of the DLS instrument, and iii) a source of filtered diluent (typically water).

The system is controlled by an AT computer, which operates under a simple, flexible, menu-driven program (MS/DOS) and serves two main functions. First, it controls the external sampler/diluter valves for the operations of sample acquisition, predilution, introduction into the Autodilution system and cell flushing. Second, it serves as an input-output device for serial communication with the DLS instrument (including data storage). In fully automatic mode the sampling cycle commences with the capture of a quantity of fresh concentrated sample. Following a short predilution cycle, the partially diluted sample is then passed to the Autodiluter, where the dilution factor is allowed to increase continuously until the scattering intensity falls to a level appropriate for the digital autocorrelator and consistent with the considerations discussed above. After a predetermined delay to achieve temperature equilibration with the scattering cell, the diluted sample is then analyzed by the DLS instrument. At a predetermined time the particle size distribution results are printed, the raw data stored on diskette and the fluidics system flushed with filtered water. The computer/controller then awaits the preprogrammed start of the next measurement cycle. Figure 3 shows a simplified schematic diagram of the online DLS particle sizing system, including automatic feedback control of the autodilution function.

We investigated the reproducibility of our online DLS particle sizing instrument using two samples -- a vinyl acetate latex and an oil-in-water emulsion. The former turned out to be nearly monodisperse, while the latter was relatively broad (polydisperse). The total time needed for one complete measurement cycle includes several steps: sample acquisition, autodilution, temperature equilibration, data collection, mathematical analysis, printing and storage of results, and system flushing. With the exception of data collection, the remaining functions require essentially a fixed total time -- approximately 5 minutes. The time needed for data collection (i.e. buildup of the autocorrelation function) depends on the complexity of the particle size distribution and the degree of absolute accuracy required. For both of the systems which we have evaluated (discussed below), the distributions were well approximated by the simple gaussian (cumulants) analysis -- as evidenced by values of chi-squared near unity -- permitting accurate determination of the mean particle diameter for each sample in a matter of a few minutes.

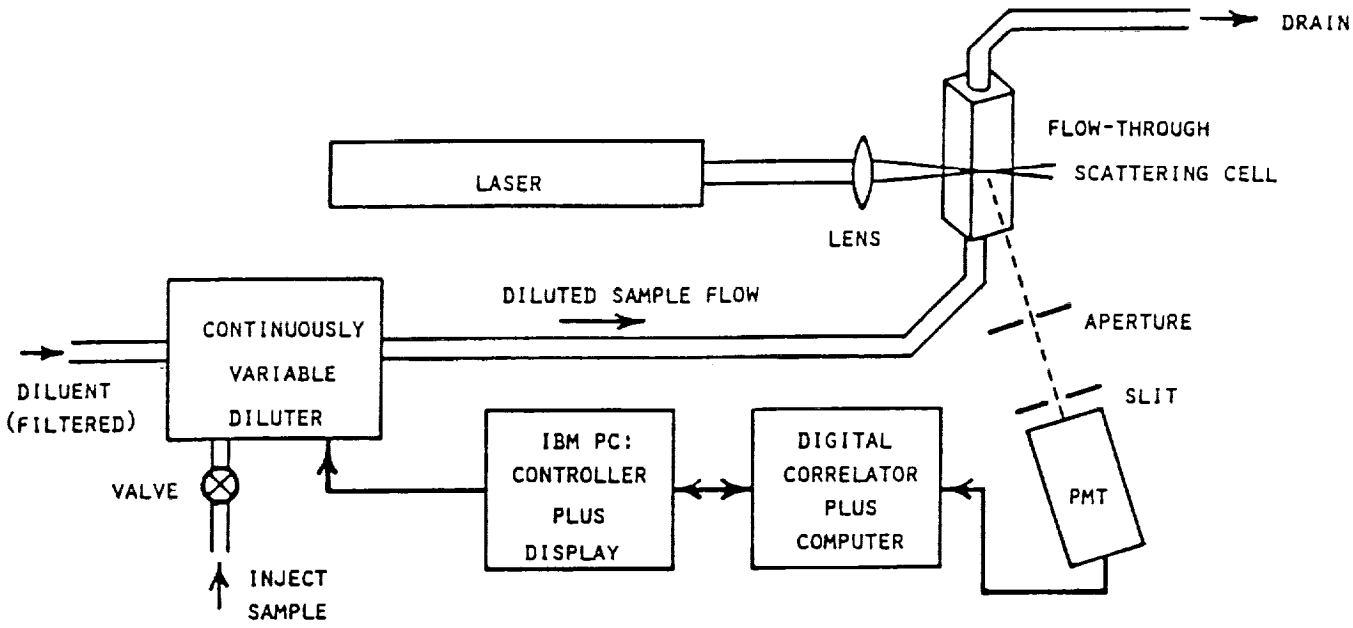

Fig. 3. Simplified schematic diagram of the online DLS-based particle sizing system, including feedback control of the autodiluter.

RESULTS - DISCUSSION

In order to judge the importance of the statistical accuracy of the autocorrelation data, it is instructive to examine the computed mean particle diameter as a function of data acquisition time. This is shown in Fig. 4 for a vinyl acetate latex suspension[14]. A quantity of the concentrated suspension was placed in a small stainless steel holding tank, pressurized with air to 10 psi and connected to the automatic sampler/diluter assembly. After the initial sample acquisition and dilution, the DLS instrument was programmed to report the results of the cumulants analysis approximately every 45 minutes, for a total of 40 minutes.

In Fig. 4 we see that the intensity-weighted mean particle diameter (upper plot) settles over time to an approximately constant value -- 160.6 nm. It appears that after a total data collection time of 8 to 10 minutes, the computed mean diameter should change by only about 1%, or less, with additional statistics. By contrast, the corresponding volume-weighted mean diameter (lower plot) fluctuates considerably over the first 10 to 20 minutes of data acquisition. This is a consequence of the relatively large changes in the C.V. (i.e. the 2nd cumulant) which occur early in the run. These variations become less pronounced over time, due to the gradual settling of the 2nd moment of the assumed gaussian distribution of particle diffusivities. The long-term settled value for the volume-weighted mean diameter for this vinyl acetate sample is approximately 155.5 nm, with a C.V. of 12% of the mean diameter.

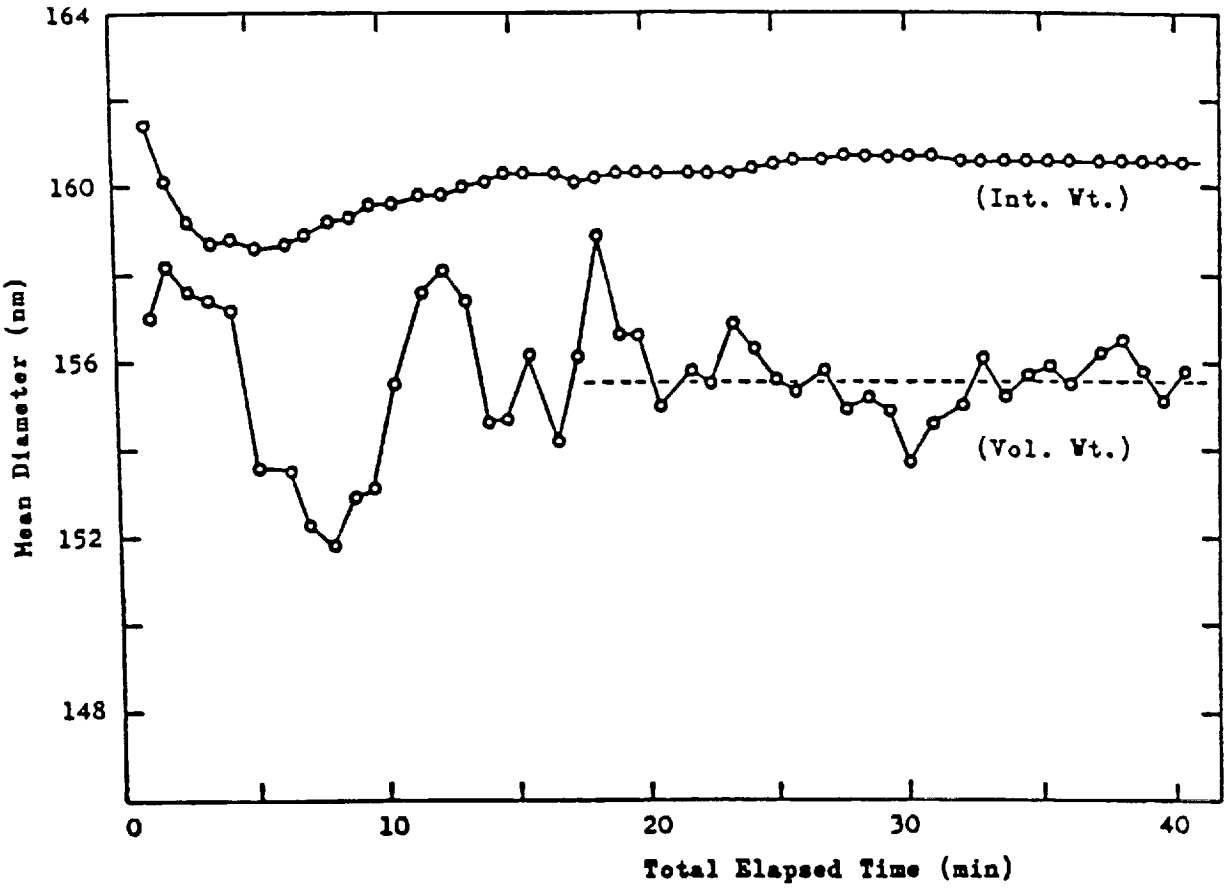

Fig. 4. Intensity- and volume-weighted mean diameter of a relatively monodisperse vinyl acetate latex suspension as a function of data collection time.

It is easy to draw two conclusions concerning the use of the online particle sizing instrument for this particular latex sample, which possesses a relatively narrow size distribution. First, in order to minimize the total data acquisition time needed for reproducible particle size results, one should focus on the intensity-weighted mean diameter (as opposed to the volume-weighted parameter), which exhibits relatively little fluctuation over time, even during the first few minutes of data acquisition. Second, it would appear that good reproducibility can be achieved (for this sample) using a data collection time of 10 minutes or less; reasonable results should be attainable after 5 minutes of data collection.

In order to challenge the speed capability of our instrument system, we carried out a series of measurements on this latex sample, using a repetition period of 15 min and a data acquisition time of 5 min. The results of 20 consecutive automatic measurements (5 hours elapsed time) of the intensity-weighted mean diameter are summarized in Fig. 5.

We observe a tight distribution of mean diameter values, with a maximum deviation with respect to the average of only about 2 nm, or only slightly more than 1%. The average for these 20 independent measurements was 160.5 nm -- almost identical to the long-time settled value found in Fig. 4. We conclude that for this relatively monodisperse latex sample the online sizing system is highly effective, with a reproducibility of better than $\pm 2\%$ for a relatively short data acquisition time of 5 minutes.

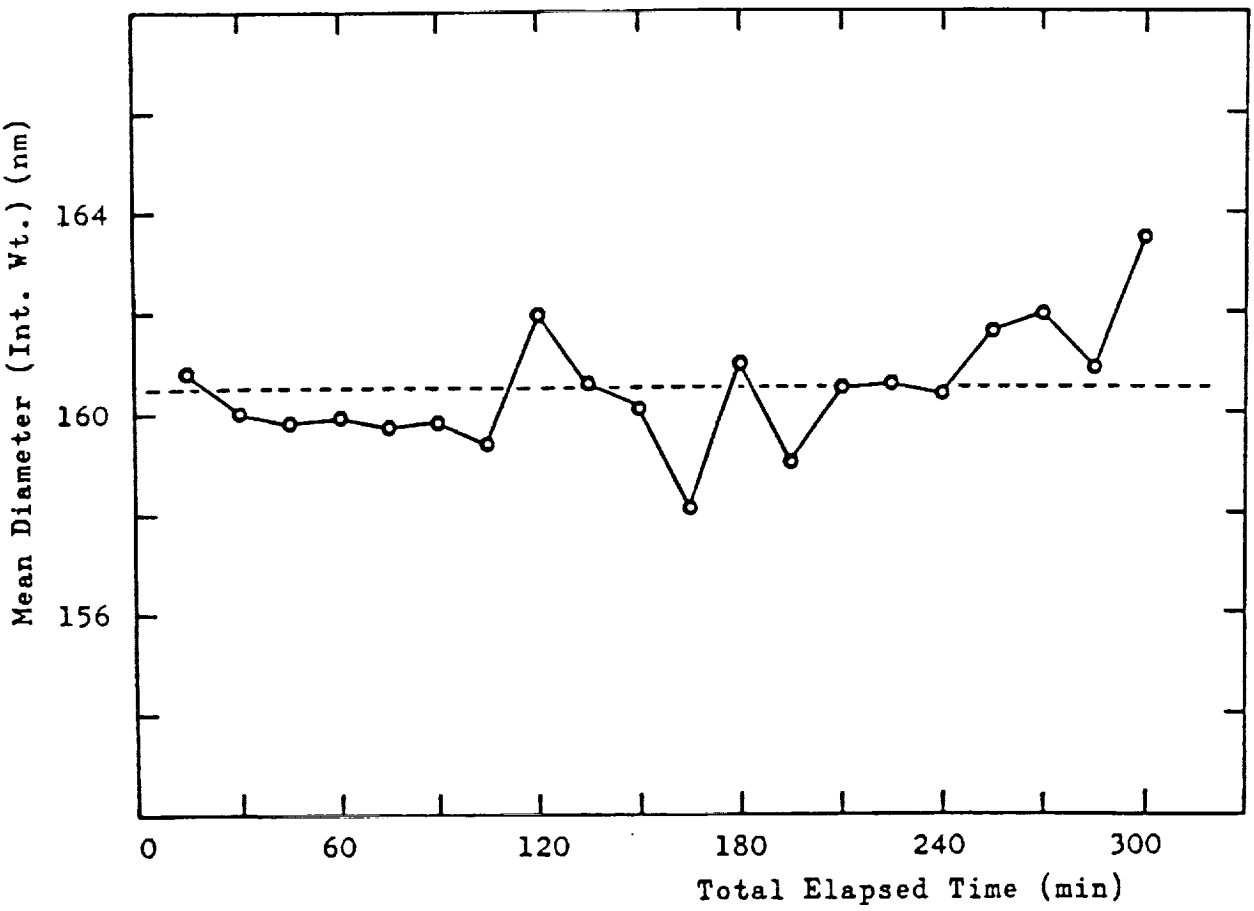

Fig. 5. Run-to-run reproducibility of intensity-weighted mean diameter for a vinyl acetate latex -- repetition period of 15 min, data acquisition time of 5 min.

We next turn to an oil-in-water emulsion (intravenous feeding fluid, made by homogenization), which possesses a wider distribution of particle diameters than the latex previously discussed. Here, the intensity-weighted mean particle diameter (long-time settled value) is approximately 225 nm, with a C.V. of ca. 30% of this mean value, and a corresponding volume-weighted mean diameter of about 203 nm. As described above, we performed online measurements on this emulsion, but in this case a fresh sample was acquired every 20 minutes, and the time of data acquisition was lengthened to 10 minutes. The results are summarized in Fig. 6.

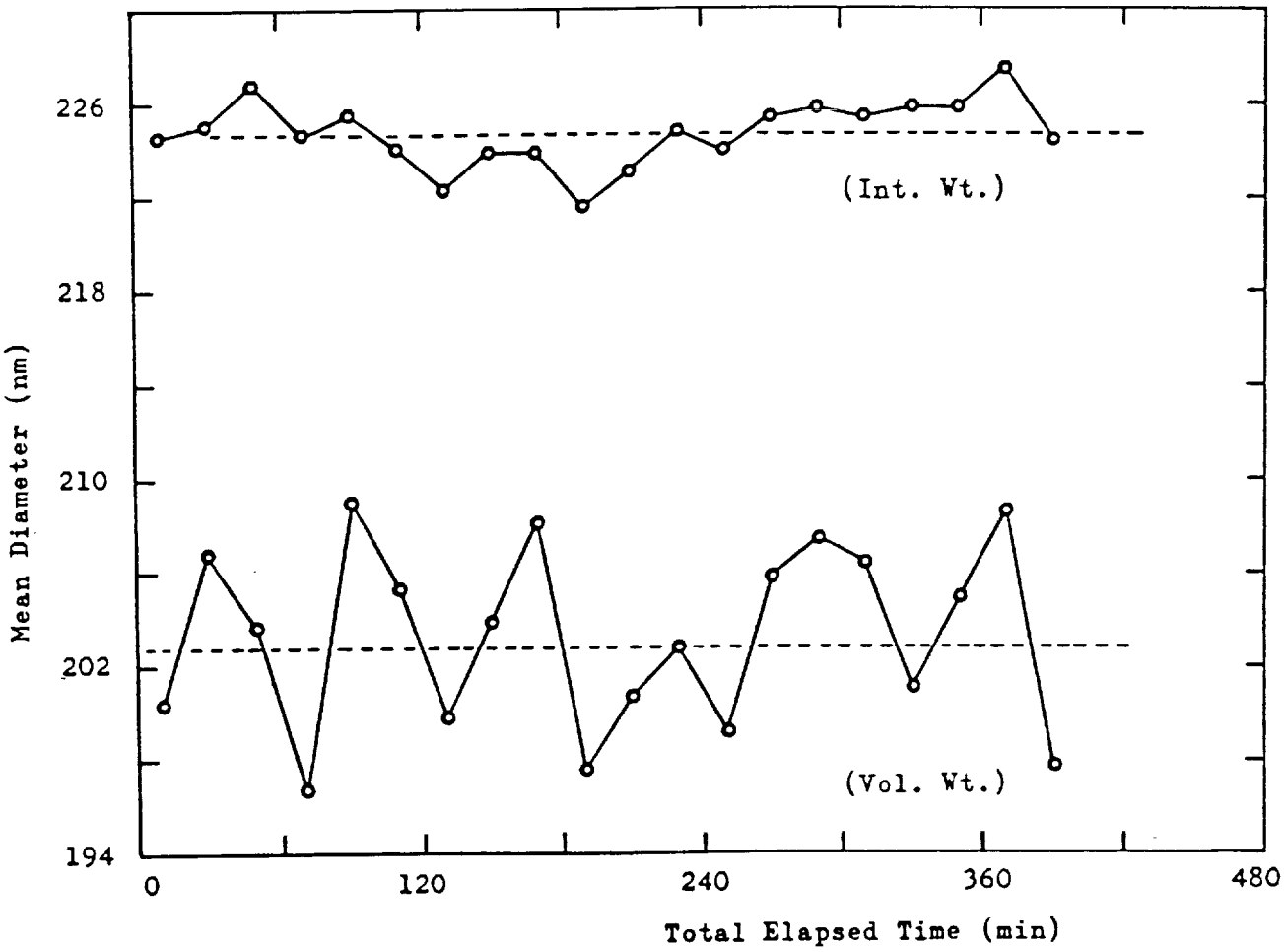

Fig. 6. Run-to-run reproducibility of mean diameter (intensity- and volume-weighted) for an oil-in-water emulsion -- repetition period of 20 min, data acquisition time of 10 min.

Here, again, we find a highly reproducible measurement of the intensity-weighted mean particle diameter (upper plot), with less than a ±2% maximum variation about the average value (224.7 nm) over the 20 independent runs in Fig. 6. As to be expected, the variations in the volume-weighted mean diameter (lower plot) are considerably larger, owing to its sensitivity to variations in the computed C.V. (2nd cumulant) of the distribution. Nevertheless, the maximum deviation of the volume-weighted values with respect to the average of the 20 runs (202.8 nm) is less than ±4%. Again, we conclude that our DLS-based particle sizing system with autodilution is highly effective as an online monitoring tool. It is able to characterize accurately both narrow and broad (single-peak) particle size distributions. For populations which are more complex than those investigated and discussed here, one would be required to lengthen the autocorrelation data acquisition time, so as to permit effective use of a nonlinear least-squares Laplace inversion procedure to extract additional information about the particle size distribution.

REFERENCES

1. Chu, B., Laser Light Scattering, Academic Press, New York, 1974.

2. Berne, B.J. and Pecora, R., Dynamic Light Scattering, John Wiley, New York, 1976.

3. Pecora, R. (Ed.) Dynamic Light Scattering: Applications of Photon Correlation Spectroscopy, Plenum Press, New York, 1985.

4. Dahneke, B.E. (Ed.) Measurement of Suspended Particles by Quasi-Elastic Light Scattering, John Wiley, New York, 1983.

5. McWhirter, J.G. and Pike, E.R., J. Phys. A: Math., Nucl. Gen., 11, 1729 (1978).

6. Pike, E.R. In Scattering Techniques Applied to Supramolecular and Non-Equilibrium Systems. (S.H. Chen, R. Nossal, and B. Chu, Eds.). Plenum Press, New York, 1981.

7. Ostrowsky, N., Sornette, D., Parker, P. and Pike, E.R., Opt. Acta. 28, 1059 (1981).

8. Gulari, E., Gulari, E., Tsunashima, Y., and Chu, B., J. Chem. Phys. 70, 3965 (1979).

9. Provencher, S., Hendrix, J., and De Maeyer, L., J. Chem. Phys. 69, 4273 (1978).

10. Provencher, S., Computer Phys. Commun. 27, 213, 229 (1982).

11. Bott, S.E. In Particle Size Distribution -- Assessment and Characterization. (Provder, Th., Ed.), ACS Symp. Series, 332, Washington, D.C., 1987, 74-88.

12. Stock, R.S. and Ray, W.H., J. Polym. Sci.: Polym. Phys. Edit. 23, 1393 (1985).

13. Koppel, D.E., J. Chem. Phys. 57, 4814 (1972).

14. The vinyl acetate latex emulsion was prepared and kindly provided to Particle Sizing Systems by Dr. T. Kourti of the Institute for Polymer Production Technology, McMaster University, Hamilton, Ontario, Canada L8S 4L7.

LIGHT SCATTERING INSTRUMENTATION FOR MICRO GRAVITY RESEARCH

Philip J. Wyatt
Wyatt Technology Corporation
Santa Barbara, California

The analysis of light scattered from an ensemble of particles has long been a preferred method for characterizing their physical properties. Instrumentation to perform the measurements which forms the basis for such analysis is available in many forms based upon a variety of different experimental techniques. A system is presented singularly applicable for making many types of measurements in a microgravity environment. The commercial version of this device, the DAWN®-F, has been used in many laboratories throughout the world to perform analyses of particular importance for both research and production. Before describing its structure and function, a few remarks concerning light scattering theory are in order.

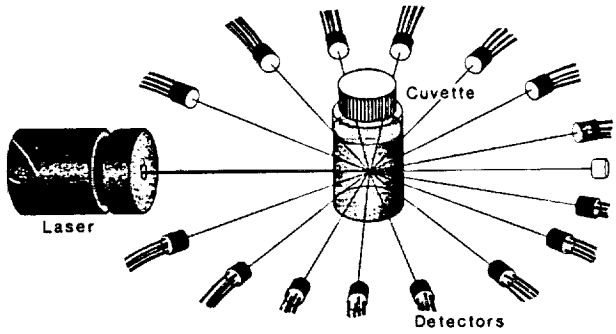

Fig. 1. Schematic representation of a light scattering experiment in a single plane.

Figure 1 presents in a schematic form the general format for a light scattering experiment performed in a single scattering plane. A "sample" is illuminated by a fine laser beam and light scattered into different directions is detected by detectors placed at different angular locations. The "sample" of the figure is contained in a transparent scintillation vial, though a number of other configurations are even more useful. The detectors shown are in general highly collimated and need not be restricted to lie in a single plane. They may be of a variety of types including transimpedence hybrid photodiodes, avalanche photodiodes, and photomultiplier tubes. Indeed, only a single detector is often employed with is made to rotate around the sample (goniometer). The particles so-measured may be simple molecules, macromolecules, bacteria, viruses and other small organisms. In general, we shall restruct our discussions to small particles, i.e. those less than a few tens of micrometers. Particles larger than this figure may be examined by light in a more direct manner. We are concerned here with using light to *infer* particle physical properties. Once

the particles of interest become very large, many of their physical properties are amenable to more direct classification. For such particles, however, we would use light scattering techniques to derive additional physical properties characteristic of their "building blocks", i.e. the molecules of which they are constructed. The physical processes responsible for creating these molecules are complex and often poorly understood. Sometimes the presence of a gravitational field affects such processes or may mask them. Accordingly, light scattering measurements of selected classes of particles and molecules within a microgravity environment could provide a bonanza of scientific results important to the understanding of these creation (e.g. polymerization) processes.

Based on the earlier work of Einstein[1], Raman[2], and Debye[3], Zimm[4] showed an important relationship between light scattering properties measured and physical properties derived:

$$\frac{R_\theta}{k^* c} = M_w P(\theta) - 2A_2 M_w^2 P^2(\theta) c, \qquad (1)$$

for very dilute particles. Here M_w is the weight average molecular weight of the particles in the scattering ensemble, c is the concentration in gms/ml, A_2 is the second virial coefficient, $P(\theta)$ is the angular variation of the scattered light as a function of the scattering angle (θ), and k^* is a physical constant depending on the relative refractive index increment (dn/dc) of the solution as the particle concentration changes, the refractive index of the pure solution absent the particles, and the vacuum wavelength of the incident light λ_o. Included in the scattering function, $P(\theta)$, are physical parameters depending on the particle configuration. Most importantly, $P(\theta)$ has the limiting form

$$P(\theta) \sim 1 - \frac{16\pi^2 n_o^2 \langle r_g^2 \rangle}{3\lambda_o^2} \sin^2 \theta/2, \qquad (2)$$

where

$$\langle r_g^2 \rangle = \frac{1}{V}\int r^2 dV, \qquad (3)$$

is the so-called mean square radius of the particle. V is the volume of the particle and the integration is performed over the particle's mass elements with respect to the distance *r* from the particle's center of *gravity*. The more commonly used term, radius of gyration, is a misnomer not to be confused with the kinematic origin of the term. Equation (2) may be written simply as

$$P(\theta) = 1 - x \qquad (4)$$

whenever

$$x = \frac{16\pi^2 n_o^2 \langle r_g^2 \rangle}{3\lambda_o^2} \sin^2 \theta/2 << 0, \qquad (5)$$

Thus for large particles, measurement at small enough scattering angles will usually satisfy Eq. (5).

Returning now to Eq. (1), the last undefined quantity, R_θ, is the Rayleigh excess factor given by

$$R_\theta = f\,[\,I(\theta) - I_c(\theta)\,]/\,I_o, \qquad (6)$$

where $I(\theta)$ is the intensity of scattered light measured from the ensemble at the angle θ, $I_c(\theta)$ is the corresponding quantity for the solvent alone, I_o is the incident light intensity, and f is the absolute calibration constant of the instrument performing the measurement. Thus the R_θ's are measured together with the concentration c and dn/dc. The weight averaged particle weight, mean square radius, and second virial coefficient are derived from these quantities. Higher moments of $\langle r_g^2 \rangle$ may be derived also. The method by which the physical parameters M_w, $\langle r_g^2 \rangle$, and A_2 are measured is usually based on the ingenious method developed by Zimm[4], aptly called a Zimm plot.

Equation (1) has a serious drawback: for mixtures of particles, it only yields weight averaged values. In recent years, however, an ideal "Maxwell's Demon" has been created to separate these particles by hydrodynamic and diffusion effects. Called Gel Permeation or Size Exclusion Chromatography[6] (GPC or SEC) this chromatographic technique separates molecules by means of specially packed columns which selectively permit the transit of molecules in terms of their effective size. Accordingly, such techniques may separate a specimen for subsequent light scattering analyses based on Eq. (1) if the concentration and angular scattering variation associated with each "fraction" so-separated can be measured. The concentration is readily measured by a sequential refractive index (R.I.) detector.

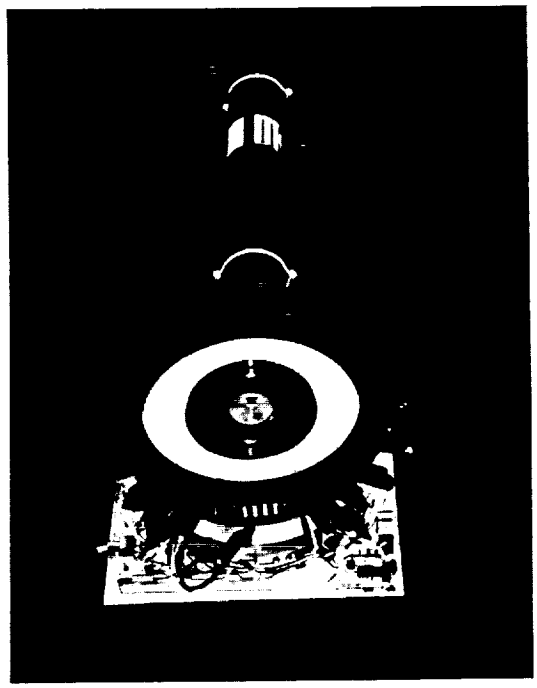

Fig. 2. DAWN-F read head.

Figure 2 presents a photograph of the read head of the DAWN-F (flow) light scattering photometer. This structure has been shown to be singularly suited for making a variety of light scattering measurements useful for GPC separations, bulk "Zimm plot" measurements, bioassays, and quasi-elastic light scattering determinations. At the center of the cylindrical aluminum block is the cell structure shown Fig. 3.
A highly polished cylinder has a through bore each end of which is attached to a stainless steel manifold permitting connection of many types of sample injection fixtures. Because the glass is selected of a refractive index greater than that of the entrained fluid, the light scattered therein is refracted before being detected by one of the 18 surrounding high gain hybrid trans impedance photodiode/amplifiers.

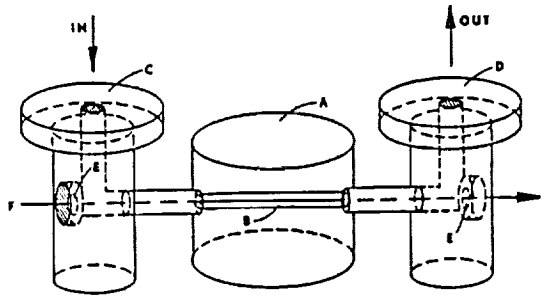

Fig. 3. The DAWN-F flow cell A with throughbore B and manifolds C and D. The laser beam enters at F through window E and exits through opposite window at E.

Figure 4 shows the refraction geometry for the rays scattered from a volume element dV into a scattering angle θ. At the interface, these rays are reflected into the angle θ' given by Snell's Law

$$n_g \cos \theta' = n_s \cos \theta, \tag{7}$$

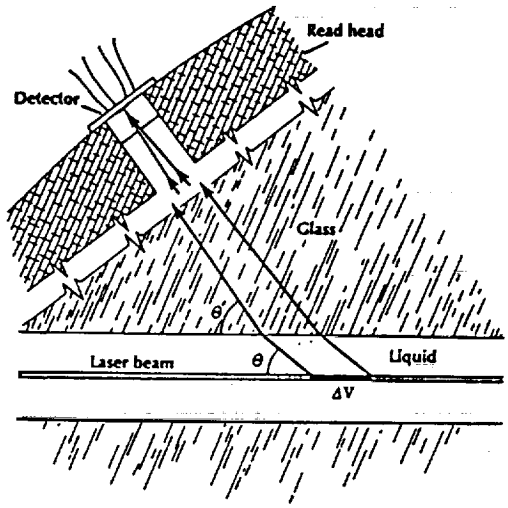

Fig. 4. Refraction of light scattered within the flow cell.

where n_s and n_g are the refractive indices of the solution and glass, respectively. Even for very small scattering angles, θ, the detectors at fixed angles, θ', do not receive scattered light from the entrance and exit windows of the manifolds themselves. Thus conventional "flair" noise is removed for this detector configuration. With the fixed detectors placed at equidistant values of cot θ', some of them are not accessible to any scattered light for certain low refractive index solvents. Accordingly, the instrument is generally operated by selecting the lowest 15 of the 18 available detectors consistent with Snell's Law, Eq. (7). For most solvents, there is usually a set of 15 detectors, the lowest of which corresponds to a scattering angle of about 10°, for scattering cells made of F2 glass with refractive index n_g = 1.61655 at 632.8 nm.

Figure 5 shows a Zimm plot obtained by successive injections of different (known) concentrations of aqueous suspensions of native xanthum gum. The molecular parameters derived therefrom corresponded to a weight average molecular weight, M_w, root mean square radius, r_g, and second virial coefficient, A_2, of

$$M_w = 10{,}128{,}000$$

$$\langle r_g^2 \rangle^{1/2} = 304 \text{ nm} \qquad (8)$$

$$A_2 = 3.17 \times 10^{-4}$$

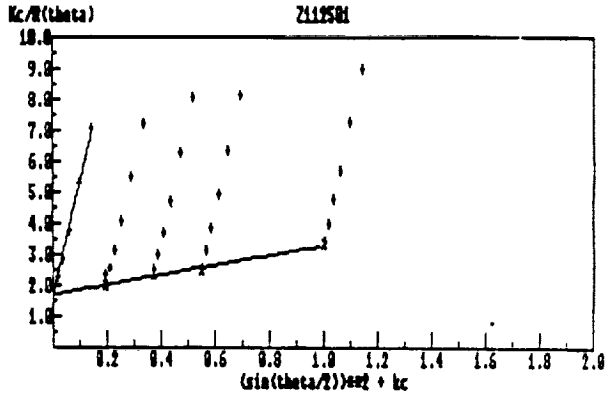

Fig. 5. Zimm plot based on the lowest six scattering angles from a Xanthum gum specimen in water. Four different concentrations were injected sequentially into the flow cell and then measured in a stop flow configuration.

Figure 6 presents a three dimensional representation of a GPC chromatogram obtained from an aqueous suspension of a polysaccharide standard with a weight average molecular weight of about 850,000. The excess Rayleigh factor as a function of retention volume is plotted for each angle. In the background is shown the RI detector response.

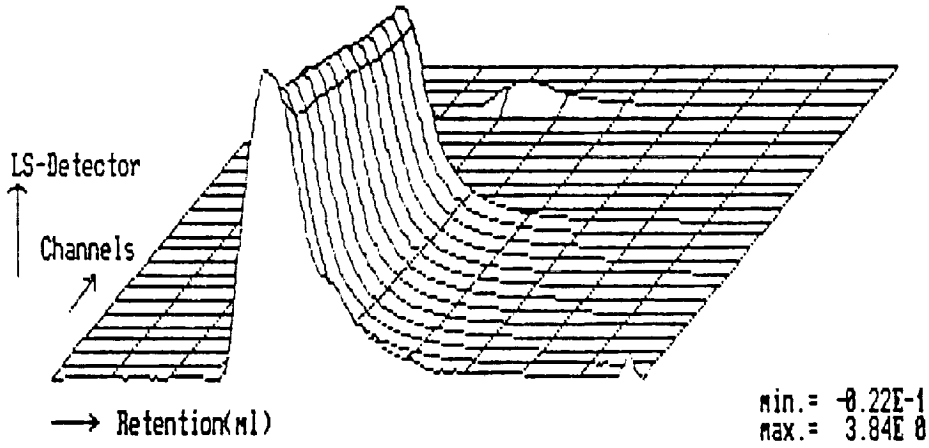

Fig. 6. Plot of retention volume versus scattering angle for a polysaccharide standard, M_w~ 850,000. Refractive index (concentration sensitive) detector is the farthest curve.

Suspensions of bacterial cells *(B. subtilis)* would produce the type of light scattering patterns shown in Fig. 7. The DAWN—F is readily converted for batch measurements by moving the cell and manifold structures and replacing them with a simple fixture to hold standard scintillation vials. The figure shows four curves (two of which are almost completely superimposed) corresponding to measurements from two replicate suspensions at 0 and 60 minutes. To one set was added a heavy metal toxicant at t = 0 min. This type of bioassay provides a rapid means for detecting toxicants in drinking water.

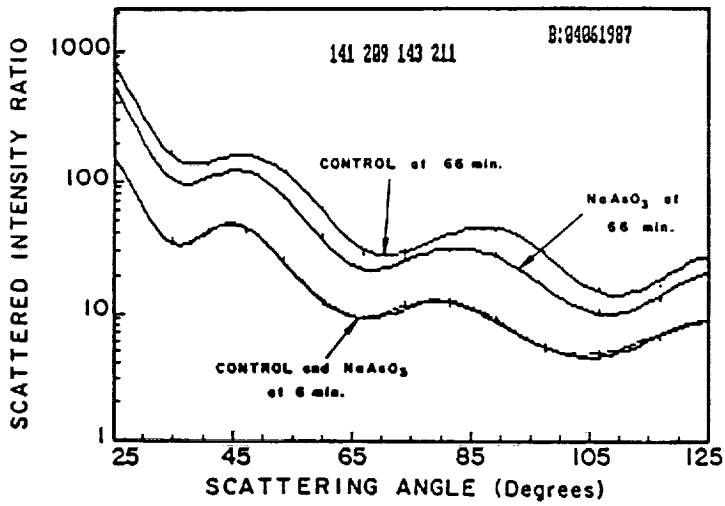

Fig. 7. Scattering from bacterial suspensions showing the effects of a water borne heavy metal toxicant.

Figure 8 shows the result of a QELS measurement using a NICOMP correlator in conjunction with the DAWN-F flow cell. A sample of two polystyrene sphere distributions was injected into the DAWN cell. A signal at about 90° was conveyed to a modest Hamamatsu 1104 photomultiplier by means of a multimode optical collimator. An 80 μm pinhole aperture was placed between the sample cell and collimator GRIN lens. The PMT signal was preprocessed with the NICOMP amplifier/discriminator. The 5 mW He-Ne laser beam was focused at the cell center with a simple plano convex lens. The high resolution of the result is due in large part to the structure of the flow cell itself. With negligible background scattering and only a small sample fraction lying between the scattering volume and the detector (the majority of the cell volume is occupied by clear glass), the cell structure seems ideal for performing fixed angle QELS experiments.

The versatility of measurements achievable with the DAWN-F read head structure is clearly evident from the foregoing discussion and illustrations. All analytical curves drawn through the experimental points have been fitted to them generally by means of Chebyshev polynomial[8] interpolations. It is clear, for example, from Fig. 7 that no number of additional detectors could have produced a more reproducible set of curves than presented there. Indeed, even the most complex of scattering patterns from sub-micrometer particles requires no more than 10 Chebyshev polynomials to fit the data in a least squares sence. One would expect similar interpolations to be equally valid for interpolating QELS data produced over an equivalent range of angles.

One remaining feature of the cell structure that should be mentioned, as well, relates to its use as a differential refractometer. Incorporating an auxiliary laser and a position sensitive detector, a sensitivity to fluid refractive index changes of one part in 10^6, or better, is easily achieved. The slight non-linearity of the system over the range of refractive

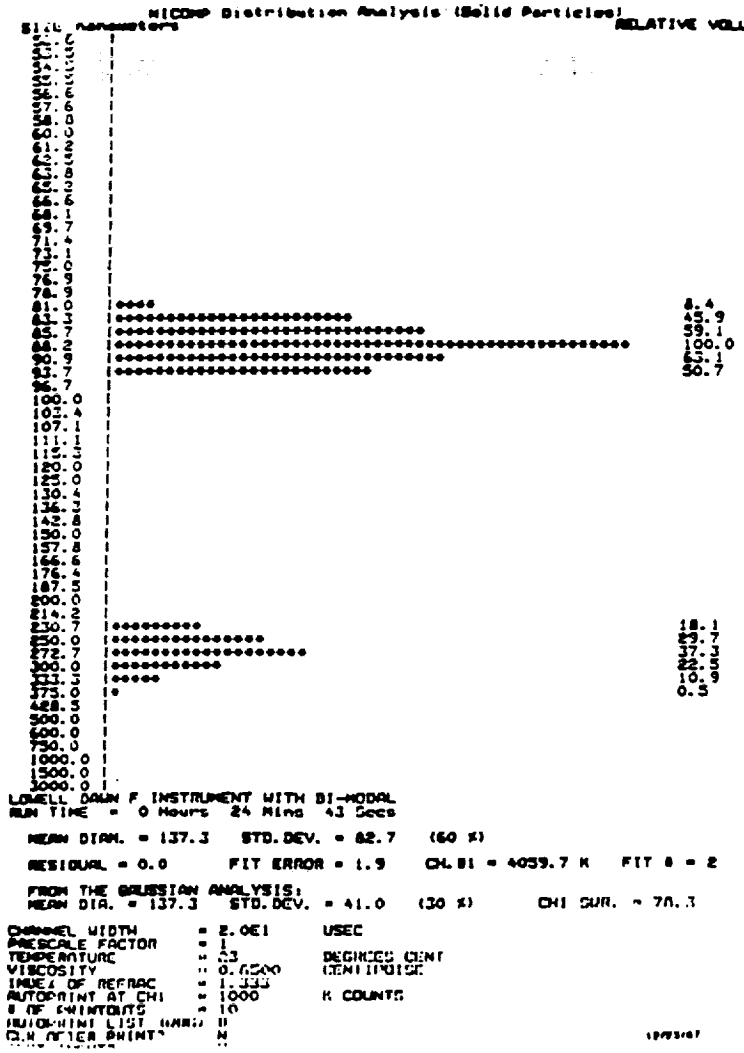

Fig. 8. Photon correlation measurement from a mixed latex sample using the DAWN-F flow cell and a NICOMP correlator.

index changes of significance for GPC measurements is easily compensated by relatively simple numerical interpolations. The truly unique aspect of this built-in refractometer is the ability it gives the total system to measure the refractive index change or solute concentration from the same volume for which a simultaneous multiangle light scattering pattern is produced. The requirement of standard GPC for accurate flow rate maintenance is thus obviated since there is no need to calculate the delay volume between the detector and columns — or for the light scattering configuration using a DAWN detector, between the light scattering detector and the concentration sensitive detector (RI). Figure 9 shows some early RI response data collected with the DAWN flow cell from a 20 µl 0.1% dextran sample of molecular weight ~600,000 injected into an aqueous stream being pumped through the cell. The spikes and other irregularities of the curve arose from pump noise since the cell and manifolds had been removed from the rigid read head structure during these measurements. Since an integrated RI detector permits deduction of each eluate's concentration, a simple hand pump could be used to perform an adequate GPC separation, reducing further the system's weight and power requirements.

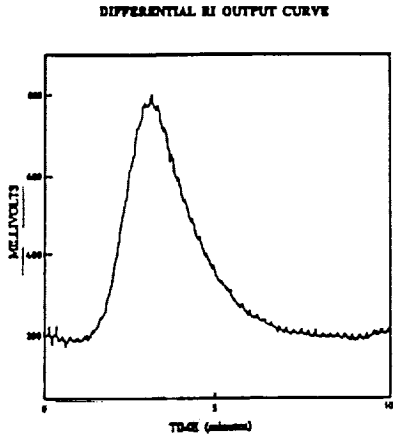

Fig. 9. Response of DAWN-F refraction cell to a 20 μl 0.1% aliquot of dextran, molecular weight ~ 600,000.

A variety of further instrument enhancements are quite reasonably implemented. For example, the gas He-Ne laser operating at 633 nm and 5mW is easily replaced by a diode laser operating at 780 nm and producing 10mW of power. The transimpedance photodiodes can be replaced by dual purpose avalanche photodiodes operated below their critical voltage for standard light scattering experiments, and above it for QELS, single photon counting experiments. Although the read head structure could be further shrunk, retaining the aluminum block structure ensures lensless collimation for all detectors in addition to good thermal and mechanical stability.

References

1. A. Einstein, Ann. Phys. **33**, 1275-1298 (1910).

2. C.V. Raman, Indian J. Phys. **2**, 1-6 (1927).

3. P. Debye, J. Physical Colloid Chem. **51**, 18-32 (1947).

4. B.H. Zimm, J. Chem. Phys. **16**, 1093-1099 (1948).

5. P.J. Wyatt, C. Jackson, and G.K. Wyatt, Amer. Laboratory **20**, (#5) 86-91 (1988); *Ibid.* **20**, (#6) 108-113; *Ibid Errata* **20**, (#7) 18 (1988).

6. W.W. Yau, J.J. Kirkland, and D.D. Bly, *Modern size exclusion liquid chromatography* (Wiley & Sons, New York, 1979).

7. P.J. Wyatt, *Rapid detection of toxicants in potable waters by laser light scattering*, Summary Report (U.S. Army Medical Bioengineering Research and Development Laboratory, Md. 1988).

8. C. Lanczos, J. Math. Phys. **17**, 123-199 (1938).

LASER LIGHT SCATTERING AS A PROBE OF FRACTAL COLLOID AGGREGATES

David A. Weitz and M.Y. Lin*
Exxon Research and Engineering Co.
Annandale, New Jersey

We review the extensive use of laser light scattering, both static and dynamic, in the study of colloid aggregation. Static light scattering enables us to study the fractal structure of the aggregates, while dynamic light scattering enables us to study the aggregation kinetics. In addition, both techniques can be combined to demonstrate the universality of the aggregaion process. Colloidal aggregates are now well understood and therefore represent an excellent experimental system to use in the study of the novel and fascinating physical properties of fractal objects. However, the ultimate size of fractal aggregates is fundamentally limited by gravitational acceleration which will destroy the fractal structure as the size of the aggregates increases. This represents a great opportunity for space born experimentation, where the reduced g will enable the growth of fractal structures of sufficient size for many interesting studies of their physical properties.

There has been considerable progress in recent years in our understanding of the process of colloid aggregation.[1] Applying the concepts of fractal geometry has provided new insight in characterizing the structure of the aggregates that are formed, while applying the concepts of scaling has lead to new insight in the time evolution of the aggregation process and the distribution of the masses of the clusters formed. Laser light scattering has played an important role in these advances.[2,3] Static light scattering can be used to probe the fractal structure of the aggregates directly. Dynamic light scattering provides a measure of the characteristic cluster radius, and can be used to measure both the kinetics of the aggregation as well as to obtain information about the cluster mass distribution.

Our increased knowledge of the details of colloid aggregation has an added, very significant benefit. It provides us with an experimental method of forming fractal structures that are well characterized, reproducible and controllable. These can be used as an experimental model to investigate the physical properties of objects that possess the unique geometry characteristic of fractals. In particular, the scale invariance of the structure of fractal aggregates is expected to lead to new and fascinating mechanical and vibrational properties, and the fractal structure characteristic of colloid aggregates is likely to have unusual dependence on external stresses, such as those induced by gravity or thermal motion.

*Also at the Department of Physics, City University of New York, New York, NY 10031.

In this paper, we present a very brief summary of the use of both static and dynamic laser light scattering to study the process of colloid aggregation and the structure of the clusters formed. We demonstrate that colloid aggregation can be described by two distinct regimes, which depend on the kinetics of the aggregation. By means of laser light scattering, we demonstrate that each of these regimes is universal, independent of the nature of the specific colloid system.

We then discuss possible extensions of experiments on fractal aggregates that may be interesting to perform in a microgravity environment. We illustrate that gravity can play an important role in the aggregation process through the differential rates of sedimentation that can exist when the cluster mass distribution is highly polydisperse. Although the lack of gravity would eliminate the effects of differential sedimentation, this can, in principle, also be done by other methods.

However, fractal structures are limited in the ultimate size that they can achieve before they collapse under the effects of gravity. Thus experimentation under conditions of reduced gravity may offer the possibility of growing considerably larger fractal structures. This could provide samples of sufficient size to facilitate the study of the novel physics predicted for objects that exhibit scale invariance.

Much of our experimentation is done using colloidal gold.[4] The colloid consists of gold spheres 75 Å in diameter with a volume fraction of about 10^{-6}. The aggregation is initiated by the addition of pyridine, which adsorbs on the surface of the gold spheres, displacing the charged ions which had stabilized the colloid against aggregation. The rate of aggregation is controlled by the amount of pyridine added, which determines the charge remaining on the surface of the spheres. Bringing the final pyridine concentration to 10^{-2} M displaces virtually all the adsorbed charge from the surface of the gold spheres. As a result, the particles stick immediately upon collision and the aggregation rate is limited solely by the diffusion of the clusters. This regime is called diffusion-limited colloid aggregation (DLCA). By contrast, if the final pyridine concentration is reduced to about 10^{-4} M, there remains a considerable charge on the surface of the colloids. This results in a substantial repulsive interaction between approaching particles, so that a large number of collisions are required before two clusters can stick to one another. This slows the aggregation rate down considerably, and this regime is called reaction-limited colloid aggregation (RLCA).

The clusters formed in each of these two regimes are fractal; however the fractal dimensions are quite different. The fractal dimensions of the clusters have been measured with a variety of techniques. Using transmission electron microscopy (TEM), the mass of a cluster can be determined simply by counting the number of particles that comprise the cluster.[5] The size of the cluster can also be directly determined from the TEM images. By studying a large number of clusters, we find that the cluster mass scales with its radius, $M\text{-}R^{df}$, where d_f is the fractal dimension. By this means, DLCA aggregates are found to have $d_f \approx 1.8$, while RLCA aggregates have $d_f \approx 2.1$. The fractal dimensions can also be determined by means of static scattering, using light,[2] X-rays[6] or neutrons.[7] All these methods give results that are consistent with those obtained from the TEM measurements.

The behavior of the two regimes of aggregation is distinguished in other ways as well. The cluster mass distributions for each regime are very different, as has been shown by TEM studies.[8] For DLCA, the cluster mass distribution is essentially independent of the mass up to a cutoff mass, M_c, and exponentially decreases above this cutoff. By contrast, for RLCA the cluster mass distribution is

dominated by a large number of very small clusters, and can be described as a power-law up to some cluster size, with an exponential cutoff above M_c, $N(M) \sim M^{-\tau} e^{-M/M_c}$, where $\tau \approx 1.5$. The shape of the cluster mass distributions have important consequences for light scattering from the aggregates.

The kinetics of the aggregation are also distinct for each regime. Since the cutoff mass characterizes the cluster mass distribution, the kinetics of each regime is reflected by the behavior of M_c. For DLCA we can represent the kinetics as a power-law, $M_c \sim t^z$, where $z=1$. This linear growth dependence is a consequence of the conservation of mass in an aggregating colloid. The dominant growth process for the DLCA occurs when two clusters of comparable size stick to one another. Thus, as the clusters become larger, the growth rate per collision increases. However, since no new mass is added to the system, the number of clusters must decrease as they grow, and the space between them must increase. Thus the time between the collisions also increases, offsetting the increased growth rate per collision and resulting in a

growth rate that is linear in time. By contrast, the kinetics of RLCA is exponential, $M_c \sim e^{At}$, where A is a rate that is determined by the sticking probability of two monomers. The increasing growth rate reflects the increase in the number of ways two clusters can stick to each other as they get larger, which increases the aggregation rate for the reaction-limited kinetics.

Light scattering has played an important role in the studies of colloid aggregation. Static light scattering is a convenient method for measuring the fractal dimension of the aggregates, while dynamic light scattering is well suited for measuring the size of the clusters and thereby monitoring the kinetics of the aggregation. Furthermore, both light scattering techniques can be used together to provide a comparison of the behavior of completely different colloid systems.

The static light scattering intensity from a single cluster can be written as $I(q) = M^2 S(qR_g)$, where the structure factor, $S(qR_g)$, is a function solely of the dimensionless parameter qR_g with q the scattering wavevector and R_g the radius of gyration of the cluster. The fractal scaling of the clusters can be used to relate the radius of gyration to the mass of the cluster, $M = (R_g/a)^{df}$ where a is the radius of a single gold sphere. The form of $S(qR_g)$ depends in detail on the structure of aggregates but it has the very general property that its limiting behavior is $S(qR_g) \rightarrow 1$ for $qR_g \ll 1$ and $S(qR_g) \sim (qR_g)^{-df}$ for $qR_g \gg 1$. Thus, for small clusters, where $qR_g \ll 1$, the static light scattering is insensitive to the internal structure of the aggregate, and the intensity scales as M^2 and is independent of q. By contrast, for larger clusters, the static light scattering is sensitive to the fractal structure of the aggregate and scales as q^{-df}, directly reflecting the fractal dimension. However, the scattering intensity from each cluster at a given q scales as M, rather than M^2, when $qR_g \ll 1$. For a distribution of clusters, the measured scattering intensity is simply the sum of the scattering intensities from the individual clusters, weighted by the cluster mass distribution function, N(M).

As an example of the static scattering from fractal aggregates, Fig. 1 shows a logarithmic plot of several sets of data obtained from DLCA clusters at different stages of aggregation. The solid lines through the data represent fits using the N(M) obtained from TEM studies and the $S(qR_g)$ obtained from a fit to the structure factor calculated for computer-generated DLCA clusters. At high q, the internal fractal structure of the clusters is resolved, and the intensity displays the linear behavior expected for a power law in the logarithmic plot. However, at smaller q, the clusters are sufficiently small that $qR_g < 1$, and the fractal structure is no longer resolved so the intensity becomes independent of q. For the larger clusters,

the fractal dimension can be measured directly from the slope of the scattering curves. This is illustrated in Fig. 2 where we compare the scattered intensity from DLCA aggregates with RLCA aggregates. Both sets of data are linear and their slopes

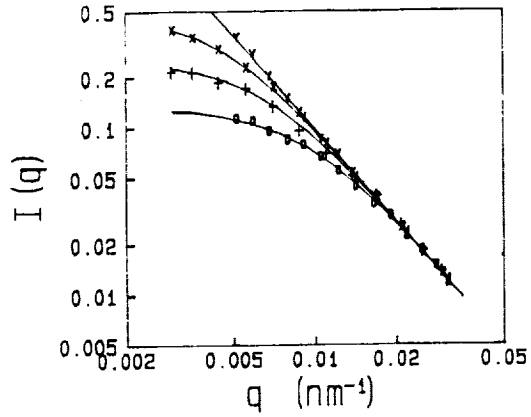

Figure 1.

Scattered light intensity from DLCA clusters at various stages of aggregation. As the average cluster size increases, the saturation of the scattering intensity at small q decreases, and the power-law dependence expected for fractal aggregates is approached. The solid lines are fits to the data using the measured cluster mass distribution and the structure factor obtained from calculuations using computer-generated DLCA clusters.

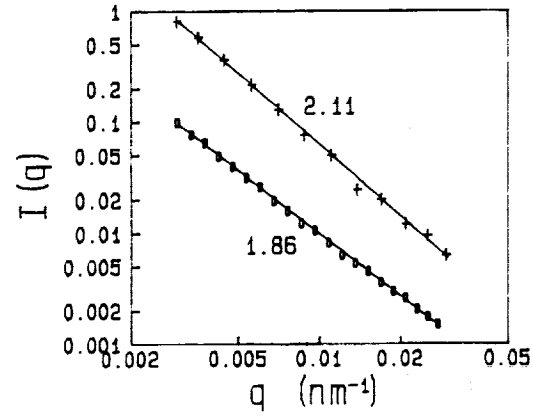

Figure 2

Scattered light intensity from colloid aggregates formed under both DLCA (upper curve) and RLCA (lower curve) conditions. The fractal dimensions of the aggregates can be determined by the slopes of the data, and are $d_f \approx 1.85$ for DLCA and $d_f \approx 2.1$ for RLCA.

give $d_f \approx 1.85$ for DLCA and $d_f \approx 2.1$ for RLCA. These values are consistent with all other experimental measurements of the fractal dimensions.

Dynamic light scattering also provides additional important information about fractal colloid aggregates. The characteristic cluster size can be determined with dynamic light scattering from the measured hydrodynamic radius. The kinetics of the aggregation process can be monitored by measuring the time evolution of the cluster size. In addition, dynamic light scattering can also provide some information about the cluster mass distribution. However, to quantitatively interpret the results obtained with dynamic light scattering, we must include the contribution of rotational diffusion to the decay of the autocorrelation functions measured experimentally. Because fractal objects possess structure on all length scales, the scattered light intensity will fluctuate as the cluster rotates. Thus, when $qR_g > 1$, rotational diffusion of the aggregates will also contribute to the decay of the autocorrelation function.[9]

There are several ways that can be used to determine the contribution of rotational diffusion to the decay of the autocorrelation function. Perhaps the most convenient way is through the introduction of an effective diffusion coefficient, D_{eff}, which describes the decay of the field autocorrelation function, $G_1(t) \sim \exp(-q^2 D_{eff} t)$, and includes the effects of rotational diffusion. The effective diffusion coefficient can be calculated using computer simulated clusters and is found to be a function of

qR_g only, allowing a scaled form of D_{eff} to be determined. An example of this scaled function is shown in Fig. 3, which represents the results of calculations[9] for about 300 clusters simulated using a model for DLCA. We plot D_{eff}/D, where D is the translational diffusion coefficient. As can be seen from the data, at small qR_g, rotational diffusion makes no contribution as the internal structure of the clusters is not resolved. However, when $qR_g \sim 1$, rotational

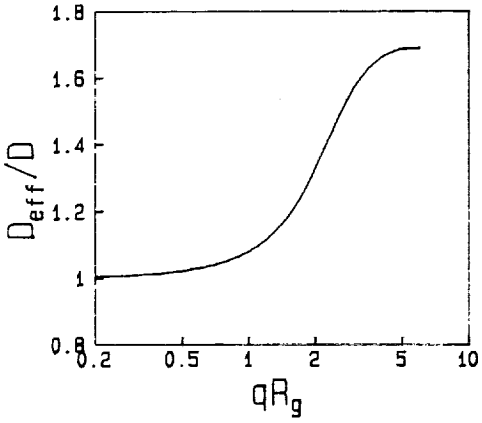

Figure 3

The calculated D_{eff}, normalized by D, as a function of R_g for computer-generated DLCA clusters. The variation with qR_g is due to the effects of rotational diffusion.

diffusion begins to contribute and the decay rate increases. For large qR_g, the contribution of rotational diffusion saturates, and $D_{eff}/D \approx 1.7$.

These results can be used to calculate the first cumulant of the measured autocorrelation function, which must also include the effects of the cluster mass distribution. We obtain an averaged effective diffusion coefficient,

$$\bar{D}_{eff} = \frac{\sum N(M)M^2S(qR_g)D_{eff}}{\sum N(M)M^2S(qR_g)} \qquad (1)$$

Because of the contribution of rotational diffusion, $\bar{D}_{eff}$ will depend on q, even if the cluster mass distribution is monodisperse. This is illustrated in Fig. 4, where we show data obtained from DLCA clusters whose cluster mass distribution is relatively monodisperse. In Fig. 4 we plot $\bar{D}_{eff}$ as a function of q for clusters whose size is such that $q\bar{R}_g$ varies from <1 at small q to >1 at large q. Here we use $\bar{R}_g$ to denote the radius of gyration of the average cluster size. The solid line represents the calculated value using Eq. 1 and the form for D_{eff} shown in Fig. 3.

Figure 4

The average effective diffusion coefficient for DLCA clusters as a function of q. The variation of $\bar{D}_{eff}$ with q is due primarily to rotational diffusion as shown by the predicted behavior including the contribution of rotational diffusion (solid line) and without the contribution of rotational diffusion (dashed line).

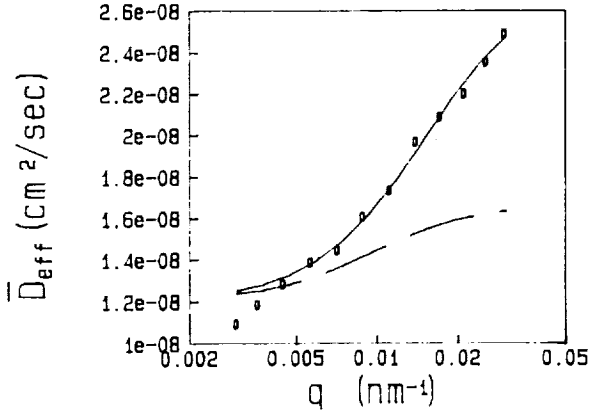

The agreement between the calculation and the experimental data is excellent. The variation of $\bar{D}_{eff}$ with q is due almost entirely to the contribution of rotational diffusion. This can be seen by comparison with the dashed line which represents the predicted behavior without including the effects rotations. The variation of $\bar{D}_{eff}$ with q is much weaker than observed.

Measurements of the first cumulant of the autocorrelation function provide a very sensitive method for collecting together a great deal of information about the aggregation process.[3] This can be done by using a master curve to describe the behavior of the first cumulant as a function of $q\bar{R}_g$. Experimentally, we measure the first cumulant as a function of q for the angles that are accessible with our equipment. This measurement is then repeated as the aggregation proceeds. However, since we expect the cluster mass distribution to exhibit dynamic scaling, its shape should remain the same at all times, provided the mass is normalized by $\bar{M}=(\bar{R}_g/a)^{d_f}$. Thus the data for the first cumulant measured at different times can be scaled onto a single master curve of $\bar{D}_{eff}$ as a function of $q\bar{R}_g$.

The shape of this master curve is very sensitive to several important features of the aggregation process. It depends on the structure and anisotropy of the aggregates through its dependence on the static structure factor and the contribution of rotational diffusion. It depends on the cluster mass distribution which also leads to a dependence of $\bar{D}_{eff}$ on $q\bar{R}_g$. However, the shape of the master curve does not depend on the details of the particular colloid used, as such colloid

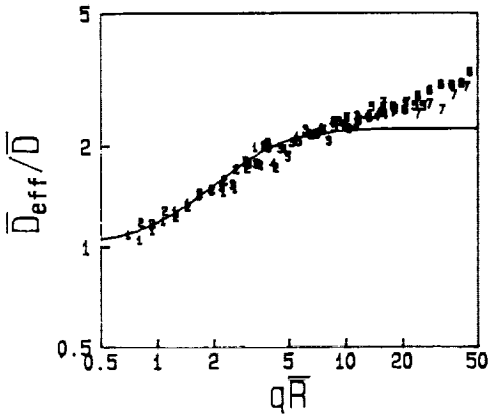

Figure 5

Master curve showing the normalized scaled effective diffusion coefficients, $\bar{D}_{eff}/\bar{D}$, for DLCA gold clusters as a function of the normalized wavevector, $q\bar{R}$. The different symbols represent data sets obtained at different times in the aggregation process. The solid line is the calculated master curve for DLCA.

specific parameters as the single particle radius are scaled out of the curve. Thus the shape of the master curve can be used to critically compare the behavior of completely different types of colloids. Furthermore, using our knowledge of the details of the aggregation process, and the structure of the aggregates, we can calculate the master curves for each regime of the aggregation.

An example of the master curve obtained for colloidal gold aggregated by DLCA is shown in Fig. 5. Each symbol in the graph represents a different set of data. Each set of data has been scaled so it lies on the single curve shown. The scaling is done by shifting each data set along the diagonal of the logarithmic plot until it lies on the same curve as the preceding data set. Thus the scaling parameter represents the radius of the average cluster that characterizes the distribution at that time, $\bar{R}$. This radius could also be determined by dynamic light scattering at $q\rightarrow 0$, when rotational effects are negligible and when the intensity weighting of all clusters scales as M^2. The solid line is the calculated master curve, and is in very good agreement with the data. The dependence on q of this master curve is due almost entirely to the contribution of rotational diffusion.

The great power of using this approach to present the dynamic light scattering data is in the comparison of the behavior of different colloids.[3] In particular, we can investigate the universality of the modern description of colloid aggregation. To do so, we use three completely different types of colloids: colloidal gold, colloidal silica and polystyrene latex. Each colloid is comprised of a different material, each colloid consists of particles of different radius, each colloid forms different interparticle bonds upon aggregation, and the aggregation of each colloid is initiated in a different manner. However, all three colloids can be aggregated either very rapidly or very slowly, exhibiting both diffusion-limited and reaction limited regimes of aggregation.

Master curves were obtained for each colloid in both regimes of aggregation. Once the data are scaled onto the master curves, there are no adjustable parameters remaining, and the master curves can be directly compared. The results of this comparison are show in Fig. 6(a) for DLCA and in Fig. 6(b) for RLCA. In each case, different symbols are used for the data obtained with the different colloids. However, for each regime, the master curves for the different colloids are indistinguishable. This demonstrates conclusively that the aggregation processes are indeed universal. The clusters formed by each colloid must have the same structure as characterized both by their fractal dimensions and by their anisotropy. Furthermore, the cluster mass distributions produced by the aggregation processes in each regime must be identical. The kinetics of the aggregation process can be determined by the time dependence of the scaling parameter for each colloid. Universal behavior is found in this as well. For DLCA clusters, all data sets

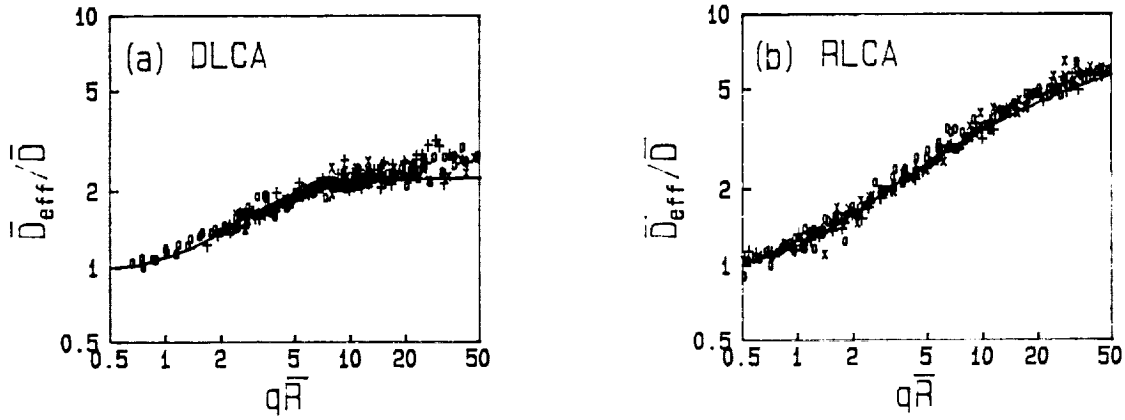

Figure 6

Master curves for (a) DLCA and (b) RLCA for three entirely different colloids: gold (o), silica (+) and polystyrene (x). The data from each of the colloids is indistinguishable for each regime of aggregation. This is a conclusive demonstration of the universality of each regime of aggregation. The solid lines are the calculated master curves for each regime.

exhibit a power-law behavior consistent with z=1. For RLCA all the data sets exhibit exponential behavior. Finally, static scattering confirms that the fractal dimensions are universal, with all the colloids having $d_f \approx 1.85$ for DLCA and $d_f \approx 2.1$ for RLCA.

The solid lines through the data in Fig. 6 are the calculated master curves for each regime and are in excellent agreement with the data. The RLCA data is seen to have a much larger dependence on q than the data for DLCA. This reflects the effects of

the power-law cluster mass distribution, which leads to an additional q-dependence. To obtain the calculated curve shown, it is necessary to use τ=1.5, as expected from the TEM studies, and to include the contribution of rotational diffusion.

The results shown in Fig. 6 demonstrate that our understanding of the process of colloid aggregation, and the structure of the aggregates that result, is quite complete. Furthermore, light scattering, both static and dynamic, provides an excellent probe of the aggregation process and the fractal clusters. Therefore colloidal aggregates can provide an experimental system to produce fractal objects under well known and reproducible conditions, and with a structure that is very well characterized. These structures can then be used to study the potentially interesting physical properties that are expected for fractal objects. Of interest here are the properties that might be best studied under conditions where the gravitational acceleration, g, is nearly zero. There are two different effects of gravity that can be considered: the effect on the aggregation process itself, and the consequences of gravity for the type and ultimate size of the fractal clusters that can be formed.

Gravity can play one immediate and important role in the process of aggregation. All the modeling of the aggregation process assumes that the cluster mass distribution is uniform in the sample. However, in the case of RLCA, a very broad cluster mass distribution is formed, which will lead to vastly different rates of gravitational settling for the clusters of different sizes. The drift velocity due to gravity of a cluster is $v=m_o Mg/6\pi\eta R_H$, where η is the viscosity of the solution, and R_H is the hydrodynamic radius, and $m_o=(4/3)\pi a^3\Delta\rho$, with $\Delta\rho$ the difference between the densities of the colloid and the fluid. The hydrodynamic radius of the clusters

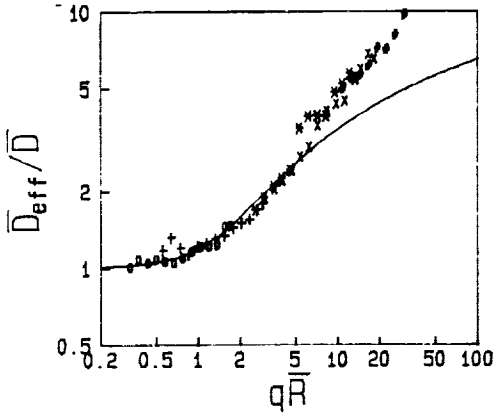

Figure 7

Master curve obtained for gold aggregated by RLCA without using g≈0 on average. The differential settling rates of the clusters changes the cluster mass distribution, leading to the change in shape of the master curve. The calculated shape without gravitational settling is shown for comparison by the solid line.

scales with the radius of gyration, $R_g=\beta R_H$, where $\beta\approx1.0$ for RLCA clusters. The ratio of the settling velocities of the largest clusters to the monomers is $V=M^{1-1/d_f}$. For RLCA the largest clusters can easily attain masses well over 10^6, which will lead to settling velocities that are three orders of magnitude larger than the monomers. Furthermore, for gold, $\Delta\rho\approx18$, leading to significant gravitational drift velocities for the larger clusters. For example, for clusters with $R_g\approx1$ μm, which corresponds to $M\approx3\times10^5$, $v\approx1.7$ mm/hr.

These large drift velocities, and concomitant large differential sedimentation rates can have significant effects on the aggregation kinetics and the cluster mass distributions. We demonstrate the consequences of this in Fig. 7, where we show a master curve obtained from colloidal gold aggregated by RLCA under conditions of normal gravitational acceleration at the surface of the earth. The results are clearly different from those expected from the theoretical calculation, which is shown by the solid line. This difference is a result of the differential settling

which causes a change in the cluster mass distribution, and which may in turn change the aggregation kinetics. The shape of the resultant master curve is clearly changed. Indeed, all the data presented in Fig. 6 for RLCA had to be obtained under conditions of g≈0, at least on average. This was achieved by using a tall cuvette as the sample container, filling the container right to the top and then sealing it. The sample container was then inverted every 15 minutes, to achieve g≈0 on average. The amount of settling that occurs for even the largest clusters in 15 minutes is relatively insignificant.

For these experiments, we were able to achieve an effective g≈0 on earth. However, there are other very interesting questions that would require space born experimentation to achieve the necessary g≈0. Many of these involve the investigation of the physical properties of fractal objects. One of the most important features of a scale invariant structure is the power-law dependence of its mass-mass correlation function, $g(r) \sim r^{-3-df}$. As a consequence, the density of a fractal object decreases as its size increases. This directly reflects the very tenuous structure that typifies a fractal object. However, this tenuous structure also means that the mechanical strength and rigidity of a fractal structure decreases with increasing size. Indeed, a fractal aggregate is predicted to ultimately become unstable and collapse under its own weight as its size increases.[10] While the largest size an aggregate can achieve depends on the details of the interparticle bonding and on the size of the individual particles, it is nevertheless limited by some upper bound. The only way to avoid this is to eliminate the effects of gravity, which would be conveniently achieved in a space born experiment.

It is difficult to test the consequences of a reduction of g experimentally in the laboratory. However, we can instead measure the effect of an increase in g on the structure of the aggregates, to investigate the scaling of the gravitational forces.[11] The effect of gravitational forces on aggregates in solution is to apply a shear stress on the aggregates due to their drift velocity. To investigate the effects of such a shear stress on the structure, we prepared a sample of gold aggregates by DLCA and subjected them to a varying amounts of shear stress by forcing the solution through a narrow capillary tube at different flow rates. The structure of the aggregates was probed by static light scattering both before and after they were subjected to the shear. Typical results are shown in Fig. 8, where the lower curve is the light scattering intensity obtained from the unsheared sample and the upper curve is that obtained from the sample subjected to the shear. The structure has clearly been modified by the shear stress, as the apparent slope of the scattering intensity has increased at smaller q, corresponding to larger length scales. This change in the scattering behavior is consistent with a restructuring

Figure 8.

The intensity of the scattered light from unsheared (lower curve) and sheared (upper curve) DLCA gold clusters. The fractal structure at long length scales is distorted by the shear as indicated by the change in slope of the scattering curve.

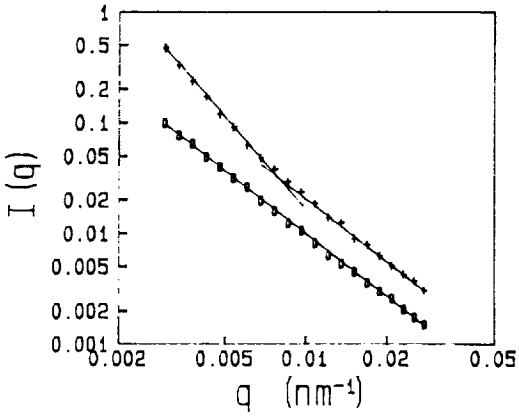

of the fractal cluster to form loops at longer length scales that would increase the rigidity of the structure and its ability to withstand the shear stress. Additional experimental data suggest that the restructuring always occurs at length scales larger than some characteristic length, whose value depends on the shear rate. These results clearly indicate that the fractal nature of a structure would be destroyed at large length scales by gravitational acceleration. This detrimental effect would be essentially eliminated by the reduction of g in a space born experiment.

The ability to form very large fractal structures that would be possible in space represents an important opportunity to do novel and interesting science. Since we can quantitatively describe the structure of a fractal object, we can also predict many aspects of its physical behavior. A tenuous, random and inhomogeneous structure such as fractal aggregate is expected to have very unusual properties. For example the spectrum of phonon states will likely be dramatically altered, and new, localized states, or fractons, are expected to occur.[12] Other transport properties on fractal structures should also be altered considerably. Furthermore, the mechanical properties of fractal structures will also be very different than those expected for objects that are homogeneous. To experimentally investigate these effects would require fractal objects of reasonable size with which experiments can be performed. Colloidal aggregates represent an excellent experimentally achievable example of fractal objects with well characterized structure and fractal dimensions. However, the size of the aggregates that can be produced with true fractal structure is ultimately limited by gravitational acceleration. One potential way to circumvent this limitation is to produce the fractal colloid aggregates in space under conditions of $g \approx 0$.

There is a second very interesting set of experiments that could be performed under conditions of $g \approx 0$. Virtually all experiments on colloidal aggregates performed to date have been carried out with colloidal suspensions. However, the fluid that surrounds the aggregates can significantly modify the behavior of the fractal structures that are produced. For example, the viscous damping in the fluid will probably preclude the observation of fracton modes for colloidal aggregates in solution. In addition, many interesting mechanical properties of fractal aggregates may be obscured by the presence of the surrounding fluid. To remove the fluid without destroying the fragile fractal structure is extremely difficult. However, it may be possible to actually form the aggregates themselves in a gas or in vacuum, without the surrounding fluid. If this could be done fractal structures of arbitrarily large size could conceivably be formed for studies of their physical properties. Moreover, the process involved in this formation would be significantly different than aggregation in a fluid because the mean free path of the diffusive motion of the clusters would be considerably larger. Thus the aggregation process would most likely involve ballistic motion rather than diffusive motion. This would represent a different regime of aggregation that could be studied. It would, however, be desirable to find a system that could be controlled in a fashion analogous to the colloidal suspensions for these experiments.

To conclude, we have shown how static and dynamic light scattering has been used extensivley in the study of colloid aggregation. Light scattering techniques provide a simple, yet powerful method of measuring many important features of coloidal aggregates. These colliodal aggregates are currently very well understood and thus represent an excellent example of an experimentally achievable fractal object. Therefore, they can be used to investigate the fascinating new physics expected for fractal structures. However, the very fragile mechanical structure of the tenuous fractal objects results in their structure being unstable under normal

gravitational acceleration, limiting the ultimate size of fractal aggregates. This limitation can be avoided by growing the fractal aggregates in space, under conditions of reduced g. This represents an important opportunity to study the properties of truly novel materials in space that would otherwise not be possible.

We thank H.M. Lindsay, R. Klein, R.C. Ball and P. Meakin for their extensive contributions to this work.

REFERENCES

1. D.A. Weitz, M.Y. Lin and J.S. Huang, in *Physics of Complex and Supermolecular Fluids*, ed. S.A. Safran and N.A. Clark (Wiley-Interscience, NY, 1987), p. 509.
2. D.A. Weitz, J.S. Huang, M.Y. Lin ans J. Sung, Phys. Rev. Lett. 54, 1416 (1985).
3. H.M. Lindsay, M.Y. Lin, D.A. Weitz, R.C. Ball, R. Klein and P. Meakin, J. Opt. Soc. Am., in press.
4. D.A. Weitz, M.Y. Lin and C.S. Sandroff, Surf. Sci. 158, 147 (1985).
5. D.A. Weitz and M. Oliveria, Phys. Rev. Lett. 52, 1433 (1984).
6. P. Dimon, S.K. Sinha, D.A. Weitz, C.R. Safinya, G.S. Smith, W.A. Varaday and H.M. Lindsay, Phys. Rev. Lett. 57, 595 (1986).
7. D.A. Weitz, M.Y. Lin, J.S. Huang, T.A. Witten, S.K. Sinha and J.S. Gethner, in *Scaling Phenomena in Disordered Systems*, ed. R. Pynn and A. Skjeltorp (Plenum, New York, 1985), p. 171.
8. D.A. Weitz and M.Y. Lin, Phys. Rev. Lett. 57, 2037 (1986).
9. H.M. Lindsay, R. Klein, D.A. Weitz, M.Y. Lin and P. Meakin, Phys. Rev. A38, 2614 (1988).
10. Y. Kantor and T.A. Witten, J. Phys. (Paris) Lett. 45, 738 (1984).
11. H.M. Lindsay, M.Y. Lin, D.A. Weitz, P. Sheng, Z. Chen, R. Klein and P. Meakin, Faraday Discuss. Chem. Soc. 83, 153 (1987).
12. S. Alexander and R. Orbach, J. Phys. (Paris) Lett. 43, L-625 (1982).

AGGLOMERATION OF CERAMIC POWDERS

James D. Cawley, Judith LaRosa, and Fredrick Dirkse
Department of Ceramic Engineering
The Ohio State University
Columbus, Ohio

A research program directed at a critical comparison of numerical models for powder agglomeration with experimental observations is currently underway. Central to this program is the quantitative characterization of the distribution of mass within an agglomerate as a function of time. Current experiments are designed to restrict agglomeration to a surface, which is oriented perpendicular to the force of gravity. These experiments are discussed with reference to: their significance to ceramic processing; artifacts which may be avoided in microgravity experiments; and the comparison of information available in real space (from optical microscopy) to that in reciprocal space (from light scattering). The principal machine requirement appears to be a need to obtain information at small scattering angles.

Introduction

In general, ceramic processing is a powder technology in which powders are manufactured, formed into a compact, and consolidated through heat treatment. Although the final piece may have the same chemical composition as the starting powders, it is often the case that a mechanical mixture of different powders is used which undergo a desired chemical reaction during the heat treatment.

Control of the state of agglomeration is important for technological reasons[1]. Agglomerates are necessary for many conventional forming operations such as dry pressing, slip casting, and plastic forming. However, the residual porosity in a fired ceramic, which can strongly affect the optical, thermal, and mechanical properties of the material, is an artifact of the porosity in the green body. This is intimately related to the packing of the primary particles within the agglomerate and the packing of the agglomerates to form the compact. Frequently, it is desired to crush agglomerates in the latter stages of powder compaction in order to achieve high packing densities. Clearly, the control of the agglomerate population is an important process control variable, and successful control implies the ability to quantify agglomerate characteristics in a meaningful way.

It has long been realized that a quantitative characterization of the agglomerate geometry is important to a complete understanding of colloidal suspensions. For example, Michaels and Bolger[2] quantitatively characterize agglomerate structure through a term C_{ap} which is the reciprocal of the solids packing density within the agglomerate. Firth[3] and Firth and Hunter[4] have shown C_{ap} to be an important parameter in describing the rheology of agglomerated colloidal suspensions.

Beginning with the seminal work of Forrest and Witten[5] on the structure of agglomerates of metallic smoke particles, it has been realized that many agglomerates are fractals. In a fractal agglomerate, the average packing density of the agglomerate decreases as it grows, so that within an agglomerate, the density is a maximum at the center of the agglomerate and drops off as a power law when increasingly larger volumes are considered, i.e. for a three dimensional system,

$$\rho = \beta \cdot r^{(D-3)} \qquad \text{Eqn-1}$$

where ρ is the density of solids within a sphere of radius r around the agglomerate's center of mass, β is a geometrical constant, and D is defined as the fractal dimension. A significant feature of fractal growth is that both β and D are constants which do not depend on variables such as time available for agglomeration.

The objective of the research currently underway is to examine the effects of process variables on the structure of agglomerates. The approach is to follow the evolution of the agglomerate on the scale of the individual particles. The process variables are viewed in terms of the forces resolved on the particles. For example: alterations in the electrolyte chemistry change the magnitude (and sometimes the sign) of interparticle forces; mixing introduces shear forces; the presence of a suspension medium gives rise to both Brownian motion, or stochastic force, as well as hydrodynamic forces; and the presence of gravity adds a systematic force. The influence of these process variables is being studied principally through the effect each has on the geometry of resultant agglomerates. This is quantified following a fractal approach. Numerical simulations, both Monte Carlo and Molecular Dynamics, are being investigated in addition to experimentation. The results of the simulations will not be discussed here except for their role in guiding experimentation.

Monte Carlo simulations have shown that (in the absence of rearrangement within the agglomerate) interparticle forces do not have a significant effect on the distribution of mass within the agglomerate. As a result, experiments are currently being restricted to agglomeration at the zero point of charge, i.e. when the only significant contribution to the interparticle force is van der Waals attraction. The importance of Brownian motion, or random walk particle trajectories, has been clearly established by the numerical simulation of Witten and Sander[6] and the large body of work which has followed, notably that of Meakin[7]. The current research focus is the role of hydrodynamic forces, principally how collision probabilities depend on fluid flow around and through existing agglomerates. The effect of gravity is being examined to determine how it complicates experimentation.

The most obvious complication introduced by the existence of gravity is that particles initially suspended in a liquid medium will settle to the bottom of the container. Further, larger agglomerates settle more rapidly. Although the density of fractal agglomerates decreases with increasing size, the settling rate increases since it also depends on size to the second power. Thus, experiments in three dimensions are subject to agglomerate collisions due to relative velocities between agglomerates (that are not typically included in numerical models). The typical densities associated with ceramics, 3.0 - 4.0 g/cm^3, make it impractical to restrict experimentation to particles sufficiently small to avoid settling. For this reason, ground based experimentation is currently being restricted to two dimensions.

Experimentation

The experimental arrangement is very straightforward and is based on the work of Onoda[8]. A small hole is drilled through an aluminum slide, and a drop of a very dilute ceramic powder suspension is placed in this hole and is supported by surface tension. The powder particles settle under the influence of gravity to the lower surface. Since the particle concentration in the volume in low, virtually all of the particles settle to the lower interface without experiencing a collision. Once settled, the particles are constrained to move on a surface and agglomeration occurs. A schematic of the experiment in shown in figure 1. The upper portion of the figure illustrates the physical arrangement, and the lower portion shows the distribution of particles within the drop once agglomeration has started. Typical conditions are the following: 0.4 μm Al_2O_3 powder (3.96 g/cm^3) at 0.001 volume percent; pH = 8.2; 4 mm hole in a 2 mm thickness. The agglomeration process has been observed in real time using optical microscopy (focussed on the lower surface of the drop) and is currently being approached using static light scattering.

It is useful to analyze how this experimental arrangement is similar to and differs from the situation being modeled in either Diffusion Limited Aggregation[6] or Cluster Cluster Aggregation[9,10]. The standard DLA algorithm is executed within a lattice (typically a square lattice) which is seeded at the center. Subsequent particles are added randomly along an approximate circle which is far away from the growing agglomerate. The only path by which a particle may be incorporated into the agglomerate is by a random walk from the region outside the agglomerate. In the case of CCA, the lattice is initially populated with a given number of particles which are then allowed to undergo simultaneous random walks. The number of particles in the system is not a function of time. Neither situation completely describes the experiments.

In the initial stage of the experiment, the number of particles per unit area is low, and the growth of agglomerates appears to take place independently, resulting in structures reminiscent of DLA. At later stages these agglomerates collide and link to form large structures like those predicted by CCA (however agglomerates appear to collide as a result of drift rather than Brownian motion). The early stage in not truly DLA for two reasons: one is that neighboring agglomerates compete for particle additions; the other is because there exists a finite probability that particles can settle to the

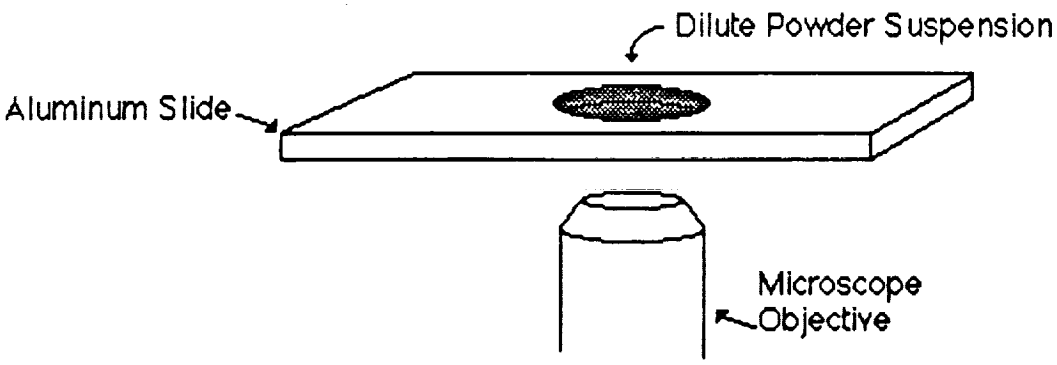

Figure 1a. Schematic illustration of the experimental arrangement for observing agglomeration on the lower surface of a drop.

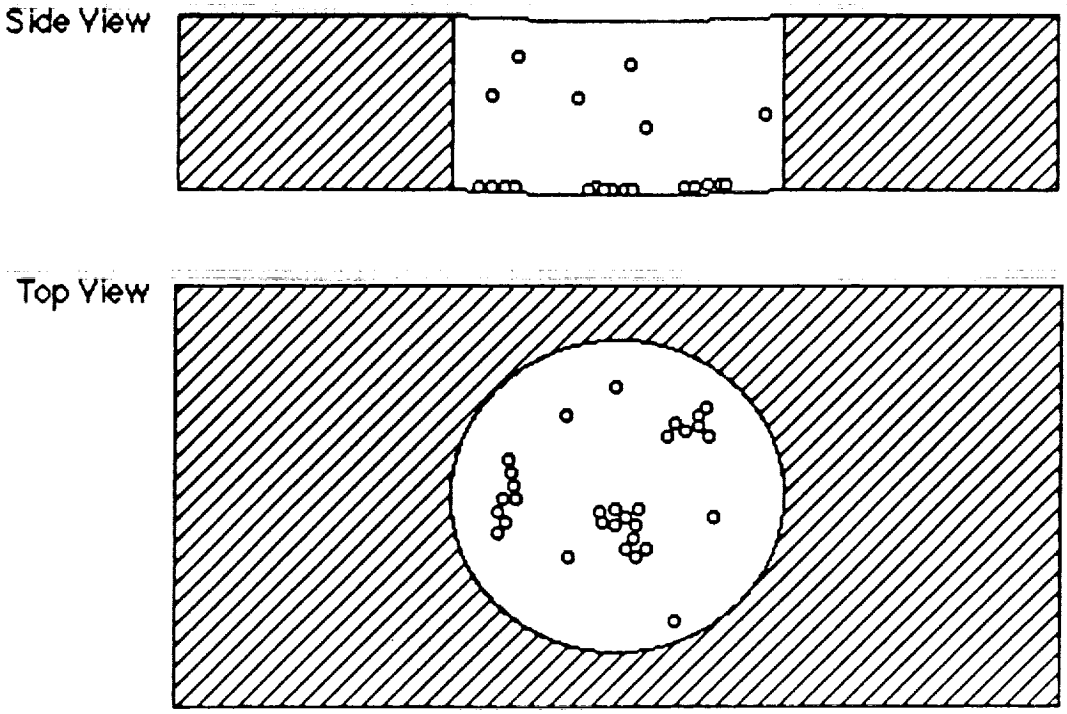

Figure 1b. Schematic illustration of the distribution of particles within the drop. Particles within the volume of the drop rarely collide and agglomeration is restricted to the lower surface of the drop.

interface such that they arrive in the plane within the interior of the agglomerate. The first effect biases the growth of agglomerates away from neighboring agglomerates. The second gives rise to agglomerates which have densities greater than what is predicted by DLA. This second effect also allows the interior of rings (commonly occurring in CCA) to be filled. The end result of these experiments is typically a plane filling structure, i.e. D = 2. Thus, in these experiments a fractal dimension (if at all appropriate) is not truly a constant since it appears to be time dependent. A time sequence of agglomerates* of 0.4μm Al_2O_3 at a pH of 8.2 which illustrates the time dependence of the particle number density is shown in figure 2.

These effects can be seen in two Monte Carlo simulations which are distinguished from simple DLA because particle additions are allowed to occur within any unoccupied lattice site to simulate particles settling from above. In the first simulation, a 200x200 square lattice was initially populated with 10 fixed particles. The rationale for using a set of fixed nucleation sites is that in the experiments, several clusters will simultaneously form on the lower surface of the drop. After some time, these will become sufficiently large to be regarded as immobile relative to the singlets. The cluster population which grows from the fixed nucleation sites will mimic this set. The top and bottom of the square were subjected to periodic boundary conditions while the left and right were treated as impermeable surfaces that did not trap random walkers. Random walkers were randomly added, and clusters were allowed to grow until a left to right percolation path was created. The results of this experiment are shown in figure 3. In the initial phase of the experiment, ramified clusters (that have a visual appearance consistent with fractals) grew with a tendency to fill the tessellation. As they approached one another they tended to densify rather than link together. This is a direct consequence of the fact that the random walker has a higher probability of entering the system in between adjacent dendrite arms on a single cluster than in the small area left between neighboring clusters. When percolation does occur, the filled fraction of the lattice is ϕ_c=18,344/40,000 = 0.4586 in striking agreement with the value of 0.45 for percolation in two dimensions by random population of sites[11].

The second simulation was designed to test whether the clusters which grow in this competitive situation are indeed fractal. In order to maximize statistics, the growth of a single agglomerate in a single "cell" was monitored. This experiment involved seeding the center of a circular region in a square lattice with a single particle and introducing random walkers at random within the circle. To make the circular region equivalent to the cell surrounding each agglomerate in the first experiment, the boundary was treated as impermeable. Four stages of growth are illustrated in figure 4 along with a standard log-log plot of number versus radius of the sampling interval. Although a typical ramified cluster was formed, it is clearly not fractal. The amount of mass near the periphery is substantially in excess of the expectation for a fractal as evidenced by the bump in the log-log plot between values of 4 and 4.5 on the horizontal axis. Again this is a purely geometrical result. The most probable location for the random walker to be introduced is the large openings between the dendrite tips. This is equivalent to particles having a higher probability of settling to the surface in regions which are

*Photo sequence taken by K. Langguth while a graduate student at OSU.

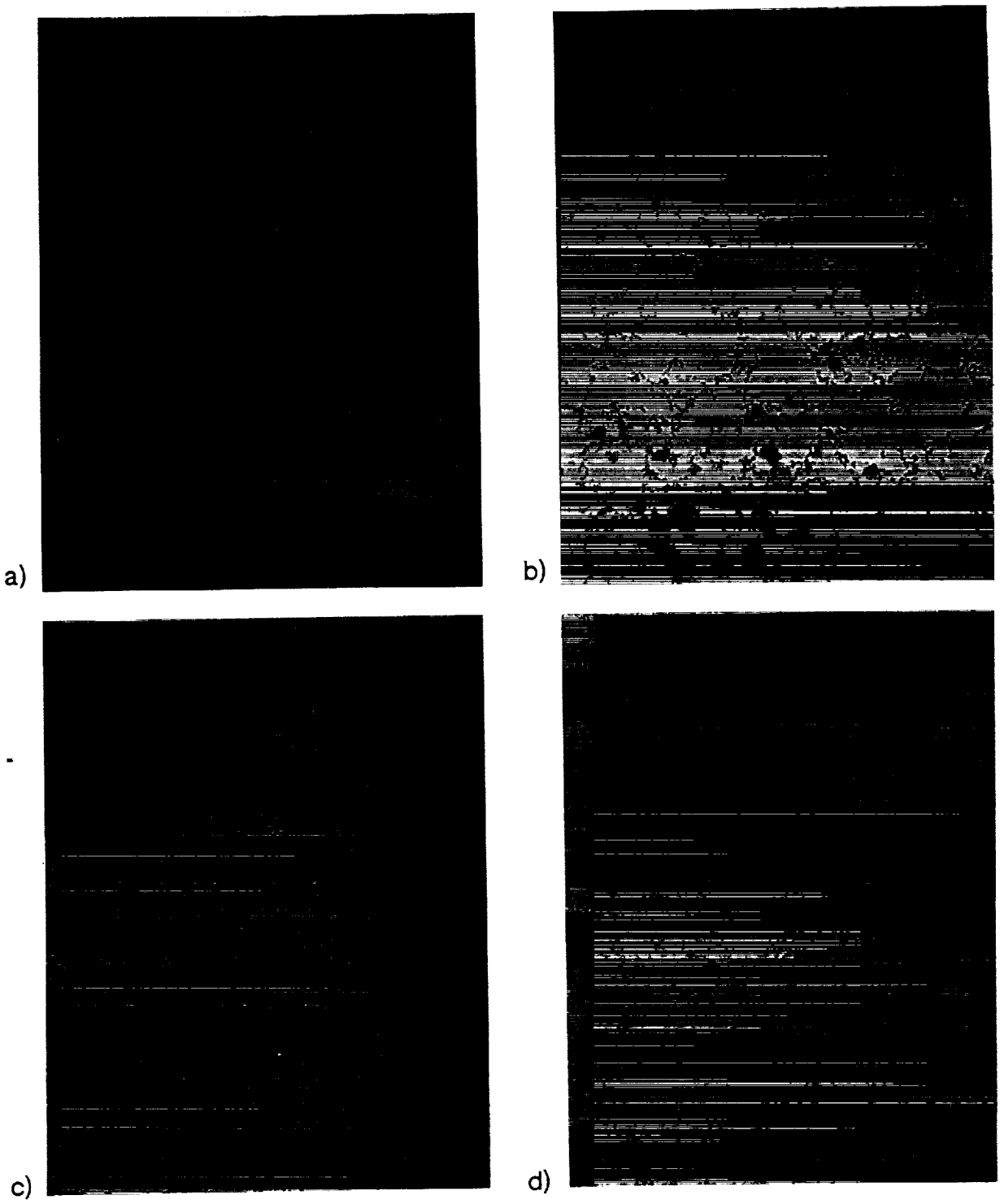

Figure 2. Optical photomicrographs of the lower surface of a 0.003 % suspension of Al_2O_3 after a) 7.5 min., b) 11 min., c) 15.5 min., d) 20 min. Both the increase in the number density of particles as a function of time and the two dimensional character of the agglomerates are clearly evident. The small particles in the image are nominally 0.4 μm and the large are 4.0 μm.

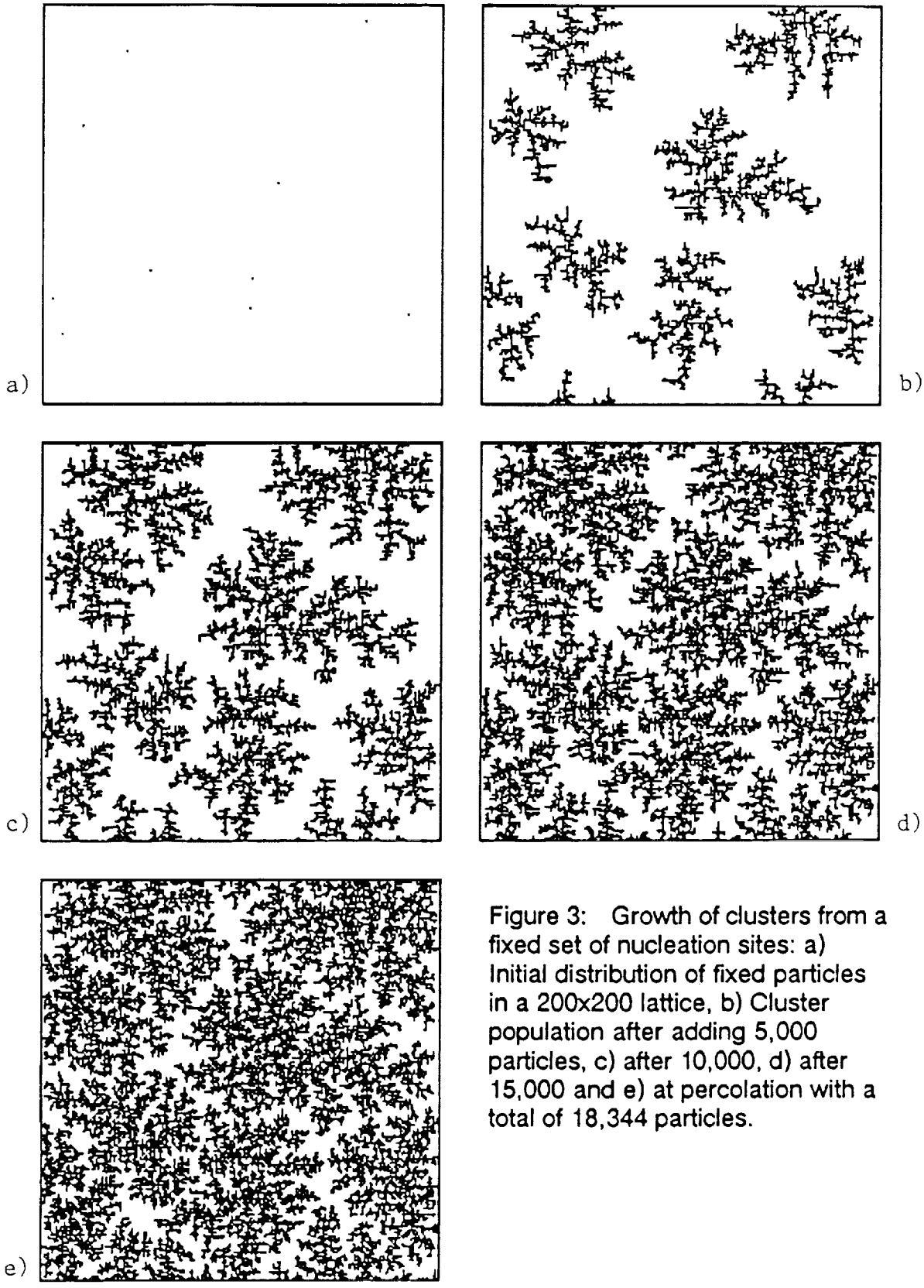

Figure 3: Growth of clusters from a fixed set of nucleation sites: a) Initial distribution of fixed particles in a 200x200 lattice, b) Cluster population after adding 5,000 particles, c) after 10,000, d) after 15,000 and e) at percolation with a total of 18,344 particles.

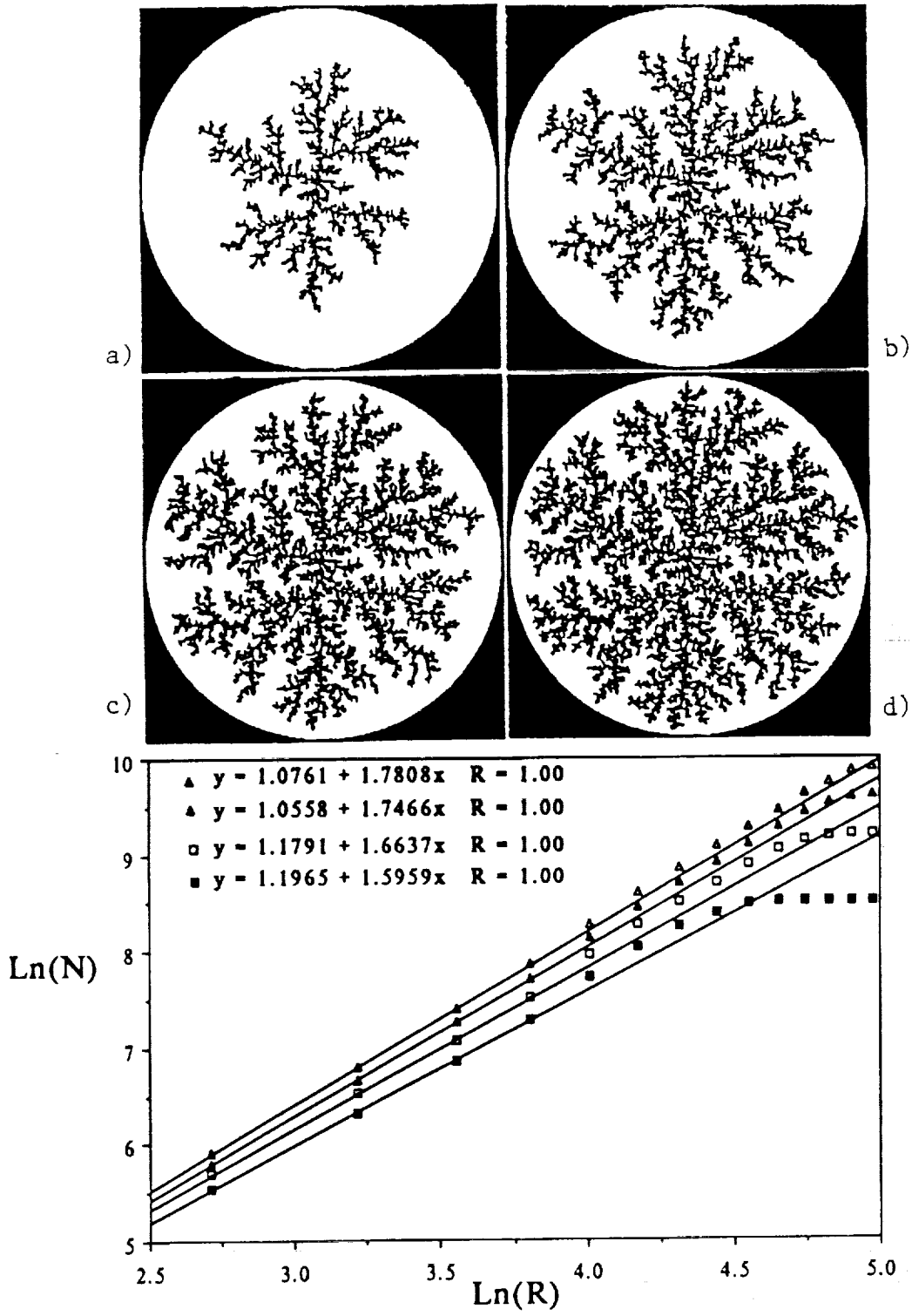

Figure 4: Modified DLA simulation in which particles are added at random to any unoccupied site. The upper portion of the figure shows the evolution of the agglomerate after: a) 5,000; b) 10,000; c) 15,000; and d) 20,000 particle additions. The lower portion of the figure is log-log plots which clearly indicate that the resultant structures are not fractal.

sparsely populated. The magnitude of the discrepancy decreases as the cell fills, finally converging to a straight line with a slope of 2 upon complete filling.

Experimental confirmation of this result is necessary. In the simulation, particles are not allowed to settle to already filled sites. This is equivalent to assuming that particles which settle onto the top of a second particle stick to the top and therefore never arrive in the plane of observation. In real systems, however, particles which settle on top of another may rotate into the plane. This would increase the rate of filling near the center of the agglomerate and might compensate for the mass accumulation near the tips and restore the agglomerate to fractal status.

The only experimental results which have been quantified resulted from agglomeration of 0.4 μm Al_2O_3 in a mildly convective environment (Peclet number on the order of 10). In this situation, small agglomerates are driven together by convection in the liquid and lead to structures reminiscent of CCA agglomerates. A tracing of a large agglomerate, which formed 22.5 minutes into the experiment, is shown in figure 5 along with its log-log plot of number of particles within circles of systematically varied radii. It can be seen that apart from a transient near the agglomerate center, it is well described by a fractal dimension of 1.54 which is in good agreement with CCA simulation. Further quantification is underway to determine precisely the degree to which the agglomerates resulting from this geometrical set-up are fractal, and in particular, the role of convection is being examined.

Application of Light Scattering and Optical Fourier Transforms

Our experiments will be restricted to the use of static light scattering. The analysis of total intensity versus scattering angle has been used in the determination of fractal dimensions of agglomerates imbedded in both two dimensional [12] and three dimensional space [13]. Earth based experimentation will initially be restricted to the analysis of two dimensional agglomerates using the experimental set-up pictured in figure 6. This represents a sample cell which has been designed to fit into the NASA Lewis Laser Light Scattering Facility. Two principal features of this design should be noted: first, the path of the laser beam is modified by the presence of the prism such that it will probe the sample perpendicular to the plane on which agglomeration takes place; secondly, a charge coupled device video camera will be used as a two dimensional array detector allowing the simultaneous collection of data over a range of scattering vectors.

The signal that results from the ground based experiments is expected to be an Optical Fourier Transform of the two dimesional agglomerates which form on the lower surface of the cuvette combined with a background signal resulting from the population of singlets which remain suspended in the fluid above. Characterization of the background may be approached using a horizontal laser beam which does not sample the agglomerates. Interpretation of the signal will follow the analysis of Allain and Cloitre[12].

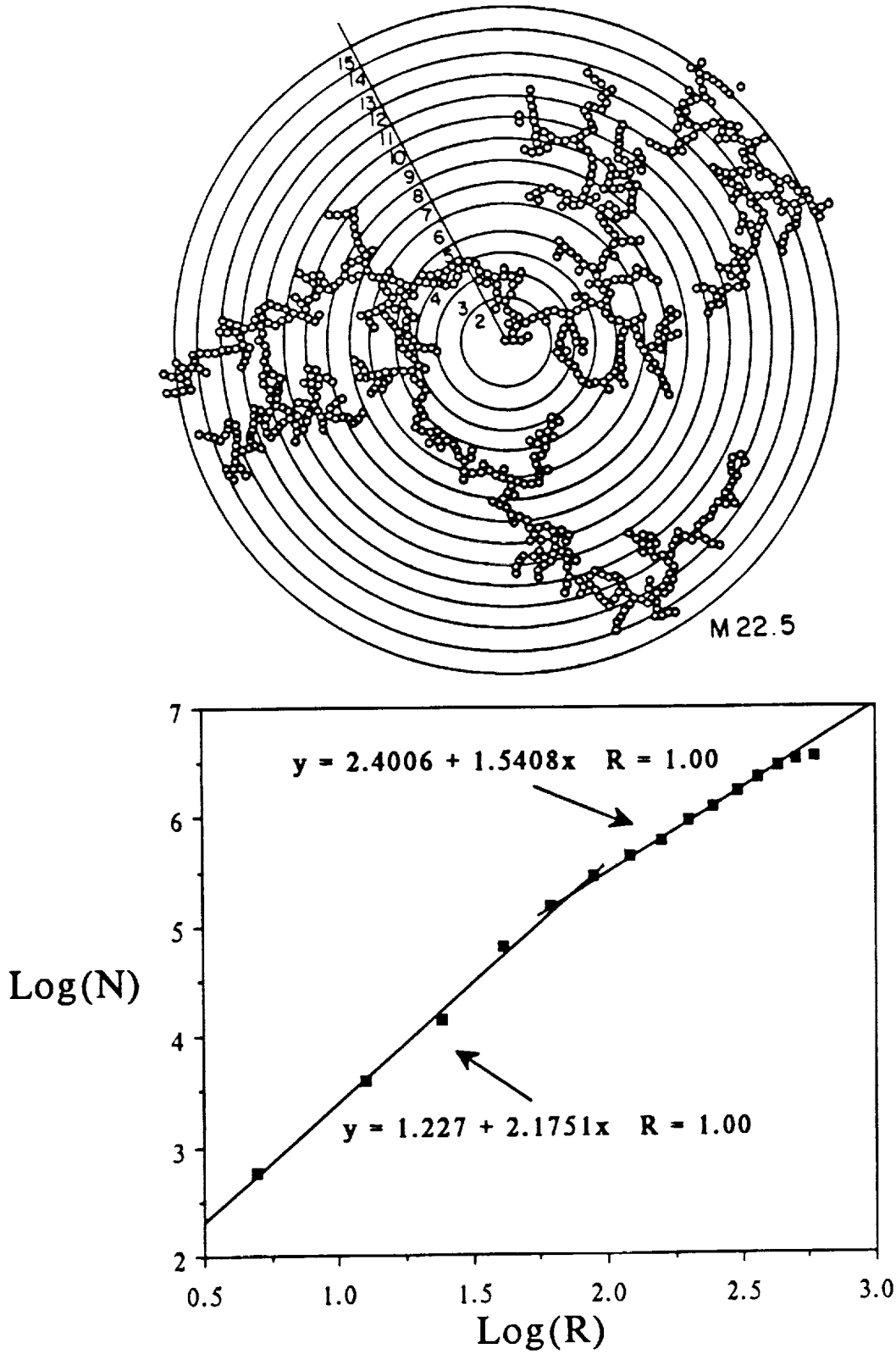

Figure 5: Tracing of an agglomerate of 0.4 μm Al_2O_3 formed on the lower surface of a drop along with a log-log plot which suggests it is fractal and has a dimension of 1.54.

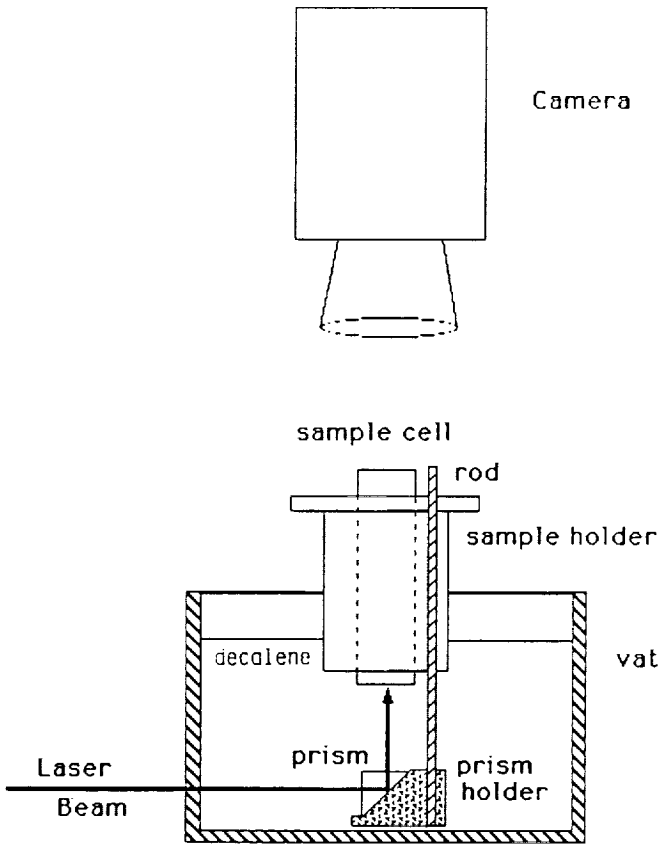

Figure 6: Schematic of the sample cell to be used in conjunction with the NASA Laser Light Scattering Facility.

The distribution of particles in the agglomerate is probed only with scattering vectors, k, which satisfy the inequalities

$$1/R_g \leq k \leq 1/a \qquad \text{Eqn-2}$$

where R_g is the radius of gyration, and a is the particle size[12]. The scattering vector is defined as

$$k = 4 \pi n \lambda^{-1} \sin(\theta/2) \qquad \text{Eqn-3.}$$

This equation may be used to define the parameters for a particular experiment. For instance, it is useful to calculate the scattering angle, θ, which satisfies the right hand inequality of Eqn-2 since only scattering from angles below this value will contain information about the agglomerate. Its value depends on the wavelength of the illuminating radiation, λ, the index of refraction of the suspension medium, n, and the particle size. The results of calculations for this upper scattering angle are presented in Table 1. These results emphasize the importance of small angle measurements. Many powders of interest in ceramic processing are on the order of 0.5 microns. Even with illumination with red light, 680 nm, the information is compressed below 17°. For

Table 1. Upper Scattering Angles Calculated for a Range of Particle Sizes Using Two Wavelengths of Radiation

Particle Size	Upper Scattering Angle λ = 680nm, n = 1.3	Upper Scattering Angle λ = 514nm, n = 1.3
0.1	50°	36°
0.2	42°	18°
0.3	28°	12°
0.4	21°	9°
0.5	17°	7°
0.6	14°	6°
0.7	12°	5°
0.8	10°	4°
0.9	9°	4°
1.0	5°	4°

the purposes of analyzing agglomerates of these relatively large particles, the maximum wavelength is preferred. Clearly, the most sensitive variable is the actual particle size, and in experiments using Fe_2O_3, this can be controlled during powder synthesis[14].

The prospect of obtaining information in both real space (using mass distribution obtained by optical microscopy) and reciprocal space (using light scattering) will provide the opportunity to make critical evaluations of the respective techniques. Such information will greatly increase the reliability of information gathered from three dimensional agglomeration experiments since obtaining real space information with the necessary spatial resolution is very difficult. For example, the consequences of polydispersity can be directly tested.

Summary

Agglomeration experiments are underway which are restricted to two dimensions in order to eliminate artifacts due to settling under the influence of gravity. Simulations of this experiment suggest that in a purely diffusive environment, this experimental set up will likely produce agglomerates which are not fractal due to competition between growing neighbors. However, the experimental data which have been collected on agglomerates grown under mild convection is consistent with interpretation as a fractal and has a dimensionality consistent with CCA. A significant advantage to the two dimensional experiments is the ability to collect information in both reciprocal space and real space.

Three dimensional agglomeration experiments are more relevant to the issues associated with ceramic processing. These experiments will require a microgravity environment to avoid both settling under gravity and thermal convection currents in the fluid. These structures will be most easily probed in reciprocal space, and information gathered from the two dimensional experiments will be of direct use in subsequent interpretation.

References

1. J. W. Halloran, "Role of Powder Agglomerates in Ceramic Processing," in Adv. in Ceramics Vol. 9, Forming of Ceramics, (American Ceramic Society, 1984)

2. A. S. Michaels and J. C. Bolger, "Sediment Height and Sedimentation Rate of Kaolinite Suspensions," Ind. Eng. Chem. Fund., 1, 153 (1962).

3. B. A. Firth, "Flow Properties of Coagulated Colloidal Suspensions, II. Experimental Properties of the Flow Curve Parameters," J. Colloid Interface Sci., 57, 257 (1976).

4. B. A. Firth and R. J. Hunter, "Flow Properties of Coagulated Colloidal Suspensions, I. Energy Dissipation in the Flow Units," J. Colloid Interface Sci., 57, 248 (1976) and "Flow Properties of Coagulated Colloidal Suspensions, III. The Elastic Floc Model," J. Colloid Interface Sci., 57, 266 (1976).

5. S. R. Forrest and T. A. Witten, "Long Range Correlations in Smoke-Particle Aggregates," J. Phys. A12, 1109 (1979).

6. T. A. Witten and L. M. Sander, "Diffusion Limited Aggregation, A Critical Phenomena," Phys. Rev. Lett. 47, 1400 (1981).

7. P. Meakin, "Diffusion-Controlled Cluster Formation in 2-6 Dimensional Space," Phys. Rev. A27, 1495 (1983).

8. G. Y. Onoda, personal communication.

9. P. Meakin, "Formation of Fractal Clusters and Networks by Irreversible Diffusion Limited Aggregation," Phys. Rev. Lett., 51, 1119 (1983).

10. M. Kolb, R. Botet, and R. Julien, "Scaling of Kinetically Growing Clusters," ibid 51, 1123 (1983).

11. Zallen, The Physics of Amorphous Solids (Wiley-Interscience1983).

12. C. Allain and M. Cloitre, "Optical Fourier Transforms of Fractals," in Fractals in Physics, L. Pietronero and E. Tosatti, Eds. (Elsevier Science Publishers 1986).

13. D. W. Schaefer, J. E. Martin. P. Wiltzius, and D. S. Cannell, "Fractal Geometry of Colloidal Aggregates," Phys. Rev. Lett. 52, 2371 (1981).

14. S. Hamada and E. Matijevic,"Ferric Hydrous Oxide Sols: IV. Preparation of Cubic Hematite Particles by Hydrolysis of Ferric Chloride in Alcohol-Water Solutions," J. Col. Inter. Sci., 84, 274 (1981).

THEORY OF MICROEMULSIONS IN A GRAVITATIONAL FIELD

J.F. Jeng and Clarence A. Miller
Department of Chemical Engineering
Rice University
Houston, Texas

A theory of microemulsions developed previously is extended to include the effect of a gravitational field. It predicts variation with position of drop size, drop volume fraction, and area per molecule in the surfactant films within a microemulsion phase. Variation in volume fraction is greatest and occurs in such a way that oil content increases with increasing elevation, as has been found experimentally. Large composition variations are predicted within a middle phase microemulsion near optimal conditions because inversion from the water-continuous to the oil-continuous arrangement occurs with increasing elevation. Generally speaking, gravity reduces solubilization within microemulsions and promotes separation of excess phases.

1. Introduction

The force produced by the earth's gravity has well known effects on a large scale such as the arrangement of phases in the order of increasing density in a test tube. Our interest here is in its effect on microstructure. Since microemulsions are considered to be mixtures of two types of domains, oil and water, separated by surfactant films, regardless of the detailed microstructure, it is pertinent to ask (a) if the density difference between oil and water has any effect on the equilibrium behavior of the microemulsions and, if so, how large is the effect, and (b) whether the

interfacial tensions between the microemulsions and the excess phases are also influenced by gravity.

Reports of gravitational effects on microemulsion systems are few. Only in the last few years have initial experiments in this area been carried out. Rosen *et al.* (1,2) reported gradients in composition and in properties such as density and electrical conductivity at, and only at, optimal salinities for both pure and commercial surfactants. In particular, they found evidence of an oil-rich composition in the upper portion of the middle phase and a water-rich composition in the lower portion. All their experiments were conducted under isothermal conditions in the earth's gravitational field.

Similar results were reported by Good *et al.* (3,4) based on experiments using light scattering and ultracentrifugation. In addition to gradients in composition, they also reported gradients in drop size. The presence of two species of particles in the middle phase, one denser and the other less dense than their respective continuous media, was suggested, a finding consistent with the results of Hwan *et al.* (5).

Rossen *et al.* (6) raised questions about some of the above experiments and also conducted experiments on microemulsion systems of different compositions, including the three-phase region. The results of their ultracentrifugation experiments indicated a wide compositional variation among samples taken at different distances from the axis of rotation.

In this paper, we extend the theory of microemulsions developed by Jeng and Miller (7) to include the effects of gravity or centrifugation. Although Rossen *et al.* (6) studied such effects theoretically using binary and ternary regular solution models, the present work is the first which explicitly incorporates the effect of microstructure in microemulsion systems. A more complete account of this work has been given by Jeng and Miller (8).

2. Theory

2.1 General Thermodynamic Considerations

Consider a system which consists of N components and is in an equilibrium state at constant temperature T and external pressure P_o. The system is placed in a container of fixed shape, e.g., a test tube, and is under the influence of a gravitational or centrifugal field. Equilibrium requires that, for any component in the system, the sum of the ordinary chemical potential μ_i and the gravitational potential should be uniform. That is,

$$\mu_i + m_i\psi = \text{constant} \tag{1}$$

where m_i is the molecular weight of component i and ψ the gravitational (or centrifugal) potential per unit mass.

We assume that the solution is incompressible and that no volume change occurs upon mixing. Then the quantities n_i, which designate the number of moles of each component per unit volume, are no longer independent because the sum of the volume fractions $n_i v_i$ is unity, where v_i is the molar volume of species i. If we use the equations of hydrostatics to express the pressure change with position in terms of ψ, we can write the derivative of Eq. (1) in the following form for an N-component system (9):

$$\sum_{j=1}^{N-1} \left(\frac{\partial \mu_i}{\partial n_j}\right)_{T,P,n_k} dn_j + (\rho_i - \rho) v_i d\psi = 0 \tag{2}$$

where ρ_i and ρ are the densities of pure component i and the local solution mixture, respectively. Eq. (2) is the basic equation for systems involving more than one species in equilibrium at constant temperature and under the above-mentioned conditions, and is generally referred to as the equation of sedimentation equilibrium. Note that its first term represents the diffusion force (per mole) of component i while the second term represents the net sedimentation force. They have opposite effects on the system and are balanced at equilibrium.

In a gravitational field, where field strength is uniform throughout the system,

$$d\psi = gdz \tag{3}$$

where g is the gravitational acceleration and z the elevation above an arbitrary reference level.

2.2 Application to Microemulsions

Note that Eq. (2) is equally suitable for molecular solutions, colloidal dispersions, and microemulsions. In the case of molecular solutions, a strong field (e.g., high rotation rate centrifugation) is required to induce detectable stratification except near critical points. For colloidal dispersions, gradients in particle concentration are strongly dependent on particle size and on the density difference between the particles and the continuous phase. Since microemulsions are closely related to conventional colloidal dispersions, it is of interest to examine how they are affected by gravity.

Consider a system which consists of three components, oil, water and surfactant, and which forms a microemulsion with or without excess phases at equilibrium. The difference between a conventional colloidal dispersion and a microemulsion in a gravitational field is that, in the former, particle size is uniform while in the latter, it may vary with position. The microemulsion drops are assumed to be spherical and of uniform diameter at each elevation. The equations for hard spheres supplemented by van der Waals attaction have been employed with the duplex film model to derive expressions for the chemical potentials of all components in a gravity-free environment (7). These expressions can be readily applied to the same system in a gravitational field by substituting into Eq. (2). In this manner we find

$$\left(\frac{\partial \mu_i^m}{\partial \eta}\right)_{R,A_s}\left(\frac{d\eta}{dz}\right) + \left(\frac{\partial \mu_i^m}{\partial R}\right)_{\eta,A_s}\left(\frac{dR}{dz}\right) + \left(\frac{\partial \mu_i^m}{\partial A_s}\right)_{\eta,R}\left(\frac{dA_s}{dz}\right)$$

$$= -(\rho_i - \rho) v_i g \qquad , \qquad i = o,w,s \tag{4}$$

$$\left(\frac{\partial E}{\partial \eta}\right)_{R,A_s}\left(\frac{d\eta}{dz}\right) + \left(\frac{\partial E}{\partial R}\right)_{\eta,A_s}\left(\frac{dR}{dz}\right) + \left(\frac{\partial E}{\partial A_s}\right)_{\eta,R}\left(\frac{dA_s}{dz}\right)$$

$$= 0 \tag{5}$$

where μ_i^m is the chemical potential of component i in the microemulsion phase. Also the concentrations n_i have been expressed as functions of R, η, and A_s, which are drop radius, the volume fraction of the dispersed phase, and the area per surfactant molecule in the films, respectively. The quantity E may be considered to be the chemical potential of the drops. Because E must be zero at each elevation within the microemulsion, its derivative must also vanish.

According to the Gibbs-Duhem equation, only three of the above four equations are independent. In this study, we choose those for μ_o^m, μ_w^m and E. It is convenient to choose μ_o^m and μ_w^m and not μ_s^m because, when a microemulsion is in equilibrium with pure excess phases, the chemical potentials of oil or water or both can be related to those of the respective excess phases. But since all the surfactant is assumed to stay in the microemulsion phase, its chemical potential is not readily related to that of the excess phases.

3. Results

Imagine that a microemulsion in equilibrium with one or more excess phases is sliced into many thin layers with the cutting plane perpendicular to the direction of the field. Due to the gravitational (or centrifugal) forces,

compositions and other properties will, in general, be different in different layers. At the interface, where the first slice coexists with the excess phase, gravitational effects across the interfacial region are assumed negligible. Hence, the equilibrium between this layer and the excess phase can be treated as if both were in a gravity-free environment. Values of R, n, A_s and other properties of this first slice are thus obtained according to the procedures described by Jeng and Miller (7). Gradients of R, n and A_s at this position are calculated by substituting these values into Eqs. (4) for oil and water and Eq. (5). The values of R, n, A_s, etc., of the next slice are estimated from these gradients and then used, in turn, to calculate the gradients there. And so forth.

Results obtained by this method include phase continuity (O/W or W/O), R, n, and A_s and their gradients, composition, density ρ, interfacial tension γ_d and bending energy H_d of the drop surfaces, drop concentration n_p, and local solubilization parameters V_o/V_s and V_w/V_s at every elevation. The calculations also determine the types of interfaces and their tensions at the elevations where microemulsions meet excess phase(s).

Unless specified otherwise, calculations are made based on a sample size of 10 ml in a test tube which has a cross sectional area of 1 cm^2. The volume ratio of the components in the overall sample is V_s: V_o: V_w = 2.5: 48.75: 48.75, the same as used in previous calculations (7). Unless otherwise indicated, the earth's gravitational field is that acting on the microemulsion.

3.1 Compositional Paths on Ternary Phase Diagrams

Jeng and Miller (7) presented a predicted series of ternary phase diagrams for gravity-free oil-water-surfactant systems. At small values of the natural radii R^* (O/W) and R^* (W/O), phase diagrams corresponding to

Winsor I and II equilibria, respectively, were found. At large R^* (O/W) and R^* (W/O), especially near the optimal natural radius $(R^*)_{opt}$, diagrams with three-phase regions corresponding to Winsor III were predicted. Since incompressible fluids were assumed, the phase diagrams are independent of pressure if other variables are held constant.

Calculations of phase boundaries for these diagrams were carried out by varying values of $\Delta\mu_o$ and $\Delta\mu_w$, the differences between the chemical potentials of oil and water in the microemulsion and those of pure oil and water, respectively. The composition of a "middle-phase" microemulsion is that for which both $\Delta\mu_o$ and $\Delta\mu_w$ are equal to zero. A microemulsion in equilibrium with excess water has $\Delta\mu_w = 0$ and $\Delta\mu_o < 0$, while a microemulsion in equilibrium with excess oil has $\Delta\mu_o = 0$ and $\Delta\mu_w < 0$. For a single-phase microemulsion, both $\Delta\mu_o$ and $\Delta\mu_w$ are negative.

In this section, we explore the usefulness of these diagrams to represent the variation in composition with elevation for a microemulsion in a gravitational field. If the composition variations are calculated as described above and plotted on the ternary phase diagram which represents the system, they form a continuous curve, as shown in Figures 1 and 2. Such a curve is called a compositional path.

Figure 1 shows compositional paths for a Winsor I equilibrium. System composition and properties are the same as those of Figure 3 of reference (7). The paths begin on the two-phase boundary, where microemulsions are in equilibrium with excess oil, and extend into the interior of the neighboring single-phase region. The calculations indicate that drop radius R and the area per surfactant molecule A_s change little with elevation, but the volume fraction η of the oil drops is larger in the upper portion of the microemulsion, as might be expected.

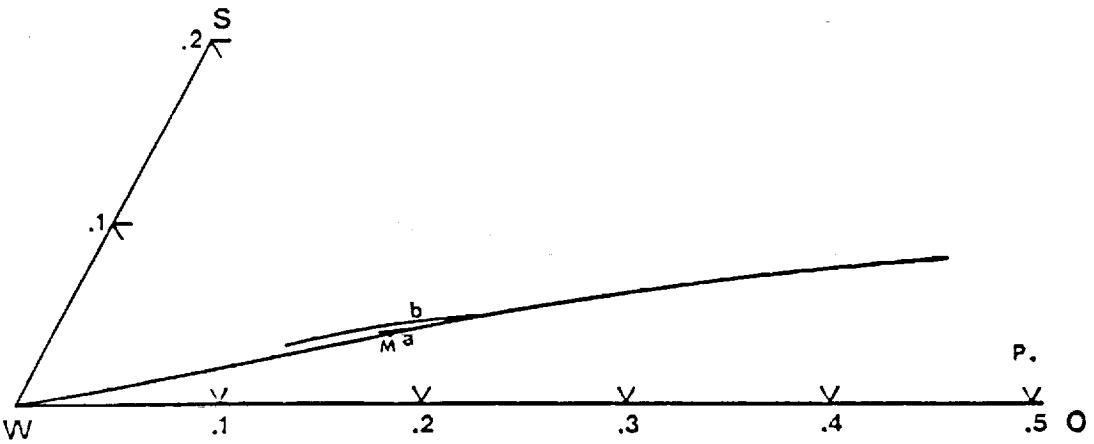

Figure 1. The effect of sample size as depicted by compositional variations in a partial ternary phase diagram. The system is the same as in Figure 3 of ref. (7). All samples have the same overall composition, P. Point M for Og. Curve (a) for total sample height of 10 cm at lg, curve (b) the same for total sample height of 100 cm.

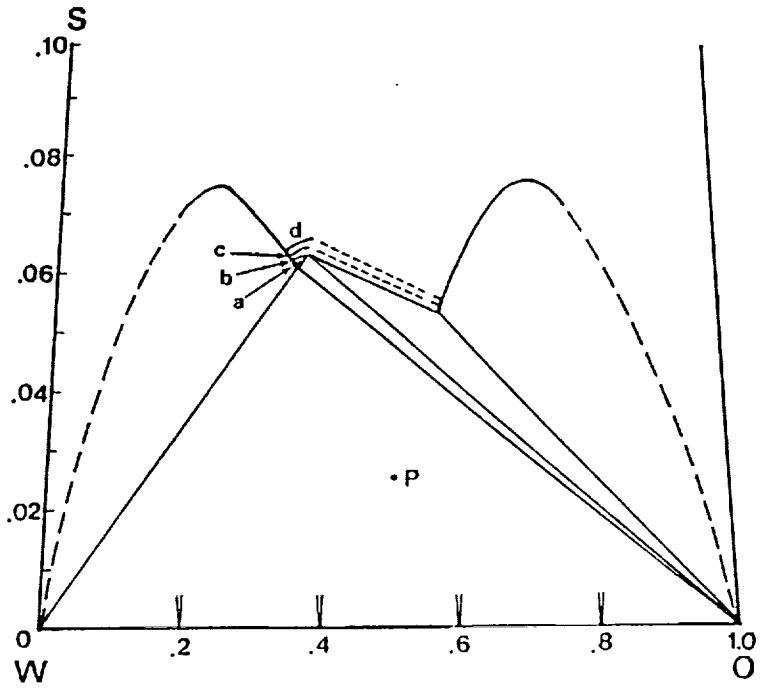

Figure 2. Compositional paths and the effect of sample size for a system with natural radius slightly larger than the optimal value. The system is the same as in Figure 4 of ref. (7). Total sample height (a) 5 cm (b) 10 cm (c) 20 cm (d) 30 cm.

Particularly noteworthy are the strong dependence of path length, i.e., total composition variation, on sample size and the shift in the local composition of the microemulsion at the interface. Path a is relatively short because the drops in this microemulsion are relatively small. Similar behavior is seen for Winsor II systems (10).

Figure 2 shows compositional paths for a three-phase system near the optimal R^*. Again the overall composition and system parameters are the same as for a previous calculation. The paths of Figure 2 exhibit some characteristics quite different from those of Figure 1. Paths a and b, for instance, begin with initial compositions on the microemulsion-oil boundary, extend into the single-phase region above the three-phase triangle, move toward the other two-phase lobe, and end at points on the microemulsion-water boundary. These paths, although entirely within the O/W microemulsion region, are longer (when plotted to the same scale) and hence overall composition variations are greater than in Figure 1 for Winsor I behavior. Since the drop sizes and dispersed volume fractions are larger near optimal conditions, these larger gradients in composition and in other associated properties are expected.

Particularly striking is that paths can pass through a discontinuity in composition where an inversion occurs from a W/O to an O/W microemulsion. In these cases (paths c and d) the "middle phase" actually consists of an upper W/O part and a lower O/W part. For calculations initiated at the W/O microemulsion - oil interface, inversion occurs when the chemical potential of surfactant in an O/W microemulsion having the local chemical potentials of oil and water falls below that of the corresponding W/O microemulsion. The method for calculating this chemical potential difference is described in reference (7). Because composition changes discontinuously at the inversion point, the

difference in composition between the portions of the microemulsion in contact with oil and water becomes quite large, as paths c and d of Figure 2 indicate.

Note that inversion occurs in this case for microemulsions of sufficiently large sample size, i.e., those of sufficient height. The minimum height required for inversion decreases as R^* approaches $(R^*)_{opt}$. At $(R^*)_{opt}$ itself inversion occurs for any nonzero height and substantial concentration variations should be seen. This result is consistent with the experimental observations of Rosen and co-workers (1,2) discussed previously. Since, for given conditions, the inversion point can be located precisely by the theory, the ambiguity in phase volumes found by Jeng and Miller (7) for the four-phase region at $(R^*)_{opt}$ is no longer present when gravity is considered.

Table 1 shows the calculated variation of microemulsion properties with elevation for another system near its optimal R^*. Local values of drop radius, volume fraction, density, and composition are given at the interfaces with excess oil and excess water (t and b) and on both sides of the inversion point (bi and ai). Clearly, most of the differences between the properties at t and b is a result of the discontinuity in composition at the inversion point, as indicated above. We note that if thermal fluctuations were taken into account, a more gradual variation in composition would be expected. The effect of gravity on overall properties of the microemulsion phase such as volume (height) and solubilization parameters is also indicated in Table 1.

The compositional paths of Figures 1 and 2 indicate that, at least in the absence of inversion, the average surfactant concentration in the microemulsion phase is greater when gravity is present than when it is not. That is, the volume of the microemulsion phase decreases and that of the excess phase(s) increases when gravity is taken into account.

The increased concentration of drops produced by gravity at certain locations within the microemulsion should also promote earlier separation of a

TABLE 1. Effect of Gravity on Microemulsion Phase Behavior With Natural Radius Slightly Smaller than the Optimal Value.

System: Same as of Figure 6 of Reference (7).

R^* = 390 nm (W/O)

$(R^*)_{opt}$ = 406.4 nm (W/O)

(I) Overall Properties

	Without Gravity	With Gravity
h (cm)#	4.76	4.41
h_i (cm)#	-	3.06
V_O/V_S	10.17	8.34
V_W/V_S	7.88	8.44

(II) Local Properties

	Without Gravity	With Gravity @			
		t	bi	ai	b
Type	W/O	W/O	W/O	O/W	O/W
R (nm)	17.85	17.40	17.55	14.28	14.19
n	0.428	0.425	0.443	0.404	0.399
A_S (nm^2)	0.4995	0.4994	0.4994	0.4989	0.4989
ρ	0.8817	0.8811	0.8876	0.9489	0.9503
Φ_S	0.0525	0.0534	0.0553	0.0615	0.0611
Φ_O	0.5340	0.5363	0.5126	0.3257	0.3212
Φ_W	0.4135	0.4102	0.4284	0.6127	0.6177

@ t, top; bi, before inversion;
ai, after inversion; b, bottom.

#h is overall height of microemulsion phase

h_i is height of interface with excess oil above inversion point.

second excess phase, i.e., transition to Winsor III behavior from Winsor I or II. Accordingly, gravity should modify the phase volume diagram in the general manner illustrated in Figure 3. In addition to the overall phase volumes, this figure illustrates schematically the relative volumes of O/W and W/O microemulsions present for conditions near $(R^*)_{opt}$ where inversion occurs within the middle phase. Even though composition within such middle phases changes abruptly at the inversion point, composition of the overall middle phase varies continuously with R^*. In contrast, the gravity-free analysis (7) predicts a discontinuous change in middle phase composition at $(R^*)_{opt}$.

3.2 Interfacial Tensions

As Figures 1 and 2 show, gravity alters microemulsion compositions at the elevations where interfaces with excess oil and/or water exist. As a result, interfacial tensions should change as well. The methods for calculating interfacial tensions are described in reference (7).

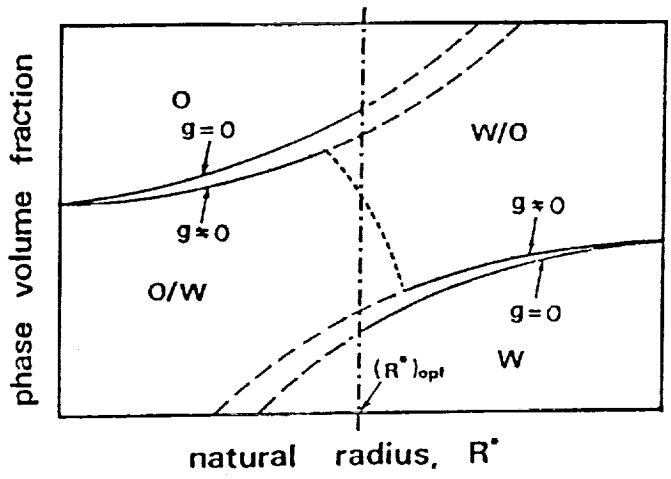

Figure 3. Schematic illustration of the effect of gravity on phase volume fractions, phase continuity, and interfacial structure of a microemulsion system. ——, Type I interface; ---, Type II interface; ·····, locus of inversion points when g≠o.

For a Winsor I equilibrium (Figure 1), gravity produces an increase in oil solubilization at the interface and thereby causes a small decrease in interfacial tension. Representative results are given in Table 2. Behavior is similar for cases of Winsor II equilibria (10).

TABLE 2. Comparison of Equilibrium Interfacial Tensions With and Without Gravity.

Systems: Same as in Table 5 of Reference (7).

	Without Gravity		With Gravity	
	γ_{mo}	γ_{mw}	γ_{mo}	γ_{mw}
a	0.1602	-	0.1601	-
b	0.0438	-	0.0435	-
c	-	-	-	-
d	0.00738	0.00277	0.00707	0.00338
e	0.00426	0.00379	0.00395	0.00406
f	0.00359	0.00409	0.00364	0.00433
g	0.00339	0.00429	0.00346	0.00372
h	0.00269	0.00611	0.00271	0.00553
i	-	-	-	-
j	-	0.0357	-	0.0353
k	-	0.1449	-	0.1446

All units are in mN/m.

Only sample f exhibits inversion within the middle phase for this system.

If there is no inversion within a microemulsion coexisting with both excess oil and excess water, one of the interfaces is a monolayer (Type I), the other a much thicker interface between the microemulsion and its excess continuous phase (Type II), as illustrated in Figure 2 of reference (7). For instance, in paths a and b of Figure 2, the Type I interface is between the uppermost part of the O/W microemulsion and excess oil, while the Type II interface is between the lowest part of the O/W microemulsion and excess water. As Table 2 indicates, the tension of the former interface decreases and that of the latter interface increases when gravitational effects are considered.

When inversion occurs within the middle phase, as for paths c and d of Figure 2, the interfaces with both excess oil and excess water are of Type II. This result differs from that of the gravity-free case (7), where the interface with one excess phase is of Type I and that with the other excess phase of Type II except at the optimal R^*. Our calculations indicate that interfacial tension generally decreases when one of these interfaces is changed from Type I to Type II as a result of gravity-induced phase inversion.

4. Conclusions

A theory of microemulsions with spherical drops developed previously has been extended to include the effect of gravity or centrifugation. It provides information on gradients within a microemulsion phase of equilibrium properties such as drop radius and dispersed volume fraction. Near optimal conditions abrupt inversion from a W/O to an O/W microemulsion can take place with decreasing elevation within the overall "middle phase". When such inversion occurs, the composition difference between extremities of the middle phase is substantial, as has been observed experimentally. Otherwise, composition variations are relatively small in an ordinary gravitational

field, especially for microemulsions with small drops. Other specific conclusions are the following:

(1) The effect of gravity is to decrease the volume of the microemulsion phase, solubilization parameters, and interfacial tensions of Type I interfaces, and to increase interfacial tensions of Type II interfaces and surfactant concentration in the microemulsion. Although not investigated here in detail, gravity seems to promote the initial separation of excess continuous phase from a microemulsion, e.g., excess water from an O/W microemulsion.

(2) In a gravitational field, phase inversion occurs when the system is near its optimal natural radius. This inversion region increases with increasing sample size and field strength.

(3) In all cases oil content increases and water content decreases with increasing elevation for oils less dense than water. The variation in composition occurs mainly by variation in the volume fraction of drops, with changes in drop size having only a secondary effect. Surfactant concentration is highest where drop concentration is maximized, whether this situation occurs at the top or the bottom of the microemulsion phase.

(4) Including gravity removes the ambiguity in phase volumes at the inversion point found in the gravity-free analysis of Jeng and Miller (7). It also yields an overall middle phase composition which varies continuously with natural radius R^* instead of changing discontinuously at $(R^*)_{opt}$.

References

1. Rosen, M.J., and Li, Z-P., J. Colloid Interface Sci., **97**, 456 (1984).

2. Zhao, F., Rosen, M.J., and Yang, N-L., Colloids Surfaces, 11, 97 (1984).

3. Good, R.J., Ho, J.T., Broers, G.E., and Yang, X., J. Colloid Interface Sci., **107**, 290 (1985).

4. Good, R.J., van Oss, C.J., Ho, J.T., Yang, X., Broers, G., and Cheng, M., Colloids Surfaces, **20**, 187 (1986).

5. Hwan, R.N., Miller, C.A., and Fort, T., Jr., J. Colloid Interface Sci., **68**, 221 (1979).

6. Rossen, W.R., Davis, H.T., and Scriven, L.E., J. Colloid Interface Sci., **113**, 248, 269 (1986).

7. Jeng, J.F. and Miller, C.A., Colloids Surfaces, 21, 247 (1987).

8. Jeng, J.F. and Miller, C.A., Colloids Surfaces, 28, 271 (1987).

9. Fujita, H., "Foundation of Ultracentrifugal Analysis", John Wiley and Sons, New York (1975).

10. Jeng, J.F., Ph.D. Thesis, Chapter 4, Rice University (1986).

PROPOSED USES OF LASER LIGHT SCATTERING INSTRUMENTS FOR POLYMERIZATION STUDIES

Lon J. Mathias, Charles E. Hoyle and Kevin McLaughlin
Department of Polymer Science
University of Southern Mississippi
Hattiesburg, Mississippi

Samuel P. McManus
Department of Chemistry
University of Alabama in Huntsville
Huntsville, Alabama

James M. Caruthers
Department of Chemical Engineering
Purdue University
West Lafayette, Indiana

and

Michael L. Runge
Science Research Laboratory/3M
3M Company
St. Paul, Minnesota

INTRODUCTION

The understanding of monomer and polymer diffusion processes in dilute and concentrated solutions is of fundamental importance for evaluating and predicting homo- and copolymerization kinetics. A recent paper[1] summarizes in detail the effects of polymer diffusion on copolymer composition in the high conversion regime. In this portion of a copolymerization reaction, viscosity effects maximize the importance of polymer diffusion in controlling copolymer composition and especially molecular weight. However, the effect of polymer diffusion is also important at low conversion and during dilute solution polymerizations although the effect is markedly reduced. A major problem with predicting copolymer composition throughout a copolymerization process is that accurate polymer diffusion constants are not known[2]. When coupled with uncertainty in how monomer diffusion effects copolymerizations, it is not surprising that complete and accurate models have not been developed for copolymerization reactions.

Microgravity offers a unique environment for studying polymer diffusion and polymer polymerization reactions. The absence of convection currents, which are the major mode of mixing at the molecular level on earth, are eliminated or reduced in the microgravity environment. More importantly, the prediction of unique copolymer composition development in microgravity (discussed in detail below) will allow controlled formation of new compositions of matter. The absence of mixing at the molecular level should produce unique short-block copolymers available for the first time for comonomer compositions which normally lead to random or long-block copolymers under good mixing.

We propose the investigation of fundamental polymer diffusion and polymer polymerization processes in microgravity. Because of the complexity of polymerization diffusion and kinetics measurements, a cooperative effort is required based upon the interdisciplinary nature of polymer research and drawing on individual areas of expertise of the coauthors. This effort will involve fundamental studies of monomer and polymer diffusion; their effect on initiation, propagation and especially termination kinetics rate constants; and the accurate evaluation of copolymerization reactivity ratios in microgravity. Table 1 summarizes the coauthor's area of expertise.

Table 1. Requirements for microgravity polymerization studies.

Photoinitiation	- Hoyle/USM
Molecular Modeling of Polymerization Processes	- McLaughlin/USM
Copolymer Kinetics	- McManus/UAH
Diffusion Measurements and Predictions	- Caruthers/Purdue
Light Scattering and Molecular Characterization of Polymers	- Mathias/USM

This paper will present our expectations concerning experimental design for these studies and especially will describe an evaluation technique for in situ monitoring of polymer diffusion and polymerization kinetics in microgravity. Fundamental to this study is the availability of a versatile multi-angle laser light scattering spectrometer sufficiently small for incorporation in microgravity reactors.

EXPERIMENTAL PARAMETERS AND DESIGN

Photoinitiation and Photopolymerization

Typical photoinitiators will be employed with UV and pulsed laser light sources. This will allow careful control of the initiation process as well as direct determination of initiation, propagation, and termination rate constants. Professor Hoyle at USM has established the methodology for detailed kinetic evaluation of homo- and copolymerization reactions using photoinitiation and phototermination processes[3].

Molecular Modeling of Polymerization Processes

Molecular modeling will be carried out at several levels building upon simple models and results, and extending to more detailed calculations. Microcomputer techniques will be employed initially to establish overall calculation parameters, and to examine simple statistical models for diffusion-controlled monomer incorporation into copolymers. These will be extended to minicomputer and finally supercomputer calculations on systems at USM and at the Marshall Space Flight Center in Huntsville. These modeling efforts will provide a theoretical basis for the selection of appropriate comonomer compositions for maximizing the effects of microgravity on copolymerizations. They will also facilitate prediction of propagation and termination rate constants, and molecular weights of homo- and copolymers formed in microgravity.

Diffusion Modeling and Calculations

Diffusion measurements involving mass transport across a concentration gradient are complicated by the enthalpy of mixing which causes convective mixing. This problem is compounded during vinyl polymerizations because of the enthalpy of polymerization which is generally much greater than the mixing enthalpy. Thus, measurement of both low and high molecular weight materials is difficult to do accurately on earth. In microgravity, the contribution of convective mixing can be eliminated and accurate diffusion constants measured. Proposed research will involve initial computer modeling of diffusion, especially polymer diffusion, coupled with design and execution of microgravity measurements.

Modeling of the diffusion process will provide insight into the effects of experimental parameters on the measurement accuracy. Variation of concentration, temperature, and solvent-polymer interactions can be estimated alone and collectively. In addition, the effect of chain stiffness on the mechanism of polymer diffusion will also be calculated. Finally, the presence of convective mixing at various values of mixing enthalpy will allow estimation of the effect of this variable on the measurements. Description of the expected results is given in the Discussion section.

Monomer Selection for Copolymerizations

Comonomers chosen for study, both theoretically and in ground-based experiments, are summarized in Table 2. These monomers were selected by polymer synthesis researchers at UAH (McManus) and USM (Mathias). The rationale for selection involves choice of monomer compositions in which r_1 is large while r_2 is small. The reactivity ratio pairs should lead to the compositions which, in the absence of convection, will display the greatest difference in microgravity compared to well-mixed systems not under diffusion control.

One concern in the choice of comonomers is that the rate of propagation may be just comparable to the rate of monomer diffusion, and thus show only marginal differences. To maximize differences in the diffusion rates for the two comonomers, we have also included methacrylate-terminated macromonomers in Table 2. Macromonomers are polymers or oligomers possessing terminal vinyl functionality, in this case a methacrylate unit. It has recently been demonstrated that the relative reactivity of such terminal groups is essentially identical to that of methyl methacrylate in copolymerizations with a variety of methacrylate esters and styrene in well-stirred systems[6]. In quiescent systems, however, diffusion of macromonomers will be greatly reduced compared to small molecules and will result in copolymerizations that will reflect the greatest effects of microgravity.

Table 2

Monomer 1	r_1	Monomer 2	r_2
methyl methacrylate	1.35	acrylonitrile	0.18
methyl methacrylate	1.20	methyl alphachloroacrylate	0.30
methyl methacrylate	2.53	vinylidene chloride	0.24
methyl vinyl ketone	1.78	acrylonitrile	0.61
vinyl chloride	2.00	vinyl acetate	0.30
2-vinyl pyridine	1.13	styrene	0.55
2-vinyl thiophene	3.10	styrene	0.35
methacrylate-macromonomer	1.0	methyl methacrylate	1.0
"	0.47	styrene	0,52
"	1.35*	acrylonitrile	0.18*

*estimated values based on behavior with other monomers

Light Scattering Spectrophotometer

The design of this instrument is based on that presented in the proceedings announcement. Maximum versatility is required for carrying out a number of different types of measurements in microgravity, either simultaneously or in a sequential manner. These measurements are discussed in detail in the Discussion section.

Polymer Analysis

Copolymer composition, and homopolymer and copolymer molecular weight and molecular weight distributions, will be determined directly in microgravity (when appropriate) and in the laboratories at USM. Copolymer compositions will be evaluated at the molecular level using high field NMR. This will allow direct comparison of the molecular incorporation of comonomer units based on differences in chemical shift related to comonomer sequences. The molecular weight measurements will be carried out with presently available methods based on stand-alone light scattering spectrometers as well as coupled systems utilizing SEC (size exclusion chromatography) with mass and molecular weight detectors. The latter will include in-line viscometric as well as light scattering detectors for evaluation of homopolymer compositions and molecular weight distributions. Application to copolymer systems is more difficult and requires extensive evaluation of the light scattering behavior of the copolymers specifically selected.

The measurement of diffusion processes, both of preformed polymers in the microgravity environment, and of homo- and copolymers as they are formed in the microgravity reactor, will be carried out based on initial modeling study predictions and calculations carried out both at USM (McLaughlin) and Purdue University (Caruthers). These measurements will use light scattering as well as other techniques such as infrared, UV spectroscopy, and differential refractometry to directly monitor the diffusion process of polymer molecules in dilute and concentrated solutions. The LALS instrument will be coupled with other spectroscopic techniques to provide complimentary data. The availability of spectrometers for space science, some of which are currently under development, is vital for this effort.

DISCUSSION OF EXPECTED RESULTS

In this paper, we will not discuss in detail the synthetic requirements, the copolymer composition measurements, or the molecular modeling experiments to be carried out. We focus instead on the use of laser light scattering as a detection and monitoring method for in situ evaluation of polymer kinetics and polymer diffusion

processes. The experiments required are presently not possible with available spectrometers. The ultimate success of these experiments, and the fundamental examination of other polymer processes in the microgravity environment, all depend on the availability of appropriate instrumental capabilities. Because light scattering is one of the most sensitive techniques for polymer characterization and analysis, it will allow a broad spectrum of experiments dealing with polymerizations and polymer properties in microgravity.

Homopolymer and Copolymer Diffusion Studies

Let us first outline experiments that will evaluate simple diffusion rate constants for homopolymers and copolymers in selected solvents and with respect to molecular weight. Figure 1 illustrates two configurations of cell designs and measurement protocols for such evaluations. In the first cell, a simple determination of total concentration with respect to time is measured. Light scattering intensity is directly related to concentration if the molecular weight and refractive index variables for this polymer in the given solvent are known. Using this technique, a simple concentration-time plot can be obtained showing the amount of polymer passing through a given volume of the cylindrical cell. Diffusion begins when the sample compartment partition is opened to allow the concentrated solution of polymer to interact with the pure solvent in the LALS sample cell. Mass transport can be calculated knowing the dimensions of the cell and the time-dependent concentration of the polymer at any given point in the cell.

The second configuration shown in Figure 1 illustrates a more precise monitoring of the diffusion process. Either sequential measurements across the cell using the same source and detector is made, or an array detector is used which allows virtually simultaneous measurements along the cell's linear direction. The former requires mechanical motion of the sample or the detector, or the use of electronic switching with an array of light-pipe sensors. The latter would involve a series of matched laser sources and detector windows in which, after appropriate calibration, the absolute concentration of migrating polymer is measured physically along the cell. Diffusion begins at one side and polymer migrates linearly through the cell. This technique provides for automatic baseline compensation and allows continuous monitoring of the diffusion process throughout the cell. Any changes of diffusion rate with change in local concentration would be directly detected.

FIGURE 1. Possible LALS configurations.

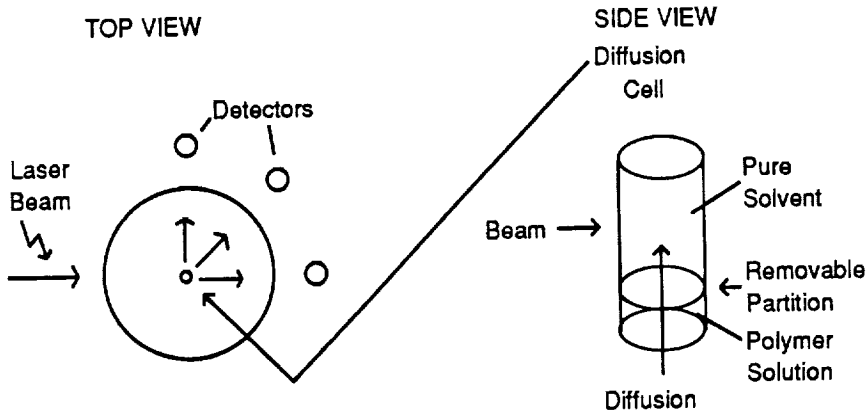

STACKED LALS UNITS FOR SIMULTANEOUS
DIFFUSION/MASS TRANSPORT MEASUREMENTS

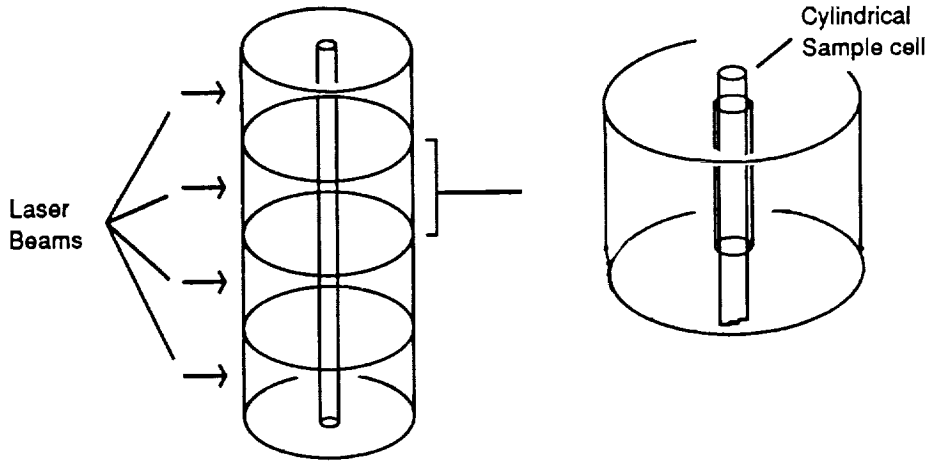

Both of these cell designs and measurement protocols allow evaluation of diffusion in the absence of convection. For polymer molecules, whose inherent molecular weight and size reduce their diffusion constants much below those of small molecules, the rate of diffusion in the absence of convection is normally very low. Accurate measurement of such diffusion constants is not possible on earth. In addition to the value of the obtained data for application in earth systems, diffusion constants are needed for determination of the rate constant values described below.

Relationship of Polymer Molecular Weight to Diffusion and Convective Mixing

In radical polymerizations, chain termination involves reaction of two active chain ends through coupling or disproportionation as shown in Figure 2. This process is facilitated by convective mixing. In contrast, chain propagation occurs mainly through diffusion of monomer molecules to the active chain end. The overall rate constants that are important in these processes are R_p, rate of propagation, and R_t, rate of termination. The former is proportional to the concentrations of active chain ends and monomer. The latter is proportional to only the concentration of active chain ends. Based on theoretical determinations established previously and tested experimentally, the kinetic chain length, DP, equals R_p/R_t^3. It is clear from this equation, that any changes in R_p or R_t will effect DP. Propagation is facile under normal conditions and in the absence of gravity, and little change in the rate of propagation is expected. Termination, however, should become more difficult in the absence of convective mixing and should lead to a decrease in R_t. The overall effect should be a considerable increase in DP over a well-stirred system.

FIGURE 2. Termination by coupling vs disproportionation.

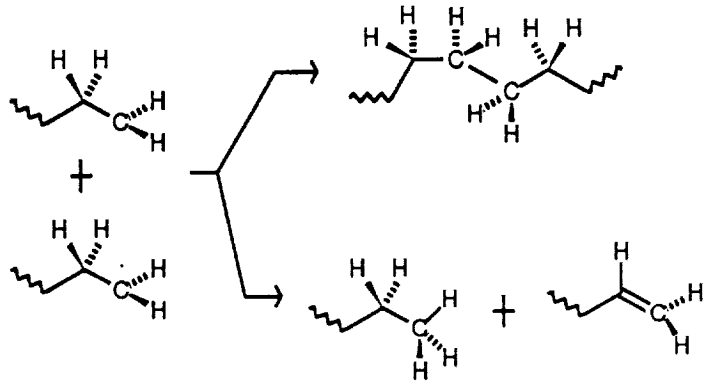

It is clear that the dependency of molecular weight on mixing and therefore the mechanism of mixing, should affect molecular weight. Once the diffusion rate constant is known for a given polymer molecule with respect to molecular weight of that molecule in the solvent chosen, one can accurately calculate the individual rate constants for propagation and termination. This information has previously not been available because convective mixing swamps diffusion controlled processes.

Copolymer Composition Studies

This study will involve selected comonomer mixtures that will allow maximum differences between earth and the microgravity environments. Let us first discuss copolymerization in general, and the reactivity ratios associated with given monomer pairs. Then we will describe expected behavior in microgravity, the experimental design, and how a laser light scattering detector can be used in its evaluation.

In a typical copolymerization process, the two comonomers have different reactivities with respect to active chain ends. The reactivity of each monomer depends not only on its inherent reactivity, but also upon the radical chain end with which it is reacting. This leads to four equations given in Figure 3. It is the ratio of the rate constants for a given monomer reacting with the two possible chain ends which is the important variable in determining sequence composition.

FIGURE 3. Reactivity ratio definitions.

$$--M_1^* + M_1 \xrightarrow{k_{11}} --M_1M_1^*$$

$$r_1 = k_{11}/k_{12}$$

$$--M_1^* + M_2 \xrightarrow{k_{12}} --M_1M_2^*$$

$$--M_2^* + M_2 \xrightarrow{k_{22}} --M_2M_2^*$$

$$r_2 = k_{22}/k_{21}$$

$$--M_2^* + M_1 \xrightarrow{k_{21}} --M_2M_1^*$$

While we do not have time to discuss all possible combinations of r_1 and r_2, let us describe in depth the combination chosen for the microgravity experiment. If $r_1 >> 1$ and $r_2 << 1$, a copolymer sequence should be generated in which monomer 2 is incorporated in long blocks with occasional incorporation of single molecules of monomer 1. This is depicted in Figure 4. Of course, the overall rate of incorporation of each monomer depends not only on its relative rate constants but upon its relative concentration as well.

FIGURE 4. Typical copolymerization with good mixing.

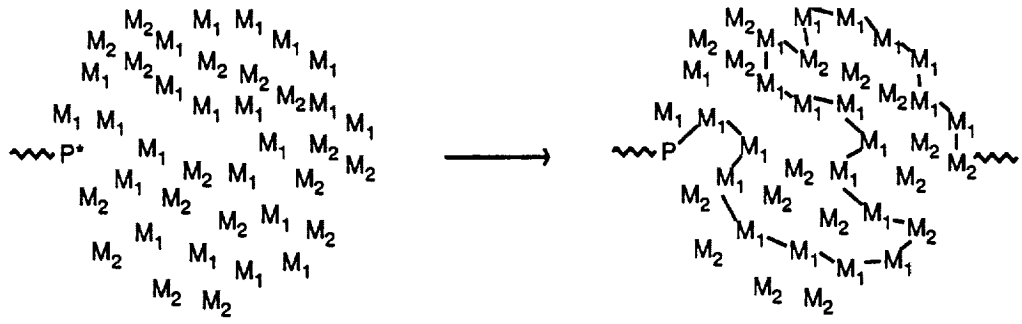

Selecting a monomer mixture of 50% of each monomer, for example, it should be clear that a copolymer will be obtained initially in which monomer 1 is the predominant monomer. As conversion continues, however, the concentration of monomer 1 decreases more rapidly than that of monomer 2. This leads to a situation in which the higher concentration of monomer 2 gradually leads to its greater incorporation into the growing copolymer. The copolymer composition changes as monomer 2 concentration increases, and the individual rate constant affects are overcome by concentration effects. At complete conversion in a batch reactor, this leads to an overall or average copolymer composition of approximately 1:1 despite the fact that the composition of individual chains formed at different levels of conversion will be very different from a 1:1 ratio. The properties of this mixture of copolymers will be very different from those of a copolymer which is homogeneous throughout.

Figure 5 outlines schematically the series of steps envisioned for a copolymerization in which not only diffusion of the polymer molecule is reduced, but monomer diffusion becomes slow and comparable to the rate of propagation. In the absence of convective mixing, the growing radical chain end thus occupies a "fixed" volume containing the average bulk concentrations of monomer 1 and monomer 2 that are available for reaction. In this microenvironment, the more reactive monomer 1 is preferentially incorporated into the growing polymer chain causing the local concentration of monomer 1 to decrease, and the local concentration of monomer 2 to increase. If sufficient time is available for further propagation within this microenvironment, but insufficient time for inward diffusion of the two monomers to re-establish the average concentrations, then the rate of incrorporation of monomer 2

should momentarily increase. This will result in a markedly different copolymer composition than if convective mixing occured. The assumption, of course, is that the rate of diffusion of the monomers is slow with respect to chain propagation. Ways of controlling the relative diffusion processes are to choose monomers whose relative reactivities are most different; change the temperature and viscosity of the reaction medium; or select monomers whose reactivites are essentially unchanged while their diffusion rates vary. The last involves macromonomers versus low molecular weight monomers. In all cases, it is necessary to know the absolute diffusion constants for polymers and monomers in the environment chosen.

The molecular weight detection apparatus, i.e., the light scattering spectrometer, will function as the combined conversion and molecular weight detection apparatus. Only low conversion polymerizations (<20-30%) will be used in these studies to limit the effect of changing monomer ratios with extent of reaction. Also, since molecular weight will probably vary with conversion and with relative diffusion constants of monomers and polymers, the results of homopolymer and copolymer diffusion studies, coupled with the ground-based evaluation of light scattering variables for these copolymer systems in the solvent selected, will allow direct determination of polymer growth with respect to time. Ground-based analysis of the copolymer compositions after return to earth will allow molecular level determination of comonomer incorporation. This information will allow calculation of all relevant rate constants in the reacting system. Even small differences in monomer diffusion under microgravity conditions should lead to marked effects on copolymer composition that should be readily measurable.

The copolymerization experiment was chosen to facilitate the determination of relative rate constants rather than absolute rate constants. Rate constant evaluation is notoriously difficult, requiring a large number of repetitive measurements of high precision and accuracy. However, the evaluation of relative rate constants is much less demanding. This is true especially when the relative constants are chosen so as to maximize their differences. The copolymerizations described above do this in terms of reactivity ratio differences. The copolymer obtained is thus a molecular level recording device for the relative diffusion and reactivity rates for the comonomers in the copolymerization process.

Figure 5. Diffusion controlled copolymerization; $r_1 >> 1$, $r_2 << 1$.

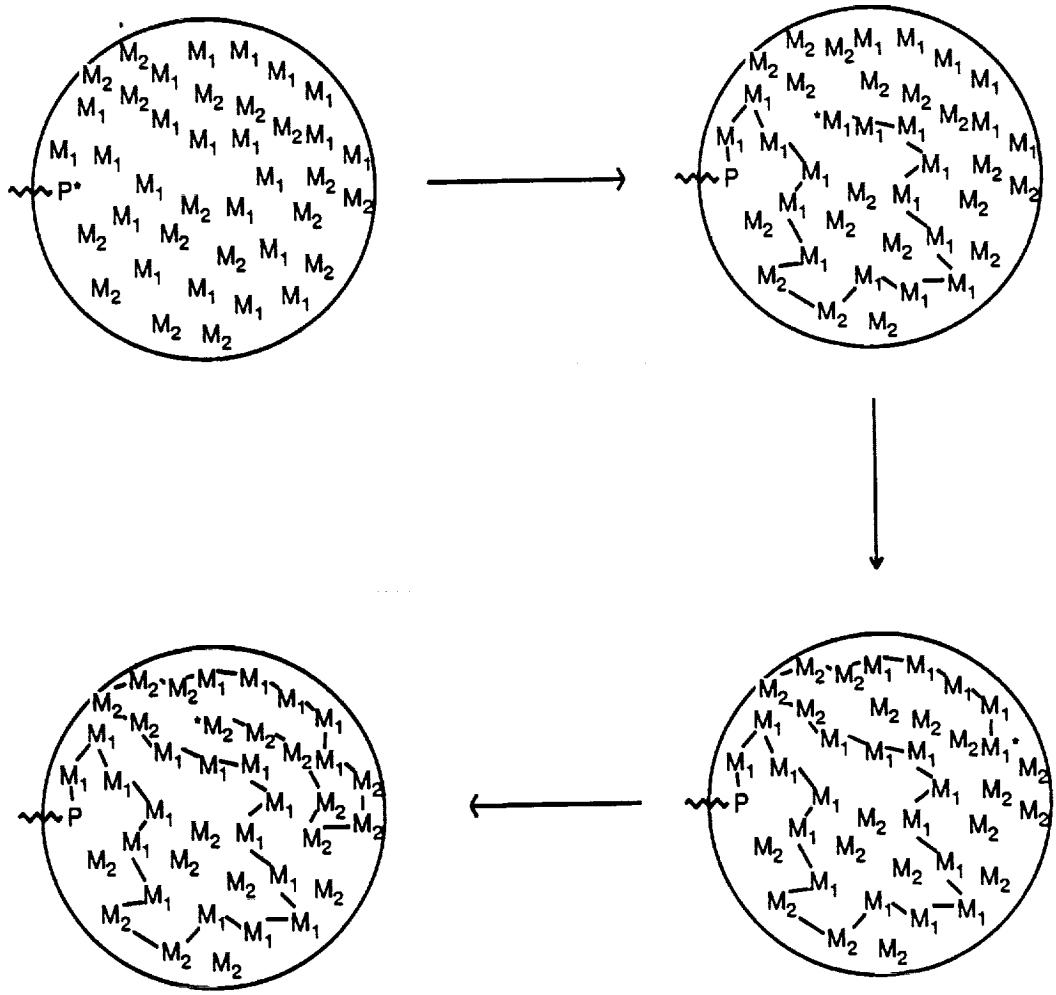

We believe that these experiments will therefore provide fundamental information about polymers that will have both theoretical and practical application. Fundamental to the study of these systems is the availability of the sensitive detectors of molecular weight and molecular motion. Light scattering spectroscopy provides the necessary analytical method, especially if it is available in conjunction with other detection techniques such as refractive index, infrared, and perhaps ultraviolet spectroscopy. While we have not discussed combined techniques above, it should be clear that enormously greater information would be available using more than one analytical method. One can envision a process in which the diffusion process is

monitored by both a molecular mass method (such as IR or UV) as well as a molecular weight sensitive method (light scattering). For example, in a single experiment, one could take broad molecular weight distribution polymer sample and measure the relative rates of diffusion for molecules based on their molecular weight.

Conclusions

The experiments described above will allow determination of fundamental monomer and polymer properties. The diffusion rate constants to be measured in the absence of convective mixing have not been accurately measurable on earth. This data will provide new insights into the fundamental behavior of polymers in a variety of situations important to their formation and processing. For example, molecular weights and distributions are directly dependent on the relative diffusion behavior of monomers and polymers. Processing of polymers, either in solution or from the melt, involves molecular reorganization and motion. The combination of convective mixing with diffusion determines the ability of polymers to effectively orient into crystalline domains. A further example is provided by copolymerizations at high conversion. In this regime, which is industrially important on earth, the diffusion constants of monomers and polymers become extremely important. The copolymer composition throughout the reaction must be amendable to calculation and prediction. This is currently not possible without accurate knowledge of polymer and monomer diffusion constants.

References

1. Sharma, D. K.; Soane, D. S. **Macromolecules**, 1988, **21**, 700-710.
2. Hjertberg, T. **J. Appl. Polym. Sci.**, 1988, **36**, 129-140.
3. Hoyle, C E.; Trapp, M.; Chang, C. H. **Prpnts. Polym. Mat. Sci. Eng.**, 1987, **57**, 579.
4. Odian, G. "Principles of Polymerization," 2nd Ed., John Wiley, N. Y., 1981.
5. Tsukahara, Y.; Tanaka, M.; Yamashita, Y. **Polym. J.**, 1987, **19**, 1121-1125.

POLYMER SOLUTION PHASE SEPARATION: MICROGRAVITY SIMULATION

Lawrence C. Cerny
Department of Chemistry
Utica College
Utica, New York

and

James K. Sutter
National Aeronautics and Space Administration
Lewis Research Center
Cleveland, Ohio

In many multicomponent systems, a transition from a single phase of uniform composition to a multiphase state with separated regions of different composition can be induced by changes in temperature and shear. The density difference between the phase and thermal and/or shear gradients within the system results in buoyancy driven convection. These differences affect kinetics of the phase separation if the system has a sufficiently low viscosity. This investigation presents more preliminary developments of a theoretical model in order to describe effects of the buoyancy driven convection in phase separation kinetics. Polymer solutions were employed as model systems because of the ease with which density differences can be systematically varied and because of the importance of phase separation in the processing and properties of polymeric materials. The results of this project indicate that the kinetics of the phase separations can be performed viscometrically using laser light scattering as a principle means of following the process quantitatively. Isopycnic polymer solutions were used to determine the viscosity and density difference limits for polymer phase separation. From these methods, it was possible to examine polymer-polymer interactions in a θ-solvent. The rheological measurements were extended to detect the phase separation and to define the critical temperature. The results are tentatively explained in terms of a free energy expression which combines both thermodynamics and hydrodynamics.

INTRODUCTION

The study of phase separation processes is an active area of research in polymer science. There is strong evidence that theories describing phase separation in polymeric systems may have direct applications to low molecular weight systems as well as inorganic materials. Recent work on polymers avoids convection effects by using high viscosity systems such as bulk polymers or concentrated solutions. Current theories usually do not include consideration in both the experimental work and the theoretical analysis. It is anticipated that the results will be applicable to commercial processes such as controlling the morphology of the polymeric materials and improving the efficiency of both chemical and biological separation processes. It is anticipated that this work will be of increased importance to NASA because of the opportunity for controlling the extent of buoyancy driven convection during phase separation experiments using the microgravity environment of the shuttle and space station. This work indicates that small solutions density differences in ground based experiments can be used to simulate results of space experiments. This investigation will supplement the current program in microgravity science which is now aimed at metal alloys and crystal growth.

Recently there has been a great deal of interest in both the experimental and theoretical aspects of the kinetics of phase separation. This is evident from the number of presentations that were reported at the "Symposium on Polymer Blends" at the American Chemical Meeting in New Orleans, LA in August 1987 (1).

The kinetics of the spontaneous growth of concentration fluctuations of spinodal decomposition has attracted a great deal of attention because:

(1) Polymers with high molecular weights allow the study of the unmixing process to be followed in the early stages of the reaction. Mixtures of small molecules are usually limited to the final stages of the unmixing.

(2) Polymer molecules in these mixtures, again because of their size, permit the valid investigation of a linear theory within the time reference of the experiment. Therefore, polymers are very desirable molecules. Also, the architectural geometry can be modified in polymers to present another significant molecular parameter.

Most theories, which have their origin with small molecules, have neglected the polydispersity which so commonly occurs in the preparation of commercial polymers. Corrections for this property have recently been reported and indicate changes in the binodal curve (2).

(3) Also polymer-solvent systems have a unique situation in which the interactions between the two vanish. This is called the θ-condition (3). In theory, at least, this allows one to examine polymer-polymer interactions, in the absence of polymer-solvent effects.

For polystyrene, it is also possible to alter the molecular configuration. That is, besides the linear polymer, it is possible to form star (4) and comb (5) molecules. This fact adds an additional dimension. The same molecular weight polymer, because of its configuration, will be more compact and therefore the types of polymer-polymer interactions will reflect this parameter.

An important feature of this investigation relates to the use of the experimental technique of light scattering. This physical measurement allows an accurate means of following the kinetics of the phase separations, both in solution and in films. The determination of the θ-condition has been adequately described by Orofino using light scattering methods (6). More recently, the dynamical aspects of phase separation in polymer blends have been reported by time-resolved light scattering techniques for films (7,8).

Another added feature to simulate microgravity relates to the fact that in several polymer-solvent systems exhibiting the θ-condition, it is possible to attain an isopycnic situation. This is particularly unique and offers an added parameter in need of detailed investigation.

Silberberg and Kuhn reported some very interesting phase separation and miscibility experiments using viscometric techniques (9). They were able to show that in certain demixed liquid-liquid systems stirring can affect the solubility and/or miscibility of the phases. In some cases this amounted to a situation corresponding to a temperature change of 10 C or a 1.15-fold dilution. From these early investigations, they were able to relate the shear rate of the mixed solution to a temperature change and the size of the droplet particles (10). These studies were extended by VerStrate and Philippoff using polystyrenes in di(2-ethyl hexyl) phthalate (11). It was clearly shown that the temperature of the cloud point in this θ-system, was strongly dependent upon the shear stress. Recently, Berg and Moldover (12) examined exponent near the consolute points. Even with simple liquids, there was quantitative evidence for viscoelasticity near the critical point.

The current investigation presents some preliminary studies on polymer-polymer interactions in θ-solvents and explores the use of rheometry for phase changes.

EXPERIMENTAL

A. Polymers. The initial work employed polymers which are commercially available. The preliminary studies used polystyrenes which have narrow molecular weight distributions. This means that the heterogeneity ratio, Weight Average Molecular Weight/Number Average Molecular Weight, is less than 1.10. These are linear polymers with molecular weights in the range of 51,000 to 411,000. The

characterization information such as molecular weight, viscosity and heterogeneity ratio is provided by the supplier. However, these parameters were carefully reviewed.

B. Solvents. The solvents to be used met two important criteria. First, they must be θ-solvents, that is, at a specific temperature, called the θ-temperature, there are no polymer-solvent interactions and the system behaves ideally. This is analogous to the Boyle temperature for a real gas. Second, the density at or near the theta point should be approximately the same as the polymer. An isopycnic system could be used to simulate the microgravity environment of the shuttle or space station. To date the solvents meeting both these criteria are diethylmalonate, diethyloxalate, and mixtures of these two.

All of the solvents were characterized with respect to the density function of both the temperature as well as the polymer concentration (6).

Since the density of the polymer is also critical, the relationship given by Fox and Flory (13) was used.

C. Viscometers. The visometric measurements were made in three different types of viscometers; a Cannon-Ubbelohde capillary semi-micro dilution viscometer (14), a Brookfield concentric cylinder viscometer and a modified Zimm-Crothers low rate of shear rotational viscometer (15). The viscometers were thermostated with water baths whose temperature was controlled to ± 0.01 C.

RESULTS AND DISCUSSION

The initial viscometric measurements were made with mixtures of well-fractionated polystyrene polymers in a 1 to 1 (by volume) of diethylmalonate and diethyloxalate. This is a θ-solvent for polystyrene at 48 C (16). It was the intent of these measurements to evaluate polymer-polymer interactions in a θ-solvent by means of the Stockmayer-Fixman equation (17). These authors suggest that the equation between the intrinsic viscosity, $[\eta]$ and the molecular weight M,

$$[\eta] = K\, M^{1/2} + 0.51\, \Phi_o B M \qquad (1)$$

can be used to evaluate both short - and long-range interactions. In this equation, K is a constant which relates the viscosity to the molecular weight, Φ_o is the Flory-Fox constant, B is a parameter measuring the polymer-solvent interactions. Therefore a graph of $[\eta]/M^{1/2}$ versus $M^{1/2}$ should result in straight line. The intercept is K and the slope is $0.51\Phi_o B$. It was anticipated that in a θ-solvent, the slope would be zero since the polymer-solvent interactions are minimum. However, in polymer-polymer mixtures, it was expected that a deviation from zero slope would be a measure of the polymer-polymer interactions. Some of these data are shown in Fig. 1 for polystyrene in 1:1 DEM:DEO at 48 C. The open circles are mixtures of two pure fractions. The data do not indicate any deviations from a zero slope. Also shown in the figure are some samples in toluene.

The early studies of Silberberg and Kuhn (9,10) as well as those reported by VerStrate and Philippoff (11) motivated the next part of the investigation. The measurements were made to examine the possibility of defining a phase transition in an isopycnic solution by rheometry. Some of these data are presented in Fig. 2. The instrument was Brookfield Viscometer Model DV-II. This is a concentric cylinder viscometer, which was run at a constant speed of 60 r.p.m. Since the unit is made of stainless steel and completely enclosed, the visual detection of the phase change was made in a test tube under similar temperature conditions. The two processes indicated similar results.

In order to incorporate both the viscometric with the visual, an all glass modified Zimm-Crothers rotating cylinder was designed. This unit also allowed the measurements to be made at lower shear rates. The viscometers were calibrated over an appropriate temperature range with the solvent. These data are shown in Fig. 3 for two shear rates. The appearance of a phase transition is quite obvious.

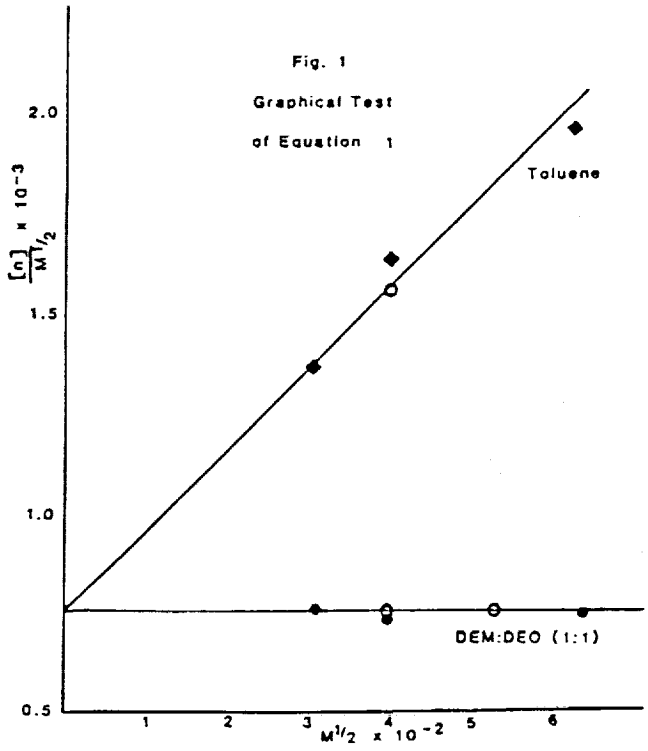
Fig. 1
Graphical Test
of Equation 1
Toluene
DEM:DEO (1:1)
$\frac{[\eta]}{M^{1/2}} \times 10^{-3}$
$M^{1/2} \times 10^{-2}$
2.0
1.5
1.0
0.5
1
2
3
4
5
6

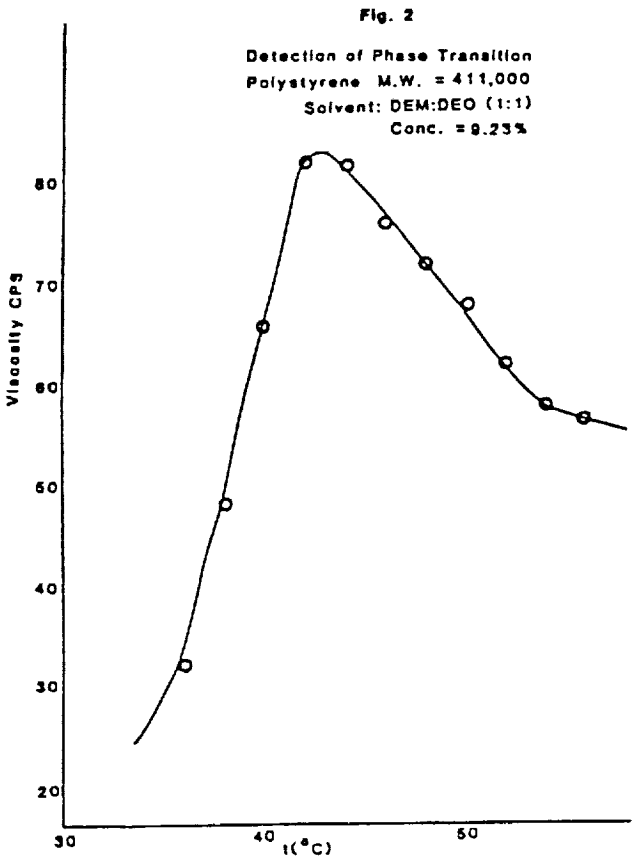
Fig. 2
Detection of Phase Transition
Polystyrene M.W. = 411,000
Solvent: DEM:DEO (1:1)
Conc. = 9.23%
Viscosity CPS
t(°C)
80
70
60
50
40
30
20
30
40
50

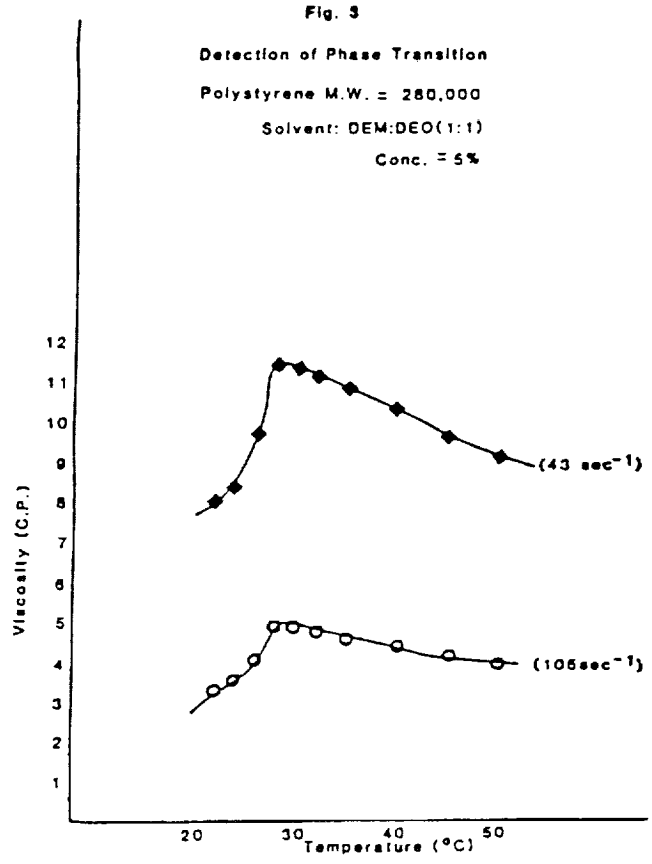
Fig. 3
Detection of Phase Transition
Polystyrene M.W. = 280,000
Solvent: DEM:DEO(1:1)
Conc. = 5%
Viscosity (C.P.)
Temperature (°C)
(43 sec^{-1})
(105sec^{-1})
12
11
10
9
8
7
6
5
4
3
2
1
20
30
40
50

The results present a phenomenon that is quite an interesting example of the interrelationship of hydrodynamic and thermodynamic effects. The behavior of a polymer solution near the upper critical solution temperature is usually given by the Flory-Huggins equation for two-components.

$$\Delta G_m = (RT)(n_1 \ln(v_1) + n_2 \ln(v_2) + \chi n_1 v_2) \qquad (2)$$

where n_i is the number of moles of component i, v_i is the volume fraction of component i, and χ is an empirical free energy interaction parameter. To this static free energy expression should be added a stored free energy term G^S, so that the free energy of mixing during flow could be given as:

$$\Delta G^1_m = \Delta G_m + G^S \qquad (3)$$

An estimate of G^S is

$$G^S = J_e P^1_{12} \qquad (4)$$

were J_e is the equilibrium compliance and P^1_{12} is the shear stress. Initial calculations with the limited amount of data available, cast some doubt on the fact that the stored free energy would be reduced by the formation of two phases. Another approach suggests that the free energy of mixing difference calculated from the cloud point temperature at rest and the cloud point temperature of the following solution should be compared with the values obtained from Eq. 4. These two methods give values of the same order of magnitude and eliminate the possibility of a clear-cut decision (11). What has emerged from these studies is the need to investigate the details of the hydrodynamic instability that may be correlated with both the cloud point curves and the compliances. What also should be taken into account for microgravity atmosphere is the interfacial free energy of formation for the two phase system. This has not been done but may be an important contribution to the interfacial energy in the current situation.

In summary, it can be reported that these preliminary results provide a sufficient basis for a further study of the rheometric determination of phase transitions and kinetics. Two approaches can be recommended: The first would be to extend the work of Berg and Moldover (12) analyzing the viscosity in terms of a reduced temperature. This would be a means of evaluating the critical exponent for the process and compare the results with binary systems. The second approach is much more involved but may provide the quantitative data needed to determine polymer-polymer interaction. In this laser light scattering, classical and/or dynamic, would be used to follow the phase separation as a function of the shear stress. From the Zimm plots, in the ternary θ-system, it should be possible to evaluate interaction parameters, radii of gyration and molecular weights. This would constitute an ideal-ideal system in which the system, if isopycnic, would have minimum gravitational effects as well as minimum polymer-solvent interactions.

REFERENCES

1) Polymer Preprints, Div. Polymer Sci., In A.C.S. Vol. 28; No. 2, p.XXVIII-XXXII, 1987.

2) Schichtel, T.E. and Binder, K., Macromol., 20, 1671-81, 1987.

3) Flory, P.J., "Principles of Polymer Chemistry", Cornell Univ. Press, 1953, p.529.

4) Bauer, B.J. and Fetters, L.J., Rubber Chem. and Tech., 51, 406-436, 1987.

5) Roovers, J.E., Polymer, 16, 827-832, 1975.

6) Orofino, T.A. and Mickey, J.W., Jr., J. Chem. Phys., 38, 2512-2520, 1963.

7) Snyder, H.L. et al., Macromol., 16, 757-762, 1983.

8) Hashimoto, T. et al., J. Chem. Phys., 85, 6118-6128, 1986.

9) Silberberg, A. and Kuhn, W., Nature, 17, 450-451, 1952.

10) Silberberg, A. and Kuhn, W., J. Poly. Sci., 13, 21-42, 1954.

11) VerStrate, G. and Philippoff, W., Poly. Lett. Ed., 12, 267-275, 1974.

12) Berg, R.F. and Moldover, M.R., J. Chem. Phys., 89, 3694-3704, 1988.

13) Fox, T.G. and Flory, P.J., J. Polym. Sci., 14, 315, 1954.

14) Cerny, L.C., et al., J. Appl. Polym. Sci., 12, 581-591, 1968.

15) Lin, O.C.C., Macromol., 3, 80, 1970.

16) Abe, M. and Fujita, H., J. Phys. Chem., 69, 3263-3267, 1965.

17) Stockmayer, W.H. and Fixman, M., J. Poly. Sci. C, 1, 137, 1963.

PROTEIN CRYSTAL GROWTH IN MICROGRAVITY

William M. Rosenblum* and Lawrence J. DeLucas†
University of Alabama in Birmingham
Birmingham, Alabama

and

William W. Wilson
Department of Chemistry
Mississippi State University
Mississippi State, Mississippi

INTRODUCTION

Protein crystallography is a powerful technique used to determine the 3-dimensional structures of biological macromolecules. The structural results from protein crystallography are important for understanding structure/function relationships of nucleic acids and proteins, and for elucidating the mechanisms by which enzymes, receptors, hormones, etc. function in biological systems. Recently, these crystallographic studies have become of considerable interest to the pharmaceutical, biotechnology and chemical industries, as promising tools in drug design, protein engineering, and other biological applications. Within the pharmaceutical industry, for example, protein structure information can be helpful in the development of novel drugs.

Compounds can be designed that selectively bind to specific sites within target proteins, thereby inhibiting or altering their activity (1-5). A number of

*Department of Physiological Optics and Optometry.
†Center for Macromolecular Crystallography.

major pharmaceutical companies have now established protein crystallography groups to pursue this approach of rational drug design.

An equally promising application of protein crystallography involves protein engineering (6-14). Molecular biologists use the detailed structural information to identify areas of interest within the protein, which they subsequently alter via site-directed mutagenesis. It is believed that this approach will prove to be of tremendous practical value for the design of modified enzymes, and for the development of proteins that have carefully engineered physical and biological properties. Applications of site-directed mutagenesis are expected to increase, and several protein crystallography groups in academic institutions and in biotechnology oriented companies are expanding their programs to exploit the potential of this technology.

An additional application of protein crystallography involves the design of synthetic vaccines (15-18). Recent studies have indicated that effective vaccines might be designed using synthetic peptides which mimic protein sequences found on surfaces of target proteins. The three-dimensional structure information provided by protein crystallography can be utilized to identify important structural features for peptide design.

The majority of the experimental procedures involved in protein structural analysis have become much less formidable. However, most protein crystallographers would single out protein crystal growth as the remaining major bottleneck of the field. Most macromolecules are extremely difficult to crystallize and many otherwise exciting and promising projects have terminated at the crystal growth stage. Proteins and other biological macromolecules often yield small microcrystals readily, but it can then take

several years of trial-and-error experimentation before crystals can be grown that are suitable for a complete structural analysis.

There is evidence that larger and higher quality crystals can be grown in space, under microgravity conditions. Fundamental studies of crystal growth in microgravity have been of great interest (19) from the very beginning of the space program. The major motivation behind these studies is the expectation that the elimination of density-dependent flow effects, which occur during crystal growth on earth, may beneficially alter the crystal growth process. Since gravity also produces sedimentation effects that may interfere with the uniform growth of crystals, there has been additional motivation for space studies of materials that crystallize from solution.

As early as the Apollo program, crystal growth experiments in microgravity were performed using various inorganic and organic materials. These studies have continued into the Spacelab program and, although still in a preliminary stage, have indicated that microgravity can improve crystal homogeneity and decrease the number of defects in crystals (20-25). Since protein crystals are stabilized by relatively weak interactions, they might be especially affected by fluctuations in the growth environment, including those caused by sedimentation or convection in gravitational fields. Recently a number of laboratories around the world have begun investigating the effects of gravity on protein crystal growth. Littke and John (21) reported the first space experiments, which involved the growth of lysozyme and β-galactosidase crystals on Spacelab I. Their preliminary studies indicated that space-grown protein crystals are considerably larger than crystals of these proteins obtained under the experimental conditions on earth. In an effort to further investigate the potential of microgravity for protein crystal growth, crystallographers from

the University of Alabama at Birmingham, along with scientists from the University of Alabama in Huntsville and the George C. Marshall Space Flight Center, initiated a comprehensive research program to study protein crystal growth. More than forty Co-Investigators from a number of academic, industrial and government laboratories are now involved in this project, which is directed at fundamental ground-based and space investigations of protein crystal growth. The space experiments have involved prototype hardware development and crystal growth on five different shuttle flights.

HARDWARE DEVELOPMENT

Although several different techniques are used to grow protein crystals (26), our initial hardware designs concentrate on the vapor diffusion method. This procedure typically involves the slow precipitation of protein in droplets of solution by vapor pressure equilibration against a solution containing a higher concentration of the precipitating agent. This method was chosen for several reasons:

1) Most protein crystallography laboratories have extensive experience with this method and a large percentage of the protein crystals described in recent publications have been obtained using this technique.
2) This technique is particularly amenable to crystallization experiments involving small quantities of proteins. This feature is attractive since many of the proteins of interest are available in only milligram amounts.
3) In a microgravity environment, relatively large stable droplets of the protein solutions can be formed with minimal surface contacts, thereby decreasing possible nucleation sites and eliminating the extensive wall effects that generally accompany crystallization experiments on earth.

Figure 1 shows the principle behind the design of the apparatus developed for protein crystal growth by vapor diffusion techniques. Each experiment takes place within a sealed chamber that has a volume of approximately 2 cm^3 with clear plastic windows for visual and photographic monitoring of crystal growth. The back chamber windows are covered with a polarizer to enhance photography of the crystals growing within the droplets. Prior to activation of the experiment, the protein solutions are contained within syringes, which are stoppered during launch and landing. Growth is activated by withdrawing the stopper and extruding the protein solution onto the syringe tip using screw-operated pistons. The protein droplet equilibrates with a wicking material saturated with an equilibration reservoir. After the crystallization experiment is complete, the protein solution containing the crystals is withdrawn back into the syringe and the stopper is reinserted on the tip. One entire unit contains twenty-four crystal growth chambers (Figure 2) and occupies 17 x 5 x 1/2 inches of space. The apparatus is easily stored in a number of different locations within the middeck area of the space shuttle.

The first stage of the shuttle experiments emphasized hardware development. For these initial experiments, it was felt that the hardware should be as simple as possible; should not require power; should occupy minimal space; should be self-contained; should permit easy photography of the crystallizing solutions; and should be designed for operation by crew members unskilled in protein crystal growth techniques. It was felt that this might facilitate frequent flight opportunities that could be used to test a variety of hardware modifications to optimize the final design. This prototype hardware was expected to be useful for testing concepts and developing basic techniques for protein crystal growth in space. However, it was clear that it would be of limited value for performing systematic experiments in protein

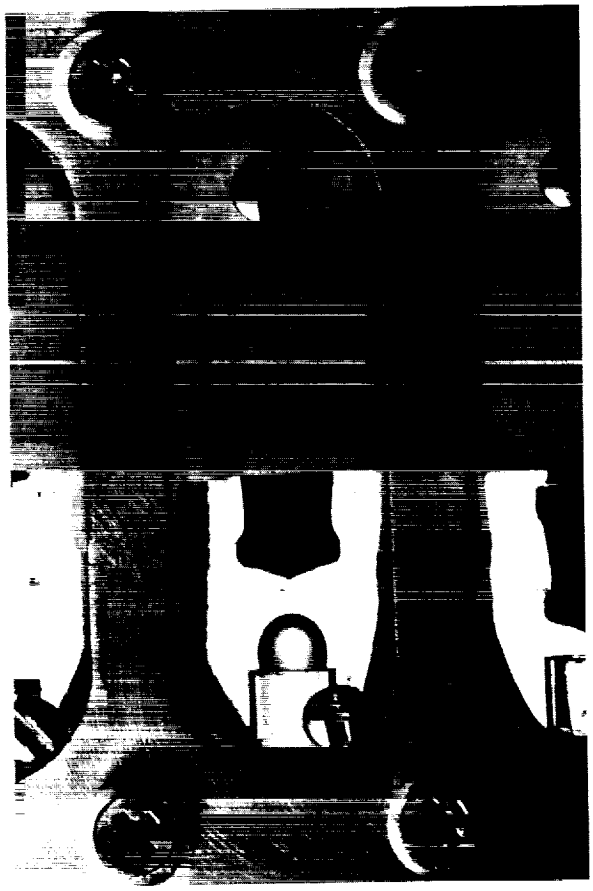

Figure 1.- Vapor diffusion crystal growth technique. The bottom screw in the window is removed to add reservoir solution and the top screw hole is used as a vent. The O-ring plunger that is used to stopper the sample syringe is protruding from the wicking material.

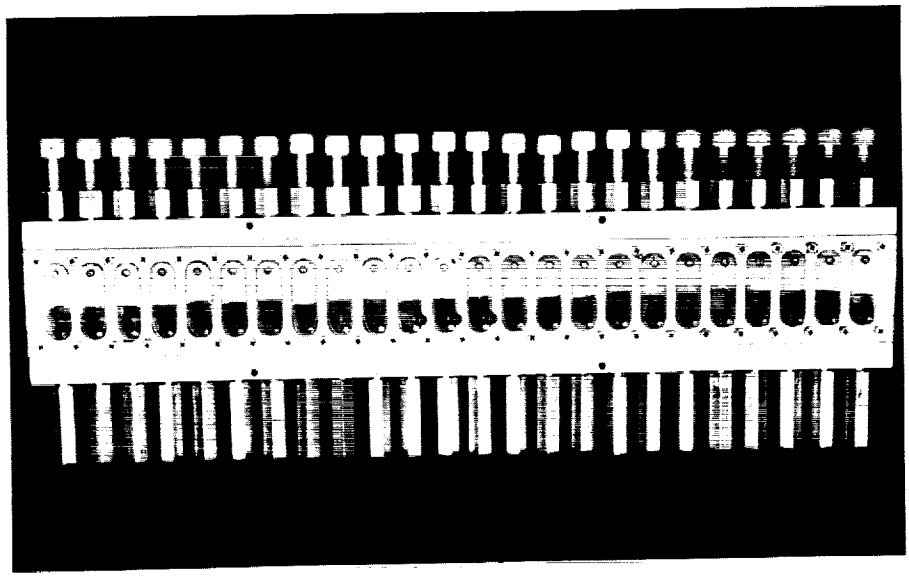

Figure 2.- Vapor diffusion crystal growth hardware. One complete unit consists of 24 syringes and opposing plungers.

crystal growth, since relatively few samples could be included and important variables such as temperature could not be controlled.

The preliminary experiments were performed on four shuttle flights (STS-51D in April 1985, STS-51F in July 1985, STS-61B in November 1985, and STS-61C on January 1986). The experiments were performed in the middeck area of the shuttle using small amounts of space available in the lockers that occupy one wall. The general procedure was: (1) to store the hardware within a locker at launch; (2) remove it from the locker to activate the experiments; (3) either store it back in the locker during flight or attach it to the wall of the middeck where it could be examined periodically; (4) deactivate the experiments toward the end of the shuttle mission; and (5) restore the apparatus in a locker prior to landing.

RESULTS

The shuttle experiments were particularly useful for optimizing the major variables in vapor diffusion crystal growth. For example, it was learned that equilibration rates are significantly slower under microgravity conditions, presumably because of suppressed convection effects. As a result, the vapor equilibration chambers have been designed to accelerate these equilibration rates by increasing the surface area of the wick containing the reservoir solution, and by decreasing the distance of the wick from the protein drop. In addition, a reliable technique for seeding the droplets of protein solutions within the vapor diffusion apparatus has been developed, and has been used to grow crystals of human C-reactive protein. It is difficult to draw firm conclusions from the crystallization results thus far since important parameters, such as temperature, have not been controlled. However, our

results have been encouraging. On flight STS-51D, a lysozyme crystal was grown from an 80 µl droplet. Only one crystal grew within the drop and it was 1.6 x 1.2 x 1.2 mm in size (Figure 3). The quality of this crystal was assessed via X-ray methods and was found to be equal to the best observed for earth-grown crystals of lysozyme. We have been unable to grow a crystal this large on earth under identical conditions. Furthermore, it is interesting that all of the control experiments performed on earth have produced several lysozyme crystals within each protein drop, as opposed to the single crystal that was obtained in the microgravity experiment.

Shuttle flight, STS-61C, contained a total of 48 vapor diffusion crystal growth experiments using 6 different proteins (lysozyme, human serum

Figure 3.- Lysozyme crystal grown on shuttle flight STS-51D. A single crystal is attached to a polypropylene flared-tip syringe.

albumin, human C-reactive protein, bacterial purine nucleoside phosphorylase, canavalin and concanavalin B). Even though the mission was prematurely shortened, high quality crystals were obtained for each of the proteins tested except lysozyme. In addition, photographic records of the crystallization solutions in the vapor diffusion apparatus were obtained while in orbit. Figure 4 shows three of the photographs that were obtained on the shuttle. These

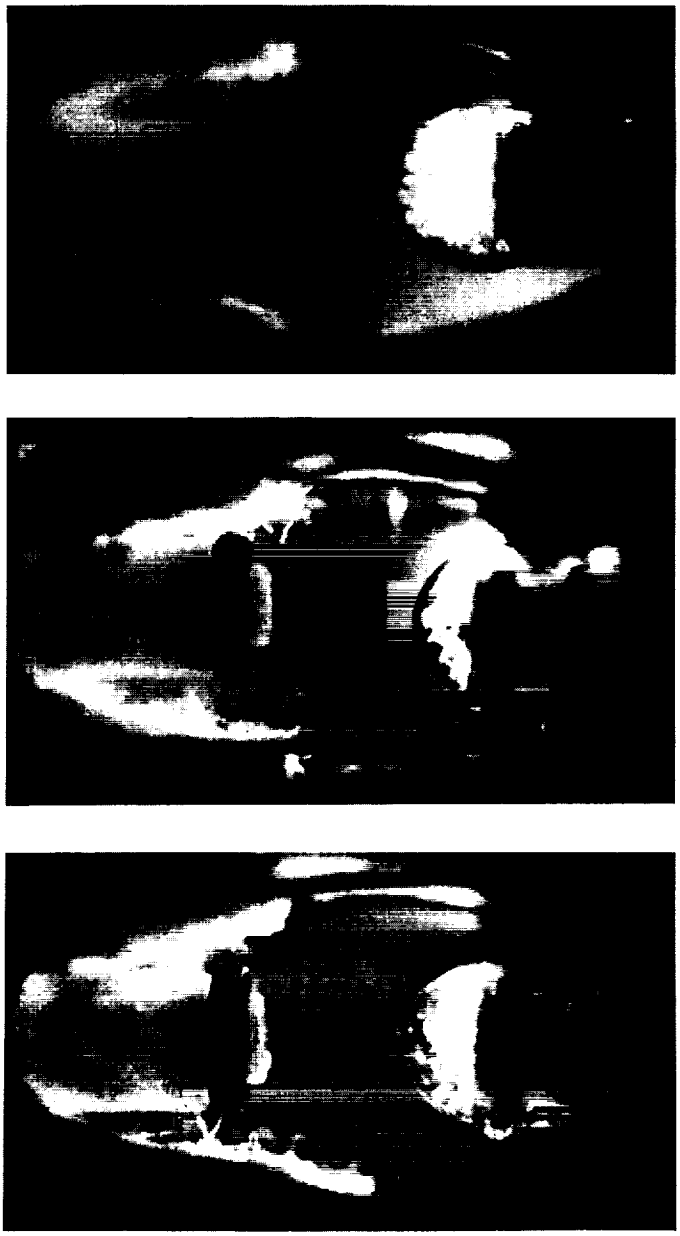

Figure 4.- Photographs of crystals grown while in orbit on shuttle flight STS-61C using the hanging-drop method: (A) Canavalin; (B) Concanavalin B; and (C) Lysozyme.

photographs and others indicate that crystal nucleation sometimes occurred on the glass syringe tips (for example, concanavalin B (Figure 4B)) and lysozyme (Figure 3) and also within the solutions away from the tips (for example canavalin (Figure 4A)). Figures 5 a, b, c, and d show photographs of some of the space-grown crystals taken within 72 hours after the shuttle returned to earth.

It appears that the elimination of density-driven sedimentation can affect crystal morphology. For example, canavalin crystals grew dispersed through the droplets in space (Figure 4A), which resulted in uniform morphologies for nearly all of the canavalin crystals (Figure 5B). Canavalin crystals grown by the identical method on earth generally form as fused aggregates at the bottom of the droplets because the crystals are more dense than the surrounding solution (Figure 6).

In the case of human C-reactive protein, an entirely new crystal form which had not previously been identified in ground-based crystal growth experiments, was obtained from the shuttle experiments. The space group for the new crystal form is $P4_222$, and it diffracts to an appreciably higher resolution than the original crystal form. The new crystal form was subsequently obtained in ground-based experiments using the shuttle hardware, so it may be influenced by altered equilibration rates or other experimental conditions that are hardware dependent. Further experiments are needed to determine how microgravity affects the distribution of these two crystal forms of human C-reactive protein.

For the most recent shuttle flight (STS-26), several important modifications were made.

(A)

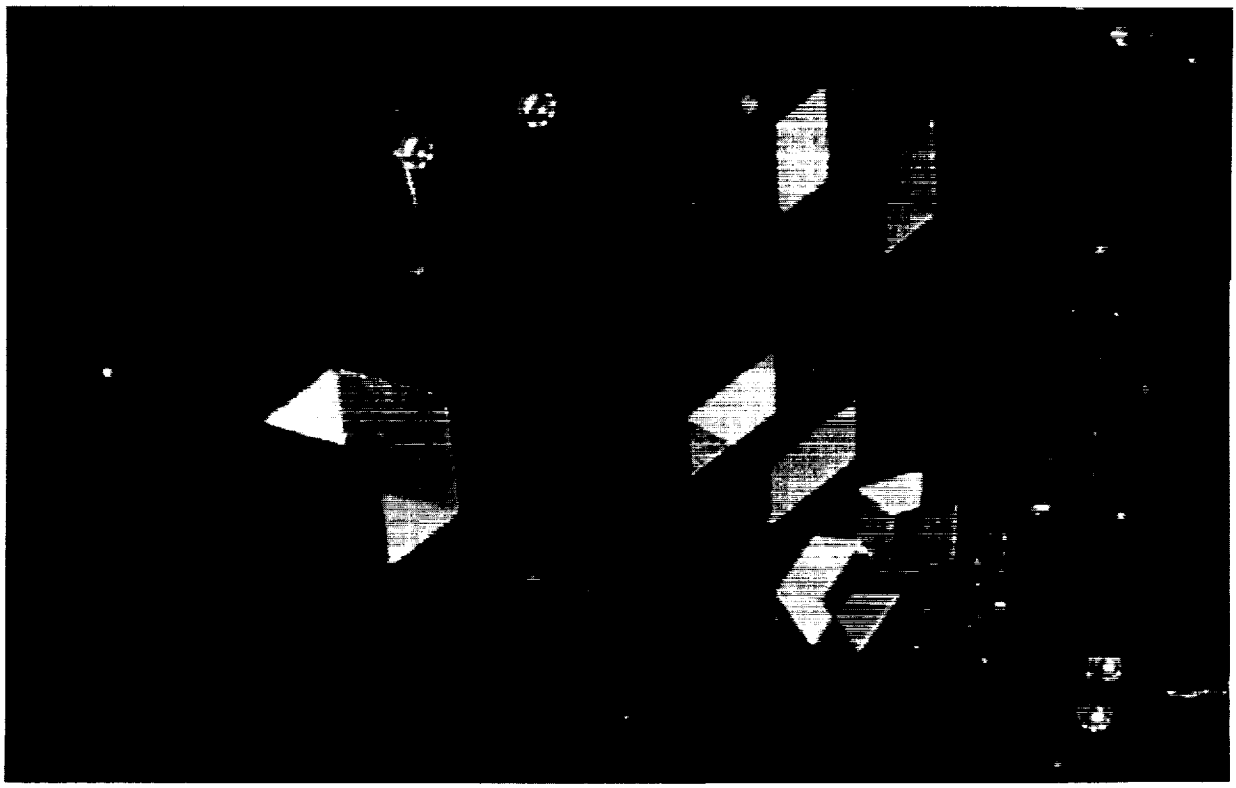

(B)

Figure 5.- Crystals grown on shuttle flight STS-61C: (A) Bacterial Purine Nucleoside Phosphorylase; and (B) Canavalin

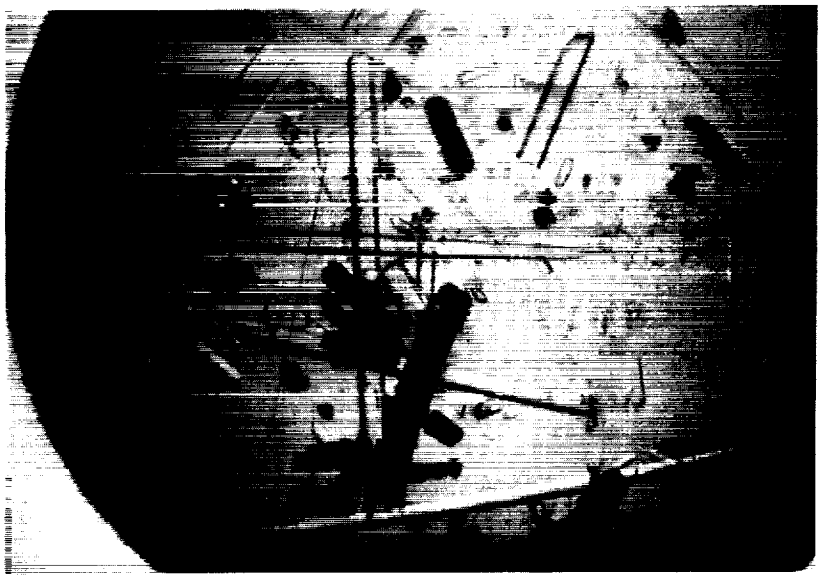

(C)

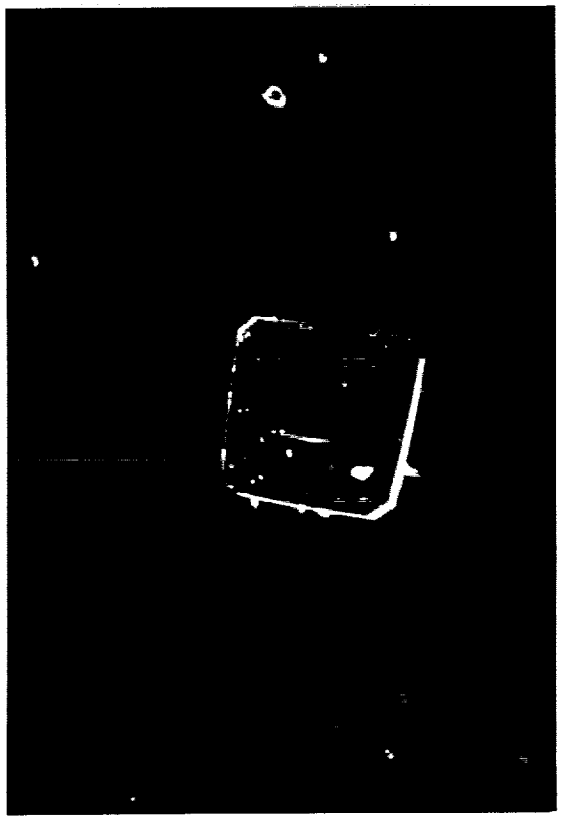

(D)

Figure 5.-(Cont.) Crystals grown on shuttle flight STS-61C: (C) Concanavalin B; and (D) Human Serum Albumin.

1) The unit is contained with a refrigerator/incubator module (RIM), so that rigorous (± 0.2° C) temperature control will exist for the duration of the crystal growth experiment (except during activation, deactivation and photography).

2) The syringe and plug mechanism has been semi-automated by linking each syringe or plug to a ganging mechanism that permits sets of syringes and plungers to be activated simultaneously.

3) A new double barrel syringe design has been incorporated to avoid premature precipitation that may result from premixing the solutions prior to launch.

Figure 6.- Earth-grown crystals of canavalin

Eleven different protein samples were flown on STS-26, utilizing a total of 60 vapor diffusion growth chambers. Crystals were obtained for all eleven proteins with nine proteins producing crystals suitable for X-ray diffraction analysis. The detailed analysis of these crystals is still in progress and therefore cannot be reported at this time.

FUTURE HARDWARE DESIGN

There are several additional modifications that are needed for the phase II/phase III generation of protein crystal growth experiments. The ganging mechanisms for plug withdrawal and drop deployment should be fully automated so that the RIM does not have to be opened during these procedures. This will avoid induced temperature changes due to exposure of the experiment to the middeck environment.

A second modification concerns monitoring the crystal growth process while in orbit. Past experiments used simple photography and visual observation. The present hardware configuration necessitates removing the RIM door and withdrawing each vapor diffusion tray (on a sliding mechanism) outside the RIM. Once fully withdrawn, individual photographs are taken of the chambers using a 35 mm Nikon camera with back lighting and a polarizing lens. Although this system has been useful for initial experiments concerned with prototype hardware development, they are inadequate for the advanced crystal growth experiments planned. A system is needed which provides detailed records of the processes that are occurring within the crystallization solutions without exposing the experiments to the middeck environment.

Scientists from the Center for Macromolecular Crystallography, the U.A.B. Physiological Optics Department, the U.A.B. Physics Department and the Mississippi State University Departments of Chemistry and Physics have

pursued in tandem, several alternative approaches for monitoring protein crystal growth experiments. The following will describe some of the data obtained from initial experiments utilizing video monitoring of protein crystals via light microscopy and laser light scattering.

The investigation of various optical monitoring techniques for protein crystal growth has been utilized so that crystal formation could be observed from the nucleation stage and throughout the growth phase.

Initial work in this lab utilized Fraunhoffer (27-29) diffraction to demonstrate the growth of lysozyme crystals. Using a He-Ne laser, it was shown that spherical scatterers produced a diffraction pattern from which one could determine particle sizes via measurement of the diffraction ring diameters. In the crystal growth cell, it was possible to demonstrate crystal size and shape and to follow changes in these parameters with time. Using an image capture system consisting of a CCD camera and an image analysis system for an IBM PC, it was possible to capture the diffraction patterns projected into the CCD and enhance the important elements of the pattern by edge enhancement and line scan software.

From this early work, it was realized that other modes of examination were needed. In particular, it was necessary to develop a system with capabilities of detecting crystals at the incipient or nucleation stage; and a microscopic system to look at larger crystals. Thus, a combined system which used laser scattering and a white light microscope was developed. A 90° laser scattering pattern was recorded on a time lapse video recorder and captured on the image processing system. The image analysis system can be used to detect the presence of small lysozyme crystals before they can be detected with

the white light microscope. The laser scattered light was shown to be present when the captured image was processed by use of digital filtering and pixel enhancement.

In conjunction with Dr. Jim Martin, who is the Director of the Medical Laser Lab, Physics Department, U.A.B. and Dr. Bill Wilson, Mississippi State University, there is an ongoing program using the Brookhaven Dynamic Scattering System. The following reviews the basis for these experiments and some preliminary results obtained.

The crystallization process is initiated by the formation of ordered aggregates of the protein molecules called nuclei (as opposed to disordered aggregates which lead to amorphous precipitation of the protein). The energetics of the nucleation stage of crystallization have been presented by Feher and Kam (30). Two distinct stages of nucleation were suggested. First, a quasi-equlibrium state between protein monomers and j-mers is established. Light scattering measurements of the average molecular size of the mixture at this stage allowed the estimation of the equilibrium constants. The measurements of Kam et al. (31) were recently repeated (by W. W. Wilson at Mississippi State University) on lysozyme and a comparison of the results is shown in Figure 7. The average diameter of the equilibrium mixture compared to that of the lysozyme monomer as determined by dynamic laser scattering is shown as a function of lysozyme concentration. There is a gradual but distinct increase in average particle size as the total lysozyme concentration is increased, consistent with a shift of the equilibrium towards the j-mers state. One interesting feature of this stage of the nucleation is that it appears to be a stationary state, that is, the formation of j-mers occurs very quickly after mixing of the solution components but the free energy change does not favor

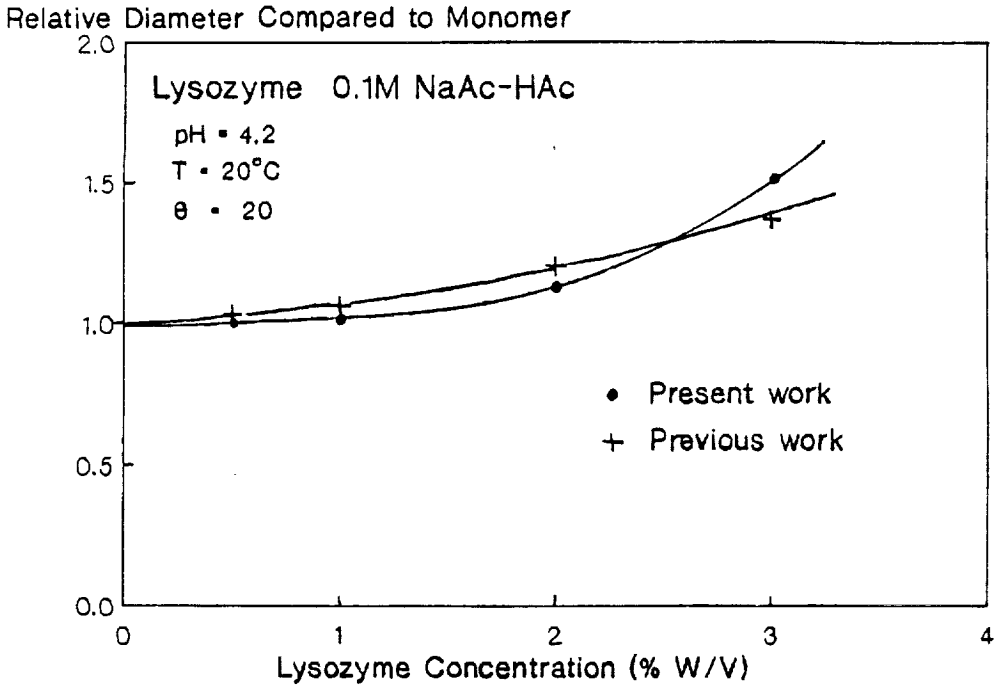

Figure 7.- Relative diameter of lysozyme aggregates in the quasi-equilibrium states.

a continuous growth process. It was observed that solutions prepared under the proper conditions for the quasi-equilibrium state are essentially static with regard to particle size changes over periods of several hours.

A second stage in nucleation is referred to as post-nucleation growth. The decrease in free energy accompanying the growth of nuclei is sufficiently large to sustain a dynamic process in which the average particle size steadily and markedly increases with time. Dynamic laser scattering (32-33) was used to monitor the average particle size during the growth stage. Figure 8 shows the results for a 3.0% (w/v) solution of lysozyme in a 0.1 M NaAc buffer with 5.0% (w/v) NaCl as precipitating agent. The experimental variable in this case was solution temperature. At the beginning of the experiment, the temperature was adjusted (30° C) so that the lysozyme solution was in the quasi-equilibrium state. The average particle size was about 5 nm under these conditions. The solution temperature was then slowly lowered so that the transition to post-

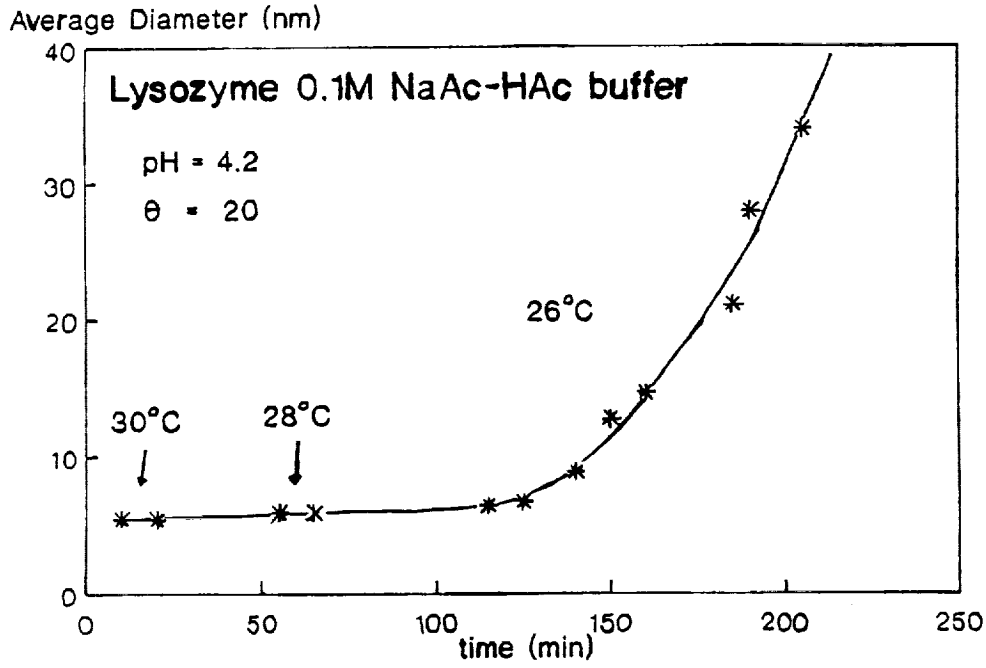

Figure 8.- Average particle size vs time for post-nucleation growth.

nucleation was carefully approached. The average particle size was monitored as the solution cooled. At 26° C, the growth continued with average particle size reaching supra-micron size. The rate of the nucleation growth is strongly temperature dependent. For example, if the final solution temperature is reduced to 24° C, the average particle size reaches the upper limit for reliable measurements by dynamic laser scattering ($\approx 3\mu$) in about 30 minutes.

An important result found from these experiments is that the post-nucleation growth can be slowed or even reversed by raising the temperature. This result suggests that temperature regulation may be an effective method for controlling the nucleation process, especially if the growth can be detected in its early stages. It is with regard to the onset of post-nucleation growth that we propose to use laser scattering intensity measurements as a monitor for the dynamic process. Figure 8 demonstrates that scattered intensity fluctuation measurements (dynamic scattering) can be used to detect this stage of crystal growth. It was also found that a measurement of the average scattered total

intensity follows closely the growth in particle size. Figure 9 shows the relative intensity, in terms of photo-counts per second, of the light scattered as a function of time for exactly the same experiment as shown in Figure 8. It is clear from Figure 7 that the post-nucleation growth stage can just as surely be identified by intensity measurements as by actual particle sizing measurements.

Although these experiments have been invaluable in determining the proper hardware design, knowledge of the true benefits of microgravity for protein crystal growth must await future shuttle flights. Future hardware design will allow monitoring and/or dynamic control of temperature, protein concentration, ionic strength, pH, and precipitating agent concentration. This is essential for accurate comparisons to be made between the space and the earth-grown crystals.

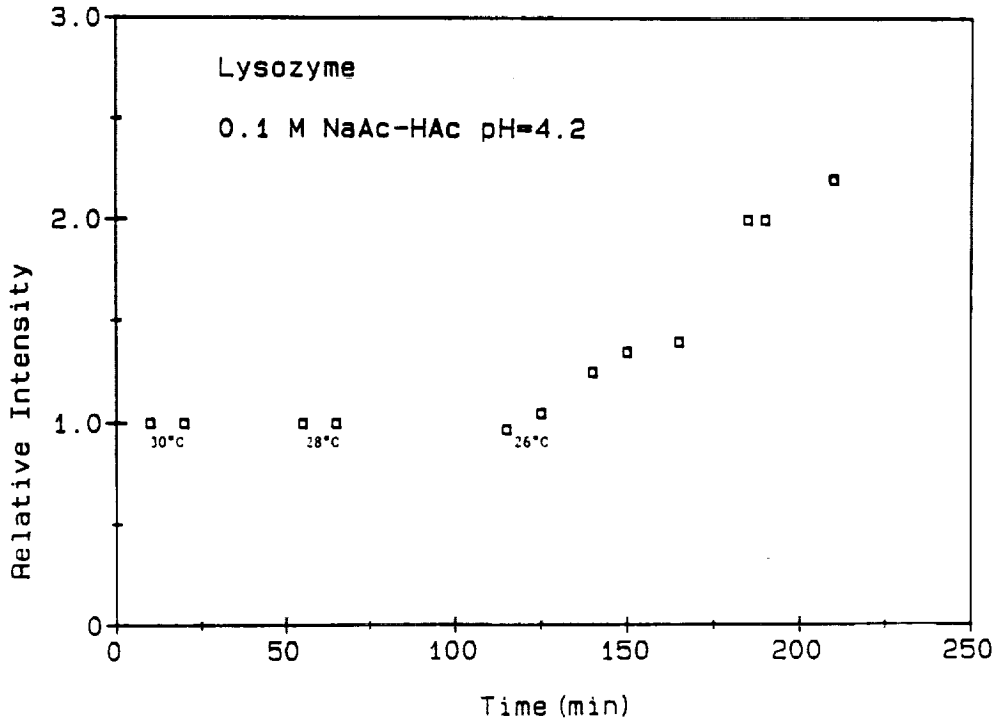

Figure 9.- Photodetector count rate vs time for post-nucleation growth.

CONCLUSIONS

Major advances have been made in several of the experimental aspects of protein crystallography, leaving protein crystallization as one of the few remaining bottlenecks. As a result, it has become important that we better understand the science of protein crystal growth and that we develop improved methods for protein crystallization. Preliminary experiments with both small molecules and proteins indicate that microgravity may beneficially affect crystal growth. For this reason, a series of protein crystal growth experiments using the space shuttle has been initiated. The preliminary space experiments have been used to evolve prototype hardware that will form the basis for a more advanced system that can be used to evaluate effects of gravity on protein crystal growth.

Various optical techniques are being utilized to monitor the crystal growth process from the incipient or nucleation stage and throughout the growth phase. The eventual goal of these studies is to develop a system which utilizes optical monitoring for dynamic control of the crystallization process.

REFERENCES

1. Blundell, T., Sibanda, B. L., and Pearl, L. Nature, Vol. 304, 1983, pp. 273-275.

2. Goddard, W. Science, Vol. 227, 1985, pp. 917-923.

3. Goodford, P. J. J. Med. Chem., Vol. 27, 1984, pp. 555-564.

4. Johanson, R. A. and Henkin, J. J. Biol. Chem., Vol. 260, 1985, pp. 1465-1474.

5. Wilson, T. and Klausner, A. Biotechnology, June, 1984, pp. 511-519.

6. Craik, C. S., Largman, C., Fletcher, T., Roczniak, S., Barr, P. J., Fletterick, R. and Rutter, W. J. Science, Vol. 1228, 1985, pp. 291-296.

7. Estell, D. A., Graycar, T. P., and Wells, J. A. Jour. Biol. Chem., Vol. 260, 1985, pp. 6518-6521.

8. Fersht, A. R., Shi, J.-P., Knill-Jones, J., Lowe, D. M., Wilkinson, A. J., Blow, D. M., Brick, P., Carter, P., Waye, M. M. Y., and Winter, G. Nature, Vol. 314, 1985, pp. 235-238.

9. Galloway, J. Nature, Vol. 314, 1985, pp. 228-229.

10. Kaiser, E. T. and Lawrence, D. S. Science, Vol. 226, 1984, pp. 505.

11. Maugh, T. H. Science, Vol. 223, 1984, pp. 269-271.

12. Perry, L. J. and Wetzel, R. Science, Vol. 226, 1984, pp. 555-557.

13. Wells, T. N. C. and Fersht, A. R. Nature, Vol. 316, 1985, pp. 656-657.

14. Wharton, R. P. and Ptashne, M. Nature, 7, Vol. 316, 1985, pp. 601-605.

15. Berzofsky, J. A. Science, Vol. 229, 1985, pp. 932-940.

16. Marx, J. L. Science, Vol. 226, 1984, pp. 819-821.

17. Westhof, E., Altschuh, D., Moras, D., Bloomer, A. C., Mondragon, A., Klug, A., and Van Regnemortel, M. H. V. Nature, Vol. 311, 1984, pp. 123-126.

18. Williams, R. J. P. and Moore, G. R. Trends Biochem. Sci., Vol. 10, 1985, pp. 96-97

19. Rindone, G. E. (editor), Materials Research Society Symposia Proceedings, Vol. 9, North-Holland, New York (1982).

20. Littke, W. and John C. Science, Vol. 225, 1984, p. 203-204.

21. Littke, W. and John C. Z. Flugwiss Weltraumfrosch, Vol. 6, 1982, p. 325.

22. Wiedemeier, H. Presented at TA-2 Preliminary Science NASA Headquarters (March, 1984).

23. Wilcox, W. R. J. Crystal Growth, Vol. 65, 1983, pp. 133-142.

24. Wilcox, W. R. J. Crystal Growth, Vol. 65, 1983, pp. 133-142.

25. Yee, J. F., Lin, M. C., Sarma, K., and Wilcox, W. R. J. Crystal Growth, Vol. 30, 1985, pp. 185-192.

26. McPherson, A., Academic Press, Orlando, Florida, Vol. 114, 1985, pp. 112-119.

27. Kerker, M. The Scattering of Light and Other Electromagentic Radiation, Academic Press, 1969.

28. Van DeHulot, H. C. Light Scattering by Small Particles, John Wiley and Sons, 1957.

29. Hecht, E. and Zajac, A. Optics, Addison-Wesley Publishing Company, 1974.

30. Feher, G. and Kam, A. Methods in Enzymology, 114, 77 (1985).

31. Kam, A., Shore, H. B. and Feher, G. J. Mol. Biol., 123, 539 (1978).

32. Pecora, R. Dynamic Light Scattering: Applications of Photon Correlation Spectroscopy, Plenum Press, 1985.

33. Chu, B. Laser Light Scattering, Academic Press, 1974.

National Aeronautics and
Space Administration

Lewis Research Center
Cleveland, Ohio
44135

NASA

Reply to Attn of

5110

24 August 88

Dear Workshop Participant:

Re: Discussion Session

An important chance for you to influence the design of NASA's reduced gravity laser light scattering instrument arises during the workshop discussion session September 8. Some seed questions and partial sketches of proposed laser light scattering instruments follow. We offer them as an outline for the discussion session and hope that they will serve as a springboard for your ideas. Our main goal will be to incorporate your ideas and suggestions. We appreciate your expertise and time and thank you in advance for helping us develop this important instrument.

Our chief task will be that of meeting the experimenters' needs. During the workshop you will hear papers asserting the necessity for reduced gravity:

(1) to study large fragile structures unobtainable in a normal gravitational environment,

(2) to answer basic science questions which can be addressed only by reducing convection currents and sedimentation effects,

(3) to quantitatively monitor existing and upcoming experiments where particle size (30 angstroms to 3 microns) and polydispersity are a concern.

Much of the workshop will concentrate on how to meet these needs technically. We hope to incorporate these ideas along with your own into an instrument we can test initially aboard NASA's Learjet or KC-135.

Cordially,

William Meyer
Workshop Organizer

Strawman Laser Light Scattering Instrument

I. Sample Holder

We are proposing two different sample handling systems, bulk and flow. The choice of which system to use is dictated by the experiments to be performed. The rest of the light-scattering apparatus is usable with either sample holding configuration.

We are considering two design concepts for a bulk system. The first contains the samples in cylindrical scintillation vials (see fig. 1). When more than one sample is used, samples are changed via a carousel. No index matching fluid is used; the consequent flare problem is alleviated by the high spatial resolution optics described in part III.

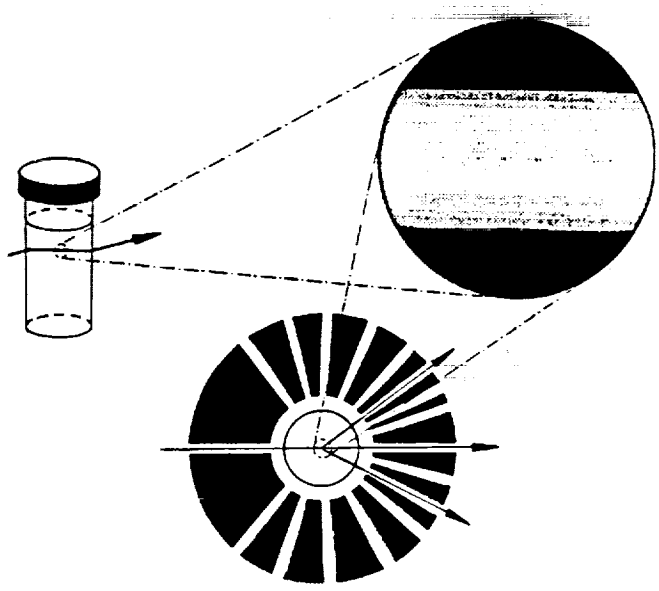

Collimated detector layout of DAWN B; field-of-view in upper right; typical cuvette in upper left

fig. 1

The second sample-holder design is a thick glass cylinder containing a horizontal bore with optical flats at each end. This design avoids flare problems by moving the flare from the sample holder outside the path of the detectors.

One proposed flow system is that used in Wyatt Technology's DAWN (see Fig. 2).

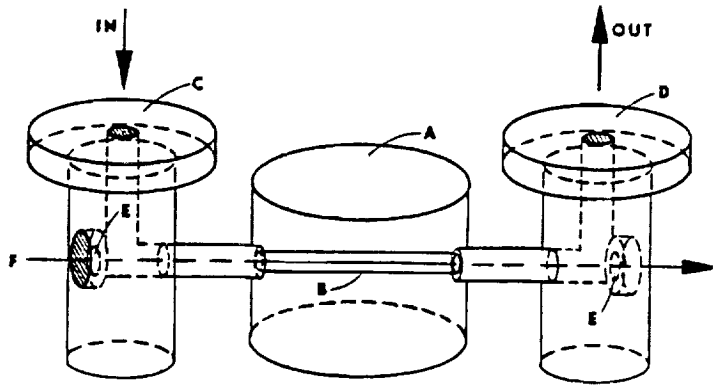

Flow cell schematics

fig. 2

II. Laser Source

We intend to use a focused laser diode which emits light at 680 nm [780 nm] to illuminate the sample. R.G.W. Brown's work has shown that these diodes make fine sources for laser light scattering. They are rugged, small, and power-efficient. Also, by mounting them directly to the aluminum block containing the sample and its associated receiving optics, we eliminate vibration-induced movement of the laser beam within the sample. In this way, the same part of the sample is always illuminated.

The small size of the solid-state lasers allows us to easily juxtapose two or more of them. This has two advantages. First, we achieve reliability through redundancy. Should one of the lasers fail, we can still continue the experiment. Second, we effectively increase the number of scattering angles. For the bulk system with the scintillation vials, we use two lasers of the same frequency. By changing the angle of the incoming beam, we effectively double the number of scattering angles. If the second laser is attached to a stepper motor, a continuous range of scattering angles is accessible.

Changing the angle of the incident beam is not possible with the flow system or its equivalent horizontal-bore bulk system (see fig. 2). Here we can change the scattering vector by changing the frequency of the incoming beam (e.g. 550 vs. 680 nm).

III. Receiving Optics

It is not feasible to use an index matching fluid when performing a laser light scattering experiment in a microgravity environment. We therefore must devise other ways to minimize flare light.

In the flow system or the horizontal-bore bulk system, flare is minimized by the cell shape itself (see fig. 2).

For the scintillation vial bulk system, we can reduce flare via an optical masking system which will be addressed in Cheung's paper and which appears in figure 3.

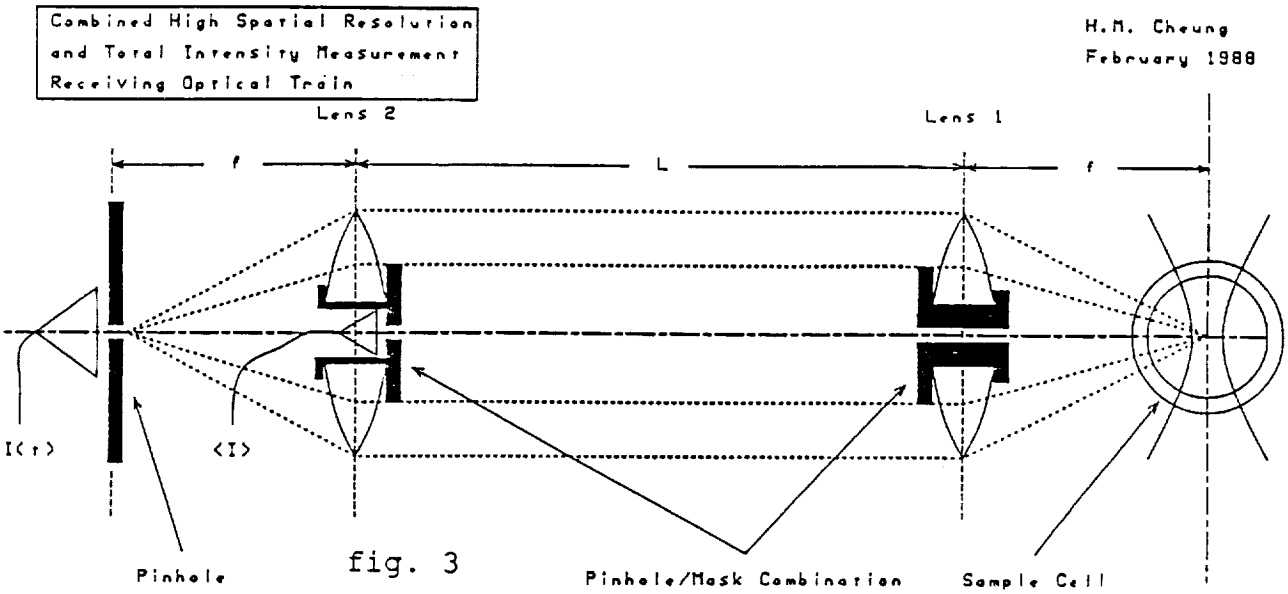

fig. 3

This system blocks flare with a mask whose size depends upon the scattering vector.

IV. Detectors

We plan to have several detectors placed at fixed angles in an aluminum housing (see fig. 4)

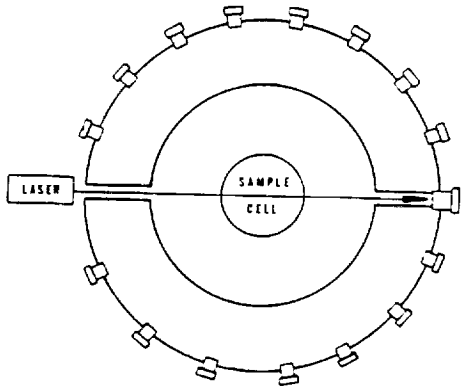

fig. 4

which will contain the sample cell, laser(s) and receiving optics, and detectors. Avalanche photodiodes (APDs) are proposed as detectors. This alleviates the concerns about high voltage, temperature drift, and power consumption associated with photomultiplier tubes. APDs are biased at about 250 volts. By changing the bias, one can switch from

single photon counting to total intensity measurements. APDs consume about one watt of power, most of which goes to the built-in Peltier cooler used to lower the dark count. The dark count is constant and around 100 counts/sec at -20 C. The high speeds necessary to do single photon counting are achieved by built in active quenching circuits. We are proposing a count rate of up to 20 MHz (10 MHz at lower angles) with a dead time as low as 20 to 100 nanoseconds. This will depend upon the experimenters needs as outlined at the workshop.

V. Correlators

A number of single card correlators for light scattering measurements are under development. They are all capable of being reduced to one or two chips and allow the storage of real time correlograms. At least two of these correlators will be described during the workshop presentations.

We envision placing one correlator at each detection angle, provided the number of detection angles is small (five or fewer). This again gives us reliability through redundancy. If many fixed detection angles are shown to be needed, each correlator will be multiplexed between several angles.

The number of correlator channels needed and the channel spacing are matters for debate. We are considering the use of exponential channel spacing and its concomitant

need for 8 to 16 channels. This stands in stark contrast to the conventional linear channel spacing with hundreds of channels.

We hope to create efficient algorithms for the extraction of particle size distributions using the work of Cumins and Staples (Langmuir 1987,3, 1109-1113). The improved algorithms are to be based on Maximum Likelihood methods (see Numerical Recipes, Press, et. al.). This work by Edwards will be made available to the builder of NASA's reduced gravity laser light scattering instrument.

We would like to thank Wyatt Technology and Mike Cheung for their kind permission to use the figures in the preceding pages.

Operational Questions

1. Should we measure polydispersity?
   Range, resolution?

2. Should we measure polarization?

3. Should this be a bulk-sample instrument, flow, or both?
   This is partially dictated by whether the experimenter wants the samples back.

4. Should we add a refractometer for index of refraction measurements in-situ?

5. Should we consider the use of telescience? How much control should experimenters have from the ground?

6. Do we need classical and dynamic light scattering in one instrument?

7. How will samples be prepared?
   How will they be contained and stored?
   Who will keep track of sample history?

8. Temperature control - Probably Peltier coolers
   Shall all samples be kept at the same temperature?
   Equilibration times?
   Temperature range?
   Accuracy
   Stability (plus or minus 0.1 or 0.0001 degrees C)

9. Should we provide an accelerometer?
   Do we need acceleration data in real time?

Discussion Outline:

I. Samples

II. LLS Hardware

III. Operating Parameters

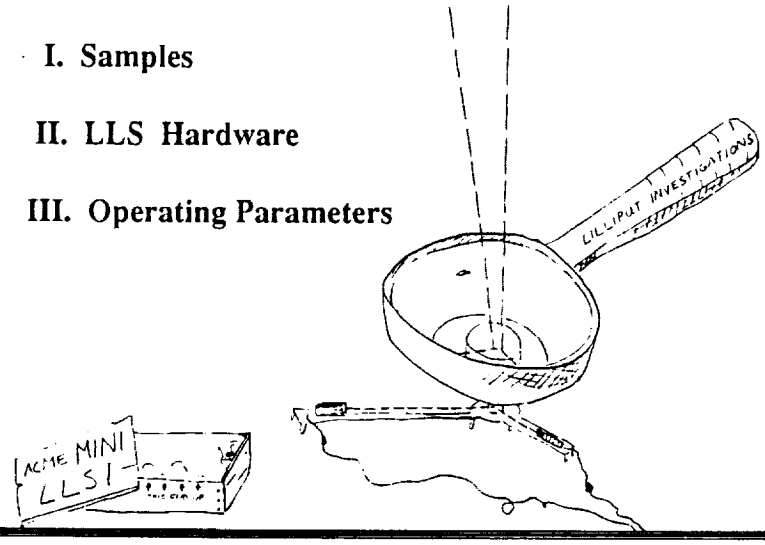

Samples:

Containment
- Bulk or flow sample cells?
- Method of experiment activation?

History
- Storage (thermal requirements, etc.)
- Acceleration Data

LLS Hardware:

Laser Source
- number of lasers?
- laser wavelength?
- solid state?

Detectors
- dark count (less than 100 counts/sec)?
- count rate (greater than 10 MHz)?
- dead time (less than 100 nsec)?
- number of angles and their spacing?
- APDs?

LLS Hardware (cont.):

Receiving Optics

Correlators
- real time?
- number of correlators?
- number of channels in correlator?
- channel spacing (exponential)?
- single chip?
- maximum likelihood?

Operating Parameters:

Polarization Measurement

In Situ Refractometer

Telescience
- Experiment control from ground?
- Amount of information needed?

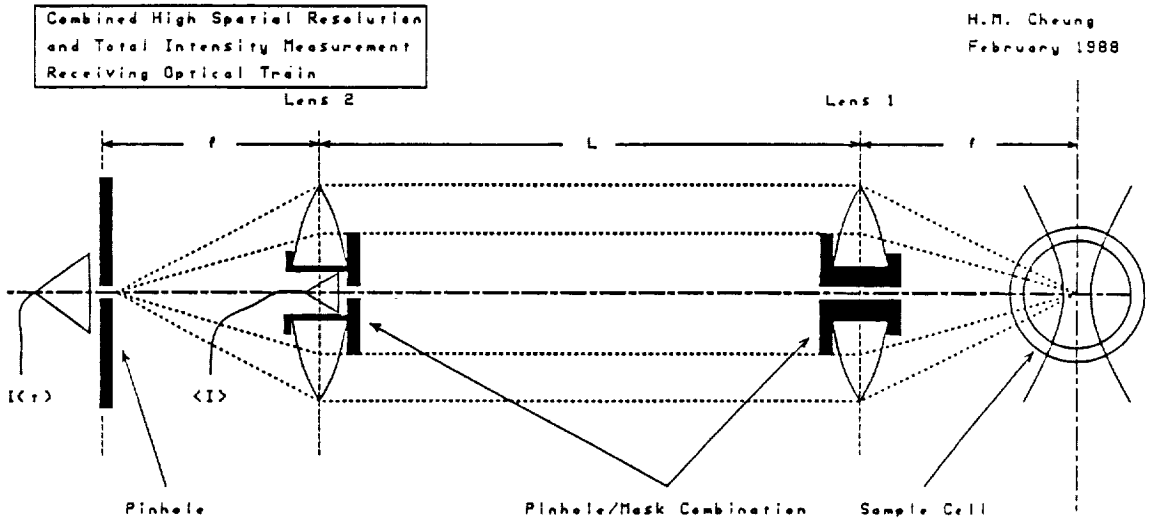

TRANSCRIPT OF PROCEEDINGS

NASA LASER LIGHT SCATTERING WORKSHOP

DISCUSSION GROUP 1

SHERATON HOPKINS HOTEL

CLEVELAND, OHIO

THURSDAY, SEPTEMBER 8, 1988

3:00 P.M.

PARTICIPANTS:

Thomas Glasgow, Leader

Robert Edwards, Co-leader

Robert Brown

David Cannell

Larry DeLucas

Harbans Dhadwal

Robert Gammon

Andrus Lattik

Samuel McManus

David Nicoli

Jeff Shaumeyer

Jim Sutter

Bob Thompson

Walther Tscharnuter

David Weitz

T. GLASGOW:

Thank you for your participation. It has been a very interesting session to me. It has been a very interesting year, as we have had this activity going on for about a year now. Bill Meyer has been with us just a year and a week, and he has been running the laser light scattering program for us here at Lewis. He has been consistently enthused and pleased with the degree of help and cooperation he has gotten from all the investigators and builders of hardware around the country and around the world.

Next week Bill is going to write a letter to headquarters in which he will give the executive summary of this entire conference. In a few pages he must summarize the value of what we have done today, and include suggestions for what NASA headquarters should do with this program in the upcoming year and years. He will have to make recommendations as to hardware development, selection of experiments, and the interrelation between the selected experiments and the hardware to be developed. When we originally wrote the proposal for this work, before Bill joined us, we really didn't know how many wonderful things were going on around the world in this business; how many people were working on the technological advances that we would need to make a space flight apparatus. In the discussions over the last day and a half here we have been very pleased to see that a number of things are ready, examples being Robert Brown's very nicely made compact solid state instruments. And is there anything stopping us from taking one of those and putting it on-orbit? They look just the right size to put next to the protein crystal growth experiment.

Robert Brown's
Compact LLS Instruments

R. BROWN:

I think they can be made smaller, by maybe a third or more. What I didn't mention yesterday is that they are entirely solid state; there are no moving parts. Everything is bonded within with UV-curable glue. They are shim adjusted and bolted down, so you can throw them around or whatever you want to do with them, and they will stay in alignment. They are rock solid, and I think that's important.

T. GLASGOW:

Did I hear you mention that the licenses for this technology are being purchased by a single company?

R. BROWN:

The position is as follows. This is United Kingdom Ministry of Defense research from a bona fide research group with no commercial affiliations. The Ministry of Defense has set up a company for technology transfer from research into industry -- and that is not necessarily UK industry, although UK industry has to be approached first. That company has been assigned the rights to license patents and to return a royalty to the Ministry of Defense or the Treasury over the next few years. And the situation at the present time is that the company has licensed some of these ideas to eight different companies, which are now running their own development programs.

T. GLASGOW:

Are those licenses typically exclusive licenses?

R. BROWN:

There are exclusive licenses in specified market areas. For example, if one were to go into the biotechnological field, an area might be gel permeation chromatography.

D. NICOLI:

Could you be a little more specific as to what is licensable?

R. BROWN:

We hold patents on the designs of two of the anemometers, on the APD circuitry, and on part of the laser Doppler systems that I haven't told you about yet. There are also patents on our software, a log-log correlator. Anything we have done with correlation has a patent slapped around it. I think we now hold six patents in different correlation techniques. And then, besides the patents, we have written up and sold registered designs on such things as the thermal design of the APD housings, the mechanical designs, and the tolerances. Another issue of course is know-how. Companies don't run with these devices without access to expert consultants. As a government employee, I am not available as a private consultant, but what can be done and indeed has been done by some of these companies is to buy some of my time for a feasibility consulting study through the Ministry of Defense on a legitimate consultancy arrangement. So, there are all sorts of ways of interacting with industry.

Future Workshops

T. GLASGOW:

To help Bill Meyer compose his letter next week, one of my goals today is to get some suggestions for our future workshops, because this is an ongoing program. I would like to give a little attention right now to what you might like to see in a future workshop. As one idea, it has been suggested that we have a future workshop in conjunction with a technical meeting such as an American Chemical Society Meeting, or with one of the other user groups, if there is a good user group.

D. CANNELL:

I have some comments along those lines. In these meetings I have the impression from talking to other people who, like myself, have done light scattering for many years, that there is no strong driving need within the light scattering community to do particular experiments in space. The exception to this probably involves critical phenomena, which present real problems down here, but which are being addressed as a specially-designed experiment. Despite this perception, what I saw here, especially in the talk on crystallization of biological samples of proteins, is that you begin to develop applications of microgravity: you find out, either by chance or by good insight, that something works very well in orbit. Then I can see that you might very well wish to have a powerful analytical tool such as light scattering available to pursue these other interests. But only if it is possible to use it to monitor in real time what is happening in the unimaginable experiments to be done in the future. That seems to me to be the most legitimate rationale for light scattering in a microgravity environment. It seems to me that if you are going to have another workshop, it probably ought to focus on what the requirements for an optical LLS instrument reasonably might be. Without such a set of requirements and a set of tests to see whether the instrument meets the specified requirements, you can't have a nice competitive bidding process or have vendors able to competitively try to meet your needs. Nor do I think that you have the adequate guidance for any in-house development efforts. So my idea is that the first priority is to straighten out what everyone really wants to do, and also to realize that the wider light scattering community is not driving hard for low-g experiments. On the other hand, many of us believe LLS is a very powerful, very general technique that is extremely useful in a huge variety of situations, and it very well could be extremely useful in helping to monitor many of the experiments of interest in the microgravity environment.

T. GLASGOW:

In essence, part of what you said reflects some of the original goals for space station, where we were to have a complete, almost generic, laboratory available so that experiments could be performed no matter what the interest. We may not be able to address the LLS development efforts in your suggested manner, and we probably will have to go with much more direct experiments that are driving specific needs. However, I do like your suggestion.

D. NICOLI:

To second what David was saying as to the emphasis being on what you want to do up there and what that implies about the requirements for instrumentation, some of the applications discussed today make it obvious that you could end up wanting a number of very different designs; perhaps three or four. Suppose, for instance, as extremes, you think about David Weitz's very large structures and about tiny particles that are in the Rayleigh region as they polymerize or crystallize. That could dictate the use of two very different instruments, rather than trying to squeeze all of the different requirements into one all-purpose instrument. Nobody in the light scattering community that I know of would allow his life to be tied up for two or three years thinking about developing the best generic. He would like to make a contribution, but quickly -- to decide what we want to do, try it, build a prototype, and then get on with it, rather than optimizing.

R. BROWN:

In responding to that, David just pointed out to me the basis of the whole of our own program, which is that we only wanted to do the design once. Ours is a modular concept. While all of our instruments are the same design, they are configured slightly differently. So if you wanted to change your experiment, you might just drop in new optics when you have done the basic design once in a modular fashion.

D. NICOLI:

Are you saying "A good detector is a good detector" ?

R. BROWN:

Yes, our code name for this has been "Optical Lego." All summer, we have figuratively been trying to make Lego bricks that we can then plug together as we wish to.

H. DHADWAL:

I agree with both things that have been said. In my experience, you need to have an experiment defined before you can design an optimum instrument. The work that Robert Brown has done in terms of the modular design deals with the semiconductor laser and also the avalanche photodiode detector. But I think you will agree with me that the optical part in Robert's setup is not right now a replaceable module.

R. BROWN:

The optics is indeed a module.

H. DHADWAL:

A module perhaps, but the thing is that the instrument, if it is going to be sent up, must take care of a lot of different things. We have seen a need for multiple angles, static light scattering or statistical scattering, dynamic light scattering measurements, and refractive index measurements. So all of those things have to be decided on before we can design a generic instrument. And that instrument can be designed right now. We have the technology, as we have seen, for a single-card correlator, solid state lasers, and solid-state detectors. So as far as laser light scattering in space is concerned, really one has to have the application. What does NASA really want to do in space as far as light scattering is concerned?

J. SHAUMEYER:

The people in the light scattering community all have their specialized devices, and none of them is ever going to be satisfied with a single device. But if you change the perspective to look instead at the people who could benefit from using light scattering as a tool, and this as one tool among many, then perhaps something more productive would come out of this. That would be a baseline that I would consider in planning a future workshop: LLS for people that we saw today who could use it effectively and who aren't necessarily trying to make the high precision type of measurements that require very

specialized instruments. One more observation that I want to make about the whole meeting is that the simpler you can keep an LLS device, the more likely it is to satisfy some people.

T. GLASGOW:

There have been comments that NASA has in the past built some complex apparatus that cost a lot of money, took an incredible length of time, and satisfied no one. I think we have learned our lesson about that approach.

L. DeLUCAS:

The points that have been made are exactly what I mentioned last night. I look at Robert Brown's device and I get excited because it is small, but for our particular purposes, I know we are going to want special modifications. We want a device that is a multi optical monitoring system: one that monitors at the nucleation point with laser light scattering, but that uses other monitoring techniques, perhaps diffractive and video monitoring, to follow the growth of protein crystals from the incipient stage through to their full growth. Then we might want to couple this device, using software, to a system that will control the growth process while it is happening. Now, a device like that is going to have to be dedicated solely to protein crystal growth. I can't see us going up and adapting some generic device for that. But we would like the basic technology to be developed, so that we can come to people like you and buy what is necessary, either expertise or the instrument itself, and then modify the device for our own purposes.

R. BROWN:

That is the whole point. What I've shown is only a technological development; a first try at some research prototypes in each class of laser light scattering instrument that satisfies our requirements. There must be a million other ways of doing this.

L. DeLUCAS:

Sure. The only thing is, that last night when we talked in a group I got the feeling that the main idea was to build one device that will suit a lot of different disciplines. I just don't think that can be done.

R. BROWN:

Can I answer that? Our devices weigh 125 grams, and if they were made of plastic rather than metal they might weigh just a few grams. They are considerably smaller than 16 cubic inches, or whatever the figure was that Bill Meyer was talking about. There is no reason why one couldn't make a number of small instruments and put them all in the same allotted volume. Perhaps a sample could even move around from instrument to instrument. The game is entirely open, isn't it?

D. CANNELL:

I think I agree with Robert. I can imagine, for example, very easily pulling out one of the solid state laser modules, focusing on your hanging droplet, pulling out one of the lens/fiber combinations with the avalanche photodiode attached to it, looking in at 90 degrees or whatever angle you like, and getting an immediate signal when nucleation has started. No development at all would be needed; just plug it in and there it is. That's the right modular approach. I think it offers an incredible flexibility that can meet these unknown unimaginable future needs of experimenters in the microgravity environment.

L. DeLUCAS:

Our problem is that we are not going to have one hanging droplet per mission, we are going to have 300 to 600. And we are going to want each of them monitored via a computer at specific times throughout a two week mission on the shuttle or a three month mission on the space station. Now, it seems to me that we need to build a system that is specific for that scenario.

D. CANNELL:

These devices are so small and low cost that I can even imagine using 300 lasers and 300 fibers and 300 photodiodes if you want to.

R. BROWN:

Even better, there are ways of multiplexing optical fibers in a solid state fashion using nonlinear crystals where you can get a fanout. You can bring a beam across and launch into a different fiber so that you can have 40, 50 fibers going into one laser and again have 40 or 50 fibers returning down to one detector. There are all sorts of games that we haven't played yet.

S. McMANUS:

It seems to me that what would serve us best at this point would be to have us deliver some wish list ideas to Bill or to some other group and let them respond to us about how feasible they seem. Also, we should determine some requirements for our experiments and learn whether they can be met.

T. GLASGOW:

I might mention that in this workshop, we intentionally minimized the number of investigators invited, and also limited the areas represented to aggregation and polymer science, roughly speaking. We avoided making this workshop all-inclusive because we felt that if we were describing the specifics of a lot of experiments, we wouldn't have time to address the technology questions that we wanted to pursue first. However, I do agree with Professor McManus that we have to get input from a number of experimenters on what they are going to need.

S. McMANUS:

It seems to me there is no problem with our needs being met by the technology available around the world. Our requirements are going to be somewhat similar to Larry's and somewhat different, but I think we can solve that problem by using duplicate instruments. These devices shouldn't be that expensive compared to the price of an experiment.

T. GLASGOW:

In your view, then, the device would simply be an add-on to the experiment. The experiment would be built as originally planned, and you would essentially use laser light scattering as an additional data source for your experiment.

S. McMANUS:

That's the way I would see it.

Space Experiments using LLS

H. DHADWAL:

This is sensible if laser light scattering is what you want to do. But I think everybody in the field will agree that there are not many space applications right now; we don't have any need that mandates doing laser light scattering in space. Now, the talks on protein crystal growth are very interesting, but from what I've heard today, I don't know if laser light scattering would be very useful for that. Other techniques, such as video cameras and diffraction, may work better than photon correlation spectroscopy. Given that, if NASA still wants to do laser light scattering in space, it must look hard to see what it wants to accomplish with LLS. I cannot overemphasize how important it is to find the applications.

D. NICOLI:

One approach might be for NASA to decide through workshops and other means which experiments it wanted to orbit, then give those experimenters synopses of the technical capabilities of the people who are most knowledgeable about hardware. Then the onus would be on each experimental group to make its own contacts and to optimize the hardware design for its own experiments. NASA's overview would be to identify any commonality. This way every experiment would have its own equipment and own approach but would be encouraged to use the best technology available.

T. GLASGOW:

One of the goals of the Advanced Technology Development program is to try to centralize the overview, with the hopes that one area will then provide the technology for numerous experiments and cut down the cost of the discrete development of these things.

D. NICOLI:

But, Tom, isn't there this famous experience about committees getting a camel in designing a horse? Small research groups wouldn't have that problem.

T. GLASGOW:

Yes. We can get camels.

D. NICOLI:

It seems that there are lot a bases to cover. Why worry that you've covered all of them? Isn't sufficiency rather than optimization the goal in a lot of cases? If the real interest is in the experiments and their science payoff, then why not say that each experiment has its own solution, and I don't particularly care if the equipment can cover all the bases?

T. GLASGOW:

The experiments will inevitably be the driver. If the experiments don't drive the equipment, we won't have the equipment.

D. NICOLI:

If we have equipment in search of experiments it's not good. But when an experimenter thinks about what he wants to do and how to make his measurements, shouldn't the onus be on the experimenter? What do you think about that, Dave?

D. WEITZ:

I think if you put too much of the onus on the experimenter, there won't be many experiments. To be honest with you, I can think of experiments that I might do in space. Maybe I'd continue some of the work I'm doing now. But when I'm asked to put a lot of effort into designing and building hardware, then I have to ask if it is really worth my effort. If I ask, "What is the science that really needs to be done in space?," it's pretty minimal right now. But if there were a well-designed laser light scattering facility in space, and if using it didn't take up a whole lot of my time, i.e. if I could just drop some samples in and run tests really quickly, then I'd be willing to spend some time thinking about imaginative things that I might do in space.

T. GLASGOW:

I'd like to ask for a little clarification. Are you suggesting that there should be a number of experimental facilities available, that are easy for experimenters to use, and that the availability of those facilities might indeed encourage people to come up with ideas to use them?

D. WEITZ:

Right, particularly if they're well designed, relatively flexible facilities. For example, if the low-g facility were just a basic light scattering apparatus that I could mimic in my laboratory, I might find that I could duplicate an existing ground-based experiment to see what I could really learn in a low-g environment. Otherwise, I would limit myself to what I could do in my laboratory, without spending five years setting up a space experiment and going through space worthiness, qualifications, etc. With a facility, I could presumably design experiments around what was available, and that would serve as a means of generating new ideas that ultimately would require different equipment, different facilities. So I'm viewing this as a way of generating really novel and new ideas rather than letting currently existing ideas drive me. Maybe this is one way to inspire people to think of new microgravity experiments.

J. SHAUMEYER:

Inspiring people to think of things is terrific. However, I would love to avoid this facility syndrome that we've had to fight off several times. That is, some instrument is built or designed which costs a great deal of money and doesn't work very well, and so it's instantly turned into a facility. Then NASA insists that everyone should use it, but finds nobody will touch it because it was too specific to a particular job. By contrast, Robert Brown may be on to something with his modular approach. And, as Dave Nicoli said, maybe the emphasis should not be on a facility or a general-purpose instrument, but on making technology easily available for each experimenter to put together a unique package. Having modular technology well in hand, but simple enough that it can be restructured easily, would save a lot of effort over developing a complete instrument from the ground up for a specific job. This does indeed put some of the onus on the experimenter, but that's nothing new. You have to match some hardware to an experiment sooner or later in order to make your measurements.

R. EDWARDS:

There's an old proverb that says if all you have is a hammer, everything tends to look like a nail; and I've noticed that we are not immune to that syndrome. If somebody comes into my lab and says he has a measurement to make, I'm going to tell him about laser light scattering, even though there are other perfectly good methods. I actually did this; the other day I did a measurement for somebody using a fancy-dancy $150,000 laser anemometer. I could have done it with a pitot tube, except that I couldn't find one. The point is, there really are other technologies besides laser light scattering to measure things that people in polymer science or biotechnology want to know. And so I'm getting a little worried about limiting our approach too much by looking for laser light scattering experiments, or by setting up a laser light scattering facility and seeing what kind of moths it attracts. It strikes me that maybe the conversation ought to go back to where it started, which was whether it makes sense to go to meetings like ACS meetings to solicit ideas for space experiments. Also, we could hold other workshops such as this one, where NASA gets a little better handle on what's available in the outside world.

B. THOMPSON:

I'm kind of an outsider here; my area of expertise is fluids and combustion and structures. But one of my assignments now has to do with developing facilities on space station. One of our problems in trying to develop these facilities is coming up with a good set of reference experiments from which we can at least set some envelopes for this facility. If you're thinking about putting light scattering experiments in a facility on space station, we're developing those facilities now. The hardware will be cut within the next few years. So it's imperative that the experiments that are going to be using light scattering be defined as well as they can at this point. I see a lot of polymer scientists and chemists and others around here who might use the space facility. I'm not sure whether a facility like ours is applicable to these disciplines, but I think it could have some possibilities. I would suggest to this assembly that you go out and discuss with others, maybe in combustion or other disciplines, what you'd like to do. That's certainly going to help you eventually get the right hardware up there on space station.

D. WEITZ:

As someone who would consider using that space facility, I'd like to reiterate my point about ease of use. As a scientist, you always have several things that are competing for your attention. Therefore, you can't afford to invest a lot of effort in order to use a facility. This has got to be something that's recognized. The ability to use the facility has to be a relatively straightforward thing. The process must be so standard that you can readily proceed the way you normally do with experiments: i.e. try a lot of different things to sort out what you ultimately want to do.

B. THOMPSON:

We're discussing here what can be done in space. I don't think you're going to have the luxury of plentiful on-orbit time on Space Station, and certainly not on Spacelab. Therefore, you can't just try a lot of things. In-space projects are going to have to be well thought out experiments, with a good solid rationale for conducting them. We have done or proposed many experiments on fluids and combustion, and have found that if you don't have good, solid justification for doing that science in space, the experiment just doesn't happen.

T. GLASGOW:

The joint cooperative agreement that we signed to develop an LLS apparatus for space flight charges us with investigating whether there is reason to take such an instrument into space. We have to do that carefully, over a period of time, to find out whether there are investigators who absolutely need this capability. Their need has to be so great that they are willing to go through the agony, pain, and years of preparation to make it possible. Yet, in our program we should be investigating more experiments as potentials; we should be looking at so many that maybe a third or 40 percent of them fall out along the way. Instead, we've been very conservative; we've only examined a few experiments along the way.

D. NICOLI:

Is there not a parallel to what others experienced with things like the initial design of a large neutron scattering facility? At the start there must have been fairly limited thinking about precisely what to use that beam for. And think of how it operates: users travel a distance, get to be there for a short amount of neutron beam time, spend only two or three days there and so don't sleep at all, do their experiments, and then leave. There is a selection process to determine which experiments are worth doing and how much time they are going to get. And it seems to me that those projects tie up people's lives for substantial periods of time. What are the design considerations that go into that? What are the constraints on the experimenter? Now there's going to be a microgravity LLS facility; never mind that it's up in space, it's still a facility. And people have to generate excitement about doing experiments, and have to think about what that facility should contain in terms of little widgets and gadgets that will make it work. Maybe there are some parallels to neutron scattering that would help people think about this LLS facility process.

T. GLASGOW:

Jim Sutter has been working on some polymer experiments in the laboratory that anticipate using laser light scattering. Perhaps Jim, you could say a few words about any anticipated need for use of the apparatus in space.

J. SUTTER:

Sure. We need to build microgravity facilities which are sufficiently specific that we can be assured experiments performed in them will fully respond to the science questions. The scientific problem must drive the hardware development rather than having available hardware development dictate the kinds of experiments which can be contemplated. Likewise, the experimenters have the responsibility of defining research programs which have a valid need for microgravity and a clear explanation of how microgravity will influence a process. What NASA needs to do, and we're trying to do, is to provide in an innocuous environment like this workshop, an opportunity for people who do have ideas for experiments to come forward and provide the details of what needs to be done. The important thing is that if your science does have a genuine microgravity application, and you push hard enough, you can get it done. So I encourage the PI's, and Bill does and Tom does as well, to try to pull together your specific needs and talk to us.

D. WEITZ:

I guess I really don't see a need for microgravity for a lot of things. There are only one or two things that I really feel require it.

D. CANNELL:

I think, though, that there is more dreamt of than we're aware of. I don't think that if we had asked a lot of hard questions about growing protein crystals, that we would have predicted better growth in a low-g environment. We would have said, "Maybe it'll be better, maybe worse." I think that getting experience on what happens in the microgravity environment is very important for the long range development of the whole program. And I just don't think you can see ahead of time what may or may not happen. I think that's really the rationale for trying to do a lot of experiments up there. Let a lot of them be busts, who cares? You're going to learn a lot in the trying.

D. WEITZ:

All this supports my argument that you need a facility that lets people try things; that lets people dream. I perceive that there simply aren't many experiments that require microgravity to the extent that somebody would be willing to spend ten years of his life really pushing them. So the question is, do we have the luxury or the resources to dream?

L. DeLUCAS:

I'd like to say a couple of things. Number one, we don't have the luxury to quickly do experiments in microgravity. To put an experiment in space takes a tremendous effort. It takes years to get the hardware qualified, even for a simple experiment like protein crystal growth, which requires no power on the shuttle. Number two, Dave Cannell's point about not knowing in advance what will work well in microgravity is well taken. The first time we talked with our peers about doing protein crystal growth in space, we literally got laughed at. There was even an article in Science called "The Great Crystal Caper." People just did not believe there was any merit to doing it. There are many things that we just have no idea about. So we've got to give people an opportunity to explore. The problem is how to make it easy for people to do that, because nobody wants to devote ten years to one experiment that fails. The thing that gave us our chance with protein crystal growth was that a German quickly got on the shuttle with an experiment, and we then piggybacked with McDonnell-Douglas. Had we had to go through the channels that you do today, I think we might have given up in midstream, before we knew what we had. Because of the Challenger disaster, it's very difficult now to do science on the shuttle.

J. SUTTER:

We at Lewis decided not to gear our polymer phase separation program for shuttle flight. We decided to do whatever was necessary to carry out the program in the lab. So we ended up density-matching a polymer and solvent to avoid density-driven convection. There are a lot of barriers to space flight. Until the politicians in this country provide the fiscal resources to allow us to truly experiment, it's going to be a real pain. Some of us are willing to endure that.

T. GLASGOW:

We've been having a fun philosophical discussion about the difficulties of getting into space, and how much more fun it would be if the process were a lot easier -- if we could just walk in with our equipment and step on, for example. However, I would like to get back to the questions Bill left for us to discuss. I have been neglecting the questions about equipment technology, because as I looked and listened during this conference, it appeared to me that technology is being taken care of very nicely around the world. I am left, however, with a question about correlators and polydisperse samples. Can the existing technology handle polydisperse samples well? Or should we stick to monodisperse systems?

R. EDWARDS:

I think that depends on what you're looking for. If you are interested in means and second moments of histograms, that's fine. You can get a handle on that and watch it evolve with time. However, if you want to see the bumps and wiggles on the histograms, you're in for an incredibly long experiment, and even then you may not get what you're looking for. If the histogram is a very wide distribution, you can resolve some detail about it, but you cannot see the bumps and wiggles on a narrow distribution. Multiple angle scattering is an obvious improvement, but it's not magic. It is not going to resolve the bumps on a distribution that's ten percent wide.

D. CANNELL:

I agree completely, and I think this stems from a simple scientific reality. I was a graduate student in George Benedek's group in the late 60's and early 70's, and Stuart Dubin was given the job of using light scattering to see whether lysozyme denatured. After getting nowhere for a few months, Stuart sat down one day and calculated what he would see in a solution that consisted of a bimodal distribution: two types of scatterers, each of which scattered an equal amount of light, but which differed by a factor of two in their diffusion coefficient. This seemed a very generous spacing that would give him a good chance of seeing an effect. The correlation spectrum was within a percent of what you would get from the mean of the two. Stuart told George Benedek, "George, I can't do this experiment." At that time it was impossible. Nowadays you could make a stab at it with a good correlator and very careful technique, but any little systematic errors and you're dead. You just have to realize that laser light scattering is not a good way to make statements about polydisperse samples. You cannot use it to say, "There are seven big particles and three little ones and 17 medium ones in there." On the other hand, LLS is wonderful for measuring average values such as the Z average diffusion coefficient, the weight average molecular weight, and the radius of gyration very precisely.

T. GLASGOW:

Let me restate the question. If I were following a coarsening experiment, watching ripening in a liquid, and I wanted to know whether size varied with time to the inverse one third or inverse one half, or whatever, would I be able to know?

D. CANNELL:

Yes, LLS would be excellent for that.

W. TSCHARNUTER:

Our correlator [BIC] can distinguish easily between large and small polydispersity, polydispersity being defined as the second moment. It could easily detect .02 for example or .1. It can also track the change in polydispersity with time. So the correlators are very suitable for this kind of experiment. Now, there is a question on the screen there about real time number of channels in the correlator. I think for space applications, you should use a card with 12 to 16 channels and a carefully chosen channel spacing. For many applications you don't need more than that. Our single-card correlator is fully automated, so it's easy to use. And it decreases the time needed to run an experiment by a factor of 4 to 5. Finally, it is easily possible to switch from one detector to any number of correlator cards. So if you put two or three cards in there, you can make simultaneous measurements of various angles, you reduce the time required, and you have redundancy.

R. GAMMON:

Go back one step. The reason why optical techniques deserve some real emphasis for low gravity experiments is they are a delicate probe; they don't touch the sample. They don't change anything, particularly not at the intensity levels we are talking about. There probably are experimenters who don't yet use light scattering who really ought to think about it. If they have a reason to go up and investigate delicate structures, light scattering or optical techniques in general would be ideal.

T. GLASGOW:

Are there other areas of LLS technology where we should concentrate if we are funding some work? Or are the technological aspects being brought along well, and should we instead concentrate on experiment definition and ground-based experiments?

Sample Preparation

R. BROWN:

Before we define experiments as such, there is an area that hasn't been addressed at this meeting at all. We have addressed lasers, optics, detectors, correlators, and software reduction. I think we now have all the technology we need for the next decade or two. But those of us who actually work in the labs know that the Number 1 problem is the sample quality and sample handling. And if you have got a rotten sample, you get a rotten experimental result. Yet very few people are addressing the problem of how to get really pure, clean samples. What do you do with them? How do you accurately temperature stabilize them? How do you get rid of dust? Should we use heterodyne techniques? Perhaps we should go back to square one and consider heterodyning as an option because of dust problems. Anyway, if I had some money, that's where I would put some emphasis. I know how difficult it is for me to make good samples; I have been doing this a long time and I am still not very good at it.

R. GAMMON:

There is another consideration. The samples are delicate; we need to be sure that we don't bump and shake and break them while getting them into space. I remember watching a movie at the Smithsonian in which Walter Cronkite describing the wonderful advances in crystal growth, and the astronaut kicked the experiment.

Heterodyning

R. EDWARDS:

One reason why nothing was brought up about sample preparations is probably because we all felt guilty. I felt my graduate students were incompetent and yours knew what they were doing, because that can be a problem. And about heterodyning -- I spent a lot of time working with two lasers in the early days, just to be stubborn, and I discovered all kinds of interesting things. For instance, even small lasers can push particles around. In fact, if you did it right, you could vary the power between the two beams, and you could actually listen to the beam being pushed. The stronger beam pushed the particles through, and that caused a distortion in the correlogram. Since we only ran at about 30 milliwatts, I was a little surprised. Not only that, we got vibration, even though we had a "vibration-free" table. You could even detect people dropping pencils on the floor in the next room. Believe me, one beam is better.

W. TSCHARNUTER:

I have two comments, one about dust in the samples and another about heterodyning. The way our group handles dust rejection is to make numerous short correlation measurements and compare every measurement to the previous ones, for a certain total number of counts. If a given measurement exceeds the maximum allowed deviation from the previous correlation functions, then that measurement is thrown out. The deviation can be set automatically by the instrument or manually by the operator. This works, for example, with monodisperse small particles where dust is involved and the dust data are simply thrown out. We call it a dust bin in our correlator. The total correlation function, which consists supposedly of only good correlations, is now used. Heterodyning we ran into recently with our fiber optics system. It has some advantages, and it has been used recently, but the intercept is very small. As you know, it is a two or three percent intercept rather than a 60 or 70 percent intercept. There is a so-called structure function which may be a better way of evaluating data. In this structure function, you subtract the intensity at one sample time from the intensity at a second sample time, and work with the difference. You sum the squares of all the differences. The beauty of it is that the

constant level, which in heterodyning is very high by definition, is automatically subtracted off. Experimentally, it is an exponential function subtracted from a very high value, so it looks like an inverse correlation function. The new Brookhaven Instruments Corporation correlator has the ability to calculate structure functions built into the software control.

R. BROWN:

I would like to corroborate everything Walter just said. I think we should reexamine heterodyning and structure functions. Klaus Schaetzel in the other room is well known to many of us as an instigator of this, and claims it is a great advantage.

D. CANNELL:

As a small comment along those lines, I think we should keep in mind that what matters is the statistical uncertainty, the fluctuations in the baseline from channel to channel. You don't have that in the heterodyning case. It is not that having a baseline is necessarily bad, it is the uncertainty that is the problem.

Monitoring Crystal Growth

R. GAMMON:

I have a question about the protein work being done or being planned. What tools do you use now that are optical? Do you plan to fly the same tools in the future, or are you expanding your horizons?

L. DeLUCAS:

Unfortunately, because it used to take 20 years to do a structure, people didn't care why they got crystals. So no optical techniques were developed in the last 30 years. Our interest in monitoring and controlling crystal growth conditions started because of NASA involvement. What we have established beyond a doubt is that if you control the rate at which protein crystals grow, you produce higher quality crystals. Generally, the slower the rate, the higher the crystal quality. The next concern, then, is how and when to control the rate. We are now developing techniques to slow the growth rate; we have pumping systems that will do that. But in order to know when to adjust the rate, we must know when the crystals have started growing. We would like to be able to say, "We just got a nucleation point, because we've detected an oligomer of four molecules that have come together." Actually, we don't even need to know the number four, because this is a polydisperse system. All we have to know is that nucleation has started. And the only technique that I know of to see a few molecules 40 angstroms in diameter coming together is laser light scattering. Once we've detected nucleation and started controlling the growth rate, we would like to monitor the growth with the other optical techniques that Bill Rosenblum mentioned. So that's how we got involved with optical techniques in general and laser light scattering in particular.

R. GAMMON:

I would not call that laser light scattering. It's more like the dust effect that we see. Either the sample is clear, or there are motes in it. When we see motes, we know that we didn't filter the sample well enough. When you see motes, you know that nucleation has begun. Yet I understand that light scattering is a very sensitive test for that, and is therefore very valuable to you. In fact, you need just the modular tools that we have been talking about: a nice small laser, a detector, and some optics. But in substance you don't care about the correlators or any of the rest of it; you just want a signal.

L. DeLUCAS:

That's true, we don't require correlograms to carry out our program of trying to produce good crystals in microgravity. However, that information is required in order to understand how the crystal is growing and what causes defects when they occur. Several of our co-investigators are working with correlators to try to understand these processes. For instance, there is a group in Huntsville working on that.

H. DHADWAL:

I want to come back to the correlators. I think everybody would agree that the techniques of analyzing correlation functions to get precise information have been well established over the last decade. So there is not much to be gained from putting money into that area. The idea that Walter mentioned of doing repeated measurements for dust rejection is useful in case you have a dirty sample. But it's much better to eliminate the dust right at the beginning, if possible, instead of fiddling around trying to correct the measurements later on. Now heterodyning is probably a useful area to investigate. It is used in communications because it reduces the signal to noise ratio considerably. In fact, if the correlation functions have better signal to noise ratios, it may be easier to recover polydispersity information. Nobody's really done heterodyning. I've looked at backscatter anemometers, including the original fiber optical anemometers, and they are by nature heterodyne. But at all other angles measurements have always been self beating or homodyne. With optical fibers, it may be possible to investigate whether heterodyning would be a useful technique to give us better signal to noise ratio in our correlograms.

Fiber Optics

T. GLASGOW:

How about the technology of the fibers themselves? Do the fibers behave in ways that we really don't understand?

H. DHADWAL:

The only problem I've seen that might remain to be addressed is microphony. Microphony is the picking up of external vibrations of the system. For example, if the spacecraft is shaking, that might modulate your signal. In the laboratory, using monomode fibers, there is no microphony, because monomode by definition means only a single mode is transmitted. With multimode fibers there may be some problem, but that has to be investigated.

R. BROWN:

In my experience, microphony isn't a problem. We have observed modal noise in the multimode fiber system, but only under really bad vibration conditions, such as in a very noisy lab. There are times when it is advantageous to use monomode fiber, and there are other times when it's advantageous to use multimode fiber, because they have different characteristics. For example, in low forward angle scattering, one might choose to use monomode fiber. But at all other angles one might choose multimode fiber because you get extra power, and you don't care about the intercept. One might even optimize the conditions by using a combination of fibers at different angles.

H. DHADWAL:

Using several fibers would be beneficial not only for the power considerations, but also for the spatial coherence considerations. Since spatial coherence relationships are angle-dependent, it is plausible that for each angle you might use a different probe. So I agree with all that you said.

D. CANNELL:

I have some comments about fibers as well. For the last six or seven years in my lab I have operated an instrument that I designed and built, which has 18 different scattering angles ranging from 2.5 degrees to 168 degrees. We used large multimode fibers to collect the scattered light. Once the scattered light has been imaged and selected by a slit system, it goes through large multimode fibers to get to the detector. We see no difficulty with making quasi-elastic light scattering measurements with this system. It also, of course, makes very accurate static light scattering measurements. For example, right now we are studying gold spheres diffusing through silica gels. The baseline in the correlation functions is a thousand times bigger than the amplitude of the signal, and it still shows no significant problems.

W. TSCHARNUTER:

You're talking about using all the fibers as receivers. Now, we have also used fibers as launchers from the laser, and in that case it has got to be monomode. It is impossible to use multimodes because of the speckle pattern.

H. DHADWAL:

Yes, I think we all agree with that; if you want to use a fiber as a transmitter, it must be monomode and probably also polarization- preserving. However, you pay the penalty that the launching becomes difficult and maintaining the launch is difficult. So you ought not to do that unless it's really necessary.

R. BROWN:

I second that very strongly. I avoid using fibers to get the laser light into the cell, because the fibers attenuate the light and create so much hassle. I only use them as receivers, unless I'm really forced to do it the other way.

R. EDWARDS:

Well, there are situations for which fiber optics as transmitters are desirable. For instance, I have an experiment which will be hung over the ocean surface. And if something goes wrong and the experiment falls into the ocean, I'd rather lose the fiber than my laser. There are also applications in wind tunnels and high vibration areas where people want really good vibration compensation, so they use fibers. And lasers of your size aren't going to lose much power in the fiber.

W. TSCHARNUTER:

I fully agree with Robert, it's a hassle to use a fiber as a launcher. But we do it because our sample is 30 or 40 meters away from the laser, and the fiber does work.

R. BROWN:

Recall that I did say that fibers shouldn't be used as launchers unless absolutely necessary. And indeed there are situations where it is absolutely necessary.

T. GLASGOW:

Is it fair to summarize by saying that we need not give much attention to correlator development?

R. BROWN:

Yes.

W. TSCHARNUTER:

The only development I could think of right now is to go from a single card to a single chip, which is very expensive. Since there aren't that many correlators sold in the world, this development certainly is not feasible from a business perspective. For a government agency, maybe it would be.

Proposed LLS Instrument Design

R. BROWN:

Actually, we're all just walking around the mountain by discussing individual components of a laser light scattering system. Let's try to climb the mountain by having a go at a system design. I will just present some ideas and then we can argue about them, OK? If I were designing this, I would use a diode laser and miniature optics, and I would have three sets of replaceable miniature optics to give me either a 5, a 50, or a 500 micron beam at the center of a small sample cell. With the 5 micron beam I can do things like number fluctuation spectroscopy. With 50 microns I can cope with most concentrations, about ten to the fourth to ten to the ninth particles/ml. And with 500 microns, because I know I don't have sedimentation problems in microgravity, I can perhaps look at much lower concentrations. I would then choose perhaps five angles on each side of the scattering plane. Say forward scattering, 20 degrees, 60 degrees, 90 degrees and 150

degrees; I'm choosing these arbitrarily. My reason for choosing 90 degrees is so that I can do cross-correlation experiments. I would put a polarization analyzer in my receiver, so that I could do dynamic depolarized light scattering if I wanted to. Now I'm left with specifying the types of fibers that I want to run out to those angles I mentioned earlier. For the forward angle, my preference would be monomode fiber, because I know I can get pretty high resolution with it. It may not be sufficient, but I think I would compromise between how far forward I could get and what fiber I use. At all the other angles I would probably choose multimode, because then I've also taken care of classical light scattering. At one or two of the angles I might well put a monomode fiber right beside the multimode, and perhaps have a heterodyne capability. And at all the rest I would probably have a self beat, or homodyne, capability. So I now have 10 or possibly 15 fibers coming out. I would put an APD detector at the end of each one. Most of the detectors would have to be passively quenched, not actively quenched, because of the current capability of technology. But for the forward scattering angles I would use actively quenched APD's, in order to increase the dynamic range. I would expect to go up to a 10 or 20 megahertz counting rate. Now that I have the signals from the detectors, I would probably want to put quite a few single board correlators up there. Maybe half a dozen or a dozen of them, if they were small enough. And I do believe that their size will come down dramatically over the next year or so. I would support all the channels entirely. And because we're doing dynamic light scattering, I would use a 12 to 16 point logarithmically-spaced logarithmic-channel correlator and/or structurator. The structurator does have significant advantages in certain operating regions, and I think an experimenter might want to have that capability. And then you've obviously got to have sufficient storage. And the rest, then, is data processing algorithms. There are a variety available for log-log, geometric spacings, and so forth. At this stage, I wouldn't want to choose precisely what the data processing algorithm is; it may well be experiment-dependent. So I would want to leave a piece of storage area in the computer where I could put in my own program, according to my experiment.

H. DHADWAL:

What Robert has described is the idea of having all the different techniques -- number fluctuation spectroscopy, classical light scattering, depolarized dynamic light scattering, and cross correlation -- in the same instrument. I basically agree with the idea. One thing he didn't mention, though, was the shape of the cell; that must be considered, too. Also, one could incorporate refractive index measurements into the instrument. Really, we all agree that it would be best to use a semiconductor laser, APD detectors, and single board correlators of the type Walter [Tscharnuter] described. Perhaps we don't need 6 to 12 correlators, though. We could use one or two, and multiplex them. And the specific optics that are necessary would, I think, depend on the application. We should examine that more carefully.

W. TSCHARNUTER:

I agree with everything that Robert said. As far as structurators are concerned, we at Brookhaven Instruments have them built into our single card correlators. A software switch, i.e. hardware with a software control, controls whether the card operates as a correlator or a structurator.

LLS with Moving Samples

T. GLASGOW:

I have a question about an experiment I'd like to do, and actually the protein crystal growth people have a similar problem. We want to use light scattering to watch a coarsening experiment in a free floating droplet. There is no contact with any walls. We might want to do this at high temperature, to watch phase separation and coarsening in a glass. Obviously, then, the position of the sample is not well defined, as it is in a conventional light scattering instrument. Will we run into severe problems?

R. GAMMON:

Is it wrapped ultrasonically?

T. GLASGOW:

It can be. OK, let's say it's wrapped ultrasonically. But even then, it's not as well positioned as are the samples in a tube. And the radius is going to change during the process, because of the gain and loss of mass from the liquid. Is that going to present us with a problem?

L. DeLUCAS:

The light scattering people need to answer that, but I want to point out that one way to avoid the problem of shining a laser beam into a drop is to monitor the drop through the barrel of a syringe. We have looked at ultrasonic and electrostatic means to support a drop. There is too much vibration with ultrasonic. Using electrostatic can affect the protein itself, because the proteins are charged and the electric field will actually cause them to migrate in the solution. So we see problems utilizing that technique, but I am not going to rule it out. In fact, one of our co-investigators is funded by NASA to try to develop that technique. Now I will let the light scattering people answer your question.

R. EDWARDS:

If you are willing to put in some sort of control system to track the position of the drop, it really doesn't sound all that difficult. It shouldn't be all that hard to track a drop that's just moving around a little bit in microgravity.

R. GAMMON:

It does seem that the low-gravity situation would be an advantage, because the drops you are trying to track would move slowly. Some systems could essentially look at that as a bulls-eye, and by locating the center of the interference pattern could keep a beam on the drop.

R. BROWN:

That's one way to do it. Another thing that Larry DeLucas and I have been discussing over here is that since the experiment is in such small gravity, the photon pressures needed to actually move the proteins around would be considerably less than we need down here on earth. It is just a thought.

Telescience

T. GLASGOW:

Bill [Meyer] left me with a few more questions. We have already answered the ones about polarization and in situ refractometry, by recommending that both of those be included in the instrument. The next question pertains to telescience. Telescience is always of interest to us as a way of getting information back to the experimenter in a reasonable time so that, (1) he can monitor his experiment, and (2) he can control or change his experiment from the ground. So the question is whether we should include telescience capability with the laser light scattering apparatus. And if so, how much and what type of information needs to be telemetered back?

R. GAMMON:

I am not a great believer in telescience. However, I could imagine making good use of it if it were sending back enough data in real time or near real time to reconstruct an operational screen, like the ones that you have when you stand at your own lab apparatus. It wouldn't have to send back the entire data stream in real time, just enough to recreate the screen, so that the experimenter on the ground is able to watch as if he were with the experiment.

H. DHADWAL:

That is only useful if he has enough control to do something.

R. GAMMON:

He gets to watch the evolution of the experiment to help make decisions. He still has to decide what to do and relay that up to the astronaut running the experiment. It's not the

same as directly controlling the experiment, yet it is still quite valuable to watch the numbers coming up on the screen and to be thinking along with the person who can exercise direct control.

T. GLASGOW:
How massive would the requirements be to send that kind of information? It depends on whether we are sending the data as it comes from the photon counters or whether we are --

R. GAMMON:
No, not the photon counts. Imagine that you have common software. You know how to reconstruct the screen on the ground, so you only have the data on the screen up there sent to you. That way it's cheap, and requires only a low data rate.

W. TSCHARNUTER:
I agree with that. The amount of data to be downlinked from an LLS experiment is really not excessive, unless you want to use a lot of channels. But we've assumed we need only 12 or 16 channels. If we downlinked that, along with some temperature data, about every 30 seconds, the experimenter would have plenty of information. Everything else can be reconstructed using software on the ground. If the experimenter and the astronaut are using the same software, they will view the same screen. There are probably a few other parameters that I'm not thinking of right now, but the point is, only a very limited amount of data are necessary.

R. GAMMON:
I said I was not a great believer in telescience, because the telescience I had heard about in the past had to do with transmitting high resolution video in real time. For most experimenters, that is overkill, and is unnecessarily expensive. But I think there is some level well below that, which would be extremely useful to experimenters for a small price.

L. DeLUCAS:
Our group has been asked the same question, do we need telescience? One of the important variables in our experiments is when to seed. It is difficult to train an astronaut to do that, because even when we do it in our lab, we often find it doesn't work. We then look at what happened, and make a decision on when to try seeding again in the very same solution. Having light scattering data sent down to us that allows us to look at the seed and monitor where we are in the growth process can help us make a decision on what to do. For example, if nothing happened to the edges of the seed, we could tell the astronauts to put another seed in there in ten more hours. We can make real time decisions like that. So there is a good reason for our knowing what is happening up there.

T. GLASGOW:
For the remaining few minutes, I would like to take suggestions from the floor.

Raman Scattering

R. GAMMON:
There are some other tools related to light scattering, such as Raman scattering, that would be useful to the polymer scientists and the protein scientists. Raman scattering requires a different kind of spectrometer, which is in many ways much harder to mount. Yet it could still take advantage of the technology mentioned here: the small, compact lasers, the improved detectors, and the increased quantum efficiency. The same holds true for Fourier Transform spectrometers. Once miniaturized, Raman and Transform spectrometers would fly very well, and would add an analytical capability to materials experiments. Maybe a footnote could be added to the report, that there are other light scattering technologies, which we haven't touched on, that would be very appropriate for materials science in space.

R. EDWARDS:

I was thinking the same thing earlier: of all the optical designs I have been hearing about at this workshop, none have been incompatible with Raman or Transform spectroscopy. So I figured that those capabilities would be a relatively easy add-on when the time comes.

H. DHADWAL:

I agree with Bob [Gammon] that a miniature Raman spectrometer would be very interesting. The only ones I've seen so far have been three or four feet long.

S. McMANUS:

In our symposium paper that Lon Mathias is going to send in, he has mentioned several instruments. We gave a lot of thought to what instruments we wanted to propose for our polymer experiments, and the laser light scattering seemed to be the simplest and smallest -- we had already talked with Bill about recent technological developments. I hear that some of these other techniques will also be available on the space station. But for an individual experiment, I think you have to limit yourself to one program and two kinds of devices to give you some information back.

R. GAMMON:

Let me just respond in the spirit of the workshop that I'm excited about the miniaturization that we've heard about. And it's certainly worthwhile to have a real-time analytical tool such as Raman scattering for materials experiments.

R. BROWN:

May I comment on that? There are people I know of in Yorkshire, England who have used diode lasers, avalanche photodiodes below the breakdown point, and a double holographic monochromator. This is a tiny, lightweight monochromator that literally sits in the palm of your hand. With this, they have done perfectly successful Raman spectroscopy on the standard compounds such as benzene. They've digitized their analog information and used multichannel analyzers. I'm sure we could improve on that with digital photon counting techniques. The point is, these things can be done right now; we don't have to consider it a future extension.

R. GAMMON:

Yes, the diode lasers and multichannel analyzers have already given Raman scattering two orders of magnitude faster spectra. Couple that with an APD, and we have a real system. Furthermore, the system would have the analytical power corresponding to infrared, but it could be used on transparent samples or odd shapes, things that you wouldn't use infrared on. It's really ideal. It's delicate; you don't touch the sample or have to change the sample in any way. It's got all the advantages of the optical systems we've talked about already, and yet it's analytic and specific.

Closing Remarks

T. GLASGOW:

If there is nothing else anyone would like to bring up, I suggest we adjourn. I thank you for coming, and hope to see you at a future workshop. I assure you that Bill and I will be as close to each of you as the telephone. We all look forward to having our experiments in space in a few years; and it will be due to your contributions that this will happen. Thank you.

TRANSCRIPT OF PROCEEDINGS

NASA LASER LIGHT SCATTERING WORKSHOP

DISCUSSION GROUP II

SHERATON HOPKINS HOTEL

CLEVELAND, OHIO

THURSDAY, SEPTEMBER 8, 1988

3:00 P.M.

PARTICIPANTS:

William Meyer, Leader	MaryJo Meyer
H. Michael Cheung, Co-leader	Clarence Miller
Rafat Ansari	Syed Qutubuddin
Steven Bott	James Rollings
James Cawley	William Rosenblum
Paul Chaikin	Rudolph Ruff
Benjamin Chu	Gilbert Santoro
Ivan Clark	Klaus Schätzel
Tony Cox	June Tveekrem
William Fredericks	John Wiencek
Andrew MacGregor	William Witherow
Lon Mathias	Philip Wyatt

W. MEYER:

What I'm going to do first is give you an overview. Before the workshop, we sent each of you a copy of our "straw man" design for an in-space laser light scattering (LLS) instrument. That design is by no means carved in stone, so please feel free to suggest changes. We need your input in order to build this instrument to satisfy the requirements of your space experiments. The questions we would like to address are divided into three categories: sample containment and handling, LLS hardware, and on-orbit operational considerations. First we will discuss samples. We want to know how the samples should be contained, specifically, should we use bulk or flow cells? How precisely does the sample temperature need to be measured and controlled? Do we need to measure the small vibrations to which the sample is exposed, i.e. should we mount an accelerometer on the LLS instrument? How much information is needed about the sample's history before the experient is turned on? Finally, what is the best way to activate the experiment? Then we will move our discussion into hardware concerns. For example, we will talk about what kind of laser source we want. I think what we have heard about Robert Brown's work will help a lot in that area. We need to consider the specifications of the detectors. Do we really need a ten MHz count rate? Some top experts in light scattering say that we probably don't need more than 100 kHz or 1 MHz. What kind of dead time do we really need? We can probably live with 100 nsec, but should we try harder? We need to discuss detector placement. How many angles do we need? How many should be static, and how many should be dynamic? Should we put detectors on both sides so we can do cross-correlation? Another concern is receiving optics. We are pursuing parallel developments in optical masking and in fiber optics. We need to compare these technologies to see which performs better at small angles. Then we will talk about correlators. Within the next year, we will have the capability of developing a software correlator. But perhaps it would be better to use hardware correlators. Single-board correlators now exist, and they could possibly be reduced in size to a single chip. Do we need a single-chip correlator, or is a single-board correlator sufficient? Lastly, we are concerned with operational capabilities such as polarization measurements and refractometry. Should we design the instrument so that one can both measure and change polarization? Should in-situ refractometry be included? Finally, how much interaction, if any, is required between the principal investigator on the ground and the astronaut running the experiment? In other words, do we need telescience? That's a preview of coming attractions. First, I would like to discuss samples. Could I have some input from the experimenters on what you need for samples? I've heard strong preferences on both sides of the bulk vs. flow cell issue.

Sample Cells

P. WYATT:

If you have a bulk sample in space, how do you get rid of air bubbles in the sample? If any air gets into a scintillation vial, it won't just nicely rise to the top the way it does on the ground.

W. ROSENBLUM:

We haven't had that problem. In our case, the samples are suspended droplets, and there is no way for air to get in. For samples in vials we siliconize the vials or remove the bubbles by reverse hypodermic suction. There are other methods as well.

S. QUTUBUDDIN:

Our microemulsion experiments require bulk rather than flow systems. We form a microemulsion and polymerize it to obtain a porous solid. The morphology and porosity of the solid depends on the initial microstructure of the microemulsion. We have studied one system so far, a styrene. Another application would be to use two monomers, one hydrophilic and one hydrophobic. Then you can do simultaneous polymerization of the two monomers to create a type of polymer composite, having both hydrophilic and hydrophobic properties. We are able to do all the experiments on earth, but we lack

control of the porosity and morphology of the solid structures. Performing the experiments in micro-g would give us that control. Dr. Miller's theory indicates that gravity affects the process after the polymerization reaction has started. If we can slow down the polymerization reaction, we can hope to recapture the initial microstructure of the microemulsion. The porosities that we've gotten so far are in the sub-micron range, but the ultimate goal is on the order of 100 Angstroms.

W. MEYER:

What size bulk cells would you want?

S. QUTUBUDDIN:

About one cubic centimeter would be sufficient.

W. MEYER:

Lon [Mathias], do you have any thoughts on bulk versus flow?

L. MATHIAS:

We can't use a flow system; we do static experiments on drops. The carousel concept for bulk samples has been mentioned, but I'm not sure how to incorporate that into the design. Furthermore, we do photopolymerization, so we require illumination of the samples. The instrument therefore must be able to accomodate photoinitiators or other light sources. It also should be mobile. And if we are going to incorporate Phil Wyatt's refractive index and dn/dc measurements, that will require more changes to the design. What I'm getting out of this is that it would really be helpful to make a list of different experiments, their requirements, and how those requirements affect the design of the LLS instrument. There's got to be a compromise between the experiments and the equipment, and I'm not sure where that compromise is going to occur.

P. CHAIKIN:

My requirements don't fit in either the bulk or the flow categories. First of all, I would like to have a cell in which I can change the sample by adding or removing a small amount and mixing. That's actually fairly easy. But I also would like to do scattering experiments in a cuvette cell when the sample is under shear. That's a different matter entirely.

W. FREDERICKS:

The idea of a multi-detector, multi-angle, classical and dynamic light scattering system is great, but the real problem is how to shape the sample cell. There is a great variety of experiments that people want to do, and none of the existing sample cells seem universal enough for all the experiments.

W. MEYER:

We could perhaps have a modular design, with interchangeable read heads, so that for some experiments we would use a flow-through cell, for others a bulk cell, and for yet others a shear cell.

B. CHU:

It seems to me it is very important to establish some general specifications for the instrument, and deal with specific requirements on a case-by-case basis. It is not possible to design an instrument to do everything because the cell configuration is different for different experiments.

J. ROLLINGS:

I have a question for Bill Rosenblum. How difficult is it to focus the laser beam onto your spherical drops? If that focusing is critical, you might be designing something that's almost doomed to failure.

W. ROSENBLUM:

Very good point. We have had a lot of experience with this and we have come to several conclusions. One is that the hanging droplet method is probably the worst method we could ever incorporate. The motivation for doing it was that the sample would not touch any walls, and so would supposedly be interference-free. But imaging through a drop, or pointing a laser at it for light scattering, is awful. We also tried a suggestion from Klaus Link in Germany to prepare the crystals in Tygon tubing, and then seal the tubes, like little sausages. We flew that configuration in the Chinese rocket that just went up. We couldn't image through that any better; it acted as a strong cylindrical lens and distorted the image. For optical imaging, rectangular cuvettes would ease our life a lot, but they obviously wouldn't work for multi-angle light scattering. I'm not sure how to design a combined system.

A. MacGREGOR:

If you have a hanging droplet from one hypodermic, why can't you put another hypodermic on the bottom to get sort of a cylindrical surface using the surface tension? That should ease your problem and it would also constrain it top and bottom. Or, why not put a fiber optic probe right into the droplet?

W. ROSENBLUM:

We did think of extending a fiber optic probe through the syringe and into the droplet, but the crystallographers didn't like the idea. I'm not quite sure why. But you are right, that would be an easier way to inject light into the samples.

W. MEYER:

So our conclusion on sample cells is that we need a variety of them.

Temperature Control

We now need to touch on temperature control: what range and stability do we need? A range of 20 to 40 degress C was stated in some of the presentations today. Could each of you tell us what range and stability is required for your experiment?

S. QUTUBUDDIN:

The range we would like is from 20 to 60 degrees C, with stability of plus or minus 0.1 degrees C.

W. FREDERICKS:

Generally, in isothermal crystal growth we need temperature control to within a few hundredths of a degree over the entire region of the cell, from the vapor sink to the liquid.

W. MEYER:

If we have plus or minus a hundredth of a degree Kelvin, is that good enough?

W. FREDERICKS:

I would think that would be quite adequate. [Other people in the room nodded, and nobody voiced any objections.]

J. WIENCEK:

Besides having a close temperature tolerance, many experiments need to ramp or step-function the temperature in a very precise fashion. To get good stability in the ramping functions or step-functions or response times, the dynamics of the whole system must be considered. You are going to have to heat every metal part that's in contact with the scattering cell.

W. MEYER:

That's a good point. We had initially thought of using Peltier coolers. It seems that we can easily control within a hundredth of a degree Kelvin with Peltier coolers. We won't get step functions, but we will be able to control the ramping.

A. MacGREGOR:

One brief comment. Peltier devices won't heat above 80 degrees C, so if someone wants to go higher, you will have to find another source of heating and cooling.

I. CLARK:

You don't include uniformity on your list of temperature concerns. For some experiments I would think that would be much more critical than stability. Also, I am puzzled as to the scope and intent of this discussion. Are we trying to develop an instrument only for the experiments that are present, or are we considering other applications too?

W. MEYER:

We do have some experiments now which we are using as a departure point, but the possibility exists to broaden the scope. If we can accomodate other applications without completely redesigning the instrument, we will be delighted. Our initial phase is to keep the instrument as simple as possible. For example, we will probably stick to homodyning to avoid vibration problems. We can work on the next generation's machines later, but initially we just want something that will work. Your comments are very valuable to us. Thank you. Any other concerns on temperature?

Sample Handling

Then let's talk about the sample storage and history. One potential problem occurs when several samples need to be equilibrated at different temperatures before performing the LLS measurements. Should we store all these samples at different temperatures, or are the experimenters willing to equilibrate them one at a time, while they are in the LLS instrument? I know some of the microemulsions take a long, long time to come to thermal equilibrium.

S. QUTUBUDDIN:

Yes, some microemulsion systems do take a long time to equilibrate. But by careful studies on the planet earth we can find systems that will equilibrate within an hour or so. So equilibration time and history should not be a problem for the microemulsion studies.

W. MEYER:

Is this the kind of situation in which an astronaut could just pull a tube out of the rack and insert it into the LLS instrument, and then just wait for the sample to equilibrate?

S. QUTUBUDDIN:

Right, something similar, very simple. We don't need any elaborate mixing.

W. MEYER:

Are there other concerns on samples and containers?

J. TVEEKREM:

Do any of these samples need to be prepared and stored in a clean room to minimize dust problems? The samples will have to sit for a long time while undergoing checkout and integration at Kennedy Space Center.

W. ROSENBLUM:

Dust is one of the main killers for photon counting, so there will have to be some container cleaning done. We have to use methods such as peristaltic pumping through filters to try to clear the sample of dust. It is difficult, but dust can be removed successfully. Bill Wilson in Mississippi, for instance, has achieved very clean samples, so I don't see that as a major problem.

W. MEYER:
Other comments? When I spoke with David Cannell last night, he said it is very, very important to choose your container carefully, so that you can put an incredibly smooth finish on it to cut down flare. Any thoughts along those lines?

P. WYATT:
For bulk sample cells, flare shouldn't be a major problem as long as the scattering angle is above 20 degrees. So we need to know how small of an angle is required for these experiments.

W. MEYER:
I believe that some of the people studying colloids want to go down to five degrees or even two degrees.

P. WYATT:
I should point out, there is a large company in this country that decided to compare specialized 10 ml containers to the the ten cent scintillation vials, which we know do not have particularly good quality. They wanted to find the best cell that can be manufactured, given no restrictions on money. And they spent a tremendous amount of money only to find that the difference between a ten cent scintillation vial and the best that money can buy was negligible, except at small angles. But at small angles, a cylinder is a very cumbersome geometry to use anyway. One has to be concerned with the inner and outer diameters of the cylinder, the quality of the glass, and the polishing technique used.

W. MEYER:
Robert Brown raised an interesting point the other night; he has found that flare doesn't seem to launch into fiber optics. Have you experienced this in your research, Ben [Chu]?

B. CHU:
We've found we can exclude the stray light by looking at a finer section of the beam, but, you know, all of these are related factors.

W. MEYER:
It looks to me like we are talking about receiving optics, so let's skip to that. We have heard proposals for fiber optics that sound wonderful. We also have some work going on with optical masking, which should help a great deal, though the performance at small angles remains to be seen. Would you like to comment on that, Mike?

M. CHEUNG:
I'm going to talk about lenses that are large compared to microlenses and fiber optics. One advantage of using full size optics is that the light collection efficiency is much higher. Of course you can emulate that with the fiber optics by using larger lenses up front or focusing it down smaller. But this causes problems because if you are focusing smaller on one side of the lens it means you are collecting from a larger area on the other side of the lens. I think the best system will ultimately prove to be a hybrid, which uses a slit-shaped mask to cut flare and then a GRIN lens to couple into a fiber optics probe. I don't think anybody doubts that fiber optics are the best way to transport light to the detector.

W. MEYER:
Would you share some of your experience with us, Ben Chu? What is the minimum angle you can attain?

B. CHU:

First, let me point out that the only major difference between using microlenses and large lenses is the physical limitation of how close you can get to the main beam, and where the light trap can be located. There is not much argument on that. With "regular cells", for self diffusion, our minimum scattering angle is two degrees. We are using a solution of solid particles in cyclohexane where the solvent scattering is five percent of that of the solute.

P. WYATT:

You got those low angles using a cylinder cell?

B. CHU:

No, we used a prism light scattering cell. The design is published in Review of Scientific Instruments, [59 (5), May] 1988.

P. WYATT:

Okay. I think this is important, because I sense a belief here that you can take a cylindrical cell, combine it with the right kind of optics or masking, and do light scattering at very low angles. Maybe that would work if you had a half-meter diameter cylindrical cell, but I don't think that size would serve our purposes.

K. SCHÄTZEL:

Of course, the diameter is the most important consideration in using a cylinder cell. But the nice thing about cylinder cells is that it is so easy to measure all angles. With elongated cells it is much easier to do the smaller angles, but you can't do the large ones. For a universal instrument we need the capability to measure at both large and small angles. We could use both cylindrical and elongated cells, but then we would have to have two samples. If we tried to combine cylindrical and elongated geometries in a single cell, we would end up with a rather awkwardly-shaped cell. So I think we will have to live with the limitations of cylindrical cells and compensate as best we can with receiving optics.

W. MEYER:

It looks like we have two possible working solutions for receiving optics. I suspect that we will try to develop both and make comparisons. Any other thoughts?

Number of Scattering Angles

P. CHAIKIN:

Do you expect to have a detector array rather than single detectors?

W. MEYER:

We hadn't included that in the initial design, but if that's a request, we do need to know it. Do you need a two dimensional array, or would it suffice to just add a linear array for low angles?

P. CHAIKIN:

For the experiments I'm thinking of I need a two dimensional array, because under shear the structure factor distorts and I want to know the structure factor in all directions.

W. MEYER:

What range of angles do you need for the two dimensional array?

P. CHAIKIN:

I was thinking of maybe 45 degrees half angle, 90 degrees full.

W. MEYER:

That eliminates the standard detector cell. We may have to use a unique read head for your experiment. I'm sure that won't be a problem, because I think it will interface well with the rest of the hardware.

B. CHU:

If you are interested, we are building an instrument similar to that, but it is only for on-earth applications.

W. ROSENBLUM:

We do need multiple angle scattering, at least in the scattering plane, to deal with polydisperse systems. When you have a polydisperse system, it is very difficult to know in advance how many angles and which angles are going to be needed to determine the polydispersity. There are papers that show that multi-angle detection is the way to go.

B. CHU:

That depends on how big the particles are. If they are very large, so that the static structure factor shows big changes due to polydispersity, then multi-angle scattering will play an important role. But if you have smaller molecules with a range of sizes, then multi-angle scattering will not help too much.

W. MEYER:

For multi-angle scattering, what spacing would you recommend between the angles? Would you use logarithmic spacing?

B. CHU:

About one detector every degree. That, of course, means there are over 150 data points.

W. MEYER:

We may be able to do that simply by moving the laser, since we have a finite number of detectors. As we move the laser it will shift the scattering angles.

S. BOTT:

It seems to me that before we can solve any of these problems of instrument design, we need to know two things -- the sample volume, and the lowest scattering angle required. Given those two things, I think there are any number of people in this room who would converge on the same solution to this problem. Then the next thing to find out is how many angles are needed; that again depends on the type of experiments you want to do.

A. MacGREGOR:

There seems to be an assumption here that you are only going to build one instrument. But as Robert Brown showed, it is possible to drastically reduce the size and cost of lasers and detectors. You then have the option of including more than one instrument in the same experimental volume. The instruments could share the same electronics, but would have different functions.

W. MEYER:

That's a very good comment. The instruments would also be useful just for people to play with, to find out how they act on the ground before we take them into micro-g. To follow up on Steve Bott's comment, why do we need to know the sample volume?

S. BOTT:

You need to know the volume because that determines whether you can use a cylindrical cell or whether you have to use some kind of flat or multi-faceted cell. Secondly, you need to find out how low an angle is really necessary. You shouldn't just say, "We have to go to an extremely low angle"; you must specify the angle. It is important to define both the volume and the angle because the smaller the sample volume and the lower the angle, the greater the difficulties you have to overcome.

W. MEYER:

Can you tell us a bit about the difficulties? How small an angle do you use in your work? The reason I say this is because when I ask experimenters to define how low an angle they want, they say, "How low can you get?"

S. BOTT:

I know, that's the easy answer; the hard answer is specifying a definite angle. I haven't been particularly concerned with going to a low angle, but we have designed instruments that go down fairly easily to five degrees. To go lower than that I would take a different approach.

Light Scattering through Hanging Droplets

W. FREDERICKS:

I think Andrew MacGregor had an excellent point in that there is no way you are going to accommodate all the experiments that people want to do with a single cell geometry. Some people need large samples, but there is a good reason why the hanging drop method is so attractive to people who grow protein crystals. Some of those proteins are so expensive they make gold go out of style. When you stop to think that perhaps a few tons of human liver get processed to yield a few micrograms of a protein, you can see why the cost is incredible. That's why the crystal growers choose the hanging drop method, because it takes the smallest volume of very expensive proteins.

S. BOTT:

I think that brings out why you need to define the combination of the sample volume and the lowest angle. Frequently when you are working with those very small volumes you are also working with very small crystals within the volumes. With the very small crystals you rarely need to go to extremely low angles, because the quantity that matters is the scattering vector times the size of the particle.

I. CLARK:

It seems that once you start going to the very small drop sizes or small-radius containers, the sample will start acting as a cylindrical or spherical lens. That lens will converge the laser beam and make it difficult to determine the precise scattering angle. Do you have a need to know the angle precisely?

S. BOTT:

The answer is definitely yes, because the data are analyzed by fitting for variables in an exponential. The argument of the exponential goes as q-squared, and q goes as sin(theta/2), so every error in theta gets squared and exponentially magnified. Of course, the behavior of the sine function comes into it, too. If the angle is off a little bit at 90 degrees, it doesn't matter so much, but if it's off a little bit at 2 degrees, the error is extremely important.

I. CLARK:

My concern really is what happens when your laser beam diameter becomes a significant fraction of your sample size. If you fill your whole sample with laser beam, the transmitted beam will no longer be collinear.

W. ROSENBLUM:

I've done light scattering through drops, and yes, you are right. Aligning the beam is tough; if you miss the center of symmetry, the beam walks around and you get reflections from the walls of the droplet. But in larger-volume sample containers, such as the standard Brookhaven cuvette, you don't suffer as much from that problem.

P. WYATT:

Isn't it true that when you get to very small angles you see more and more of the sample by foreshortening? Your sample fills up the acceptance angle. I would think that when you get to small angles you'd have more problems accounting for the foreshortening than for the error in the measurement itself.

J. ROLLINGS:

I've got another question about the drop experiments. If the water vapor is constantly drying, doesn't the drop itself change shape and force you to refocus constantly? How do you account for that?

W. ROSENBLUM:

Yes, the drop size and position do change. There is usually a wick in the bottom of the cell, and water or solvent is drawn out of the droplet through the wicking, thus causing crystallization to occur. Accounting for this is not a solved problem by any means. You must understand that photon counting is not a preferred method for monitoring crystal growth in hanging drops because of just the problem you have stated.

S. BOTT:

Light scattering from drops seems to be a unique problem, which maybe should be treated separately from the problems of scattering from bulk samples.

Number of Scattering Angles (continued)

W. MEYER:

Let me relay a discussion I had with David Cannell last night. He uses log spacing, and he has 18 angles on one side of the detector head and 18 on the other side. Furthermore, his fibers are optimized for either static or dynamic light scattering. He says he can essentially see anything he wants, and he has never found a system that his instrument didn't work well with. This testimony of experience suggests that we can work with a surprisingly small number of angles. Do we have thoughts contrary to that?

B. CHU:

I think that would be the case for micromolecules, but for very large particles it would limit your options. If you want to separate the internal motions of the particles from the translational motions, you have to optimize the measurement time of the correlation function. When you have only a few fixed angles, even log spaced, this may not allow you to optimize the measurement time. Also, when the particles are very big, the static structure factor is very useful. To determine the static structure factor accurately, 18 angles will not suffice; you need about one per degree. This is done in X-ray scattering: people have determined the size distribution of particles, i.e. the polydispersity, by examining the maxima and minima of the static structure factor.

W. MEYER:

One thought we had was to use a laser that moves; moving the laser is equivalent to moving the angles. If you have one moving laser and ten fixed angles, then you can fill in the gaps between the angles.

B. CHU:

In my experience, moving lasers doesn't usually work well.

W. MEYER:

That's good to know. We had also thought of changing q by changing the frequency of a laser. We can vary q by up to five degrees that way.

P. WYATT:

The number of detectors that you need for any type of particle is, I think, of the order of 2ka, which is one per degree when you get out to sizes of about 20 microns. But at 20 microns, a polydispersity of about half a percent will wipe out most of the patterns you see, so how do you get more information?

B. CHU:

Otto Glatter in Austria has some papers coming out that deal with this particular problem. But remember, you are looking at large particles where all the maxima and minima are separated, not at smaller particles, where you can't resolve polydispersity at all.

W. MEYER:

So if we had a working range of up to three microns, you're saying we would not need nearly as many angles?

B. CHU:

In this case you can go higher. You can look at sizes which are bigger, but I haven't made any detailed estimates of how big.

K. SCHÄTZEL:

I would like to make two comments of support. The first is that one major justification for doing experiments in space is the lack of sedimentation in microgravity. On earth, sedimentation is not a problem for ten nanometer particles, but it is a problem for ten micron particles. So I suppose there will be quite some interest in working with big particles in space. The second comment is that we should consider whether to detect all angles simultaneously or to detect them in some time-slotted fashion. Since the detectors have become small and cheap, and since we all know the experiment is going to be very expensive to send up there, I should think you would go for the most efficient detection scheme, and that would be parallel detectors.

W. FREDERICKS:

In addition to sedimentation, another problem that is solved by going to a microgravity environment is convective flow. This is quite important for crystal growth. Since the particles do not have to be large in that case, there may be interest in small particles.

K. SCHÄTZEL:

This sort of justifies what I said earlier, that you really need the full angle range and a high resolution if you want to study both the small and large particles at the same time. That's fairly obvious. Instead of avalanche photodiodes, we could use alternative detectors such as a charge coupled device, camera-type device, or line array. Certainly that would do for the static light scattering measurement. I don't think we are really talking about dynamic light scattering at something like 200 angles. That would take an incredible number of correlators.

W. MEYER:

How many angles are we referring to when we talk about dynamic light scattering?

K. SCHÄTZEL:

Well, with the present size of correlators, I don't think you would go significantly beyond ten or so.

Detectors

J. WIENCEK:

What about the background radiation? With all the solid state devices you are talking about putting into this, are you going to have radiation damage and will the detectors be detecting background radiation?

A. MacGREGOR:

There are two points on that. Number one, we do provide space qualified APDs. Number two, yes, there is some deterioration. The deterioration isn't significant, however, unless the radiation environment is very severe -- and the astronauts wouldn't put up with that. So you wouldn't expect to see actual degradation of the basic performance, but you would expect to see occasional excess dark counts.

J. WIENCEK:

That could be a problem for some of the experiments that need to run for days. I think some of these protein experiments run for days. And some experiments involve free diffusion of polymers; it takes a month for the polymers to diffuse one centimeter. So spurious dark counts could be a problem. But, of course, if the total dark count,

spurious or otherwise, is low enough, say 10 to 20 counts/sec, then it probably won't matter.

A. MacGREGOR:

Klaus [Schaetzel] just pointed out that an APD has a much smaller cross section to intercept radiation than does a photomultiplier tube. In fact, all the devices in the LLS instrument are going to have lower cross sections than anything we have made before. We are actually talking about something that's maybe 400 microns across and 30 to 50 microns thick, so the probability of interception is quite low. You are more likely to get scintillation in your sample, I think, than dark counts in your detector.

W. MEYER:

That's good to know. Since we are talking about detectors, let's discuss them in a little more depth. What level of dark counts do our experimenters need to worry about? Is a hundred counts per second, with a variance of ten, sufficiently low? How about 36, with a variance of six?

S. BOTT:

Before answering your question, I would like to second what Klaus Schaetzel said, that it would be a very good idea to use a completely separate set of detectors for the classical light scattering part, and to use a lot of them. In the work that I did, I used 50 for the classical light scattering part, then I just detected selected angles for the dynamic light scattering part. The classical and dynamic detectors should have completely different collection optics, because the needs are quite different. Secondly, you can use only a limited number of correlators, so you should multiplex several PCS inputs into each correlator. For example, if you have a dozen PCS angles, you might use three correlators and multiplex four fiber optics into each.

W. MEYER:

That also has the advantage that if one dies, you can switch it out of the circuit.

S. BOTT:

As for your question about dark count, I would suggest using really cheap photodiodes for the classical light scattering portion, since that's not nearly as sensitive to dark counts, and then define the dark counts that you want based on the PCS requirements alone.

W. MEYER:

We do have an option to use the same angle for both static and dynamic light scattering simply by changing the bias on an avalanche photodiode. However, that is a bit of a compromise.

S. BOTT:

One reason that I would not recommend using that procedure is that, for optimum performance, you really need collection optics for classical versus dynamic light scattering. Secondly, it is very desirable to have numerous classical light scattering collectors, and that can be done very cheaply because high voltage amplifiers aren't necessary to amplify the simple little photodiodes.

W. MEYER:

Since we will be doing both classical and dynamic light scattering, we should try to build in as much capability as we can without compromising the instrument. This includes such things as cross- correlation, in which we do dynamic light scattering at opposite angles. We have established that the maximum acceptable dark count should be defined by the needs of dynamic light scattering. Is one hundred counts per second acceptable?

A. MacGREGOR:

The quantity to worry about is not dark count alone, but the ratio of photon detection efficiency to dark count. What hinders you from maximizing that ratio is dead time, which impinges on maximum count rate, and after-pulsing. So maybe a better approach is to ask what count rate is needed and what level of after-pulsing is acceptable for different experiments. Then we will know what the maximum ratio of photon detection efficiency to dark count will be. Does that make sense? [Participants expressed general agreement.]

W. MEYER:

What I've gathered from this group, then, is that we should use something like avalanche photodiodes for dynamic light scattering and switch to something like pin photodiodes for the static light scattering. We will probably also use different fibers, microlenses, and masks, for the two types of light scattering.

Correlators

Let's press on, then. What kind of correlators should we build in for dynamic light scattering? There is a lot of concern about the number of channels and channel spacing. My first impression is to go with some of Pike's work. He says that theoretically you only need five channels with exponential spacing, but that in reality, because of dust and other concerns, you probably need 16 channels.

M. CHEUNG:

That depends on what you are trying to do. If you have five channels you can't resolve a histogram with 18 peaks. If you are interested in resolving a trimodal distribution equivalent to 20 histogram peaks, I expect you would need at least 60 channels.

K. SCHÄTZEL:

I would like to address the questions you listed under "correlators" in your slides, since that gives a nice way of organizing a response. Obviously, the answer to the first question on the need for real time correlation must be "yes", because if we send up an expensive experiment, we shouldn't waste time waiting for computations that could be done in real time. And, of course, real time correlators exist, so there is no reason for not using them. The number of correlators used will depend largely on their size. If they are on a board, we may have five or ten. If they are simply a single chip, we may have a hundred. There are no chips available yet that can do full photon correlation functions in a reasonable way, but the technology exists. Availability is a function of the number we need. If we could order a million, companies would make them immediately. The next question was the number of channels on the correlator, and that of course is closely related to the question of optimum channel spacing. It is true, theoretically, that you can do with very few channels but then you must know exactly where those channels should be. That is, before doing the measurement you must know what the outcome of the measurement will be. That's generally a difficult problem, particularly if you want to operate in a fully automatic mode. For that reason, even for earth experiments I advocate just the opposite solution. While you could make do with a small number of channels, it is now technically possible to have one correlator board that covers the whole range of times between 200 nanoseconds and two hours, or whatever you like. You can even have two independent correlation functions if you are content with 400 nanoseconds initial time. If you do it that way, there is no chance that you will miss any important information. You always have the long-time tail, so you can always tell whether there was dust in the sample; it is not just a matter of guessing afterwards.

W. MEYER:

We can draw on the experience of some of the initial experiments to help us understand the outcome, the angles needed, and so forth. We are simply looking for the changes in the experiments when they are performed in microgravity.

K. SCHÄTZEL:

Of course. You can do the experiment with just a few channels, but it is difficult and unnecessary. If there is a simpler way, why not do it that way?

W. MEYER:

So how many channels are you recommending as an option?

K. SCHÄTZEL:

Well, to have optimum signal processing, you shouldn't just vary the lag time. You must also increase the sample time to minimize noise and maximize efficiency. However, once you vary the size of the sample interval you are varying the triangular average, and that causes a slight distortion in the correlation function. To avoid that, you need to use four to eight channels per octave. Now the question becomes, "How many octaves do you want?" The answer is probably 20 to 25, in order to cover the whole time range from below one microsecond to about one second. It is still a number that is easily stored on a disk, so there is no problem in handling the data in flight. And there is plenty of time for processing afterwards because the experimenter is not going to fly another experiment soon anyway.

S. BOTT:

How much power is available? That's going to be a major constraint on how many channels and correlators you can use.

W. MEYER:

The avalanche photodiodes, with Peltier cooling, each take a maximum of 1 watt. Then if we reduce each correlator to a single chip, the power requirements will be slight and I don't think power availability will be a concern. We will, however, have space limitations.

K. SCHÄTZEL:

The correlator board I was talking about consists entirely of CMOS chips; it doesn't take much power. And if you don't need to have the fast time scales, run it at half time and it will only use half the power.

W. MEYER:

Are there comments on Bob Edwards' maximum likelihood correlation techniques?

K. SCHÄTZEL:

Maximum likelihood correlation would be nice, it would mean you had a device which counted photons in and gave particle size out, with nothing else in between. I don't know how to build that device. One outcome of Bob's talk was that he wanted to have a zero channel in order to get noise estimates. That may not be necessary because if you do a well defined experiment and you know the number of photons that you count, it is very easy to compute the noise. He also wanted a programmable position and number of channels. That is a good idea if you can only have a few channels, but if you can have them all, programming their position isn't necessary.

W. MEYER:

Point well taken. Are there other thoughts on correlators? How many should we have, assuming we multiplex them?

Date Downlinking and Telescience

J. TVEEKREM:

Doesn't the number of correlators and the number of channels -- basically the sheer amount of data we've got to analyze -- depend on whether we are going to downlink this data or store it?

W. MEYER:

Actually, we have a lot of data to start with, but once we build a correlogram it reduces rather rapidly. But since you ask, we do have a related question we should address. How important is telescience to our experimenters?

K. SCHÄTZEL:

Before we go into that discussion, I would like to comment on the question of whether to store the data or to downlink it immediately. Storage is easy; there is plenty of optical disk space. Downlinking is also feasible; a thousand correlograms contain fewer bits than a single color video image. Of course, for safety reasons we would like to have the data on the ground as soon as possible, but this is not a major issue. It's really a matter of preference whether to store or to downlink.

W. MEYER:

Okay. Regardless of whether we downlink the data or store some of it, there still may be a need to communicate with the experiment. So lets address the issue of telescience. Are the experiments sufficiently well understood that we can just set their parameters and let them run? Or will it be necessary to monitor the experiment in real time and make changes while the experiment is running?

L. MATHIAS:

I thought NASA's policy on that was pretty well established, that telescience was not encouraged.

W. MEYER:

Actually, we have some NASA people developing telescience in our lab. I live with it every day, which is one reason I thought I should ask the question.

L. MATHIAS:

It would be nice to be able to participate in the experiment. Ideally I would rather be there, but second best would be telescience. However, I think that including telescience adds a level of complexity to the design of the instrument that we may not be ready for yet.

W. MEYER:

It might be less of a problem if considered in the first generation. Perhaps we should keep this in mind when we design the initial layout.

L. MATHIAS:

One thing I liked about the crystal growth experiments was that they evolved from the very simple demonstrations to the more complicated. Maybe that's the philosophy we ought to follow here, to design something very simple first to show that it works.

W. MEYER:

Do you mean that we should not only have a simple homodyne configuration, but also a small number of angles?

L. MATHIAS:

I don't think the angles are a concern, since the detectors are apparently inexpensive, but we should focus on keeping the experiments as simple as possible, eliminating things like telescience electronics. I think that adding telescience capability, as opposed to just pushing a button and letting the experiment run, would make the experiment two or three times more complicated.

Laser Source

W. MEYER:

We have touched on telescience. Maybe we should discuss a few more hardware issues. For instance, we haven't yet talked about the laser source. The three questions

about that on my slides pertain to the number of lasers needed, the laser wavelength, and the desirability of using solid state lasers. We have seen that Robert Brown can construct a laser source from a standard solid state laser and a few dollars worth of electronics. The coherence length seems to be long enough. One concern that's not written on the slide is whether or not to use fiber optics to launch the laser beam into a sample cell. If we use fiber optics, we can thermally isolate the sample. We can also isolate all of the detectors.

P. WYATT:

There is another interesting point. I don't know how long the laser actually has to be left on. If there is no warm-up time needed, the duty cycle of the laser could be reduced tremendously. Since most light scattering measurements are normalized to the laser intensity, the laser could in principle be turned on only for the few seconds duration of each measurement.

W. MEYER:

That's true. I believe we can switch the lasers at gigahertz speeds.

I. CLARK:

That cuts down on the total usage time of the laser, which should make it last longer. However, the principal failure mode of laser diodes is thermal cycling, so it is actually more harmful to turn the laser on and off. Also, running the laser in a continuous-wave fashion for the duration of the experiment gives better stability in the wavelength.

W. MEYER:

Speaking of wavelength, could I hear some thoughts on what the wavelength should be?

J. CAWLEY:

Wavelength doesn't make much difference in my experiments.

K. SCHÄTZEL:

I would certainly prefer a visible laser. It makes alignment much easier.

A. MacGREGOR:

The standard shortest wavelength available is just barely in the visible range, around 680 nm. [Note: The laser beam power at 680 nm is 3 to 10 mW; the power at 800nm or longer is up to 5 W.] However, you can pass the beam of a standard 1060 nm solid state laser through a YAG frequency-doubling crystal to get 530 nm. It may be possible to get to even shorter wavelengths. While I can't discuss this, RCA has been asked recently to look at frequency doubling a 900 nm solid state laser beam to get 450 nm. So, you can go to visible wave lengths; whether it's worth it depends upon how much power you need and how much money you want to spend.

W. MEYER:

It sounds like the needs of all of our experimenters can be satisfied if we use a wavelength of 680 to 780 nm. With 680 we can easily see the beam. [However, the detectors have a higher quantum efficiency above 780 nm.]

Polarization

Let's move on to the operational questions. For example, a need has been mentioned for polarization measurements.

W. ROSENBLUM:

We are interested in polarization measurements. What is done now is to place polarizers on the front and back of the cells, in order to see birefringence and coloring. We are also interested in polarization changes due to scattering. In fact, since we know that the Mie diagrams depend on the instantaneous state of polarization of the scattered light, we need to be able to vary polarization to unfold some of the scattering distributions.

W. MEYER:

How will you vary it? Will you just have some detectors that respond only to vertical polarization and others that respond to horizontal?

W. ROSENBLUM:

Yes, we will certainly do that, but it is also possible to use an unpolarized laser and send the beam through a Polaroid material to change its state of polarization before it strikes the cell.

P. WYATT:

I don't know about the solid state lasers, but gas lasers have random polarization and are susceptible to mode sweeping when you try to polarize them. Are the solid state lasers polarized?

W. MEYER:

Yes, they are polarized and they can have very good mode stability. However, they present a focusing problem, because they emit an elliptical pattern.

A. MacGREGOR:

The solid state lasers are stable if they are an index-guided structure, but you have to temperature-stabilize them to keep them in the one longitudinal mode. The spatial output is essentially an elliptical beam, and the degree of ellipticity depends on the manufacturer's particular structure. So you have to specificy the degree of ellipticity to whomever is supplying your lasers.

W. MEYER:

What we are settling on using, then, is a solid state laser of wavelength 680 to 780 nm, with spatial filtering and a cylindrical lens to eliminate the ellipticity.

A. MacGREGOR:

That's true if you plan to send the beam directly from the laser diode into the cell. If you transmit through a fiber optic cable, however, the fiber can do a lot of the selecting for you. In fact, if you want to put the maximum power into a fiber optic cable, you need to use special techniques such as taping the fibers and placing the cable end close to the chip. Then you have to worry about the stability of that whole package.

W. MEYER:

Someone was talking about cementing fibers to the laser, in order to keep the laser beam and fiber in alignment.

A. MacGREGOR:

They were talking about cementing fibers straight onto the laser package you can buy from Sharp.

Refractometry

W. MEYER:

Okay. Several people have expressed a preference for in-situ refractometers. Can I ask how the Wyatt refractometer works or does this involve something proprietary?

P. WYATT:

Not anymore, although we are still finishing up our patent applications. In general, the refraction from liquid to glass depends upon the refractive index of the liquid, and with the right split photodiode detector you can measure the displacement of the beam to a fraction of a micrometer. From that, you can calculate dn [the refractive index difference] to one part in 105 or 106, and that's pretty good. The sensitivity of this trivial little device was comparable to that of the Waters 410, but with much greater stability. It is very simple to include in a flow configuration. Of course, for batch mode molecular weights you need dn/dc [the refractive index change with concentration]. Usually dn/dc is

known before the experiment begins. The exception would be in a chromatography setup where you need a continuous monitoring of concentration. You could monitor the change of refractive index to do the chromatography.

Other Concerns

W. MEYER:

Okay, we have addressed all the points I wanted to cover. I would now like to open the discussion to any concerns you have that we didn't address. What are we missing, what should we be thinking about, where do we need to go?

A. MacGREGOR:

Would you please repeat some of the drop dead dates for defining the specifications of the LLS instrument? For example, by what date do people have to tell you what experiments they want to do? And when do you need to have a preflight version of your LLS instrument?

W. MEYER:

Those dates depend on some work that we are doing and some that's being done in other labs. Within a year, we expect to have all the preliminary results, which will give us needed information about optical masking techniques, fiber optics developments, and maximum likelihood algorithms. In the meantime, we also expect that new technological developments will occur. We hope to have a working model within two years. Then it will probably take us a year to do the necessary paperwork to fly the instrument on a Learjet. So we plan to fly it within three years. People are also pushing to include it in the Fluid Diagnostics Facility, which will first fly on the Shuttle as part of a United States Materials Laboratory [USML], and eventually will fly on the Space Station. Gil [Santoro], can you tell us what the schedule is for that?

G. SANTORO:

It sounds unrealistic, but they are talking about including the Fluid Diagnostics Facility in USML-1, which is scheduled to fly in March, 1992.

W. MEYER:

We were told it would be USML number three or four, which would make it at least 2 years later. So we are probably looking at flying on the shuttle in 1994, if this becomes part of the Fluid Diagnostics Facility. In any event, those are some target dates to aim for. Any other concerns?

I. CLARK:

I would like to discuss telescience and downlinking of data a little more. As a contribution to high data rate, high resolution video transmission, Langley is working on minimizing the amount of downlinked data needed to extract pertinent features from an image. So, I would like to hear some feedback from experimenters as to what features you really need. Do you need image definition, black and white pictures, or color?

W. ROSENBLUM:

We are building a small system right now to go into the refrigerator where our crystals are being grown. It is not clear what resolution is really needed, but we have heard numbers like 0.01 mm to 0.1 mm. In any case, we need more than video transmission. One problem in the crystal business is that you can have a beautiful-looking crystal that won't diffract worth a hoot. So while visual image is a rough guide as to how the crystallization is proceeding, it alone has never proved whether a crystal is good or not.

S. BOTT:

What sort of computing power will be available to users on the Shuttle or in the module on Space Station?

W. MEYER:

I believe we can run faster than 20 megahertz with 32-bit paths. If we build in a computer as part of the experiment, then we can put in whatever computer we need and flight qualify it. I don't remember what Robert Brown said his computer speed was, but he used an Atari Mega ST4. I understand that some of the software correlator work is now being done with 16-bit paths running at 16 megahertz. One trouble we will have is that building a correlogram with 12 angles, as opposed to one angle, will cut our speed by at least a factor of 12.

K. SCHÄTZEL:

I've done a lot of work with software correlators, and I can tell you that hardware correlators are much faster. Just to give you a rough figure of merit, the performance right now is a factor of ten in favor of a signal processor over a standard microprocessor, and another factor of a hundred in favor of hardware over software. But multiplexing, of course, can also be done with a hardware correlator. You could use one correlator that is able to work at 200 nanoseconds and multiplex it between five detectors, to work at one microsecond.

W. MEYER:

That's a good comment. Once we do that, we could run the experiment with a primitive computer.

S. BOTT:

I actually wasn't thinking about software correlators when I asked the question about computing power. Instead, I envisioned doing some data analysis on board, and having the result of this data analysis determine the next experiment. There would be feedback: Instead of just having a simple list of commands, each experimental run would be based on an analysis of the previous runs.

A VOICE:

I have another concern. The instrument configuration has a lot of cool detectors spaced primarily on the side opposite the laser, which is a heat source. You may have trouble with thermal isolation, particularly during ground-based testing.

W. MEYER:

We will have to look at the thermal mass of the aluminum block into which we mount detectors, to see how many detectors we can accomodate. I imagine heating is insignificant in the DAWN instrument, but that may be due to having only 15 angles. This may be another good argument for using fiber optics; we could run the fibers below a thermal barrier.

W. MEYER:

If there are no other concerns, I'd like to review a little. We've decided on a multi-angle instrument, but how many static and dynamic angles do we need? I would like to establish upper and lower limits on the number of angles needed.

J. WIENCEK:

I think the answer lies in modular design. For general-purpose hardware, you develop a light source module and compatible detectors and correlators. Then the sample cell configuration and the arrangement of detectors can be experiment-specific.

W. MEYER:

That's true, but we still need to know how many angles are possible in order to design the instrument.

P. WYATT:

Fifteen angles will do two things. First, it will let you measure particle sizes up to 1.5 microns. Secondly, it will be compatible with standard off-the-shelf A/D multiplexers, which usually have 16 channels. So I would suggest 15 detectors or fewer; the 16th

channel on the multiplexer would be reserved for monitoring the laser intensity.

S. BOTT:
I would vote for two or three times that number for static light scattering.

B. CHU:
I still say one angle per degree is needed for static light scattering.

W. MEYER:
Okay, we have a minimum of 15 and a maximum of 180 static angles. Will we be meeting the experimenters' needs if we have perhaps half a dozen to a dozen angles for dynamic light scattering?

B. CHU:
I support what both Steve Bott and Klaus Schaetzel suggested, to use around ten angles. This is really limited by the correlators.

W. MEYER:
Since it is limited by the correlators, should we [at NASA] push for single-chip correlators? We know of two companies who can develop the technology and manufacture the chips. It would involve startup costs of tens of thousands of dollars, but after that the rest of the chips would cost very little. If it is at all financially feasible, we can make that a priority.

B. CHU:
Before reducing the size to a single chip, there are still some arguments to be settled pertaining to how the correlator should work. There are fundamentally different methods of constructing correlation functions. The method used probably depends on the people who are making correlators. There are special mechanisms involved, some of which are proprietary and which people are not willing to divulge. But I do understand the way correlation can be accumulated and the way signals should be processed. These are not necessarily the way that they are being processed.

A. MacGREGOR:
I have a policy question. We have not agreed on what is required in a correlator. When and how is that decision going to be made? It seems to me that at some stage, each of us has to either accept Bill's decisions on what the design is going to be, or find another forum for influencing the design decisions.

K. SCHÄTZEL:
As long as the chip multiplies numbers of photon counts and then sums them up somehow, nobody cares about how it is done. The important thing is that we get the right numbers.

Closing Remarks

W. MEYER:
There are still many details to be settled, and we [at NASA] will be in touch with you in the future. However, I am impressed with what has been accomplished so far. A lot of wonderful technology has been revealed at this workshop. When I began this project, my question was, "How much will we have to compromise to get an instrument that will work?" I'm amazed that after today's discussion, it looks like we won't have to compromise much at all. We may even be extending present capabilities, using new developments such as maximum likelihood correlation algorithms and combinations of dynamic and classical light scattering. And, of course, the greatest extension of all will be the ability to do light scattering in a microgravity environment. Thank you for coming. You have been wonderful.

NASA
National Aeronautics and Space Administration

Report Documentation Page

1. Report No.	2. Government Accession No.	3. Recipient's Catalog No.
NASA CP-10033		

4. Title and Subtitle	5. Report Date
NASA Laser Light Scattering Advanced Technology Development Workshop—1988	August 1989
	6. Performing Organization Code
7. Author(s)	8. Performing Organization Report No. E-4915
	10. Work Unit No. 694-03-03
9. Performing Organization Name and Address National Aeronautics and Space Administration Lewis Research Center Cleveland, Ohio 44135-3191	11. Contract or Grant No.
	13. Type of Report and Period Covered Conference Publication
12. Sponsoring Agency Name and Address National Aeronautics and Space Administration Washington, D.C. 20546-0001	14. Sponsoring Agency Code

15. Supplementary Notes

Editor, W.V. Meyer, Case Western Reserve University, Cleveland, Ohio 44106 and NASA Resident Research Associate at Lewis Research Center.

16. Abstract

The NASA Laser Light Scattering Advanced Technology Development Workshop was held September 7 and 8, 1988, in Cleveland, Ohio. Its major objective was to explore the capabilities of existing and prospective laser light scattering hardware and to assess user requirements and needs for a laser light scattering instrument in a reduced gravity environment. This workshop, which was organized by NASA Lewis Research Center, addressed experimental needs and stressed hardware developments.

17. Key Words (Suggested by Author(s))	18. Distribution Statement
ATD; Advanced Technology Development; Laser light scattering; Quasi-electric light scattering; Photon correlation spectroscopy; Avalanche photodiodes; Fiber optic probes; Microgravity; Reduced gravity; APD; Laserdiode	Unclassified – Unlimited Subject Category 35

19. Security Classif. (of this report)	20. Security Classif. (of this page)	21. No of pages	22. Price*
Unclassified	Unclassified	308	A14

NASA FORM 1626 OCT 86

*For sale by the National Technical Information Service, Springfield, Virginia 22161